The Synthesis of a Charge-Based Conjugation System to Extend the Intra-Articular Resident Time of Osteoarthritis Therapeutics

A thesis submitted to Cardiff University for the degree of

Doctorate of Philosophy of Pharmaceutical Science

Raed Mohammed Alghamdi

Cardiff University

School of Pharmacy and Pharmaceutical Sciences

April 2023

Supervisors:

Dr. Polina Prokopovich

Dr. Fabrizio Pertusati

Abstract

Osteoarthritis (OA) is a chronic inflammatory disease that affects the synovial joint structure, and there is no medication that can reduce or prevent the disease's development. The main obstacles for drugs that can slow the disease progression are penetrating the condensed cartilage network, retaining within the cartilage, and remaining within the synovial joint due to the continuous exchange of the synovial fluid. Therefore, various techniques and mechanisms of drug delivery systems have been investigated to increase the time of OA therapeutics inside the synovial joint. One of these strategies is the use of cationic delivery systems to be interacted electrostatically with the anionic cartilage components (proteoglycans and glycosaminoglycans), which will attach the carrier to the cartilage, assisting the drug to infiltrate through and retain within the cartilage as well as avoiding drug elimination during the synovial fluid exchange. In the current study, three cationic polymers, A5, A16, and A87, were chosen from the library of poly *beta*-amino polymers to be covalently conjugated to OA therapeutic (licofelone) in order to enhance the uptake and retention time of the drug within two *ex-vivo* cartilage models. Furthermore, the licofelone conjugated to A5, A16, and A87 has shown a significant increase in drug uptake and retention time inside the healthy and early simulated OA cartilage model compared to the licofelone alone. The A87-licofelone conjugate showed the highest uptake percentage of the conjugated licofelone in healthy cartilage (44 ± 4.3 % at 30 minutes) and in the OA model (26.6 ± 3.1 % at 25 minutes), while in both models, the unconjugated licofelone maximum uptake percentages were 1.4 ± 0.6 % and 1.7 ± 0.6 % at 30 minutes, respectively. Factors such as the quantity of the cartilage content, the degree of the positive charge, the intensity of the electrostatic interaction, and the quantity of licofelone conjugated to the polymers have influenced the percentage of conjugated licofelone within the cartilage. Moreover, the A87-licofelone conjugate showed no effect on the chondrocyte viability compared to untreated cells. The conjugation of licofelone to A87 has increased the uptake and retention of the drug without affecting its chemical structure and cytocompatibility.

Table of content

List of figures

List of tables

List of abbreviations

5-CNAC	(8-(N-2-hydroxy-5-chloro-benzoyl)-amino-caprylic acid)
ACN	Acetonitrile
AcOH	Acetic acid
ADAMTs	A disintegrin metalloproteinase with thrombospondin motifs
AMPA	α-amino-3-hydroxy-5-methyl-4-isoxazolepropionic acid
AUC	The area under the curve
br s	Broad singlet
BMI	Body mass index
BMP-7	Bone morphogenetic protein -7
COMP	Cartilage oligomeric protein
CTX-I	Carboxy-terminal telepeptides of type I collagen
CTX-II	Carboxy-terminal telepeptides of type II collagen
DBU	1,8-Diazabicyclo[5.4.0]undec-7-ene
DCC	N,N'-dicyclohexylcarbodiimide
DCM	Dichloromethane
dH$_2$O	Deionized water
DMAB	p-dimethylaminobenzaldehyde
DMMB	Dimethyl-methylene blue
DMOAD	The disease-modifying osteoarthritis drugs
DMSO	Dimethylsulfoxide
DMSO-d6	Deuterated dimethylsulfoxide
DTT	Dithiothreitol
ECM	Extracellular matrix
EDC	1-Ethyl-3-(3-dimethylaminopropyl)carbodiimide
EDTA	Ethylenediaminetetraacetic acid
FGF-18	Fibroblast growth factor-18
GAG	Glycosaminoglycan

GPC	Gel permeation chromatography
HCl	Hydrochloric acid
IA	Intra-articular injection
IGF-1	Insulin-like growth factor 1
iGluRs	Ionotropic glutamate receptors
IL-1	Interleukin-1
IL-6	Interleukin-6
LTB_4	Leukotriene-B4
m-AV	Multi-arm avidin
MCP joint	Metacarpophalangeal joint
mGluRs	Metabotropic glutamate receptors
MMPs	Matrix metalloproteinases
MSCs	Mesenchymal stem cells
Mw	The average molecular weight
NaOAc	Sodium acetate
NBQX	2,3-dihydroxy-6-nitro-7-sulfamoyl-benzo[f]quinoxaline
NMDA	N-methyl-d-aspartate
NMR	Nuclear Magnetic Resonance
NSAIDs	Non-steroidal anti-inflammatory drugs
OA	Osteoarthritis
PAMAM	Polyamidoamine
PBAE	Poly *beta*-amino ester
PBS	Phosphate buffered saline
PEG	polyethylene glycol
PG	proteoglycan
RP-HPLC	Reverse phase high-performance liquid chromatography
SD	Standard deviation
SEC	Size exclusion chromatography

SrR	Strontium ranelate
TGF-β	Transforming growth factor-*beta*
THF	Tetrahydrofuran
TIMPs	Tissue inhibitors of metalloproteinases
TNF	Tumor necrosis factor
UV	Ultraviolet
v/v	Volume/Volume
VEGF	Stimulate vascular endothelial growth factor
w/v	Weight/Volume
ZP	Zeta potential
λ-max	Maximum wavelength

Acknowledgment

I would like to express my gratitude to my family, wife, professors, teachers, and friends who have helped and supported me in pursuing a PhD degree.

The completion of this work would not have been possible without the assistance of my supervisors, Dr. Polina Prokopovich and Dr. Fabrizio Pertusati. I also appreciate all the guidance and encouragement that Dr. Polina Prokopovich and Dr. Fabrizio Pertusati have expressed.

Finally, none of this would have been possible without the visionary advocacy of Taibah University, Medina, SA and the Saudi Arabian Cultural Bureau, who provided the opportunity and the funding for my graduate study.

Chapter 1: **General Introduction**

1.1 **Introduction**

Arthritis is a common condition of pain and inflammation in a joint.(1) Osteoarthritis (OA) is the most common type of arthritis followed by rheumatoid arthritis.(2) In 2021, approximately 8.5 million individuals in the United Kingdom have OA, while 430,000 have rheumatoid arthritis.(2) Both diseases make the joints swollen, painful, and stiff.(2) However, OA is characterized by a chronic inflammation of the synovial joint affecting the structure of synovium, cartilage, and bone, whereas rheumatoid arthritis is an autoimmune disease.(1, 2) The current thesis will focus on OA, which has affected 528 million individuals globally, and around 80 % of these patients have been diagnosed with knee osteoarthritis.(1) Osteoarthritis can be classified as primary OA, when the cause could be attributed to aging or genetic factors. However, when there is a particular cause such as congenital abnormality or trauma (posttraumatic OA), the disease is classified as secondary osteoarthritis.(3) The two significant risk factors of OA are aging and obesity.(3, 4) Globally, 34 % of individuals aged ≤ 65 years have diagnosed with OA.(5) In 2017, 98 % of individuals with body mass index (BMI) equal to 30.1 have been diagnosed with OA.(6) Individuals with OA experience chronic pain and joint stiffness that can lead to limited working time, a poor quality of life, and depression, which impact their lives socially, mentally, and economically.(4, 6) The current disease management is mainly symptoms relief medications, such as acetaminophen, non-steroidal anti-inflammatory drugs (NSAIDs), steroids, and intra-articular injection of hyaluronic acid because OA was thought to be a wear-and-tear disease.(7-9) In early stages of OA, patients experience mild pain during movements, 10 % loss of cartilage contents, and formation of bone spurs(osteophyte). The symptoms of the disease progression are increasing articular cartilage degeneration, increasing osteophyte formation, reducing joint space, and joint swelling. The progression of OA can be slow or fast, resulting in severe osteoarthritis. In the severe stage, patients suffer from persistent severe pain and discomfort during movements because of 80 % loss of articular cartilage, no joint space (bone on bone), and a transformation of bone morphology.(10) Unfortunately, OA has no clinically approved treatment that could prevent or reduce its progression. Joint replacement surgery has been the

only structural improvement solution to OA patients.(6, 11) Despite the fact that previously OA has been considered a wear and tear disease, recent studies have confirmed that there are pathological processes involved in OA development.(11-16) Osteoarthritic articular joint shows inflammatory cytokines release, an imbalance of the articular cartilage generation/degeneration enzymes, and bone resorption.(11-16) Investigating the process of OA progression could provide therapeutic targets to prevent or reduce OA progression, which will be discussed in (1.1.2). Recognizing the enzymes that generate or degrade cartilage components as well as the inflammatory cytokines that initiate the process of OA will have a substantial impact on the future therapeutic strategies. These studies have revealed a new therapeutic class for OA known as disease-modifying osteoarthritis drugs (DMOADs).(11-16) Briefly, DMOADs inhibit the progression by targeting various OA progression pathways, which will be addressed in further depth (1.1.4).(11-16) Although DMOADs have shown significant activity against the disease progression during pre-clinical studies, unfortunately none have been approved as an OA medication because of low therapeutic efficacy and adverse effects in clinical trials.(3, 11-19) The low therapeutic benefit is due to the biological nature of the synovial joint, which has reduced the DMOADs quantity and time inside the joint. At the time, increasing the medication dose appeared to be a reasonable approach as the drug quantity was being lost at the site of action. However, the elevated dose has increased the quantity of the drug drained into the systemic circulation, which has increased the risk of side effects.(17-20) Therefore, the joint structure and physiological behaviour in the articular joint that play a role in reducing OA treatment quantity and resident time must be understood in order to build an effective DMOAD delivery system, which will be discussed next. Furthermore, developing a drug delivery system could increase DMOAD quantity and time within the synovial joint, which will enhance the therapeutic effect of these medications and reduce their adverse effects (1.1.6).

1.1.1 Structure of articular joint

Generally, the synovial joint contains three significant elements: Articular cartilage, synovial fluid, and bone (Figure 1.1). Articular cartilage is a smooth and lubricated surface on the bone end of a joint. The cartilage main function is to ease the bone mobility during body movement. Within the cartilage, there are no blood vessels, lymphatic vessels, or nerves.(21, 22)
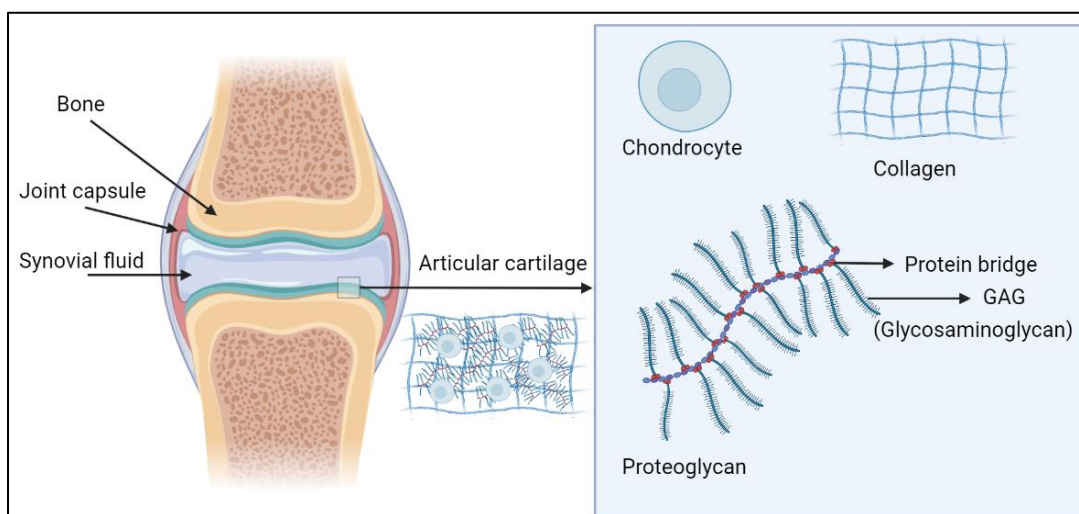
Figure 1.1: Synovial joint structure
The figure created with BioRender.com.

The articular cartilage consists of chondrocytes (1 - 5%) surrounded by extracellular matrix (ECM) (20 - 40%) and water (65 - 80%).(23, 24) Chondrocytes are the only cell type that exists within the cartilage, which initiates a microenvironment where the cell produces and maintains matrix components.(22, 25) Cartilage cell proliferation and migration are limited; therefore, healing after cartilage injury is challenging.(24, 25) The microenvironment around each chondrocyte isolates these cells from each other and prevents their migration. Cartilage cells regulate the expression of proteins that are involved in the generation and degradation of cartilage matrix components.(22)

The cartilage consists of a three-dimensional network of insoluble collagen that is crosslinked with one another. Within this network, other components that are more soluble, such as glycosaminoglycan (GAG) and proteoglycan (PG), are integrated or even chemically attached to the collagen.(26) Type II collagen and PG are the main components of the ECM (Figure 1.1).(21) Type II collagen constructs articular cartilage structure, while PGs are essential to resist

compressive pressure.(21, 24, 25) PGs consist of protein linked to linear GAG monomers.(24, 25) Glycosaminoglycans are repeating units of unbranched disaccharides that are responsible for the hydrophilicity and the negative charge of the cartilage because of the presence of anionic sulfated or carboxylated disaccharides.(21, 25) Aggrecan is the abundant and largest PG, which consists of a protein core linked to GAG via a protein bridge.(21, 25) The GAGs in the aggrecan structure are either chondroitin sulfate (sulfated N-Acetyl galactosamine and glucuronic acid) or keratin sulfate (sulfated N-Acetyl glucosamine and galactose).(21, 24, 25) Aggrecan is a negatively charged polymer under physiological conditions.(24) In addition, aggrecan can be bound via a protein bridge to hyaluronic acid, which is composed of glucuronic acid and N-acetyl glucosamine.(21, 24, 25) The negatively charged proteoglycans attract the positively charged molecules and repel the negatively charged molecules.(24) The polarity and the negatively charged ECM components attract water molecules.(25) Water assists in transporting and distributing nutrition from the synovial fluid to chondrocytes. In addition to nutrition contribution, water plays a significant role in biomechanical and lubrication processes.(21, 25, 26)

Moreover, chondrocytes are responsible for the production of local proteases. In the physiological condition, the expression of proteases is low, with a main role of tissue remodelling after injury or trauma. Proteases are enzymes that break down collagen, aggrecan, and other proteins, which result in the degradation of articular cartilage. Matrix metalloproteinases (MMPs) and a disintegrin metalloproteinase with thrombospondin motifs (ADAMTS) are the main types of proteases that are responsible for collagen and aggrecan degradation in disease conditions. Tissue inhibitors of metalloproteinases (TIMPs) are the endogenous inhibitor for MMPs and ADAMTS, which are responsible to regulate their activity.(27) Additionally, cathepsin K is a protease enzyme, mainly expressed in osteoclasts, and it is responsible for collagen degradation and bone resorption.(28) Cathepsin K degrades collagen into multiple fragments, while MMP breaks the collagen into two fragments. The mechanism of collagen degradation by cathepsin K is not well known yet.

The second element of the synovial joint is the synovia (synovial fluid), which plays significant roles as lubrication for the articular cartilage, shock absorption, and the transportation

4

of nutrition.(29) The synovial fluid consists mainly of hyaluronic acid and proteins.(29, 30) Additionally, the blood vessels are supplying the articular capsule and synovia with immune cells and nutrition.(10, 31) A synovial joint is surrounded by a synovial membrane, which produces the synovial fluid. The physiological synovia turnover is carried to the systemic circulation by venules and lymphatic vessels. (10, 29-31) Joint movements assist in the synovial fluid turnover, which occurs around 1 hour in a healthy knee.(32) The consistency of synovial fluid turnover as well as the position of chondrocytes within the cartilage network are challenging aspects for therapeutics to stay inside the joint and reach the cells, which will be discussed in 1.1.5.(17, 18, 33, 34)

1.1.2 **The pathophysiological condition of OA**

The initiation cause of OA is not well known.(3, 35) The progression of OA occurs over a period of time and involves altering the level of inflammatory cytokines and proteases within the synovial joint (Figure 1.2). Ageing, overweight, inflammation, joint abnormality, or physical injury are factors that could affect chondrocyte functionality and stimulate macrophages in the synovial fluid.(36, 37) These factors directly or indirectly activate the local immune system and initiate an inflammatory reaction.(22) Consequently, macrophages get stimulated, leading to the release of inflammatory cytokines such as interleukin (IL)-1 and tumor necrosis factor (TNF), and stimulating vascular endothelial growth factor (VEGF) and E-selectin.(3, 22) VEGF stimulates the formation of new blood vessels (angiogenesis).(3) Additionally, E-selectin expresses a new receptor, so other immune cells can be recruited to the synovial fluid. The recruitment of immune cells (T helper cells) further increases cytokine production, which stimulates the progression of inflammation.(3, 36)

Furthermore, T helper cells, macrophages, and inflammatory cytokines promote synoviocyte activities, a group of cells within the synovial membrane responsible for the production of synovial fluid, to increase protease production.(38) Additionally, interleukin-1 and TNF influence chondrocytes anabolic and catabolic activity.(37) In OA, chondrocyte catabolic activity is enhanced, whereas anabolic activity and the synthesis of new cartilage components are inhibited, which altered the expression level of MMP, ADAMTS, and TIMP in the cartilage and the synovium.(22, 27, 39-41) Studies have investigated the function and the expression level of MMP in human in order to determine which MMP is considered an OA biomarker.(27, 39-41) Accordingly, the quantity of MMPs expressed in the cartilage of patients undergoing hip replacement due to OA or a femoral neck fracture showed upregulation of MMP-2, MMP-9, MMP-13, MMP-16, and MMP-28 in OA patients.(39) Particularly, the expression of MMP-13 and MMP-28 was significantly higher compared to other overexpressed MMPs.(39) Additionally, a study has observed the expression of MMPs in the cartilage and synovial fluid of patients with OA compared to bone fracture injury.(27) In both tissues, OA patients have demonstrated a higher level of MMP-9, MMP-11, MMP-13, MMP-16, and MMP-28 compared to patients with a bone fracture injury.(27) MMP-13 is the most investigated MMP and is recognized as a biomarker

for osteoarthritis due to its robust ability to degrade the most abundant cartilage component (collagen type II).(40)

In addition to MMP, ADAMTS has shown aggrecanase activity, which degrades aggrecan in an early stage of OA, but the expression of ADAMTS's subfamily in OA was not consistent.(42, 43) However, ADAMTS-2, ADAMTS-6, ADAMTS-12, ADAMTS-14, and ADAMTS-18 have shown a constant upregulation in human osteoarthritic cartilage.(43) ADAMTS-2 and ADAMTS-14 are involved in the biosynthesis of collagen and their upregulation in OA could be related to cartilage repair process.(44) Moreover, the overexpression of ADAMTS-12 is associated with the degradation of cartilage oligomeric protein (COMP), which is necessary in the process of cartilage formation.(45) Furthermore, the substrate for ADAMTS-6 and ADAMTS-18 is unknown, and the enzymes are not involved in cartilage anabolism nor catabolism.(43) The expression level and the activity of ADAMTSs differ based on the stage of OA and the experimental model of OA. Studies have reported that aggrecanase has weak activity in late OA, which could be related to aggrecan depletion in a late stage of the disease.(42, 43) Five members of ADAMTS have shown aggrecanase activity, which were ADAMTS-4, ADAMTS-5, ADAMTS-9, ADAMTS-16, and ADAMTS-18. Moreover, ADAMTS-4 and ADAMTS-5 demonstrated the most efficient aggrecanase activity.(46) An *in vitro* study reported that ADAMTS-4 activity was induced by IL-1, but there was no evidence of ADAMTS-4 overexpression.(47) Human synovial cells and bovine cartilage cells showed an inhibition in the expression of ADAMTS-4 when treated with a combination of TNF and IL-1 inhibitor compared to untreated cells. According to *in vitro* studies, TNF and IL-1 have no influence on ADAMTS-5 activity and expression.(38, 47) Collective research data has reported different conclusions in terms of IL-1 and TNF influence on ADAMTS-5 activity and expression, which could be directly affected by the experimental procedures and conditions as well as the OA models.(48) ADAMTS-5 regulation has shown no influence by TNF or IL in synovial fibroblasts of humans, bovines, and mice, or chondrocytes of humans. On the other hand, TNF and IL-1 increase ADAMTS-5 expression in bovine and mouse chondrocytes.(48) A study on mice lacking ADAMTS-5 and wild-type mice has reported that aggrecan was protected against inflammatory cytokines in the absence of ADAMTS-5.(49) ADAMTS-4 and ADAMTS-5 evidently play a significant role in developing OA and influencing the progression of OA at an early stage. Furthermore,

cathepsin K is a protease that plays a role in the cartilage content degradation process. Overall, MMP-13, ADAMT-4, ADAMTS-5, and cathepsin K are the significant proteases responsible for the degradation of articular cartilage in OA progression.

Moreover, cytokines stimulate osteocytes, which activate osteoblasts as a repair mechanism. In the case of chronic inflammation, long-term activated osteoblasts start to form osteophytes.(36) Osteoblasts play a significant role in the OA progression by causing abnormal bone remodelling, reducing bone mineralization, and causing osteophyte formation, which affect the bone morphology and density.(50) Additionally, an *in vitro* study has suggested that abnormal activity of osteoblast can stimulate chondrocytes to increase MMP and ADAMTS production.(50) In addition, osteoblasts express cathepsin K, which is capable of degrading collagen and contributing to the breakdown of cartilage.(50) Furthermore, many of the released cytokines are pain-signalling molecules, such as prostaglandin E and bradykinin. Three out of four OA patients have mentioned persistent pain in the osteoarthritic joint.(4) IL, TNF, and VEGF are inflammatory biomarkers that are associated with OA progression.(51) Synovial fluid contents, cartilage, and bone are the main elements affected by OA progression. Therefore, the regulation of cytokines, proteases, osteoblast, and osteoclast activity are potential therapeutic target for future OA medication (1.1.4).(13)
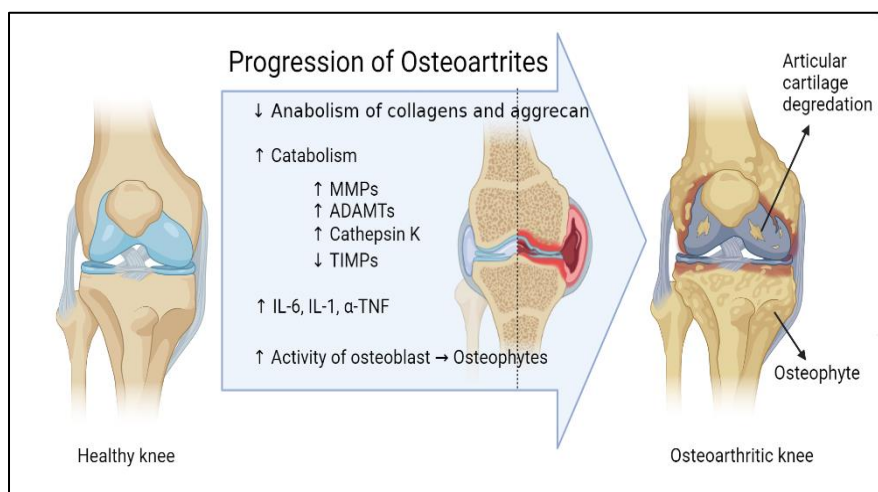
Figure 1.2: Osteoarthritis progression factors

MMP (matrix metalloproteinases), ADAMS (a disintegrin and metalloproteinase with thrombospondin motifs), TIMPs (tissue inhibitors of metalloproteinases) IL-6 (interleukin-6), IL-1 (interleukin-1), and α-TNF (alpha-tumor necrosis factor). The figure created with BioRender.com.

1.1.3 **Current treatment for osteoarthritis**

Currently, there is no cure for osteoarthritis. The recommended disease management by health professionals are acetaminophen, topical NSAIDs, and oral NSAIDs, for non-pharmacological management exercise and weight loss are recommended.(7) In the case of severe pain, opioids are recommended.(7) The current treatments for OA are mostly pain management medications.(8) The mentioned medications do not improve or protect the structural integrity of a joint.(3) Their major limitations of these medications are the poor benefits for patients and the serious adverse effects due to their prolonged administration. Renal dysfunction, cardiovascular diseases, and peptic ulcer were side effects associated with prolonged administration of NSAIDs, as were skin reactions with the use of topical NSAIDs.(8) Moreover, glucocorticoid intra-articular (IA) injections every 6 weeks relieved OA pain for a short time (1 to 3 weeks), but multiple IA injections could lead to osteonecrosis due to interruption of the blood supply.(7, 52, 53) The analgesic effect of systemic corticosteroids was not persistent in OA patients. According to a study that compared the effect of oral prednisolone against a placebo, prednisolone has no significant analgesic effect compared to the placebo.(54) Opioid-treated patients who received morphine or tramadol showed 50 % improvement compared to placebo.(55) In addition, opioids could increase the risk of cardiovascular diseases, gastrointestinal bleeding, and mortality.(55). Eventually, an OA patient reaches the severe stage of the disease since the current medications do not act on the progression of OA. In severe cases, the only available structural modifying treatment is joint replacement surgery. According to the national joint registry, 97 % of knee and 91 % of hip replacement surgeries have been performed on patients with osteoarthritis.(6) Unfortunately, 21.4% and 17.5% of these patients continue to feel pain after the surgery, respectively.(4) Non-pharmacological treatments have also been able to relive patient symptoms. Exercise and weight loss are very effective in the management of the affected joints, as they showed a reduction in the inflammatory cytokines, inhibition of the progression of OA, and pain suppression.(7, 13, 36, 52) Regular physical activity seems to reduce the 6 % risk of having OA pain.(2) Since NSAIDs are the current prescribed medications for OA patients, a new class of NSAID derivatives is under development known as cyclooxygenase-inhibiting nitric oxide donator (CINOD).(56-59)

1.1.3.1 Cyclooxygenase-inhibiting nitric oxide donator (CINOD)

CINOD is a newly developed class of medication reduces the long-term administration side effects of NSAIDs by adding nitric oxide donating moiety. Naproxcinod, also known as nitronaproxen, AZD 3582, NO-naproxen, and HCT 3012, is a NSAID derivative of naproxen (Figure 1.3).(57, 58) Moreover, naproxcinod, which is classified as CINOD, breaks down into naproxen and a nitric oxide donor compound after absorption.(56-59) The analgesic and anti-inflammatory activity of CINOD is comparable to NSAIDs.(57-59) The addition of the nitrate group to naproxen has improved its safety profile compared to COX-I and COX-II inhibitors.(57-59) The release of nitric oxide could be the reason for suppressing the gastrointestinal and cardiovascular adverse reactions caused by NSAIDs long-term administration.(57-59) Systemic nitric oxide has shown evidence of maintaining the blood flow, increasing vasodilation, and inhibiting atherosclerosis by activating nitric oxide-dependent guanylyl cyclase.(59) Nitric oxide produced from CINOD was proven to increase gastric blood flow, mucus secretion, and bicarbonate secretion, which inhibit gastrointestinal toxicity.(59) A study on OA patients has reported that naproxcinod has a similar efficacy and improved safety profile compared to naproxen.(57, 59, 60) A phase II study on OA patients has evaluated the safety and effect of naproxcinod-different doses against 25 mg of rofecoxib (a COX-II inhibitor) and a placebo.(56) The study reported that naproxcinod has significantly suppressed OA symptoms compared to placebo but shown no statistical difference compared to rofecoxib.(56) Moreover, 750 mg twice daily of naproxcinod demonstrate a better balance between efficacy and safety than 750 mg per day and 1125 mg twice a day.(56) Furthermore, naproxcinod did not show cardiovascular complication, while rofecoxib raised the subjects' systolic blood pressure significantly.(56) Currently, naproxcinod is in phase III clinical study for the treatment of OA and other CINODs are under development.(57, 58) However, CINODs, NSAIDs, steroids, and other current medications provide symptom relief, whereas the OA disease requires medication to prevent the disease progression.
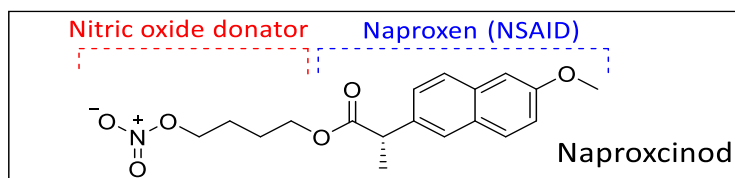
Figure 1.3: Naproxcinod structure

1.1.4 **Osteoarthritis treatment in development**

Researchers aim to discover novel therapeutics that can prevent the disease's progression since the current medications target the symptoms of OA.(11-16) These novel or repositioned drugs, known as disease-modifying osteoarthritis drugs (DMOADs), are developed to slow or prevent the disease's progression (Figure 1.4). Therefore, the OA disease development process was under intensive investigation, seeking specific OA biomarker targets for DMOADs (11, 14, 16). The progression involves cartilage degradation, inflammatory cytokines release, and bone morphology changes, which was described previously (1.1.2).(11, 12, 61) Therefore, DMOADs target cartilage catabolism, inflammatory cytokine release, bone resorption, cartilage anabolism, and chondrocyte activity (Figure 1.4).(11-16, 52) Drugs that target cartilage catabolism were designed to inhibit the primary cartilage proteases activities such as MMPs, ADMATSs, and cathepsin K (1.1.4.1). Additionally, inflammatory cytokine inhibitors can reduce IL-1 and TNF activity to slow the disease progression (1.1.4.2). Moreover, bone resorption drugs play a role in maintaining the activity of osteoblast and osteoclast and bone mineral, which is a significant element in the OA progression process (1.1.4.3). Additionally, there are molecules that have shown activity against multiple OA progression biomarkers, such as glutamate receptor inhibitors, inducible nitric oxide synthase (iNOS) inhibitors, and a dual inhibitor for 5-lipoxygenase (5-LOX) and cyclooxygenases (COX) (1.1.4.4). In addition to targeting the progression, there are DMOADs that stimulate cartilage anabolism, enhance chondrocyte activity and proliferation, and increase TIMPs expression (1.1.4.5). The effects of DMOAD have been evaluated primarily by determining the joint space changes, joint structure changes, cartilage volume changes, the quantity of OA biomarkers, and the score of the WOMAC questionnaire (Western Ontario and McMaster Universities Osteoarthritis Index).(11-16) The WOMAC questionnaire aids in the assessment of OA symptoms based on the subjects' answers.(62, 63) Most of these DMOAD could be an excellent candidate for a drug delivery system experiment to enhance their therapeutic effect since none of them is clinically approved. The discovery of DMOAD is still undergoing intensive study, and several DMOADs are in different stages of clinical studies, which will be detailed next.(11-16)
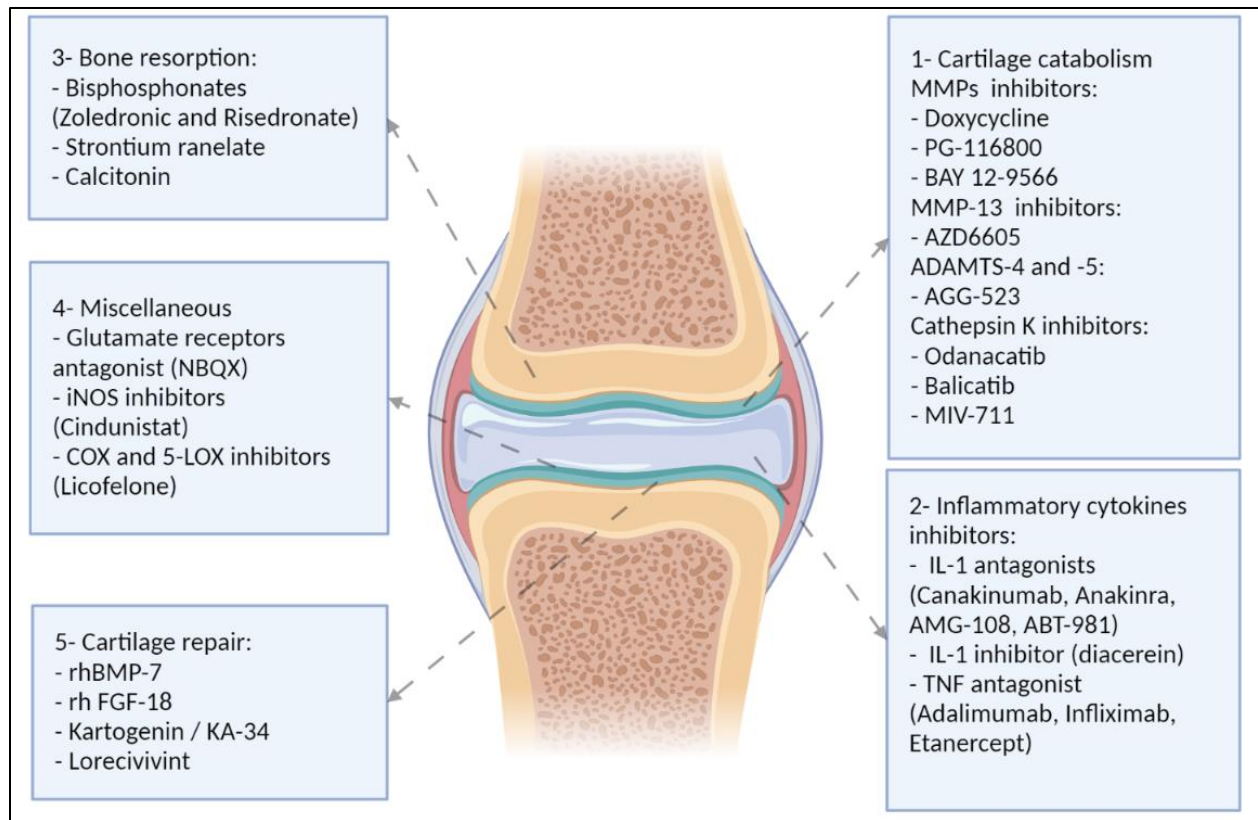
Figure 1.4: DMOADs target osteoarthritis progression factors

MMPs (matrix metalloproteinases), ADAMTSs (a disintegrin and metalloproteinase with thrombospondin motifs), rh BMP-7 (recombinant human bone morphogenetic protein -7), rh FGF-18 (recombinant human fibroblast growth factor-18), NBQX (2,3-dihydroxy-6-nitro-7-sulfamoyl-benzo[f]quinoxaline), iNOS (inducible nitric oxide synthase), 5-LOX (5-lipoxygenase), COX (cyclooxygenases), IL-1 (interleukin-1), and TNF (alpha-tumor necrosis factor). The figure created with BioRender.com

1.1.4.1 Cartilage catabolism

1.1.4.1.1 Matrix metalloproteinase (MMP) inhibitors

Matrix metalloproteinases are enzymes that play an important role in tissue developing and repairing processes during physiological and pathological conditions.(64) Doxycycline is an antibiotic with the ability to inhibit MMPs non-specifically. Despite a negligible reduction in the progression of joint space narrowing, doxycycline failed to show clinical evidence as a therapeutic agent for OA.(65) A series of MMP inhibitors, PG-116800 and BAY 12-9566, has been developed specifically to treat OA (Figure 1.5). Unfortunately, limited benefits and evidence of serious side effects were identified. Thirty-five percent of individuals who received PG-116800 treatment experienced musculoskeletal toxicity, such as joint pain and loss of motion.(66) Furthermore, clinical observation on individuals who received 100 mg of BAY 12-9566 for 3 weeks has shown an increase in collagen content. Unfortunately, hypertension, anaemia, and nausea were the major side effects produced by BAY 12-9566.(67) The major rationale behind the adverse events of PG-116800 and BAY 12-9566 is the lack of selectivity. Therefore, identifying the specific MMP that is responsible for the collagen degradation was crucial. MMP-28 and MMP-13 were identified as OA biomarkers and more selective targets than other MMPs toward cartilage degradation during the disease's development. Information regarding MMP-28 is limited, while MMP-13 has been under intensive investigation.(68) AZD6605 (Figure 1.5) is a selective and potent MMP-13 inhibitor that has demonstrated excellent preclinical results in terms of activity against cartilage degradation, safety, and pharmacokinetics.(69) AstraZeneca has reserved the right to conduct preclinical investigations on AZD6605. Inhibiting MMP-13 selectively seems to be a potential future target of OA treatment.
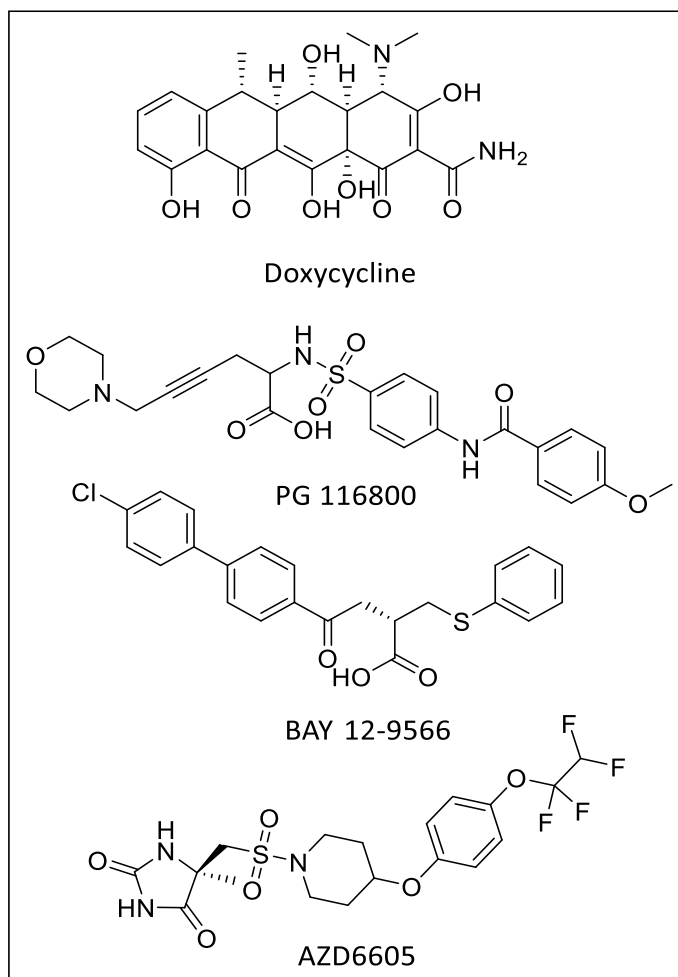
Figure 1.5: MMP inhibitors structures

1.1.4.1.2 A disintegrin and metalloproteinase with thrombospondin motifs (ADAMTS) inhibitors

A disintegrin and metalloproteinase with thrombospondin motifs is a class of enzymatic proteases that contains 19 members and is involved in cartilage anabolism, catabolism, the blood clotting process, and the formation of blood vessels.(42) The ADAMTS family contains enzymes that are responsible for collagen anabolism, such as ADAMTS-2, ADAMTS-3, and ADAMTS-14.(44) Therefore, designing a selective inhibitor toward ADAMTS, which play a role in aggrecan degradation, is essential. Studies have been reported that ADAMTS-4 and ADAMTS-5 are mainly associated with developing OA and influencing the progression of OA at an early stage; therefore, they seem interesting therapeutic targets to enhance cartilage structure and slow OA progression.(42, 46, 49) AGG-523 (Figure 1.6) is a selective ADAMTS-4 and ADAMTS-5 inhibitor

with 50 % inhibitory concentrations of 0.03 μM and 0.04 μM, respectively. Rats treated with 1 g/kg/day of AGG-523 showed a significant reduction in Ala-Arg-Gly-aggrecan fragment concentration in injured and non-injured rat knees compared to untreated rats. Furthermore, similar dose of AGG-523 in rats has shown 54 % bioavailability, t_{max} (0.25 - 1 hour), and $t_{1/2}$ (4.6 hours).(70) At a dose of 2 g/kg/day of AGG-523, the rats have shown normal behaviour with no toxicity during 4 weeks of treatment.(70) The first phase I clinical trial of AGG-523 (NCT00427687) on individuals with mild or moderate OA was conducted to investigate the effect of AGG-523 multiple-dose oral administration on the disease progression biomarkers and to evaluate the safety profile of AGG-523. Whereas, the second clinical trial (NCT00454298) was conducted to investigate the quantity of AGG-523 in patients' urine or knee joint, evaluate the effect of AGG-523 (1800 mg) after four weeks of administration, and study the safety of AGG-523 when administered once or twice a day for four weeks. The subjects in the second study were patients with severe OA undergoing knee replacement surgery. Unfortunately, the results of both studies and the administered dose quantity in the first study have not been revealed yet.
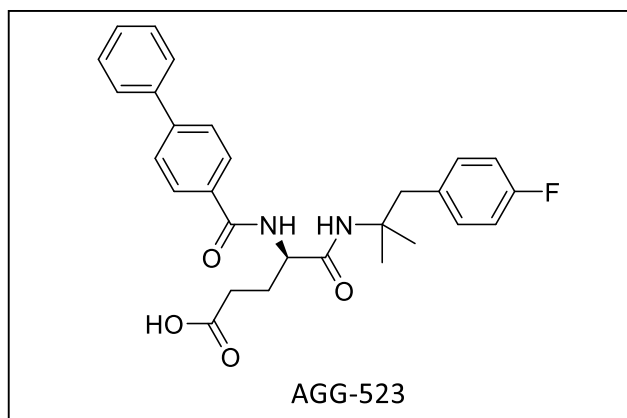
Figure 1.6: AGG-523 structure

1.1.4.1.3 **Cathepsin K inhibitors**

Cathepsin K is a cysteine protease, mainly expressed in osteoclasts, and the enzyme contributes in collagen degradation and bone resorption.(28, 71) Moreover, cathepsin K is expressed in chondrocytes, where it degrades cartilage components.(71) It has been observed that molecules that inhibit cathepsin K demonstrated a significant reduction of the OA progression biomarkers CTX-I (carboxy-terminal telepeptides of type I collagen) and CTX-II (carboxy-terminal telepeptides of type II collagen).(12) Two cathepsin K inhibitors (Figure 1.7),

odanacatib and balicatib, presented evidence of potential DMOAD by inhibiting the bone resorption biomarker CTX-I and increasing bone minerals.(28) Unfortunately, 25 mg of balicatib failed in the phase II clinical trial as it caused serious skin adverse effects such as morphea, severe skin itching, and rashes.(28, 72) In a phase II study, odanacatib (10 and 50 mg/week) showed an increase in bone minerals during 2 years of treatment.(28) However, 50 mg/day of odanacatib was terminated in phase III because of rare bone disease (atypical femoral fracture), morphea, and stroke.(73) Despite the positive results of odanacatib and balicatib against OA, both drugs have shown adverse reactions because of poor selectivity against cathepsin K.(71) Therefore, a highly selective and potent cathepsin K inhibitor was developed particularly for OA. MIV-711 (structure concealed) is a recently developed oral cathepsin K inhibitor that showed higher selectivity and potency compared to odanacatib and balicatib against cathepsin K. The drug also showed inhibition of bone degradation biomarker (CTX-I) and cartilage degradation biomarker (CTX-II).(74) A recent study (2020) reported that MIV-711 reduced OA progression with a promising safety profile during the phase II study.(75) MIV-711 at 200 mg/day has been tested on healthy individuals for 1, 10, and 28 days and demonstrated significant inhibition of serum CTX-I and urinary CTX-I and CTX-II compared to placebo.(76) Additionally, administration of MIV-711 at 100 or 200 mg/day for 6 months has shown joint structure enhancement and cartilage degradation reduction compared to placebo.(77) The drug was well tolerated during 28 days, 6 months, and 12 months of treatment and showed no sign of significant side effects compared to the placebo.(76, 77)
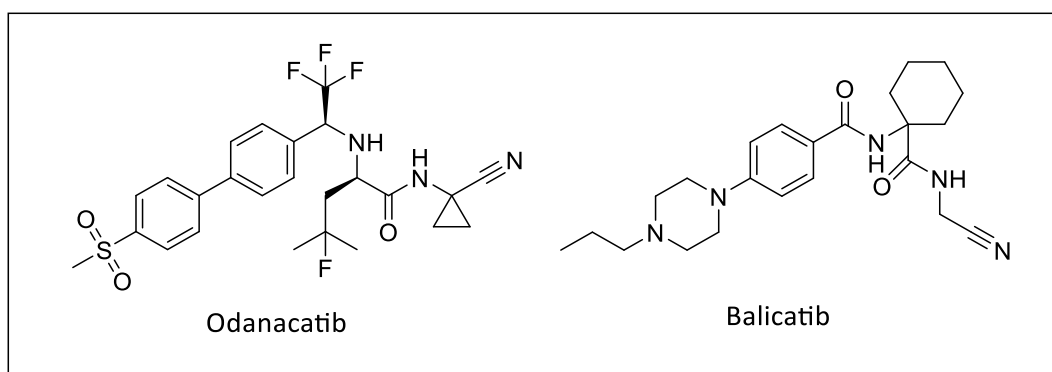
Figure 1.7: Odanacatib and balicatib structures

1.1.4.2 **Inflammatory cytokines inhibitors**

Inflammatory cytokines are significantly involved in the development of OA progression and cartilage catabolism.(13, 15) IL-1 and TNF-α are the primary inflammatory cytokines that stimulate other cytokines, prostaglandin, and nitric oxide production. Additionally, IL-1 and TNF-α are directly involved in the overexpression of MMPs and ADAMTSs.(11, 12, 14) A study on human osteoarthritic chondrocytes has reported that 10 ng/ml TNF-α significantly reduced cell viability and proteoglycan concentration compared to untreated cells.(78) Moreover, 10 ng/ml TNF-α has increased the production of IL-1β, nitric oxide, and MMPs significantly compared to untreated cells.(78) However, a combination treatment of 1 or 10 μg/ml canakinumab (IL-1β receptor blocking) with TNF-α has suppressed and neutralized the effect of TNF-α on human osteoarthritic chondrocytes.(78) A clinical trial of canakinumab (ACZ885) on patients with knee OA has shown that a single IA injection of 150, 300, or 600 mg probably has no significant effect compared to the placebo (NCT01160822). Furthermore, most of the DMOADs that have been tested against OA inflammatory cytokines were drugs prescribed for autoimmune diseases, mainly rheumatoid arthritis. Clinical trials on patients with OA knee using IL-1 and TNF antagonists were conducted. Clinical studies of the IL-1 antagonists (Anakinra, AMG-108, and ABT-981) have shown that these drugs have an acceptable safety profile, but their effect against OA progression was not significant compared to a placebo.(11, 14) The TNF antagonists, which include infliximab, adalimumab, and etanercept, were found to be ineffective against OA during the clinical studies.(13, 14, 16) Diacerein is an IL-1 inhibitor, and its exact mechanism is still under investigation. Diacerein and its active metabolite (Figure 1.8), rhein, have reduced the production of IL-1, TNF, and MMPs.(11, 79, 80) A study on patients with hip OA has reported that diacerein has significantly reduced joint space narrowing in hip OA patients compared to placebo.(81) Another study on patients with knee OA has reported improvements in OA pain, physical movement, and joint stiffness significantly compared to placebo.(82) Diacerein's safety profile and tolerability were evaluated as good to very good for patients who received 50 mg/ml and 100 mg/ml.(82) However, several subjects have reported mild to moderate diarrhoea during the clinical study of Diacerein.(81-83)
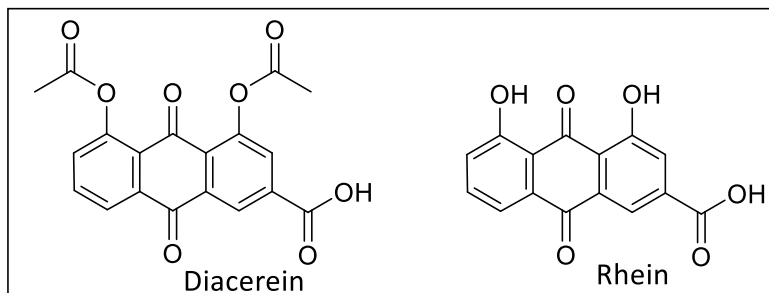
Figure 1.8: Diacerein and rhein (the active metabolite of diacerein) structures

1.1.4.3 Bone resorption

Since bone resorption is a significant OA progression factor, therapies that prevent the bone-remodelling process could be a potential treatment for OA patients. Most of the DMOADs that have been investigated against OA to inhibit osteoblast and osteoclast activity and prevent osteophyte formation are medications for osteoporosis patients or post-menopausal women at risk of bone fracture.

1.1.4.3.1 Bisphosphonates

Bisphosphonates, which are among the first line of osteoporosis treatment, can prevent bone resorption by deactivating osteoclasts and inducing osteoclast apoptosis.(84) A study on knee osteoarthritis patients has reported that 5 mg of zoledronic acid (Figure 1.9) reduces OA pain and bone marrow lesions area.(85) In addition to zoledronic acid, in patients with knee OA, risedronate (Figure 1.9) has reduced the collagen degradation biomarker CTX-II in a dose-dependent manner and significantly compared to placebo.(86) Despite the fact that zoledronic acid and risedronate have shown a potential to slow the disease progression, both have not consistently reduced OA pain and symptoms, which requires further investigation to validate the therapeutic efficacy for OA patients.(11, 12, 85-87)
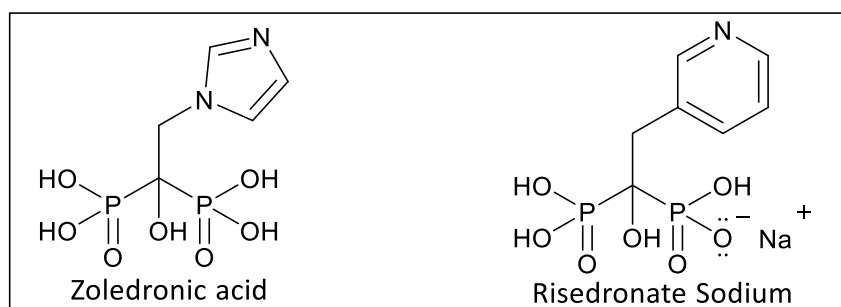
Figure 1.9: Zoledronic acid and risedronate sodium chemical structure

1.1.4.3.2 **Strontium ranelate (SrR)**

Strontium is prescribed for osteoporosis and post-menopausal women to protect them from bone fractures. Strontium ranelate (Figure 1.10) has been shown to be capable of increasing bone formation rate (88), increasing bone mineral density (89), and reducing the OA progression biomarker CTX-II.(90) An *in vitro* study has reported that SrR inhibits the expression levels of MMP-2 and MMP-9.(91) Moreover, a randomized clinical study on post-menopausal women with or without OA has stated that 2 g/day of SrR failed to reduce CTX-II level significantly compared to a placebo.(90) However, the participants were exclusively female, and they were not specifically OA patients. According to the study, the women with OA who participated had a high level of urinary CTX-II, which was reduced over time after administering 2 g/day of SrR.(90) In addition to reducing the level of CTX-II, SrR effectively alleviated OA-related pain.(90) In a phase III clinical trial, 2 g/day of SrR significantly reduced cartilage loss and bone marrow lesions compared to placebo in patients with knee OA.(92) The clinical trial included both 1 and 2 g/day SrR, however, the results have shown that the 2 g/day dose significantly reduced OA progression compared to the 1 g/day SrR and placebo groups.(92) Another study on knee OA patients has reported that 1 g/day and 2 g/day SrR have reduced joint space narrowing and urinary CTX-II significantly compared to placebo. However, the high dose of SrR has reduced OA symptoms such as pain and physical function significantly compared to a placebo.(93) The safety profile and the tolerability of SrR during the three years of study were excellent. Patients have reported common gastrointestinal disorders, whereas less than 1% of the patients have shown signs of venous thromboembolic disease. Long-term administration of SrR could lead to a significant risk of adverse reactions, for instance thromboembolism, heart attack, and allergy.(93) A recent study has mentioned the possibility of synthesizing topical SrR to be evaluated for osteoporosis treatment to enhance selectivity, reduce the dose, and reduce the risk of side effects.(89)
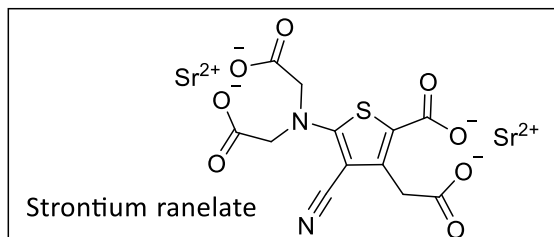
Figure 1.10: Strontium ranelate structure

1.1.4.3.3 Calcitonin

Calcitonin, which is a hormone (a 32-amino acid peptide) produced by the thyroid gland to maintain the calcium level, is used mainly to treat osteoporosis.(94) The dosage form of calcitonin was an injection or nasal spray; nowadays, calcitonin is formulated as a tablet with a carrier, 8-(N-2-hydroxy-5-chloro-benzoyl)-amino-caprylic acid (5-CNAC). The drug binds to osteoclast through calcitonin receptor changing osteoclast structure causing bone remodelling inhibition.(94) Significantly, calcitonin has shown an activity to inhibit cartilage degradation, bone resorption, and OA symptoms.(35) A phase I study on OA patients has reported that 0.6 and 0.8 mg of oral calcitonin has inhibited CTX-I and CTX-II.(95) Furthermore, a study on a small group of knee OA patients has reported that 1 mg significantly suppressed the concentration of urinary CTX-I and CTX-II and serum MMP-13 and MMP-3 after 3 months of treatment.(96) Phase III studies on knee OA patients have reported that 0.8 mg of oral calcitonin has no significant effect compared to a placebo on joint space width, and OA symptoms during two years, however, a potential to decrease CTX-I and CTX-II was observed.(97) The tolerability of calcitonin was acceptable.(95-97) Subjects who received calcitonin have shown side effects such as diarrhoea, nausea, vomiting, and headache.(95-97) Additionally, in less than 1 % of subjects, mild to moderate allergic bronchospasm induced by hypocalcaemia was observed during the treatment period.(97)

1.1.4.4 Miscellaneous

1.1.4.4.1 Glutamate receptors antagonists

There are two classes of glutamate receptors: ionotropic glutamate receptors (iGluRs) and metabotropic glutamate receptors (mGluRs).(98) Osteoarthritis studies have focused on iGluRs since mGluRs are not expressed in chondrocytes, osteoblasts, osteoclasts, or osteocytes.(99) Inotropic glutamate receptors allow ions to cross the membrane after glutamate binding.(100) Furthermore, the receptor is classified into three subclasses named after their specific ligands, AMPA (α-amino-3-hydroxy-5-methyl-4-isoxazolepropionic acid), kainate (kainic acid), and NMDA (N-methyl-d-aspartate).(98) AMPA and NMDA receptors are expressed in cartilage, bone, and synovial cells in humans.(99) Studies have reported an increase in glutamate concentration in the synovial fluid of OA patients, which can cause an increase in articular joint inflammation.(101,

102) An excessive level of glutamate increases AMPA and kainate receptor activity, which leads to the release of Interleukin-6 (IL-6).(103) An *in vitro* study on synoviocytes has reported that IL-6 expression was increased after treating the cells with exogenous glutamate.(103) Studies on the synovial fluid of patients with OA have reported that glutamate level is proportionally correlated to the level of TNF-α, IL-6, and T-cell expression and secretion.(99, 101) Therefore, the stimulation of glutamate receptors is involved in OA progression and development by increasing the release of inflammatory signalling molecules, increasing MMPs expression, and stimulating the activity of osteoclasts, osteoblasts, and macrophages. NBQX (2,3-dihydroxy-6-nitro-7-sulfamoyl-benzo[f]quinoxaline) is a competitive antagonist for AMPA and kainate receptors. NBQX (Figure 1.11) has been found to reduce both the OA symptoms and the disease progression by reducing glutamate concentration and blocking the glutamic receptor catalytic site.(103, 104) A recent study has reported that an IA injection of 2.5 mM NBQX in rats with induced knee arthritis reduced the disease progression by targeting the three significant elements in OA development, which are synovial fluid, articular cartilage, and bone.(104) In the synovial fluid, NBQX reduced synovial inflammation progression by inhibiting IL-6 release, glutamate level, glutamate receptor abundance, and knee swelling. In the cartilage, the drug reduced cartilage degradation by inhibiting MMP expression and cathepsin K.(103, 104) NBQX activity has reached the bone, reducing osteoblast activity and the accumulation of minerals, which eliminates the possibility of developing severe OA.(104) Additionally, analysing the footprints of untreated osteoarthritic rats showed abnormal gait as a result of weight bearing, whereas NBQX-treated rats re-established normal walking after one day of treatment.(104) Pre-treated rats knees with 0.25, 0.625, and 2.5 mM of NBQX reduced the pain behaviours and weight load that were induced by carrageenan.(105) AMPA antagonist has provided excellent results to be a potential OA treatment as NBQX reduces inflammatory cytokines release, reduces cartilage proteases, and inhibits bone remodelling processing. Additionally, the NMDA antagonist (MK-801 (Figure 1.11)) has inhibited the production of IL-6, IL-1β, and MMP-13 and reduced OA symptoms.(99, 106) IL-1β was proven to be involved in cartilage degradation as it increases the mRNA expression of IL-6 and MMP-13.(106) A study has reported that the release of IL-6 that was produced by GluRs stimulation after treating synoviocytes with exogenous glutamate, was inhibited by NBQX but

not MK-801.(103) Additionally, 15 hours of synoviocyte treatment with 100 µM of MK-801 increased proMMP-2 expression, while 150 µM of NBQX had no effect on proMMP-2 expression.(103) Therefore, AMPA antagonists could be a more effective therapeutic against OA than NMDA antagonists.(103) NBQX can manage glutamate receptor activity, and glutamate level, which are significant risk factors for developing inflammation, pain, and OA progression.(101, 103, 104, 106)
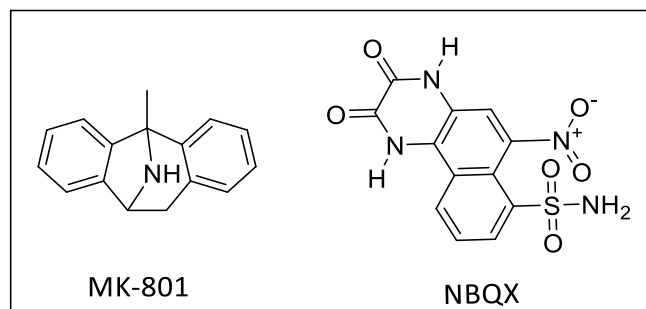
Figure 1.11: MK-801 and NBQX structures

1.1.4.4.2 **iNOS inhibitors (inducible nitric oxide synthase)**

iNOS is an enzyme that produces nitric oxide in chondrocytes and plays a role in mediating chondrocyte proliferation, inflammation, and apoptosis.(107) Most human cells require several cytokines to activate iNOS, whereas iNOS in chondrocytes can be activated by a single cytokine.(107) An elevated level of nitric oxide has been detected in the case of OA, which can enhance MMPs activity, increase cytokines production, and initiate chondrocyte apoptosis.(12, 13, 15, 107) Therefore, iNOS inhibitors could prevent or slow down the progression. Cindunistat (SD-6010) is a selective irreversible inhibitor for iNOS (Figure 1.12). An *in vivo* study of the drug has shown activity against OA, while a clinical trial showed no joint space narrowing and no inhibition of OA progression compared to a placebo after administering 50 or 200 mg of cindunistat daily.(108, 109) Cindunistat (SD-6010) is still under investigation.
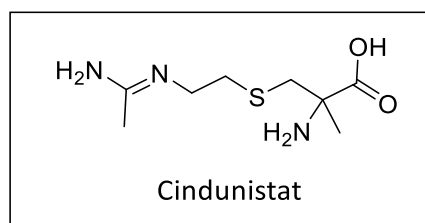
Cindunistat

Figure 1.12: Cindunistat Structure

1.1.4.4.3 **Licofelone**

Licofelone (Figure 1.13) is a dual inhibitor for 5-lipoxygenase (5-LOX) and cyclooxygenases (COX).(110) The drug has shown a well-balanced effect and potent inhibition for cyclooxygenases and 5-lipoxygenase, with 50 % inhibitory concentrations of 0.21 μM and 0.18 μM, respectively.(110) Inhibiting both COX and 5-LOX has shown improved anti-inflammation, pain alleviation, and fewer drug adverse effects compared to selective enzyme inhibitors.(110) Licofelone has shown no genotoxic potential, harm to the autonomic and central nervous systems, no effect on the cardiovascular system, and no ulceration.(111) Targeting COX selectively is the main factor in developing gastrointestinal ulceration and bronchospasm.(110) Inhibiting COX alone will shift arachidonic acid to the 5-LOX pathway, which converts arachidonic acid to leukotrienes. Leukotrienes-C4, D4, and E4 are potent bronchoconstrictors, and leukotriene-B4 is an important factor in Interleukin-1β synthesis.(111, 112) *In vitro* studies have shown that licofelone inhibits leukotriene-B4, prostaglandin E2, and IL-1β synthesis.(111-113)

Animal studies have reported that 20 and 80 mg/kg of licofelone for 26 days reduced oedema, erythema, and cartilage/bone degradation.(111, 114) Additionally, licofelone at 2.5 mg/kg for 8 weeks has reduced the activity of MMPs and collagenase, and reduced MMP-1, MMP-13, cathepsin K, ADAMTS-5 expression, and chondrocyte apoptosis.(113, 115, 116) In a clinical study on OA patients, 200 mg twice a day of licofelone showed a significant reduction in cartilage loss, a protective effect against OA, a suppression of OA symptoms, and no ulceration or bronchospasm.(112, 117) In contrast, a selective COX inhibitor, naproxen (NSAIDs), at 500 mg twice a day, has shown no effects on OA progression and ulceration.(117) In clinical studies, licofelone has been safe and tolerable, with no observed side effects during phase I study. Phase II and III studies have shown that licofelone is effective against OA progression and is able to suppress the OA symptoms. Licofelone is continuing to be investigated for OA treatment as a potential DMOAD.
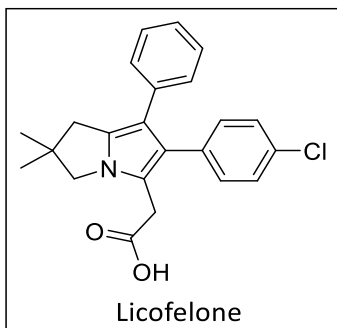
Figure 1.13: Licofelone structure

1.1.4.5 **Cartilage repair**

DMOADs primary aims are inhibiting cartilage catabolism, bone resorption, or/and inflammatory cytokine release, whereas DMOADs that target cartilage regeneration focus on increasing cartilage formation by stimulating chondrocyte proliferation and activity.

Transforming growth factor-*beta* (TGF-β) is a regulator in the process of cartilage and bone formation.(118) In the physiological condition, a high expression level of TGF-β was observed, while in the condition of OA, the expression was significantly reduced.(118, 119) Inducing TGF-β expression stimulates cartilage production, whereas blocking TGF-β shows cartilage damage and inhibits proteoglycan synthesis.(118, 120) Phase I study has investigated the activity and safety of IA injection of human recombinant bone morphogenetic protein -7 (BMP-7).(121) BMP-7 is a member of the TGF-β superfamily. The study has reported that the IA injection reduced the symptoms of OA patients with an excellent safety profile.(121) A phase II clinical trial of BMP-7 on OA patients was completed, but the results have not been posted yet (NCT01111045).

Fibroblast growth factor-18 (FGF-18) is a signalling protein that belongs to the family of fibroblast growth factor (FGF).(122) Fibroblast growth factor receptors (FGFRs) are expressed in chondrocytes and play a role in regulating cartilage anabolism and catabolism.(122) In OA animal models, IA injection of FGF-18 has shown formation of new cartilage in the lesion site, promotion of chondrocyte proliferation, and suppression of cartilage catabolism.(122-126) A study has mentioned that FGF-18 increased the expression of TIMP-1, which is an endogenous inhibitor for MMPs and ADAMSTs.(124) In OA patients, 10, 30, and 100 µg IA injection of sprifermin (recombinant human FGF- 18) have demonstrated a significant reduction in cartilage loss and joint space width narrowing compared to placebo.(127) In addition, OA symptoms were suppressed significantly in OA patients who received sprifermin compared to placebo, with no difference in adverse effects between the treated and placebo group.(127) Another study on OA patients has reported that 10, 30, and 100 µg IA sprifermin injections have enhanced the cartilage surface over time compared to the baseline.(128) However, the difference in cartilage thickness changes between treated patients and placebo patients was not statistically significant. Furthermore, a significant enhancement in bone marrow lesion was observed in treated

patients.(128) A sprifermin phase II clinical trial was done over 5 years to evaluate the effect of 30 and 100 µg in OA patients.(129) Improvements in joint space width, cartilage thickness, and cartilage volume were observed in patients who received 30 and 100 µg sprifermin. Although cartilage thickness for both 30 and 100 µg increased significantly over time, only 100 µg demonstrated a statistically significant increase in cartilage thickness compared to the placebo. At 100 µg, joint space width increased significantly over the course of treatment compared to the placebo. Comparing OA symptoms relief between sprifermin and placebo showed no statistical difference.(129) Multiple sprifermin phase II studies have reported that sprifermin can significantly enhance cartilage thickness, joint space width, and OA symptoms.(129-132)

Kartogenin (Figure 1.14) stimulates chondrogenic differentiation of mesenchymal stem cells (MSCs) and increases cartilage component reproduction.(133) Additionally, experimental observations have demonstrated that kartogenin prevents OA progression and protects cartilage from damage. A study has investigated the effects of 100 µM kartogenin IA injection in an induced OA rat model and 5 µM kartogenin in human chondrocytes.(134) In an OA rat model, kartogenin has improved OA symptoms, reduced CTX-II level, reduced MMP-13 and -3 expression, reduced inflammatory cytokine expression (IL-6, IL-1β, and α-TNF), increased TIMP-3 expression, increased the anti-inflammatory cytokine expression of IL-10, and inhibited osteoclastogenesis significantly compared to non-treated rats.(134) In the human chondrocyte, a significantly higher expression of IL-10, TIMP-1, and TIMP-3 was observed in kartogenin-treated cells compared to untreated cells.(134) However, kartogenin is a hydrophobic compound with limited water solubility, which makes the application of kartogenin as an OA therapeutic challenging.(14, 133) KA-34 is an analogue of kartogenin with enhanced potency, chemical stability, and safety profile. In an OA rat model, KA-34 has a protective effect against cartilage degradation and inhibits OA progression development.(135) Additionally, KA-34 has suppressed the level of CTX-II and increased the level of the cartilage regeneration biomarker PIIANP (serum N-propeptide of collagen IIA).(135) In both OA models, KA-34 showed an excellent safety profile with no adverse effects.(135) In 2021, the phase I clinical trial of KA-34 on knee OA patients was completed, but the results have not been revealed yet (NCT03133676).
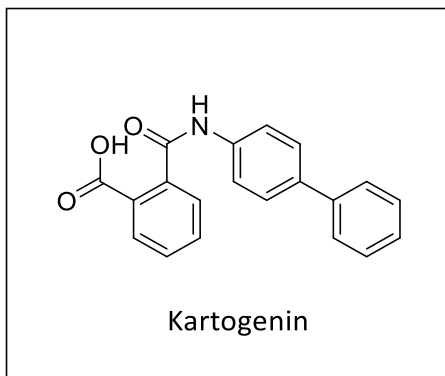
Kartogenin

Figure 1.14: Kartogenin chemical structure

1.1.4.5.1 **Lorecivivint (SM04690 or Adavivint)**

Lorecivivint (Figure 1.15) has shown a potential to slow OA progression and increase cartilage production by inhibiting the Wnt pathway.(136) The Wnt pathway is upregulated in OA and involved in increasing cartilage degradation enzymes and inflammatory cytokines production. Additionally, the Wnt pathway plays a role in chondrocytogenesis, chondrocyte activity, and tissue remodelling. Lorecivivint is a small molecule that has induced chondrocytogenesis in human mesenchymal stem cells (MSCs).(136) Furthermore, an experimental study on chondrocyte has shown that the drug has reduced MMPs expression (MMP-1, MMP-3, and MMP-13) and inflammatory cytokine production (IL-1, IL-6, and α-TNF).(136) In an OA rat model, IA injection of 0.3 μg lorecivivint significantly suppressed the expression of inflammatory cytokines and cartilage degradation enzymes (MMP-13 and ADAMTS-5) compared to non-treated OA rats. Moreover, non-treated rats showed cartilage surface loss while cartilage surface protection and OA symptom relief were observed in treated rats.(136) The safety and tolerability of three lorecivivint concentrations (0.03, 0.07, and 0.23 mg) were investigated in the phase I clinical study.(137) Moreover, the efficacy and tolerability of lorecivivint were evaluated in the phase II study. In phase II, lorecivivint-treated OA patients have shown pain and function improvement compared to placebo, but the comparison was not statistically significant at 13 weeks.(138) At 0.07 mg, lorecivivint has shown continued OA symptom improvement after 13 weeks to week 52, and the improvement was statistically significant compared to placebo.(138) In the phase IIb clinical trial, 0.07 mg has met the primary endpoint of the clinical study by showing 30 % and 50 % statistically significant improvements in

the patient symptoms reported by the questioners at 12 and 24 weeks, respectively, compared to placebo.(139) The clinical trials reported that lorecivivint was well tolerated.(137-139) Long-term phase II (NCT03706521 and NCT03727022) and phase III (NCT03928184, NCT04385303, and NCT04520607) clinical trials started recently to evaluate the efficacy and safety of 0.07 mg lorecivivint in OA patients. The results of these clinical trials are not available yet.
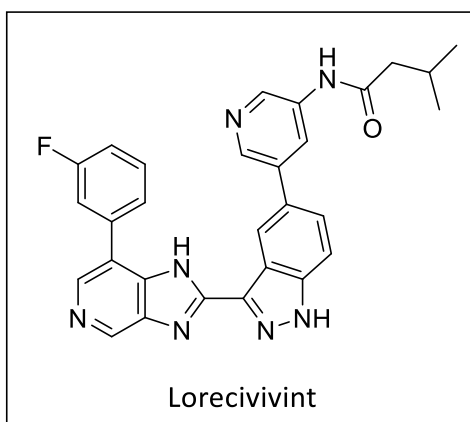
Figure 1.15: Lorecivivint chemical structure

1.1.5 **The reason of ineffective DMOADs in clinical trails**

Disease-modifying osteoarthritis drugs are designed and developed to reduce the progression of OA.(11-16) However, none of the DMOADs have been approved as a treatment for OA because of insignificant clinical results against the disease or drug adverse effects.(11-16, 140) Understanding the structure of the articular joint and the physiological processes within the joint (1.1.1), assists in reasoning DMOADs failure clinically. The first obstacle is that passive diffusion through the cartilage network is the only transportation pathway since the cartilage is avascular, alymphatic, and aneural.(25) Therefore, DMOADs have to cross through the cartilage network, which acts as a biological barrier and limits drugs from reaching their therapeutic targets because of the dense cartilage components.(17, 18) In addition to the condensed cartilage aspect, the hydrophilicity and the anionic nature of the cartilage repel the lipophilic DMOADs, which will reduce drug penetration and quantity inside the cartilage. Furthermore, after IA injection in the synovial fluid, the drug would be drained and washed away from the articular joint capsule to the systemic circulation as a result of the physiological turnover of the synovial fluid.(17, 18, 33, 34) Regarding this, a study has reported that the joint half-lives of NSAIDs, dexamethasone, and methotrexate after IA injection were 1 to 2, 3.60, and 2.90 hours, respectively.(3) Therefore, the quantity of DMOADs reaching the therapeutic target is low, and the risk of systemic adverse effects is high.(17, 18) Clinically, DMOADs have a short residence time inside the joint space, a limited access to their therapeutic target, and a limited penetration through the condensed cartilage network.(18, 33, 34) Therefore, researchers have been focusing on increasing the drug residence time within the synovial joint capsule and penetration through the cartilage by applying drug delivery system technology to OA therapeutics.(3, 17-20, 141, 142)

1.1.6 Drug delivery systems for OA therapeutics

The development of DMOADs delivery systems should be an essential priority for these therapeutics in order to overcome the biological delivery challenges in the treatment of OA.(17, 18). Generally, a suitable delivery system should be biocompatible, hydrolysable, and able to extend DMOADs duration time within the joint.(17, 18) Additionally, the size of the delivery system should be around 60 nm for drugs that target chondrocytes and bone cells so it can infiltrate through the cartilage pore size of 60-200 nm.(17, 140) The surface charge of the delivery system plays a significant role in crossing through the cartilage network mesh.(140, 143) A study on neutral and positive avidin has reported that positive avidin penetrated bovine cartilage much deeper and quicker than neutral avidin.(140) The positive charge would be electrostatically attracted to the anionic cartilage components, assisting avidin to penetrate the cartilage.(140) Furthermore, the method of loading a drug onto a carrier can affect the efficiency of the delivery system. Physically loading drugs onto the carrier has shown a low residence time of the drug within the carrier.(18) One way to solve this drawback is by conjugating the drug to the carrier via a covalent hydrolysable chemical bond.(18) A hydrolysable covalent conjugation of diclofenac to hyaluronic acid (HA) has demonstrated an extended time within the synovial fluid and reduced the concentration of diclofenac in the plasma compared to physically mixed diclofenac with HA.(144) Some DMOADs that target inflammatory cytokine release within the synovial fluid could stay within the synovia without the need to penetrate the cartilage.(17, 18). The strategic method is designing a system that prevents DMOADs from being washed away from the joint space into the systemic circulation through venules and lymphatic vessels.(17) For instance, encapsulating corticosteroid in PLGA microparticle sized 10 – 100 μm has minimized drug drainage through venules and lymphatic vessels and reduced corticosteroid plasma concentration.(145) Overall, the delivery system should extend DMOADs resident time within the joint and assist therapeutics in penetrating the cartilage network. Therefore, the DMOAD delivery system will enhance OA therapeutic activity and reduce drug toxicity. Multiple drug delivery systems have been investigated recently for OA therapeutic.(18-20, 141, 142) Studies have focused on designing a drug delivery system for current OA therapeutics such as natural compounds, NSAIDs, and steroids. However, as stated previously, these medications can only suppress OA symptoms, not

slow the progression (1.1.3). Therefore, designing and evaluating delivery systems for DMOADs is needed.

1.1.6.1 **The delivery system for current OA therapeutics (FDA approved or in clinical trials)**

Recently, researchers have been investigating design approaches to increase current OA therapeutic activity and reduce adverse effects.(18-20, 141, 142) Hydrogel, polymeric microparticles, and liposomes are the delivery strategies that have reached clinical trials. Four delivery system approaches are in the late stages of clinical trials as potential therapeutics for OA treatment, whereas FX006 is the only food and drug administration in the U.S. (FDA)-approved OA treatment and Cingal is approved in Canada and the European Union.

1.1.6.1.1 **Hydrogels**

Hydrogels are water-swollen hydrophilic natural or synthetic polymer network. Hydrogels can fill the joint space and mimic the cartilage components as a lubricant agent.(20, 141, 142) Hyaluronic acid (HA) is the most appealing hydrogel because HA is a native extracellular matrix compound. An additional advantage of HA (viscosupplementation) is that it is approved by the FDA and is being used clinically as an OA therapeutic. However, HA major limitation as a delivery system is the lack of physical and chemical mechanisms to stay within the joint space. Also, the effect of HA on pain relief is still controversial.(20, 141, 142)

Cingal is a cross-linked hyaluronic acid gel loaded with triamcinolone hexacetonide (TH) (0.204 mg TH/ mg HA). A clinical trial and phase III study have been conducted to evaluate IA injection of cingal that contains 18 mg TH and 88 mg HA in 4 ml saline.(146, 147) The formulation effect on knee OA patients was compared to HA alone and saline (placebo). A single IA injection of cingal has reduced OA pain significantly compared to HA alone for up to 3 weeks. However, throughout the trial period of 24 weeks, cingal and HA alone have demonstrated similar improvements in OA symptoms, but both treated groups have reported a significant OA pain relief during the 24 weeks compared to placebo. Additionally, a higher percent of symptom improvement was reported by cingal-treated patients.(147) The formulation of loading TH with HA has produced rapid improvement of OA symptoms starting from week one and long-lasting relief of OA pain throughout the 24 weeks.(146, 147) Two clinical trials are being conducted, the

first trial to evaluate the therapeutic efficacy of cingal on patients with hip OA (NCT04084704) and the other to compare the effects of cingal, triamcinolone hexacetonide, and HA on patients with knee OA (NCT04231318). Cingal has been approved by Canada and the European Union as an OA medication.(148)

SI-613 is diclofenac covalently conjugated to HA via a 2-aminoethanol linker (the formulation contains 11.8 % diclofenac w/w).(144) A preclinical study on an OA rat model has investigated the effect and pharmacokinetics of SI-613 in comparison with HA, a non-covalent mixture of HA with diclofenac, oral diclofenac, and phosphate buffered saline.(144) SI-613 has significantly suppressed OA symptoms compared to control groups. The formulation has shown to prolong the anti-inflammatory effect by reducing prostaglandin concentration for three days after injection, while control groups have shown no statistically significant difference compared to non-treated OA rats. Moreover, SI-613 has decreased the joint swelling significantly since day 1 of injection compared to control groups and has maintained the decrease in swelling until day 28. The pharmacokinetic study of SI-613 has shown that the plasm concentration of diclofenac was 462 times lower than the oral diclofenac and 94 times lower than the IA injection of diclofenac with HA mixture. Additionally, after a single IA injection of 5 mg of SI-613, the diclofenac has remained in the synovial fluid for 28 days with a half-life of 10.7 days.(144) In clinical studies, the IA injection preparation of SI-613 was 30 mg of SI-613 in 3 ml of citric acid-sodium citrate buffered, and the formulation was injected every 4 weeks. (149, 150) A phase II study has evaluated the efficacy and safety of multiple IA injections of SI-613, which has shown pain score improvement compared to placebo and the drug was well tolerated with no serious side effects.(149) Moreover, the phase III clinical trial has shown that SI-613 has suppressed OA symptoms significantly compared to placebo.(150) In the one-year follow-up phase III study, SI-613 has reduced OA pain since the first injection and maintained the analgesic effect until week 52.(151) Preclinical studies and clinical trials have stated that diclofenac-HA conjugate has a rapid onset of action with a prolonged analgesic effect.(144, 149, 150)

1.1.6.1.2 Polymeric microparticle

Microparticles could be natural, synthetic, or a combination of both types of polymers. The formation size of microparticles could range from 1 – 100 µm and spherical is the common

shape of microparticles.(19, 20, 142) Polymeric microparticles have shown an increase in drug retention time within the joint through different mechanisms depending on the particle size.(20, 142) For instance, 10 - 100 µm particles can penetrate the cartilage mesh, and less than 10 µm particles could be phagocytosed by the superficial cartilage cells. Furthermore, relatively large microparticles can resist washing-away through lymphatic and vascular vessels.(142) A study has found that encapsulating a drug inside bioengineered material that is larger than venules and lymphatic vessels significantly reduces the likelihood of the drug being washed away with the synovial fluid.(17) The advantages of microparticles are the sustained release of the drug and the relatively high residence time within the joint. The major limitation of microparticles is that the quantity of loaded drug is relatively low, and the long residence time in the joint could stimulate a foreign body response.(19, 20, 142)

FX006 (triamcinolone acetonide encapsulated in PLGA) is an intra-articular extended-release dosage form of triamcinolone acetonide.(152) Studies stated that encapsulated corticosteroid (triamcinolone acetonide) in PLGA (poly lactide-co-glycolic acid) microspheres can prolong triamcinolone acetonide time within the joint space.(33, 145, 153) In a rat model study, FX006 (0.28 mg triamcinolone acetonide) showed 10-fold less plasma concentration of triamcinolone acetonide compared to triamcinolone acetonide alone because the extended release of the drug limited its clearance to the systemic circulation.(145) Moreover, the PLGA microspheres size range is 20 -100 µm with a median size of 42 µm, which should be big enough to limit the clearance of FX006 via the venules and lymphatic vessels to the systemic circulation.(17, 145) In addition, FX006 has shown a more sustained efficacy and pain relief with significant improvement in joint structure in a rat model compared to triamcinolone acetonide alone.(145) In a phase II study on OA patients, a comparison of triamcinolone acetonide concentration in synovial fluid and the plasma between FX006 and the medication alone was observed. The formulation has shown a significantly extended time of triamcinolone acetonide within the joint space (3590.0 pg/ml in week 6) compared to the drug alone (7.7 pg/ml in week 6).(153) Moreover, FX006 has demonstrated a crucially low concentration of triamcinolone acetonide in plasma (966.7 pg/ml) compared to the control (11,064.7 pg/ml).(153) The extended time of triamcinolone acetonide within the joint capsule and its limited appearance in the

systemic circulation result in an increase in drug efficacy and reduce the risk of systemic side effects.(33, 152) Studies on osteoarthritic patients have reported that the OA patients who received FX006 have less average daily pain, an improvement in physical activity, and an improvement in stiffness.(33, 34) In 2017, intra-articular injection of FX006 (Zilretta™) was accepted by the FDA as a medicine for OA patients.(154)

Furthermore, EP-104IAR is a fluticasone propionate coated with polyvinyl acetate (PVA), which is a recently developed microparticle delivery system with a particle size range of 60 - 150 µm.(142) In a preclinical study, EP-104IAR maintained a long residence time of fluticasone propionate, which was 60 days.(155) Additionally, EP-104IAR has shown low plasma concentration of the drug. At 0.6 mg of EP-104IAR, the plasma concentration of fluticasone propionate was undetectable, while at 12 mg, the plasma concentration was detectable for up to 7 days with a maximum concentration of 300 pg/ml.(155) EP-104IAR was well tolerated in the animal models. A phase I clinical trial to evaluate EP-104IAR safety and pharmacokinetic was completed, but the results have not been posted yet (NCT02609126). Moreover, phase II is recruiting knee OA patients to study EP-104IAR efficacy, pharmacokinetic, and safety (NCT04120402).

1.1.6.1.3 Liposomes

Liposomes are phospholipid vesicles with a wide range of sizes, and the drug could be loaded in the hydrophilic core or lipophilic membrane depending on the drug's chemical properties (Figure 1.16).(19, 20, 141, 142) The advantage of liposomes is the slow release of the drug and their action as a lubricant for the joint. A clinical study on knee OA patients has shown that MM-II (liposomes) can reduce OA pain better, faster, and for a longer period of time than HA (hydrogel).(156) Additionally, liposomes have a relatively high drug-loaded capacity and the ability to extend the release of hydrophilic and hydrophobic agents.(19, 20, 141, 142)

TLC599 is dexamethasone (a corticosteroid) loaded in a liposomal formulation. A study on healthy rabbits and dogs has demonstrated that IA injection of TLC599 has no toxicity toward chondrocytes and cartilage.(157) Fifteen days after TLC599 IA injection, dexamethasone was detectable in the synovial fluid.(157) Another preclinical study on healthy dogs has evaluated the

pharmacokinetic and safety of a single or multiple IA injections of the liposomal formulation.(158) TLC599 IA injection every 13 weeks has shown no accumulation of dexamethasone in the plasma and prolongation of dexamethasone presence in the synovial fluid for 15 days. Additionally, dexamethasone was detectable in the synovial fluid for 120 days after a single IA injection of TLC-599.(158) Multiple and single IA injections were well tolerated by animal models.(157, 158) A phase IIa clinical study has investigated the efficacy and safety of 12 and 18 mg of single IA injection in knee OA patients for 24 weeks.(159) At 12 mg, the OA pain and symptoms were significantly reduced and maintained throughout the 24 weeks compared to placebo, whereas at 18 mg, there was no statistically significant difference. At both doses, TLC-599 was safe and tolerable.(159) A phase III clinical trial to evaluate the efficacy of two TLC-599 doses and a clinical trial to study the pharmacokinetic of TLC-599 were completed, but the results have not been published yet (NCT04123561 and NCT03754049, respectively).
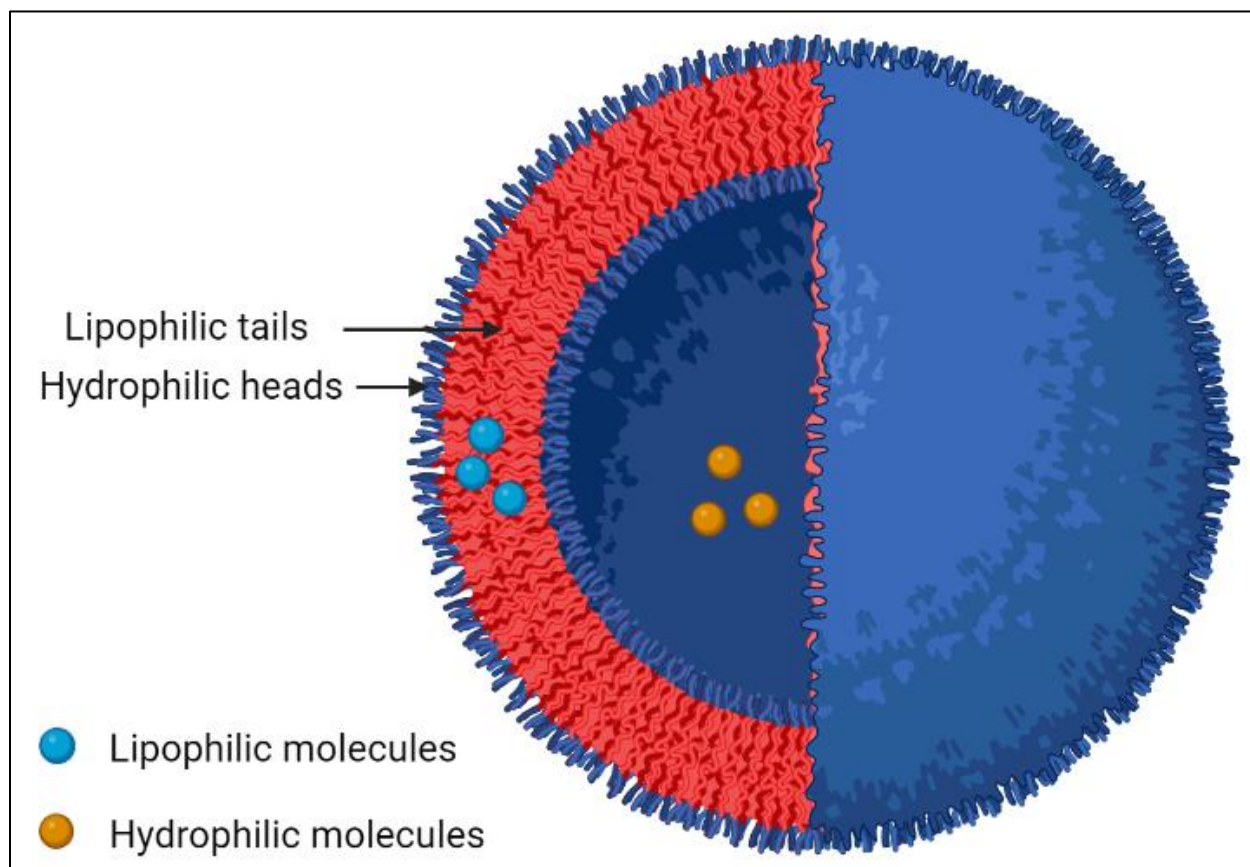
Figure 1.16: Liposome based drug delivery system

The figure created with BioRender.com.

1.1.6.2 **Examples of delivery system for DMOADs**

The majority of OA therapeutics combined with delivery systems that are in late stages of clinical trials or approved as a medication for the disease target the symptoms but not the progression. In contrast, the published studies on DMOAD's delivery systems, which are fewer than those performed on current medication (symptom relief), are in the early stages of preclinical studies. However, OA is a chronic disease that involves cartilage degradation and morphological changes in the bones, leading to joint replacement surgery even when the patient follows the prescribed medications. Therefore, focusing on developing a delivery system for DMOADs, which can prevent OA progression, should be prioritized in order to assist DMOADs be significantly effective clinically with a low risk of side effects. The primary reasons for applying a delivery system for DMOADs are to increase their retention time within the joint and limit their wash-away to the systemic circulation. Once these objectives are achieved, the therapeutic effectiveness will be enhanced while the dosage, toxicity, and systemic adverse effects of the drug will be decreased. Potentially, OA progression, OA symptoms, and OA patients' quality of life would be improved.

1.1.6.2.1 **Delivery systems of kartogenin**

There are delivery systems that are designed to extend DMOADs residence time within the synovial fluid by formulating sustained release drugs. For instance, kartogenin is a potential DMOAD that inhibits inflammatory cytokines, suppresses cartilage degradation proteases, increases chondreogensis, and increases cartilage production.(133, 134) Multiple delivery systems have been associated with kartogenin to enhance the drug water solubility for IA injection formulation and to increase the retention time within the joint.(160-165) A study has conjugated kartogenin with chitosan via a covalent hydrolysable amide bond, and the conjugate was formulated as a nanoparticle and microparticle by ionic gelation with tripolyphosphate.(160) An *in vitro* release study has shown a sustained release of kartogenin from both partial formulations.(160) At day 50, the nanoparticles released about 35 % of kartogenin, while 55 % of the drug was released from the microparticle.(160) In an OA rat model, the delivery systems of kartogenin have produced an improved OA therapeutic effect compared to control groups.

Significantly, both particle sizes have shown 24 days of residence time within the joint with no statistical difference between the formulations.(160)

Furthermore, a dual drug delivery system using pluronic® F127 and chitosan carrying kartogenin and diclofenac was developed.(161) Kartogenin was conjugated to chitosan via an amide bond, and the conjugate was covalently bonded to pluronic F127. After that, diclofenac was loaded into the core of the carrier, and the delivery system showed an independent and simultaneous release profile for each drug. Kartogenin showed a sustained release, whereas diclofenac showed an immediate release profile. In cold temperatures, the release of kartogenin was enhanced, but it maintained a sustained release profile over 14 days, whereas a rapid release of diclofenac within 12 hours was observed.(161) The purpose of this dual drug delivery system is that the diclofenac reduces OA pain and symptoms immediately, and then the kartogenin can act on OA progression. In addition, the release of diclofenac would depend on the exposure temperature.(161)

A poster illustration has reported an additional kartogenin hydrogel formulation that was prepared by conjugating kartogenin to polyethylene glycol (PEG) and then HA covalently via an ester bond.(162) In an OA rat model, HA-PEG-kartogenin hydrogel significantly suppressed the progression of OA compared to the control groups, and kartogenin has demonstrated a sustained release over 5 days.(162) The fourth formulation for kartogenin's delivery system was prepared by conjugating the drug to a polyurethane nanoparticle via an amide bond.(163) The formulation has shown an *in vitro* controlled release of kartogenin over 30 days, and the maximum percent of kartogenin released was about 20 %. In an OA rat model, a statistically significant inhibition of OA progression and cartilage protective activity was observed in the treated group compared to the control groups. Unfortunately, the pharmacokinetic of the kartogenin delivery system was not investigated. However, the cartilage protective activity of the nanoparticle formulation was maintained over 12 weeks, which could indicate a long retention time of kartogenin within the joint.(163)

Fifthly, the efficacy and the pharmacokinetic of a sustained release microparticle formulation of kartogenin with PLA (poly lactic acid) were investigated.(164) An *in vitro*

37

experiment on the cumulative kartogenin release has shown an extended release profile of the drug over 90 days. In a mouse OA model, the effect of the microparticle formulation against OA progression was significantly superior to kartogenin alone. After the IA injection, the delivery system has remained within the mouse's knee for 56 days.(164) In 2019, a formulation of kartogenin sustained release from a thermogel triblock copolymer carrier (PLGA-PEG-PLGA) after IA injection was developed.(165) The kartogenin thermogel formulation, which contains 50 μg kartogenin in 10 ml of the carrier, was investigated in a rabbit OA model. The *in vitro* release study has shown a sustained release of kartogenin from the thermogel formulation, releasing 20 % at day 1, followed by about 3 % per day, and reaching 95 % at day 20.(165) Additionally, the sustained released drug from the thermogel has shown an OA therapeutic effect by increasing collagen type II and GAG production and inhibiting MMP-13 production.(165) The studies of kartogenin delivery systems have prolonged the retention time of kartogenin within the joints, enhanced the therapeutic effect against OA, and solved the water solubility limitation of kartogenin.(160-165)

1.1.6.2.2 Delivery systems for diacerein and rhein

In addition to kartogenin, diacerein with chitosan microparticles was formulated, and since the drug has limited water solubility, diacerein dispersed in sodium carboxy methylcellulose was used as a control.(166) The *in vitro* release study revealed that 100 % of the diacerein was released from the microparticle formulation in 16 hours versus 4 hours for the control. In rats, a single oral dose of diacerein microparticles increased the maximum plasma concentration and the concentration of rhein (the active metabolite of diacerein) in the synovial fluid by more than two times and enhanced cartilage formation compared to the control.(166) Furthermore, IA injection of rhein loaded in PLGA microparticles was developed to enhance the drug's water solubility, therapeutic effect, and retention time.(167) The *in vitro* release study has shown a control release of rhein in which 45 % of rhein was released within the first day and a slow release was maintained over 30 days.(167) Additionally, the anti-inflammatory effect of the formulated drug was significantly higher compared to PLAG alone. Unfortunately, the study did not include rhein alone as a control, which could be related to the poor water solubility of rhein.(167)

1.1.6.2.3 Delivery system for the peptide (KAFAK)

Furthermore, a delivery system for DMOADs has been developed for the purpose of protection against endogenous enzymatic degradation. The anti-inflammatory peptide KAFAK (KAFAKLAARLYRKALARQLGVAA) has shown activity against OA by inhibiting α-TNF and IL-6 upregulation, with a major limitation of hydrolysis by blood and synovial proteases.(168, 169) Therefore, the KAFAK was loaded into NGPEGSS nanoparticles to prevent the degradation.(168) NGPEGSS refers to PEGylated conjugated to poly (N-isopropylacrylamide-2-acrylamido-2-methyl-1-propanesulfonate) via a breakable disulfide bond using (N,N'-bis(acryloyl)cystamine). The major advantage of NGPEGSS is that the breakdown of the nanoparticles occurs intracellularly by glutathione reductase, which protects the peptide from blood and synovial proteases. At a pH 7.4 solution, the release of KAFAK from NGPEGSS nanoparticles was constant over 3 days, while adding DTT (dithiothreitol) to the nanoparticles formulation has shown a sustained release profile of KAFAK over 3 days.(168) A follow-up study has reported that the KAFAK nanoparticle formulation has penetrated the cartilage and the chondrocyte.(169) Moreover, the peptide formulation has shown a therapeutic effect by inhibiting IL-6 production significantly, and the inhibition has improved over time.(169)

The formulation of DMOADs with a suitable delivery system is still under extensive investigation, and most of the developed systems are in the preclinical stage. The aforementioned drug delivery systems were found to enhance the DMOADs retention time within the joint and the therapeutic effect, whereby controlling the drug release from the formulation was the primary mechanism. Furthermore, the delivery systems have assisted in overcoming some of the drug limitations, such as drug water solubility and endogenous enzymatic degradation. However, the majority of these formulations featured no mechanical mechanism allowing for retention within the joint space. In contrast, cationic delivery systems have been attracting researchers due to the electrostatic interaction ability between the negatively charged cartilage components and the positively charged delivery system, which provides a mechanical mechanism for retention.(170-173)

1.1.6.2.4 Cationic drug delivery system for DMOAD

The electrostatic attraction of cationic delivery systems toward cartilage components would provide a mechanical attachment to the cartilage superficial area or allow the system to penetrate the cartilage and reach deeper therapeutic targets.(170-173) Comparing the uptake and retention time of a neutral versus cationic delivery system has shown that the cationic system penetrates the cartilage deeper and has a longer retention time than the neutral system.(140) The Bajpayee group has focused on using avidin as a delivery system for OA therapeutics, which is a positively charged glycosylated protein with an approximated dimension of 7 nm.(140) The first study investigated the cartilage depth penetration of different particle materials with different dimensions ranging from 0.9 to 15 nm. The results have shown that ≤ 5 nm particles penetrated the full cartilage thickness (1 mm) within 24 hours, while 10 nm particles gradually penetrated the full cartilage thickness within 96 hours. However, the 15 nm particle was too large to cross through the cartilage pore and was detected on the cartilage superficial area. In trypsin-treated cartilage, 15 nm was able to penetrate the full cartilage thickness within 24 hours, which could be related to the GAG depletion and cartilage pore size expansion.(140) In addition, a cartilage depth penetration comparison between avidin and neutralized avidin was observed.(140) Neutralized avidin has penetrated only half of the cartilage thickness in 96 hours, whereas avidin has diffused through the full cartilage thickness in 24 hours, with 400 times higher in quantity. The retention study has shown that 96 % of avidin remained inside the cartilage for 15 days, while 50 % of neutralized avidin diffused out during day 1.(140) A follow-up study has investigated the IA injection of avidin in rats, which showed no knee swelling or stiffness during the experimental period (7 days).(173) Moreover, the study has reported that avidin concentration has been reduced over 7 days in a time-dependent manner, starting from 5 µg/mg of joint tissue after 6 hours of injection to 0.13 µg/mg at day 7. In contrast, neutralized avidin was not detectable after 24 hours of injection. Different concentrations of avidin up to 100 µM showed no significant cell toxicity or GAG loss compared to untreated cells. However, there was a 7 % numerical difference in the percentage GAG loss between 100 µM avidin and the control group.(173)

In 2016, the Bajpayee group conjugated dexamethasone covalently via ester or hydrazone to PEGylated avidin.(172) The ester bond is for the fast release, while the pH-sensitive hydrazone bond is for the sustained release of dexamethasone. At pH 7.4, the ester-linked conjugate has released 50 % of dexamethasone in 12 hours, while the hydrazone-linked conjugate has released only 30 % of dexamethasone over 13 days. Owing to the hydrazone bond not being fully hydrolysed at pH 7.4, a cumulative release study was carried out at pH 4, where about 80 % of the drug was released within 6 days, achieving a half-life of 57 hours. At 100 µM, the avidin-dexamethasone conjugate has shown no cell toxicity compared to non-treated cells. Avidin-dexamethasone ester linked conjugate has reduced the % GAG loss induced by IL-1 significantly compared to dexamethasone alone, whereas no significant protective activity against IL-1 was observed with avidin-dexamethasone hydrazone linked.(172) The following study by the Bajpayee group has investigated the therapeutic effect of an IA injection of a 1:1 mixture solution of avidin-dexamethasone conjugates in rabbits.(174) The effect of the conjugates mixture against OA progression was significantly superior to dexamethasone alone, with a prolonged effect over 3 weeks. Avidin has proven to be a potential delivery system for OA therapeutics by diffusing through the cartilage mesh network and enhancing the therapeutic effect of dexamethasone. However, GAG loss was observed with 20 mg of avidin, which was used in the experimental study to deliver 100 µM of dexamethasone. Additionally, avidin has only 4 binding sites for biotinylated PEG, so the drug-loaded quantity is limited.(140, 174) In order to increase the loading quantity, a multi-arm avidin (m-AV) was developed, which contains 28 binding sites for the therapeutic.(175) Avidin and m-AV have exhibited comparable profiles in terms of penetration of the full cartilage thickness within 24 hours and retention time inside the cartilage.(175) Additionally, the m-AV design reduces the quantity of avidin that is required to transport a therapeutically effective dose of dexamethasone.(175, 176) In 2020, the Bajpayee group tested the therapeutic activity of m-AV-dexamethasone conjugate on bovine cartilage upon OA induction by IL-1. The conjugate was found to significantly inhibit GAG loss, nitrite release, and cell death in comparison to dexamethasone alone.(176)

In addition to avidin, positively charged peptides have been investigated for DMOADs delivery system application. According to a study on a range of positively charged cell penetration

peptides, the quantity and retention time of these peptides inside the cartilage increased in a concentration-dependent manner.(171) However, positive 16 and higher charged peptides have shown low cartilage uptake quantity because of their high binding affinity toward the cartilage components, which hindered the penetration. Additionally, 100 % of the peptides that showed a charge of +14 or higher were retained inside the cartilage for 7 days, and then 40 to 60 % of the peptides remained inside even after blocking the electrostatic interaction between the positively charged cell penetration peptides and the negatively charged cartilage components.(171) Furthermore, positive 8 charged peptide has diffused through the full cartilage thickness (500 µm) at 4 hours, while +14 and +16 crossed about 250 µm and +20 stack on the cartilage surface.(171) Therefore, the positive charge of the delivery systems should be accurately maintained because stronger electrostatic interaction will hinder the carrier diffusion.(171) In contrast, a low positively charged peptide has shown low retention time within the cartilage.(170, 171) The safety profile is a disadvantage that needs to be considered regarding the positive cell penetration peptide.(170) For instance, at 30 µM amphipathic peptide (KLALKLALKALKAALKLA-amide) has shown cell toxicity by collapsing the cell membrane. The collapsing-cell membrane has been associated with the condensed positively charged peptides, while the distribution of the positively charged amino acids has shown a safer profile on the cell membrane.(170)

Considering the previous studies on drug delivery systems, the dimension, the charge, the charge distribution, and the drug loading quantity of the delivery system should be considered in selecting a suitable delivery system for OA therapeutics. Poly *beta*-amino ester polymers (PBAE) are cationic polymers with structure diversity, which give them the ability to maintain their dimension, charge distribution, and degree, as well as drug loading quantity.

1.1.6.2.4.1 Poly *beta*-amino ester (PBAE) polymers

PBAE are positively charged polymers that provide a mechanical attachment to the cartilage through electrostatic interaction, unlike PLGA, PEG, and HA.(20, 141, 142) Additionally, the advantages of PBAE over other cationic polymers (such as poly-lysine, polyethylene imine, and poly-amidoamine) are their excellent biocompatibility and biodegradability, as well as their structural diversity, which allows the fine-tuning of their properties (Figure 1.17).(143, 177-180)

Figure 1.17 also illustrates the backbone of the polymers, which consists of ester groups and tertiary amines. These two functional groups are responsible for the biodegradability of the polymer as well as the polymer positive charge in the physiological condition.(180, 181) The ester groups are degradable in aqueous solutions with a half-life of hours.(179, 180)
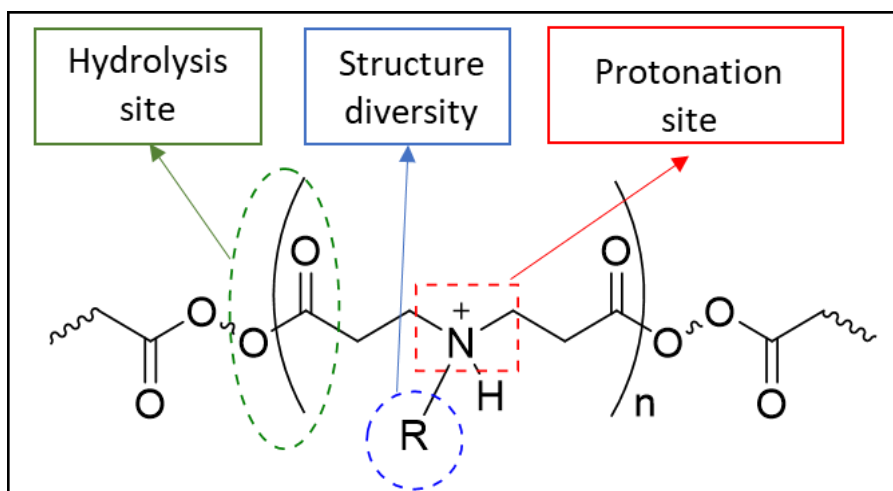
Figure 1.17: General structure of PBAE

The polymer structure, dimension, positive charge degree, charge distribution, and conjugation sites can be controlled based on the monomers selection.(143, 177-180) Therefore, the PBAE can solve other drug delivery system limitations, such as the drug loading capacity on the carrier, which was observed with avidin.(140, 174) Significantly, the positive charge of PBAE could be distributed alongside the backbone of the polymer to prevent collapsing cell membrane toxicity, which was observed with positively charged peptides.(170) Furthermore, PBAE structures could be linear, branched, or complex based on the reaction site on the acrylate and amino groups.(181) For example, diacrylate with bifunctional amines forms a linear PBAE, whereas multi-acrylates with multi-amines form a branched or complex structure of PBAE (Figure 1.18).(181) According to a study by the Bajpayee group on a range of avidin with different sizes, a smaller delivery system has a faster diffusion into deeper cartilage zone.(140) Therefore, the linear PBAE is preferred over the branched and complex PBAE structures to allow easier and faster diffusion through the cartilage mesh network. The linear PBAE is a cationic library of polymers that are synthesised from bifunctional amines and diacrylate esters (Figure 1.18).(179, 180) Regarding the biocompatibility, 10 to 100 µg of multiple PBAE polymers have shown 100 %

cell viability compared to untreated cells.(180-182) Additionally, the metabolite products of the polymers, which are the anticipated alcohol of the diacrylate and the anticipated bis(*beta*-amino acids) of the amino, have no effect on the cell viability compared to the control (Figure 1.18).(180) Moreover, the cytotoxicity studies of PBAE polymers on fibroblasts and human lung adenocarcinoma cells have shown no toxicity.(178, 180, 182) The primary approach to finding PBAE polymer was to develop a biocompatible and hydrolysable non-viral gene delivery system.(179, 180) Researchers have adapted the polymers as a delivery system for anticancer medications (such as paclitaxel and doxorubicin),(177, 183) DNA genes,(179, 180) and osteoarthritis medications (dexamethasone).(143) Conveniently, the building blocks of PBAE are commercially available. Moreover, from the perspective of their commercial applications these polymers are not expensive to prepare.(143, 177-180). The polymer synthesis is a one-step reaction with no side products and does not require the use of a coupling agent or protection group for monomers before the polymerization.(143, 177-180) Based on these findings, PBAE polymers were preferred over other delivery systems in the current study to investigate their influence on DMOAD residence time within the cartilage.
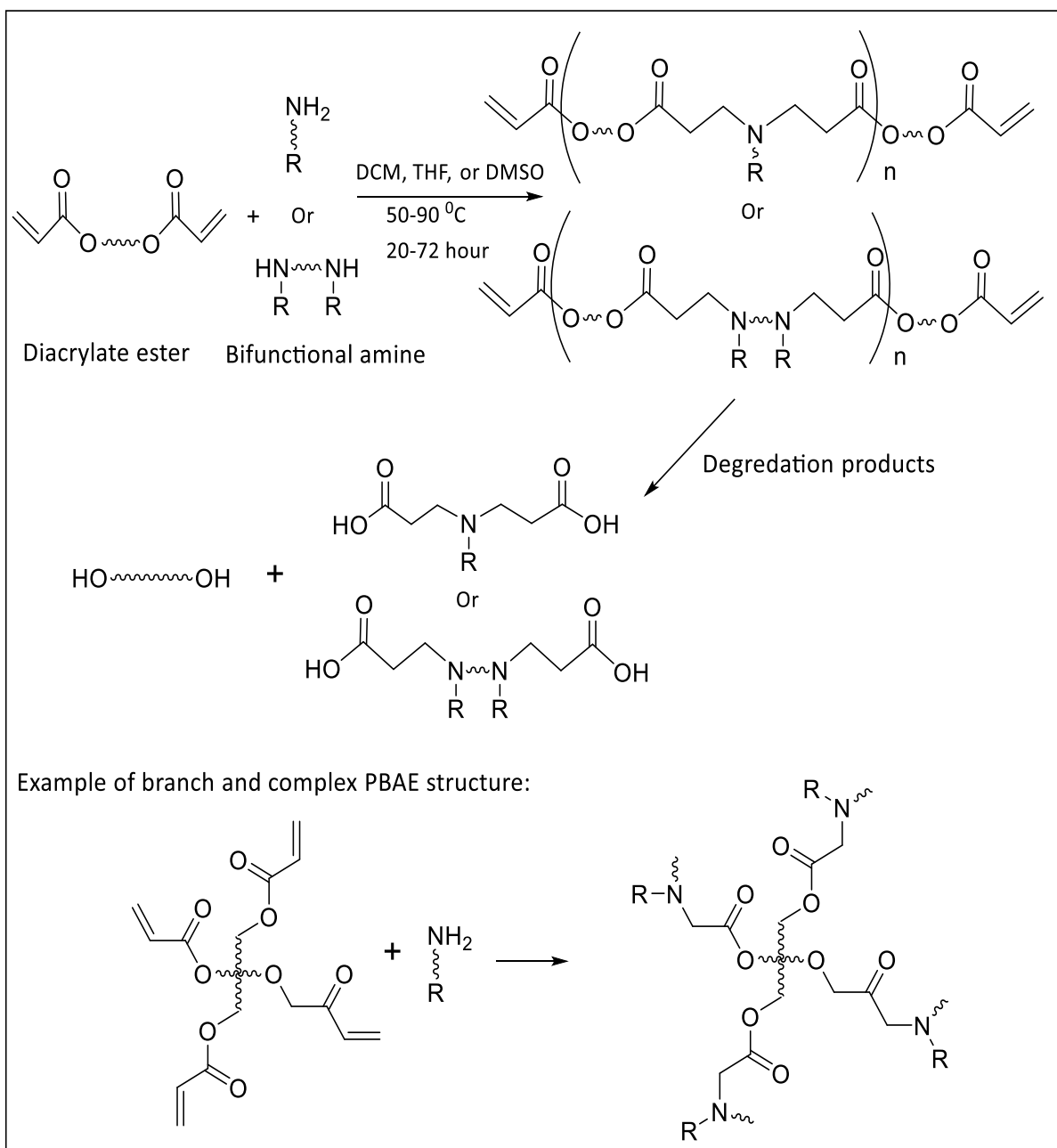
Figure 1.18: The formation of PBAE polymers, and the degradation products according to literature (143, 177-181)

1.2 Hypothesis

The conjugation of PBAE with DMOAD via a covalent hydrolysable bond will produce a positively charged PBAE-DMOAD conjugate, which will be attracted to the negatively charged cartilage component (proteoglycans) by electrostatic interaction (Figure 1.19). This attraction assists DMOADs in overcoming the biological barrier of anionic cartilage, as the positively charged PBAE polymer will mask the lipophilic characteristic of the therapeutic, allowing the penetration of DMOAD inside the cartilage, increasing DMOAD uptake quantity and retention time within the cartilage, and potentially enhancing DOMAD therapeutic activity. The successful application of PBAE as a delivery system, by enhancing the uptake quantity and retention time of the conjugated DMOAD, could similarly be adapted for DMOADs that have failed clinical trials due to poor therapeutic efficacy or side effects caused by high doses.
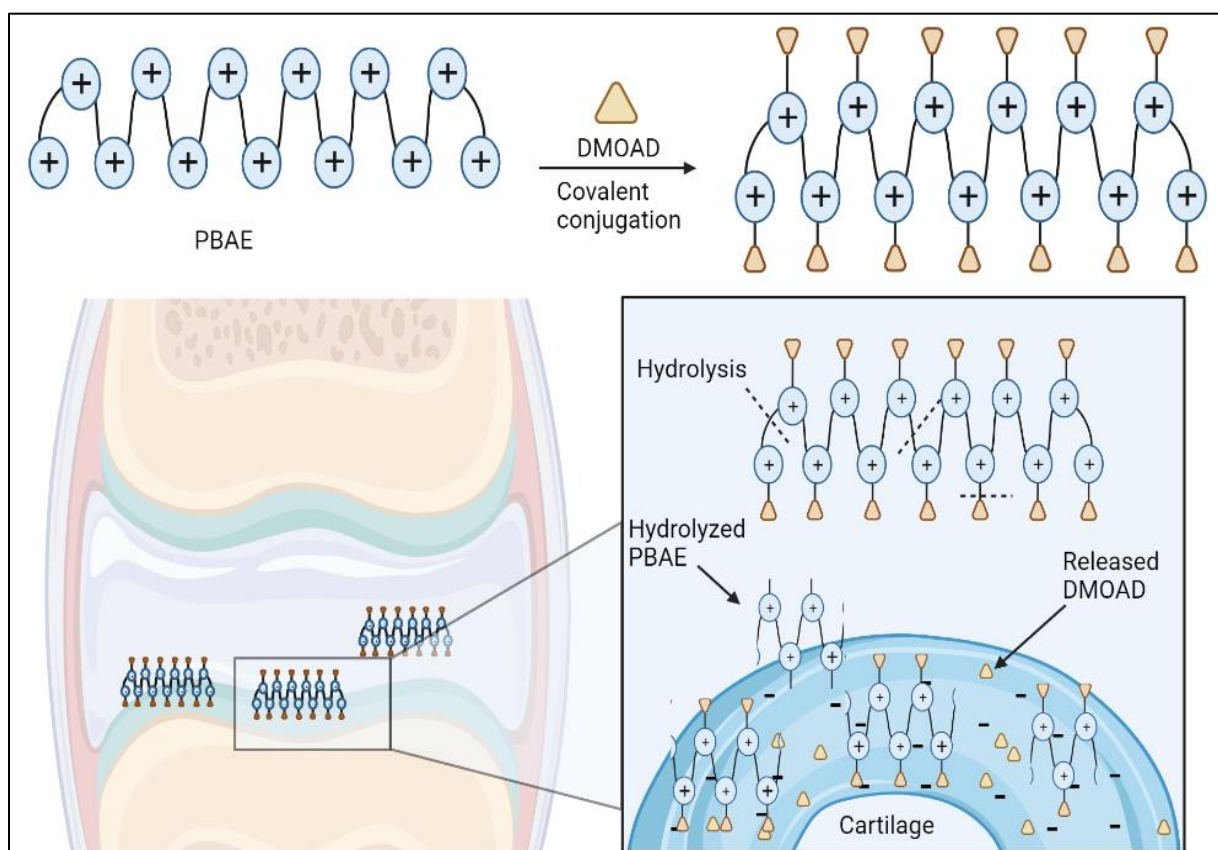
Figure 1.19: Proposed mechanism for the electrostatic interaction of a PBAE-DMOAD conjugate with the cartilage components

The figure created with BioRender.com.

1.3 Aims of the project

The aim of this study is to enhance DMOADs uptake and retention time inside the synovial joint through various routes of conjugation to a library of positively charged PBAE without affecting their cytocompatibility. As a model drug for DMOADs, NBQX and licofelone have been chosen for the study, and their therapeutic values are mentioned in (1.1.4.4.1) and (1.1.4.4.3), respectively. In the third chapter (3.1), the rationale for NBQX and licofelone selection will be discussed in detail. Furthermore, the study aims to investigate the effect of the degree of the positive charge and the quantity of conjugated drug on the uptake and retention time of DMOAD, which will be achieved by conjugating licofelone to three PBAE polymers with different physiochemical properties. Finally, a chondrocyte viability study for the PBAE-licofelone conjugate system will be observed.

1.4 Objectives
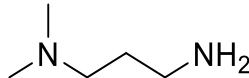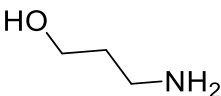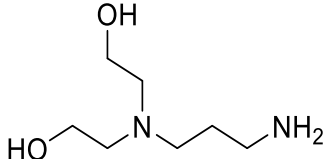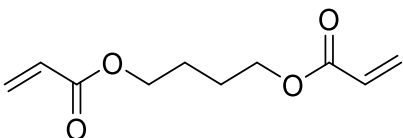
The major objective of the thesis is to develop a conjugation methodology between PBAE and DMOAD-models, and then study the uptake and retention time of these polymer-drug conjugates inside the cartilage. The experimental work is divided into four major chapters: 1) Poly *beta*-amino esters synthesis and characterization, 2) licofelone and NBQX conjugation reactions to PBAE polymers, 3) the development of RP-HPLC quantification methods for NBQX and licofelone for the release, uptake, and retention studies and an *ex vivo* early simulated osteoarthritic cartilage model, and 4) the uptake and retention time studies in healthy and OA cartilage models. The first chapter will include the synthesis and characterization of a range of PBAE polymers. Additionally, the polymers behaviour at physiological pH 7.4 as well as at inflammation pH 5 will be studied. In the second chapter, the chosen PBAE polymers based on conjugation sites and positive charge will be covalently conjugated to NBQX or licofelone, followed by the characterization of these conjugated systems. The third chapter will include the quantification methods for NBQX and licofelone using reverse phase high-performance liquid chromatography (RP-HPLC) in order to determine the quantity of the drug within the cartilage and the conjugate. Additionally, an *ex vivo* bovine cartilage model for early simulated OA cartilage was developed by treating the cartilage with trypsin solution. The last chapter will report the PBAE-DMOAD conjugates uptake and retention time studies in healthy cartilage and early simulated OA cartilage. Moreover, the most efficient PBAE-DMOAD conjugate will be evaluated for its cytotoxicity in chondrocytes.

Chapter 2: **Poly *beta*-Amino Ester Synthesis and Characterization**

2.1 **Introduction**

The linear PBAE polymers were selected over other drug carriers for multiple reasons, which were mentioned previously in (1.1.6.2.4.1). A study has reported the synthesis of over 2000 linear PBAE polymers with unique characteristics.(179) The PBAE polymers will be identified by an alphanumerical code such as **A5**, **A16**, and **A87**, where each letter represents the diacrylate and the number represents the amine (Table 2.1).(143, 179, 181, 184) For example, **A5** polymer consists of the letter **A,** which stands for the diacrylate part of the polymer 1,4 butanediol diacrylate and the number **5,** which stands for the amine part of the polymer 3-dimethylamino-1-propylamine.(143, 184) However, the alphanumerical codes could vary based on the studies library arrangement.(143, 179, 181, 184) Table 2.1 shows the names, structures, and number or letter codes of monomers that have been used in the current study.

Table 2.1: The PBAE monomers name, structure, and alphanumerical code

The amine monomer	**5**	**16**	**87**
	3-dimethylamino-1-propylamine	3-amino-1-propanol	N-(3-aminopropyl)diethanolamine

The acrylate monomer	**A**
	1,4-butandiol diacrylate

These monomers were chosen to avoid limitations, toxicity, and undesirable properties observed in previous OA drug delivery system studies, such as large size, highly positively charged, low water solubility, or condensed positive charged carriers.(140, 170, 172, 174) The structural diversity of the monomers allows controlling the positivity charge degree and distribution, the length and the molecular size of the polymer, and the amount of loaded drug.(143, 177-181, 185) For instance, **A** (1,4 butanediol diacrylate) was preferred to provide a distance between the positively charged amines and distribute the positive charge alongside the polymers (**A5**, **A16**, and **A87**), which will prevent cell membrane collapsing toxicity caused by a condensed positive charge carrier.(170) Additionally, the amines 3-dimethylamino-1-propylamine (**5**), 3-amino-1-propanol (**16**), and N-(3-aminopropyl)diethanolamine (**87**) were preferred to investigate the influence of the positive charge degree and the amount of the conjugation sites on the uptake and retention time of NBQX or licofelone within the cartilage after conjugation (Figure 2.1). The diacrylate **A** is polymerized with the amines **5**, **16**, or **87** to form three diversely characteristic polymers (**A5**, **A16**, and **A87,** respectively) (Figure 2.1). **A5** has been selected as the first PBAE to be investigated for their ability to enhance dexamethasone uptake.(143) **A16** and **A87** have been chosen based on the number of the tertiary amines and the quantity of potential conjugation sites (Figure 2.1). For example, amino-terminated **A5** has two conjugation sites but multiple amino groups, while **A16** has multiple conjugation sites but a lower number of amino groups. In contrast, amino-terminated **A87** has multiple conjugation sites and multiple amino groups.
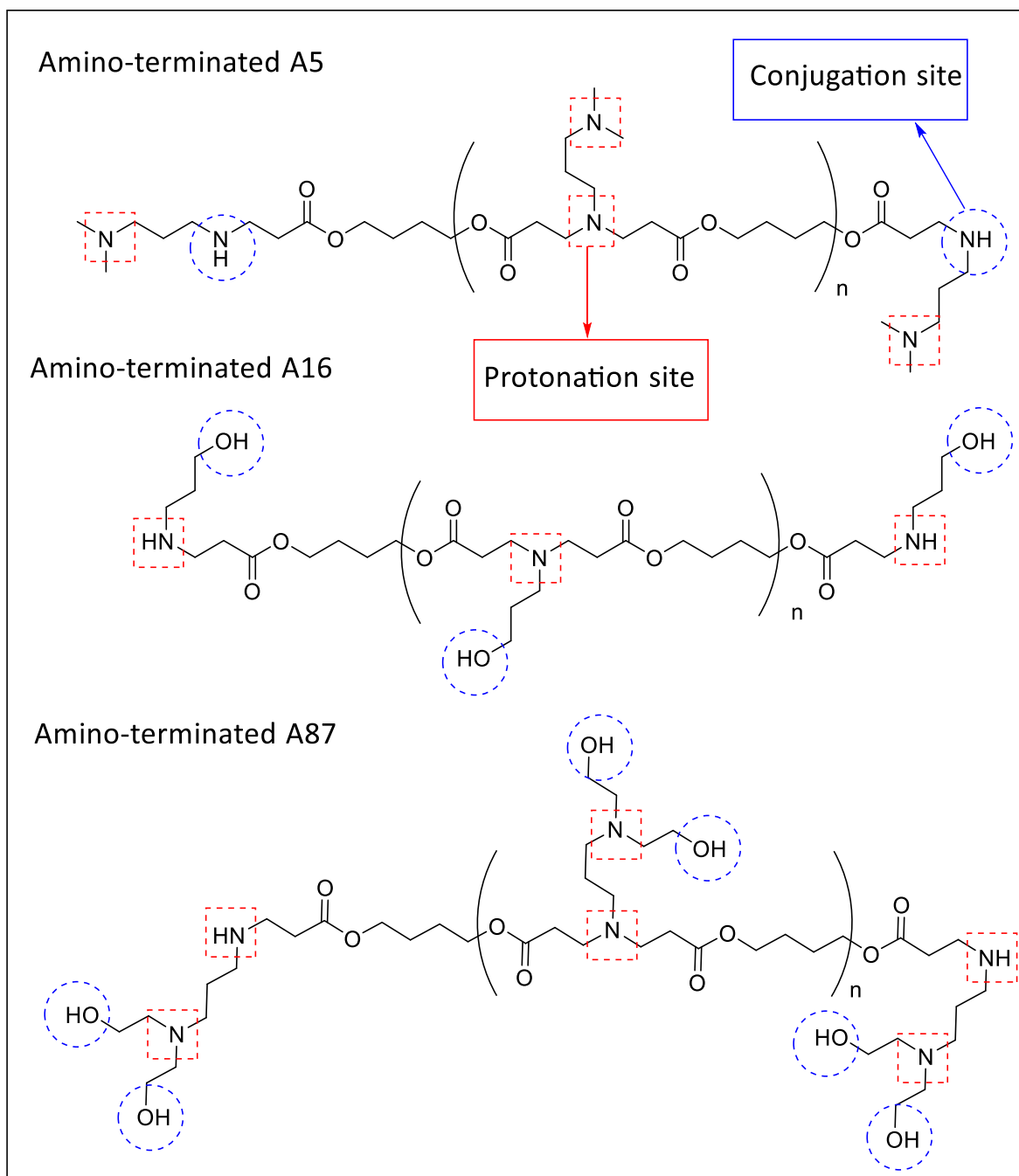
Figure 2.1: The chemical structure of amino-terminated **A5**, **A16**, and **A87**

In the literature, several reaction conditions are reported for the synthesis of PBAE.(143, 179-182, 186, 187) In general, all reactions involve a single step consisting in mixing the amine with the diacrylate solution at 50 - 90 °C for 20 - 72 hours, which was reported previously in Figure 1.18.(143, 179-182, 187) Additionally, multiple reaction solvents such as dimethylsulfoxide (DMSO) (179), tetrahydrofuran (THF) (180), chloroform (188), and dichloromethane (DCM) (143)

have been used as reaction media for the polymerization of PBAE. In this thesis, we have chosen DCM since it has proven to produce the highest product yield.(180) The reaction product was recovered by adding an anti-solvent such as diethyl ether or hexane, which reduced the solubility of the polymer and led to PBAE precipitation. The product of the reaction could be either acrylate-terminated PBAE or amino-terminated PBAE, which can be controlled by adjusting the monomers ratio. For example, combining 1.1 equivalents of the amine with 1 equivalent of the diacrylate forms an amino-terminated PBAE, and vice versa. The reaction condition for polymerization that will be followed in the current study is dissolving the monomers in DCM and then placing them in an oil bath 50 °C for 48 hours (Figure 2.2).(143, 180, 185, 186) Furthermore, the reaction mechanism of linear PBAE polymer synthesis takes advantage of the Michael-addition of the nucleophilic amino monomer to the acrylate double bond (Figure 2.2).(179-181, 186) In this chapter, the synthesis and characterization of amino-terminated **A5**, **A16**, and **A87** will be investigated.
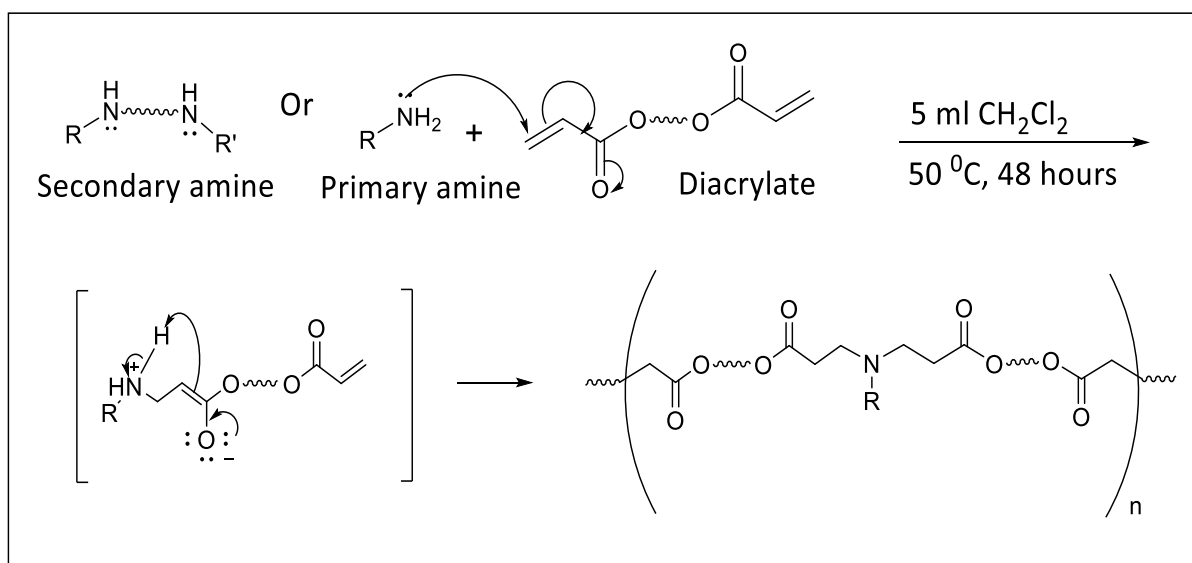
Figure 2.2: The synthesis mechanism of poly *beta*-amino ester polymers (179-181, 186)

2.2 Materials and methods

The polymer monomers 3-dimethylamino-1-propylamine, 3-amino-1-propanol, and 1,4 butanediol diacrylate were purchased from Sigma-Aldrich, while, N-(3-aminopropyl)diethanolamine was purchased from Fluorochem Limited. The solvents diethyl ether, hexane, and DCM were purchased from Fisher Scientific. Phosphate buffered saline (PBS) tablets and acetic acid were purchased from Fisher Scientific. Sodium acetate trihydrate was purchased from Honeywell. Deuterated dimethyl sulfoxide (DMSO- d6) was purchased from Sigma-Aldrich. Polyethylene glycol standards were purchased from Sigma-Aldrich.

2.2.1 PBAE polymers synthesis

Table 2.2 summarises the reaction condition of the polymerization and the quantity of the monomers that are involved in the synthesis of acrylate or amino-terminated **A5**, **A16**, and **A87**.(143, 180, 185, 186)

Table 2.2: The reactants quantity and the reaction condtion of **A5**, **A16**, and **A87** polymer synthesis

PBAE polymer	Amine	Diacrylate	Solvent	Temp. (°C)/Time	Anti-solvent
A5	553.7 µl	754 µl	5 ml DCM	50 °C / 48 hour	Diethyl ether or Hexane
A16	336.5 µl				
A87	667 µl				
Acrylate-terminated A5	503 µl	830 µl			
Acrylate -terminated A16	306 µl				
Acrylate-terminated A87	606.5 µl				

2.2.1.1 **Synthesis of A5**

Acrylate-terminated **A5** synthesis was achieved by reacting an excess of 1,4-butanediol diacrylate (1.1 equivalents, 830 μl) with 503 μl of 3-dimethylamino-1-propylamine in 5 ml of DCM in a cupped glass test tube with magnetic stirring for 48 hours in a 50℃ oil bath (Figure 2.3). After 48 hours, the acrylate-terminated **A5** polymer was precipitated by adding 50 ml of diethyl ether. Then, the tube containing the supernatant and the precipitated product was centrifuged for 5 minutes at 1500 rpm. After removing the supernatant, the product was washed with 30 ml of diethyl ether, and then the supernatant was removed; this step was repeated three times, and the remaining diethyl ether or DCM was evaporated using the rotary evaporator. The solvents were removed via rotary evaporation, followed by air-drying for 48 - 72 hours. Amino-terminated **A5** was synthesised following the same reaction procedure utilised for the acrylate-terminated **A5** this time, with an excess (1.1:1) of the amine monomer. Therefore, 553.7 μl 3-dimethylamino-1-propylamine and 754 μl 1,4-butanediol diacrylate were dissolved in 5 ml of DCM, and the mixture was stirred for 48 hours at a 50 ℃ (Figure 2.3). After 48 hours, the product was precipitated with either diethyl ether or hexane to determine which anti-solvent yields more product, which will be effective in collecting the conjugation products in the next chapter. In the acrylate-terminated **A5**, C**H₂**=C**H**- 6.3 ppm (2H, d, J= 17.10 Hz), 6.1 ppm (2H, dd, J= 10.45, 10.45, 17.10 Hz), and 5.9 ppm (2H, d, J= 10.45 Hz), 4.0 ppm (8H, br, -COO-C**H₂**-), 3.1 ppm (6H, br, -N-C**H₃**), 2.6-2.7 ppm (4H, br, -N-C**H₂**-CH₂-COO-), 2.3-2.5 ppm (6H, br, -OOC-C**H₂**- and -N-C**H₂**-), 1.7-1.8 ppm (2H, br, -N-CH₂C**H₂**CH₂-N-), and 1.6 ppm (8H, br, -OCH₂-C**H₂**C**H₂**-CH₂O-). In the amino-terminated **A5**, 4.0 ppm (8H, br, -COO-C**H₂**-), 3.1 ppm (18H, br, -N-C**H₃**), 2.6-2.7 ppm (8H, t, J=6.52, 6.52, 12.05 Hz, -N-C**H₂**-CH₂-COO-), 2.39-2.48 ppm (14H, m, -OOC-C**H₂**-and -N-C**H₂**-), 1.7-1.8 ppm (6H, br, -N-CH₂C**H₂**-CH₂-N-), and 1.6 ppm (8H, br, -OCH₂-C**H₂**C**H₂**-CH₂O-).
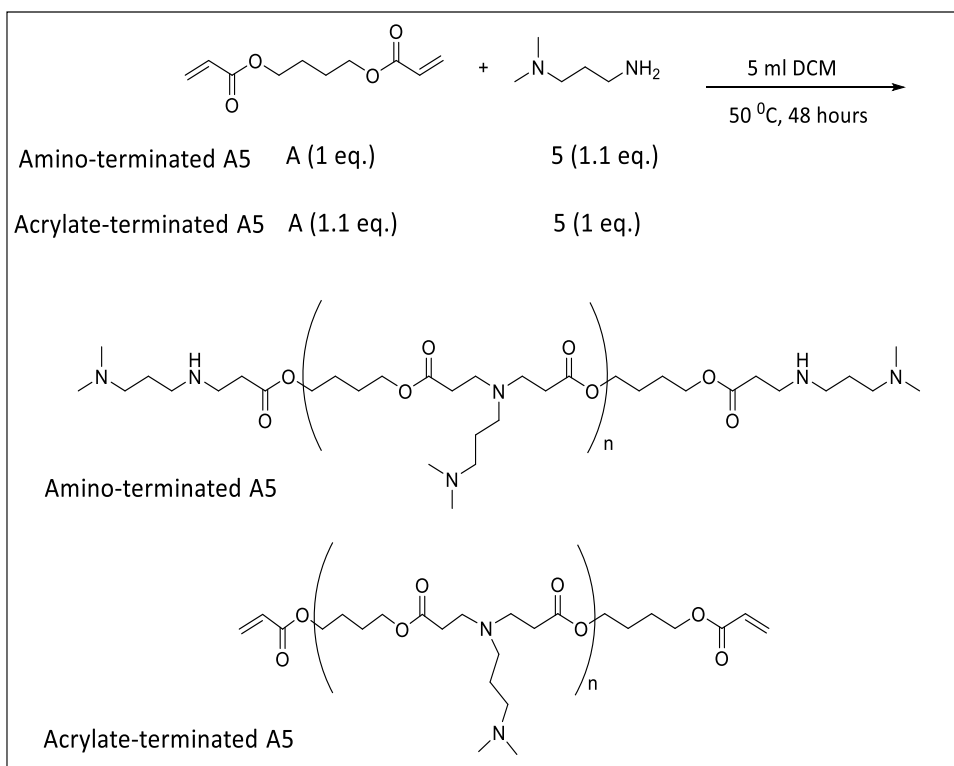
Figure 2.3: The synthesis of amino and acrylate-terminated **A5**

2.2.1.2 **Synthesis of A16**

The **A16** polymer was synthesised following the polymerization procedures of **A5**. However, in the formation of the amino-terminated **A16**, 754 µl of 1,4-butandiol diacrylate was added to 336.5 µl of 3-amino-1-propanol, while for the acrylate-terminated **A16**, 830 µl of 1,4-butandiol diacrylate is added to 306 µl of 3-amino-1-propanol (Figure 2.4). The mixture of the amine and the diacrylate monomers were dissolved in 5 ml of DCM, and then the cupped glass test tube was kept in a 50 ℃ oil bath for 48 hours with magnetic stirring. The products were obtained using either diethyl ether or hexane. In the acrylate-terminated **A16**, CH_2=C**H**- 6.3 ppm (2H, d, J= 17.73 Hz), 6.1 ppm (2H, dd, J= 10.36, 10.36, 17.73 Hz), and 5.9 ppm (2H, d, J= 10.36 Hz), 4.0 ppm (8H, br, -COO-C**H$_2$**-), 3.3 ppm (2H, m, -N-CH$_2$CH$_2$-C**H$_2$**-OH), 2.63-2.66 ppm (4H, t, J=6.93, 6.93, 13.87 Hz, -N-C**H$_2$**-CH$_2$-COO-), 2.42-2.35 ppm (6H, m, -OOC-C**H$_2$**- and -N-C**H$_2$**-), 1.6 ppm (8H, br, -OCH$_2$-C**H$_2$CH$_2$**-CH$_2$O-), and 1.51-1.45 ppm (2H, m, -N-CH$_2$C**H$_2$**-CH$_2$-OH). In the amino terminated **A16**, 4.0 ppm (8H, br, -COO-C**H$_2$**-), 3.47-3.35 ppm (6H, m, -N-CH$_2$CH$_2$-C**H$_2$**-OH), 2.6-2.7 ppm (8H, t, J= 6.84, 6.84, 13.68 Hz, -N-C**H$_2$**-CH$_2$-COO-), 2.42-2.35 ppm (14H, m, -OOC-C**H$_2$**- and -N-C**H$_2$**-), 1.6 ppm (8H, br, -OCH$_2$-C**H$_2$CH$_2$**-CH$_2$O-), and 1.51-1.45 ppm(6H, m, -N-CH$_2$C**H$_2$**-CH$_2$-OH).
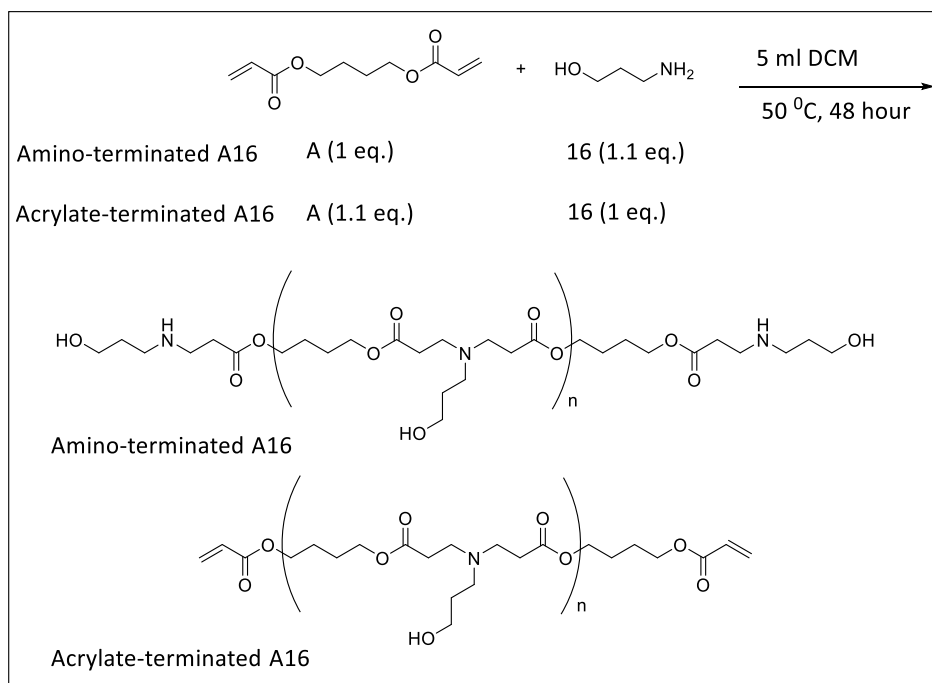
Figure 2.4: The synthesis of amino and acrylate-terminated **A16**

2.2.1.3 Synthesis of A87

The synthesis of amino- or acrylate-terminated **A87** was proceeded by maintaining its monomers ratio of 1.1:1 in favour of the desired product (Figure 2.5). In amino-terminated **A87**, 667 µl N-(3-Aminopropyl) diethanolamine and 754 µl of 1,4-butandiol diacrylate were dissolved in 5 ml of DCM. However, 830 µl of 1,4-butandiol diacrylate was added to 606.5 µl of N-(3-aminopropyl) diethanolamine in order to obtain the acrylate-terminated **A87**. The polymerization of amino and acrylate-terminated **A87** were carried out in a similar reaction condition and procedures that was discussed in **A5** synthesis. Moreover, the product was precipitated by adding 50 ml of diethyl ether or hexane to the reaction solution. In the acrylate-terminated **A87**, CH$_2$=CH- 6.3 ppm (2H, d, J= 17.65 Hz), 6.1 ppm (2H, dd, J= 10.23, 10.23, 17.65 Hz), and 5.9 ppm (2H, d, J= 10.23 Hz), 4.0 ppm (8H, br, -COO-CH$_2$-), 3.44-3.37 ppm (2H, m, -N-CH$_2$-CH$_2$-OH), 2.6-2.7 ppm (4H, t, J= 6.76, 6.76, 13.52 Hz, -N-CH$_2$-CH$_2$-COO-), 2.43-2.33 ppm (6H, m, -OOC-CH$_2$- and -N-CH$_2$), 1.6 ppm (8H, br, -OCH$_2$-CH$_2$CH$_2$-CH$_2$O-), 1.48-1.41 ppm (2H, m, -N-CH$_2$CH$_2$-CH$_2$-N-). In amino terminated **A87**, 4.0 ppm (8H, br, -COO-CH$_2$-), 3.3 ppm (6H, br, -N-CH$_2$-CH$_2$-OH), 2.65 ppm (8H, br, -N-CH$_2$-CH$_2$-COO-), 2.45-2.33 ppm (14H, d, -OOC-CH$_2$- and -N-CH$_2$-), 1.6 ppm (8H, br, -OCH$_2$-CH$_2$CH$_2$-CH$_2$O-), 1.45 ppm (6H, br, -N-CH$_2$CH$_2$-CH$_2$-N-).
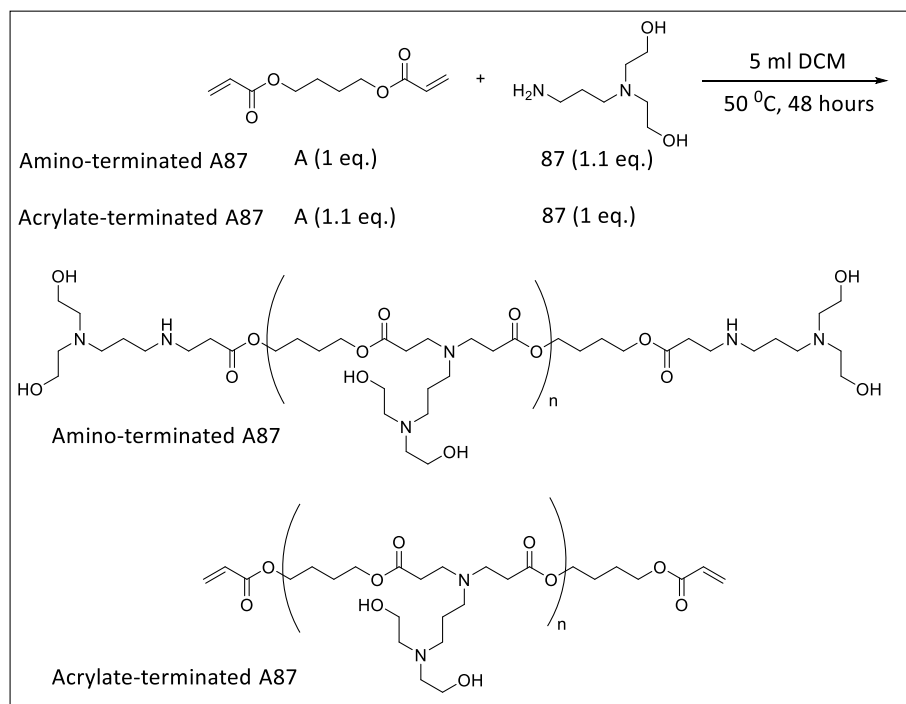
Figure 2.5: The synthesis of amino and acrylate-terminated **A87**

2.2.2 Preparation of buffers

pH meter (Hanna HI-2002 Edge®) was used for pH measurements. Buffers were prepared according to the following procedures:

- Phosphate buffered saline (PBS, pH 7.4) was prepared by dissolving 100 g of PBS tablet in 100 ml of deionized water (dH$_2$O).

- Sodium acetate/acetic acid (NaOAc/ AcOH) buffer (pH 5) was obtained by mixing (v/v) 30 % of (5.8 ml acetic acid in 994.2 ml of dH$_2$O) with 70% of (13.6 g sodium acetate trihydrate in 1000 ml of dH$_2$O).

2.2.3 Polymer characterization

Nuclear magnetic resonance (NMR) was used to determine the chemical structure of amino and acrylate-terminated **A5**, **A16**, and **A87**. The polymer average molecular weight (Mw) was determined using gel permeation chromatography (GPC) and the ^{1}H-NMR of acrylate-terminated **A5**, **A16**, and **A87**. Additionally, the polymer net surface charge was measured.

2.2.3.1 Gel permeation chromatography

A Shimadzu, RID-20A GPC system was used for determining the average Mw of amino-terminated **A5**, **A16**, and **A87** polymers at pH 7.4 or pH 5. The size of amino-terminated **A5**, **A16**, and **A87** polymers was determined based on the polyethylene glycol (PEG) standards calibration curve. The calibration curve was constructed using PEG standards ranging in size from 200 to 36000 Da (Figure 2.6). Table 2.3 shows the GPC experimental parameters for the calibration curve and experimental samples. Moreover, the GPC method was used to measure the amino-terminated **A5**, **A16**, and **A87** hydrolysis rate at pH 7.4 or pH 5 based on the average Mw reduction over time 0 - 4 days. The amino-terminated **A5**, **A16**, and **A87** polymer samples were incubated at 37$^°$C during the hydrolysis study to simulate the human body temperature. The GPC experimental samples were prepared at a concentration of 2 mg/ml of PBS buffer or sodium acetate buffer.

Table 2.3: The GPC parameters

Stationary phase	Superdex^{TM} 75, 10/300 GL
Mobile phase	100% of AcOH/NaOAc pH 5
Flow rate	1 ml/min
Column temperature	Room temperature
Detector	Refractive index
Injection volume	20 µl
Experimental time	25 min
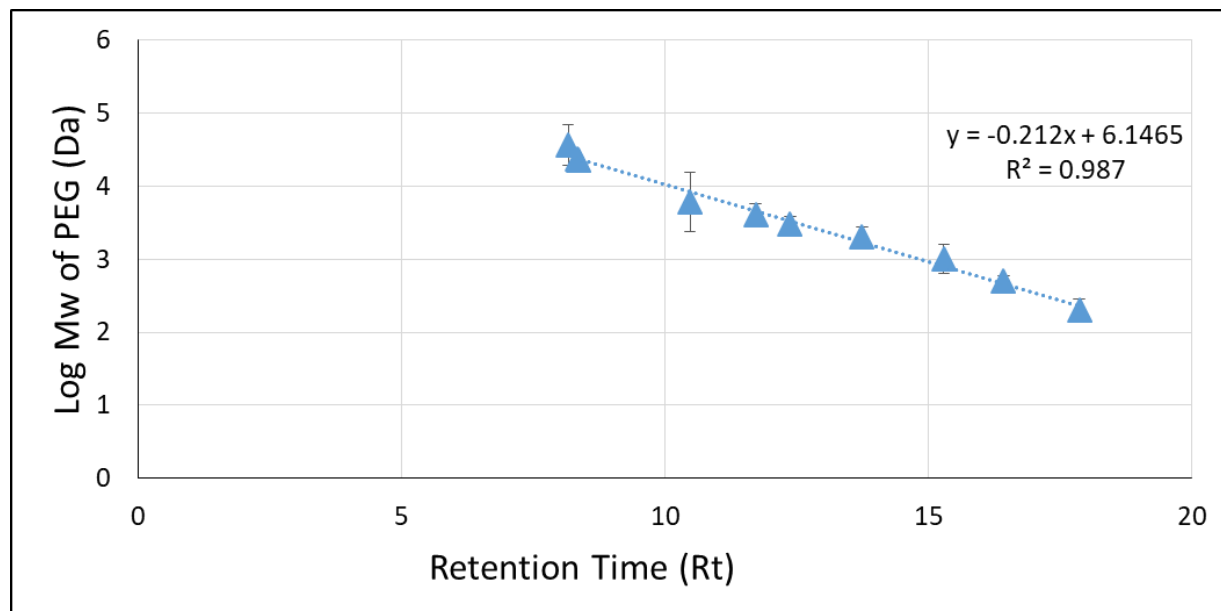
Figure 2.6: The calibration curve of polyethylene glycol standers

Bars represent (Mean ± SD of n=2)

2.2.3.2 **Nuclear magnetic resonance (NMR) spectroscopy**

The ^{1}H-NMR (Bruker, 500 MHz, BioSpin GmbH) was used to identify the structures of amino and acrylate-terminated **A5**, **A16**, and **A87**. In addition, ^{1}H-NMR was used to determine the number of repeating units (n) in the acrylate-terminated **A5**, **A16**, and **A87** following the methodology of Katherine P. and Daniel F.(189) The number of repeating units was determined based on calculating the peak area of ^{1}H-NMR and applying Equation 2.1. Then, the average Mw was calculated based on the number of the repeating units (Equation 2.2). The NMR samples of amino or acrylate-terminated **A5**, **A16**, and **A87** were prepared at a concentration of 10 mg/ml of DMSO-d6.

Equation 2.1:

$$\frac{\text{Peak area of repeating units}}{(n*\text{Number of proton in repeating units})} = \frac{\text{Peak area of end groups}}{\text{Number of protons in end groups}}$$

$$n = \frac{(\text{Peak area of repeating units}) * (\text{Number of protons in end groups})}{(\text{Number of proton in repeating units}) * (\text{Peak area of end groups})}$$

n = number of repeating units

Equation 2.2:

Average Mw = Mw of atoms in the end group + (n*Mw of atoms in the repeating units)

2.2.3.3 **The net surface charge**

Malvern Zetasizer nano ZS (Malvern Instruments Limited) was used to measure the net surface charge of amino-terminated **A5**, **A16**, and **A87** polymers, which was measured in the physiological pH 7.4 and in the inflammatory pH 5. Amino-terminated **A5**, **A16**, and **A87** polymers were prepared at a concentration of 2 mg/ml of PBS buffer or sodium acetate buffer. Then, 1 ml of the solution was placed in a zeta potential cuvette. The outcome of the surface charge is an indication of the polymer surface charge but not the exact charge because these polymers are

soluble in both buffers and do not form particles, which has been used previously with PBAE polymers.(179, 184)

2.2.4 **Statistical analysis**

A one-way or two-way ANOVA was performed between groups; for multiple comparisons followed, by Tukey or Dunnett post hoc test.(190) The data is reported as the mean ± standard deviation (SD) of three or more independent experiments. All the experiments were conducted in triplicate, unless stated otherwise.

2.3 Results

2.3.1 Polymers synthesis

The polymers acrylate and amino-terminated **A5**, **A16**, and **A87** were successfully synthesised with yields indicated in Table 2.4. The amino and the acrylate polymers have shown similar yields in similar reaction condition. With both anti-solvents, the amount of **A5** and **A16** polymer was approximately similar. However, the yield of the **A87** polymer varies based on the anti-solvent that was used to precipitate the product (Table 2.4). **A87** has shown 750 mg higher yield in hexane compared to diethyl ether. Overall, the yield of **A16** was lower compared to the yields of **A5** and **A87** polymers in hexane and diethyl ether.

Table 2.4: The average yields of A5, A16, and A87 polymers

PBAE	Anti-solvent	Yield
A5	Diethyl ether	1.93 g
	Hexane	1.84 g
A16	Diethyl ether	0.92 g
	Hexane	1.21 g
A87	Diethyl ether	1.11 g
	Hexane	1.86 g

2.3.2 Polymers NMR characterization

^{1}H-NMR was used to identify the chemical structure of the synthesised polymers. The NMR signal interpretation for **A5**, **A16**, and **A87** polymers was based on literature reports.(177, 182, 186, 191) Generally, polymers ^{1}H-NMR spectra are often difficult to interpret because of the polymer structural complexity and the protons overlapping signals. In addition to the literature reports, the ^{1}H-NMR spectra for both monomers were recorded and overlapped with the product ^{1}H-NMR spectra to aid the analysis and to confirm the proton peak assignment. Unfortunately, the solvent proton peaks that was used during the reactions appear in the ^{1}H-NMR spectrum, which is related to the physical nature of PBAE polymers. Amino and acrylate terminated **A5**, **A16**, and **A87** are very viscous liquid (resembling honey consistency), which makes solvents

evaporation challenging even after 1 hour in rotary evaporator and air-drying for 48 - 72 hours. The chemical structure of **A5**, **A16**, and **A87** polymers is relatively similar, so these polymers share the proton signals of the diacrylate and the proton signals of -OCC-C**H₂**-C**H₂**-N- units, which is the newly formed bond during polymerization. The polymers common proton signals were C**H₂**=CH- at 5.9 – 6.3 ppm, -COO-C**H₂**- at 4.0 ppm, -OCH₂-C**H₂**C**H₂**-CH₂O- at 1.6 ppm, -OOC-C**H₂**- at -N-C**H₂**-CH2-COO- at 2.7 ppm, -OOC-C**H₂**- at 2.3-2.5 ppm, and -N-C**H₂**- 2.3-2.5 ppm.

2.3.2.1 NMR signals interpretation of A5 polymers and its derivatives

Figure 2.7 reports the ^{1}H-NMR interpretation of acrylate-terminated **A5** based on previous studies and the starting materials.(177, 182, 186, 191, 192) In the acrylate-terminated **A5**, ^{1}H-NMR key peaks were at 6.3, 6.18, and 5.9 ppm, corresponding to the protons of the acrylate double bond at positions b, c, and a, respectively. The new bond formation between the amine and the acrylate group has resulted in the appearance of new proton signals at 2.3 - 2.5 and 2.6 - 2.7 ppm, which correspond to the protons at positions 4 and 5, respectively. The proton signals of (-C**H₂**-N- and -C**H₂**-COO-) at positions 4, 6, and 8 are overlapped at 2.3 - 2.5 ppm. The proton signal on the carbon next to the oxygen of the ester group (-C**H₂**-O-CO-) appears at 4.0 ppm. Additionally, (-C**H₂**-C**H₂**-) at position 3 showed a peak signal at 1.6 ppm, and the proton of (-N-CH₂C**H₂**CH₂-N-) appears at 1.8 ppm. Furthermore, the key element in the ^{1}H-NMR spectrum of amino-terminated **A5** is the disappearance of acrylate protons at 5.9 - 6.3 ppm (Figure 2.8). The disappearance of typical acrylate peaks is an indication of amino-terminated A5 formation. Moreover, the ^{1}H-NMR spectra have shown peaks at 2.6 - 2.7 and 2.3 - 2.5 ppm, which are corresponding to the protons on the two carbons that are between the amine and carbonyl carbon (positions 5 and 6, respectively). The **A5** polymers have been synthesised and the ^{1}H-NMR spectra have confirmed the formation of acrylate or amino-terminated **A5**. The interpretation of ^{1}H-NMR spectra was based on previous literature that reported the ^{1}H-NMR of PBAE polymers.(177, 182, 186, 191, 192)
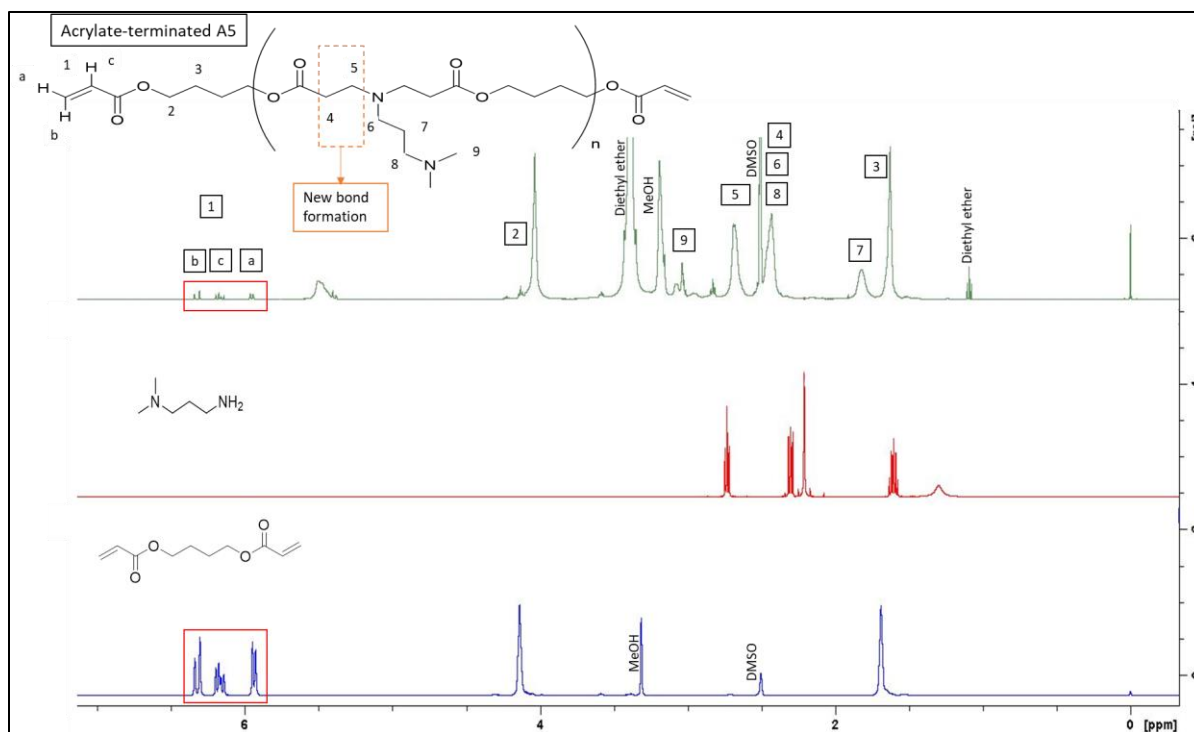
Figure 2.7: Overlay of the ^{1}H-NMR spectrum (500 MHz, DMSO-d6) of acrylate-terminated **A5** and the monomers
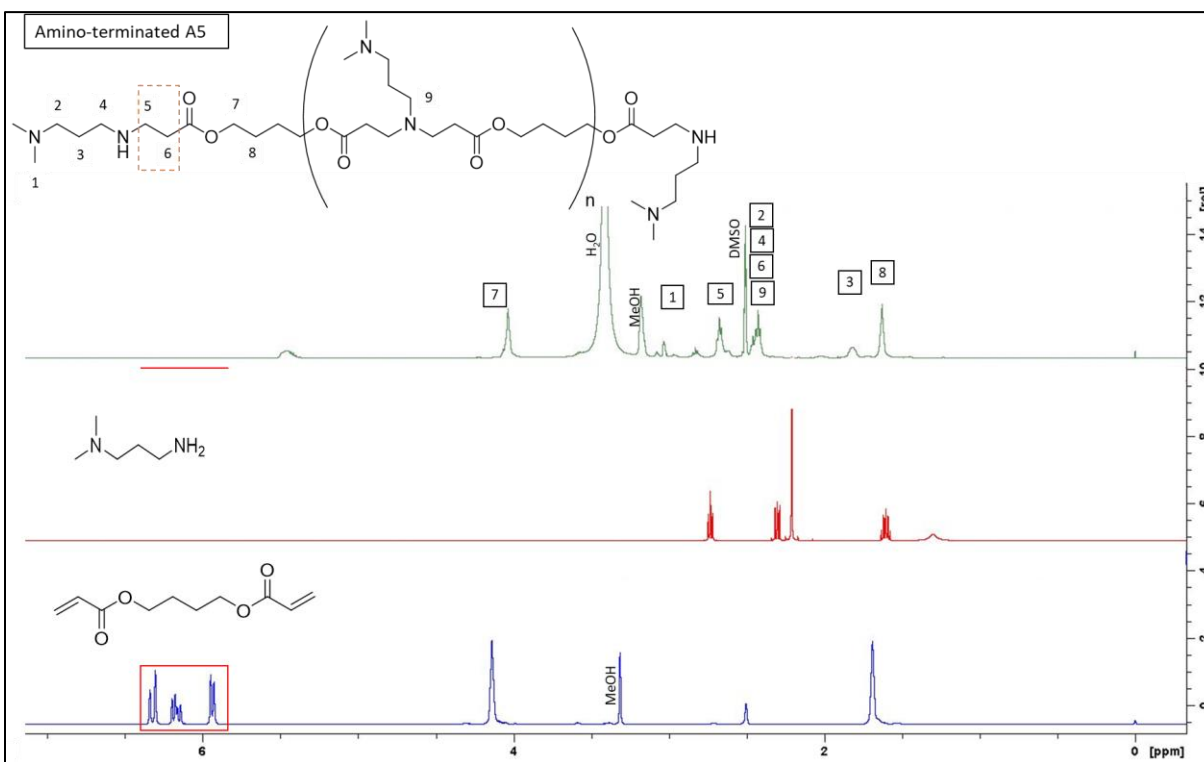
Figure 2.8: Overlay of the ^{1}H-NMR spectrum (500 MHz, DMSO-d6) of amino-terminated **A5** and the monomers

2.3.2.2 **NMR signals interpretation of A16 polymers**

Figure 2.9 and Figure 2.10 show the proton signal interpretation of the acrylate and amino-terminated **A16,** respectively. The ^{1}H-NMR spectrum of the synthesised acrylate and amino-terminated **A16** were similar to the Yi Li group ^{1}H-NMR spectrum.(192) The Yi Li group has synthesised and investigated a PBAE polymer that is similar to the **A16** structure with an additional methylene group.(192) The typical double bond protons signals of the acrylate appear at 6.3, 6.18, and 5.9 ppm, which confirm the formation of the acrylate terminated **A16**. Moreover, the disappearance of these proton peaks confirms the synthesis of the amino-terminated **A16**. The proton signals at 2.3 - 2.4 and 2.6 - 2.7 ppm, which correspond to (-OOC-C**H₂**C**H₂**-N-), respectively, confirm the bond formation between the double bond of the acrylate and the amino group. Additionally, the proton signal of (-C**H₂**-N-) is overlapped with (-OOC-C**H₂**CH₂-N-) signals at 2.3 - 2.4 ppm. The signal that corresponds to the proton of O**H** appeared at 4.3 ppm in the ^{1}H-NMR spectrum of amino and acrylate-terminated A16. In both ^{1}H-NMR spectrum, the proton signal of (-COOC**H₂**-) appears at 4.0 ppm, (-C**H₂**CH₂-) appears at 1.6 ppm, and (N-CH₂C**H₂**CH₂-OH) appears at 1.5 ppm. The ^{1}H-NMR spectrum confirms the formation of acrylate and amino-terminated **A16**.
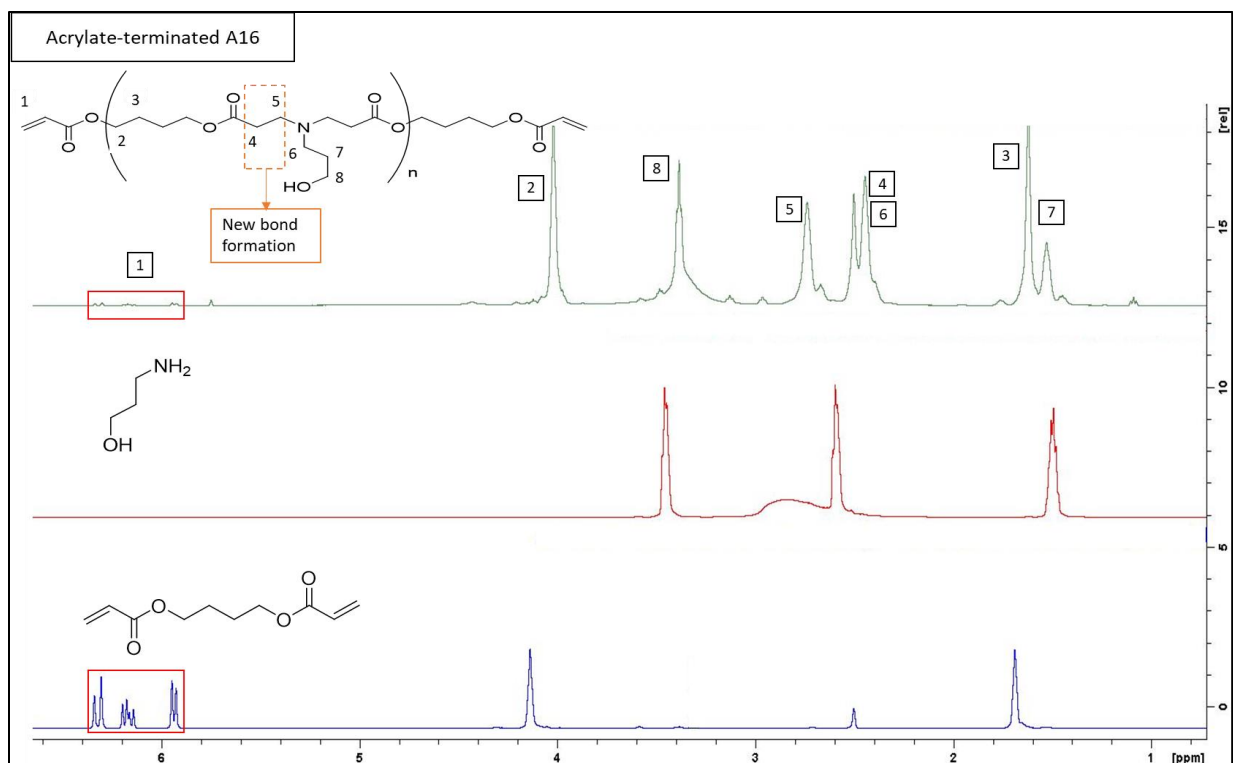
Figure 2.9: Overlay of the ^{1}H-NMR spectrum (500 MHz, DMSO-d6) of acrylate-terminated **A16** and the monomers
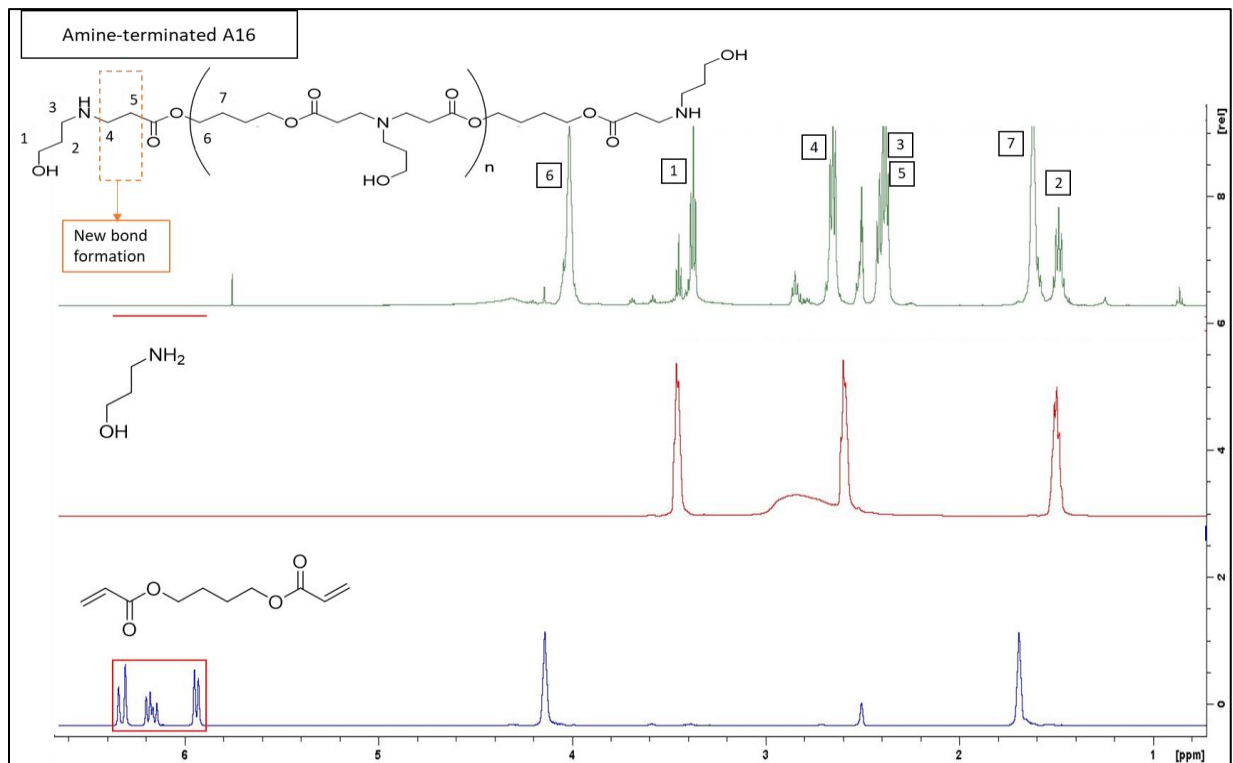
Figure 2.10: Overlay of the ^{1}H-NMR spectrum (500 MHz, DMSO-d6) of amino-terminated **A16** and the monomers

2.3.2.3 NMR signals interpretation of A87 polymers

The interpretation was based on the starting materials ^{1}H-NMR spectra and previous literature that has reported the ^{1}H-NMR of PBAE polymers.(177, 182, 186, 191, 192) The key proton signals of the acrylate-terminated **A87** appear at 6.3, 6.18, and 5.9 ppm, corresponding to the double bond protons (Figure 2.11). The protons next to the nitrogen atom peak (-C**H₂**N-) are overlapped and appeared at 2.4 ppm. The peak at 3.41 ppm corresponds to (-C**H₂**-OH). The proton peak of (-OCH₂-C**H₂**C**H₂**-CH₂O-) appears at 1.62 ppm. The hydroxyl group proton appears at 4.35 ppm. Similar proton signals appear at the ^{1}H-NMR spectrum of amino-terminated **A87**, except the protons peaks correspond to the acrylate double bond protons at 5.9 – 6.3 ppm (Figure 2.12). Since there is no proton signal corresponding to the acrylate double bond protons, the synthesis of amino-terminated **A87** was successful.
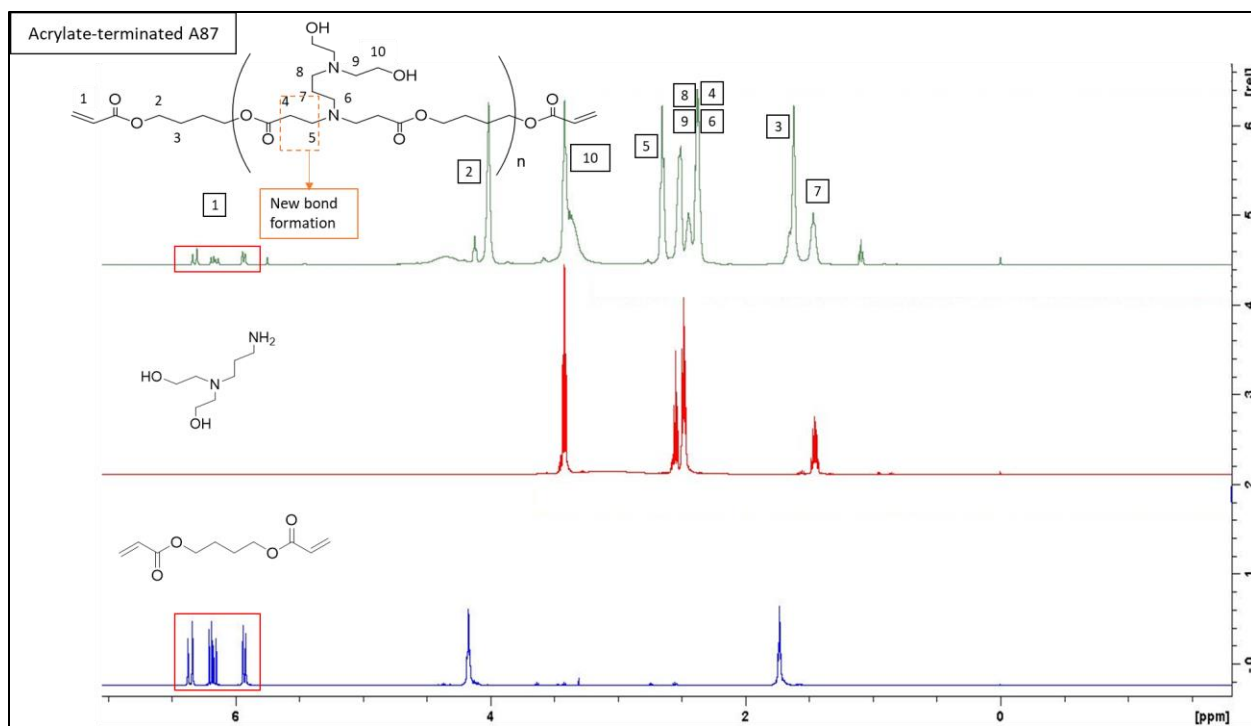
Figure 2.11: Overlay of the ^{1}H-NMR spectrum (500 MHz, DMSO-d6) of acrylate-terminated **A87** and the monomers
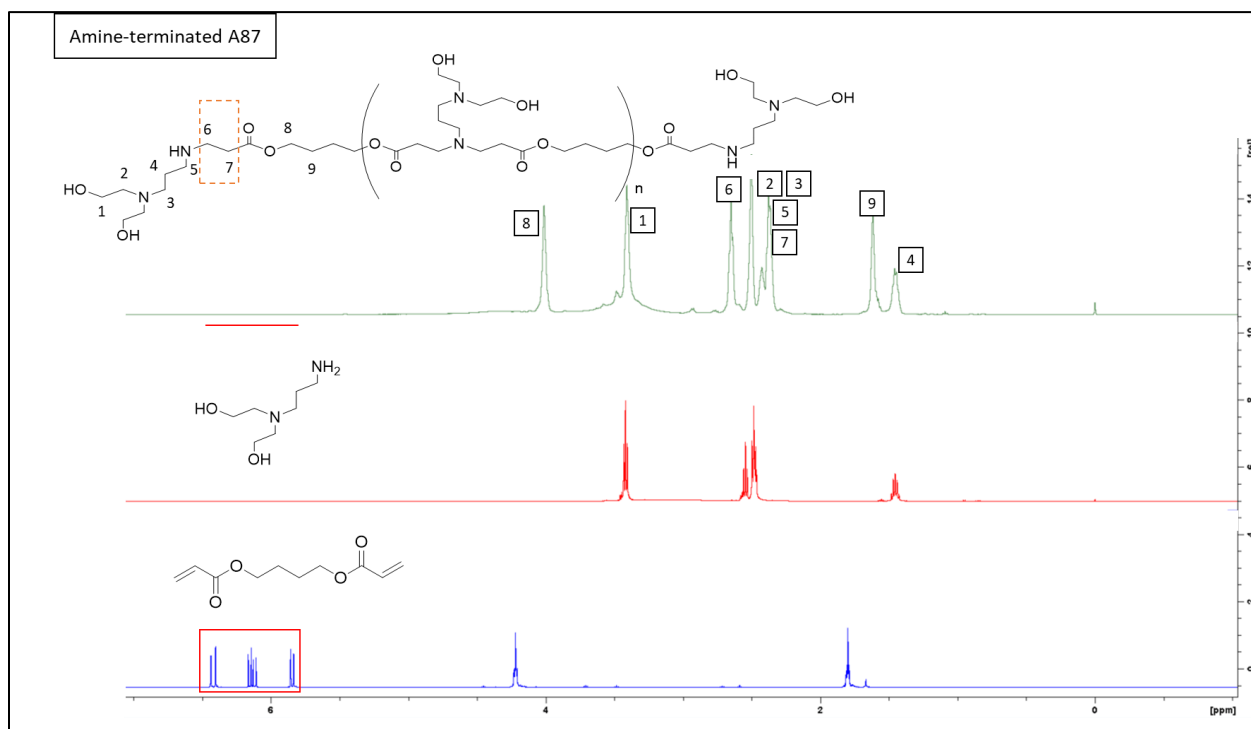
Figure 2.12: Overlay of the ^{1}H-NMR spectrum (500 MHz, DMSO-d6) of amino-terminated **A87** and the monomers

2.3.3 **Calculated average molecular weight based on the NMR spectra**

The ^{1}H-NMR spectra of acrylate-terminated **A5**, **A16**, and **A87** polymers can be used to determine the average molecular weight (Mw) of these polymers based on Equation 2.1 Equation 2.2 (on page 60).(189) The method for calculating the peak area required a single proton as a reference. Since the amino-terminated polymers do not contain a single proton and the signals overlapped, and the acrylate-terminated **A5**, **A16**, **A87** was synthesised to assist calculating the average Mw. The reason for this is the double bond protons peaks are not overlapped or in close proximity with other signals, therefore signal at 6.3 has been chosen as a reference. Table 2.5 shows the repeating units and the calculated average Mw of acrylate-terminated **A5**, **A16**, and **A87** based on their ^{1}H-NMR spectra. The number of repeating units (n) in the polymeric structure of acrylate-terminated **A5**, **A16**, and **A87** were 6.4 ± 1.1, 6.6 ± 0.27, and 5.9 ± 0.43, respectively. Accordingly, the calculated average Mw of acrylate-terminated **A5**, **A16**, and **A87** are 2,119 ± 330, 2,010 ± 76, and 2,324 ± 154 Da, respectively.

Table 2.5: The calculated repeating units (n) and the average Mw of acrylate-terminated A5, A16, and A87 based on their ^{1}H-NMR spectra (Mean ± SD)

Acrylate-terminated	Repeating units (n)	Average Mw (Da)
A5	6.4 ± 1.1	2,119 ± 330
A16	6.6 ± 0.27	2,010 ± 76
A87	5.9 ± 0.43	2,324 ± 154

2.3.4 The GPC characterization of amino-terminated A5, A16, and A87

The average Mw was determined based on the PEG standard calibration curve (Figure 2.6). In addition to determine the average Mw, the GPC method was used to determine the hydrolysis rate of amino-terminated **A5**, **A16**, and **A87** based on the Mw reduction over time 0 - 96 hours.

2.3.4.1 The polymers average molecular weight

Table 2.6 shows the average Mw of amino-terminated **A5**, **A16**, and **A87** at pH 7.4 and pH 5. The average Mw of amino-terminated **A5** is 2,580 ± 378 Da at pH 7.4 and 2,546 ± 137 Da at pH 5 (n= 4). Moreover, the amino-terminated **A16** average Mw is 1,138 ± 55 Da at pH 7.4 and 1,315 ± 103 Da at pH 5 (n= 3). The amino-terminated **A87** average Mw is 1,756 ± 260 Da at pH 7.4 and 1,739 ± 95 Da at pH 5 (n= 3). At both pH conditions, the polymers have shown approximately similar average Mw. According to the average Mw, the amino-terminated **A5** is the largest polymer followed by amino-terminated **A87** and **A16** at both pH conditions.

Table 2.6: The average Mw of amino-terminated A5, A16, and A87 based on PEG standards (Mean ± SD)

Amino-terminated	Average Mw (Da)	
	pH 7.4	pH 5
A5	2,580 ± 378	2,546± 137
A16	1,138 ± 55	1,315 ± 103
A87	1,756 ± 260	1,739 ± 95

2.3.4.2 The polymers hydrolysis studies

The hydrolysis study for **A5**, **A16**, and **A87** were conducted at pH 7.4 and pH 5 over 4 days. On the first day, the samples were analysed every hour during the first 8 hours. Under both pH conditions, a quick hydrolysis was observed for all three polymers (Figure 2.13, Figure 2.14, and Figure 2.15).

2.3.4.2.1 A5 hydrolysis study

Figure 2.13 shows the hydrolysis rate study of amino-terminated **A5** at pH 7.4 and 5. At pH 7.4, the amino-terminated **A5** average Mw was significantly decreased after 3 hours of incubation at 37℃ compared to the average Mw at the first hour. In contrast, at pH 5, a significant decrease in the average Mw of the amino-terminated **A5** begins after 6 hours of incubation at 37℃ compared to the average Mw at the first hour. Additionally, comparing the average Mw of A5 at pH 7.4 with pH 5 in respect to the incubation times has shown a significantly high average Mw at pH 5 during 2 - 4 hours of incubation. The amino-terminated **A5** hydrolysis rate at pH 7.4 is faster than pH 5. This is due to the fact that the average Mw at pH 7.4 began to show a significant reduction at 3 hours, whereas the significant reduction at pH 5 was observed at 6 hours, and the average Mw at 2, 3, and 4 hours were significantly higher at pH 5 compared to pH 7.4.
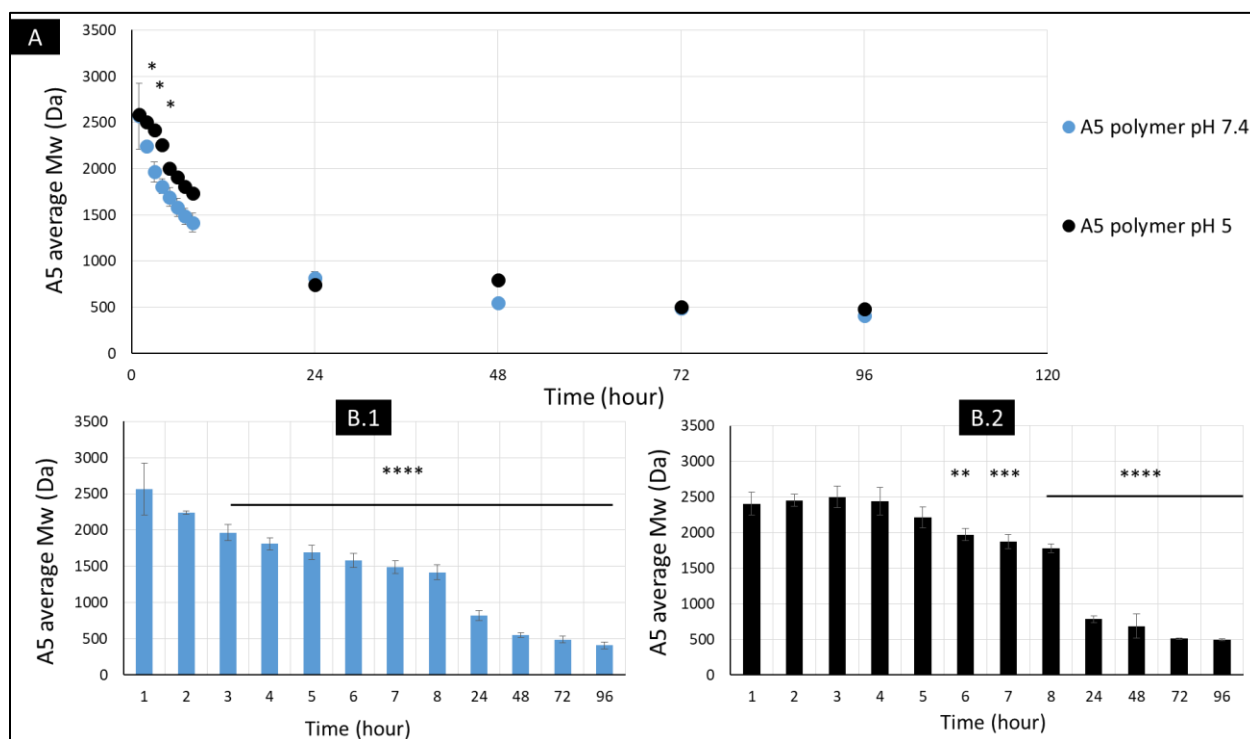
Figure 2.13: The amino-terminated A5 hydrolysis at pH 5 and pH 7.4

(A) Graph is showing a comparison of A5 average Mw at pH 7.4 with pH 5 at each time point. Circles (blue and black) represent the mean ± SD of n=4. Significant * (P<0.05) comparing A5 Mw at pH 7.4 with pH 5.(B.1) graph compares the average Mw at the first hour with each time point at pH 7.4. (B.2) graph compares the average Mw at the first hour with each time point at pH 5. Bars represent the mean ± SD of n=4. Significant ** (P<0.01), *** (<0.001), **** (P<0.0001) compared to A5 Mw at the first hour.

2.3.4.2.2 A16 hydrolysis study

The hydrolysis of the amino-terminated A16 at pH 7.4 and pH 5 over time was investigated (Figure 2.14). At pH 7.4, the reduction of the average Mw was significant after 2 hours of incubation in 37℃ compared to the average Mw at the first hour, while at pH 5, after 3 hours of incubation a significant reduction of the average Mw was observed. A numerical difference was noticed when comparing the average Mw reduction at pH 7.4 to pH 5 with respect to the time points (Figure 2.14 A). The hydrolysis rate study of A16 polymer indicated that the polymer could be degraded faster at pH 7.4 than at pH 5 because the hydrolysis began after 2 hours at pH 7.4 and after 3 hours at pH 5.
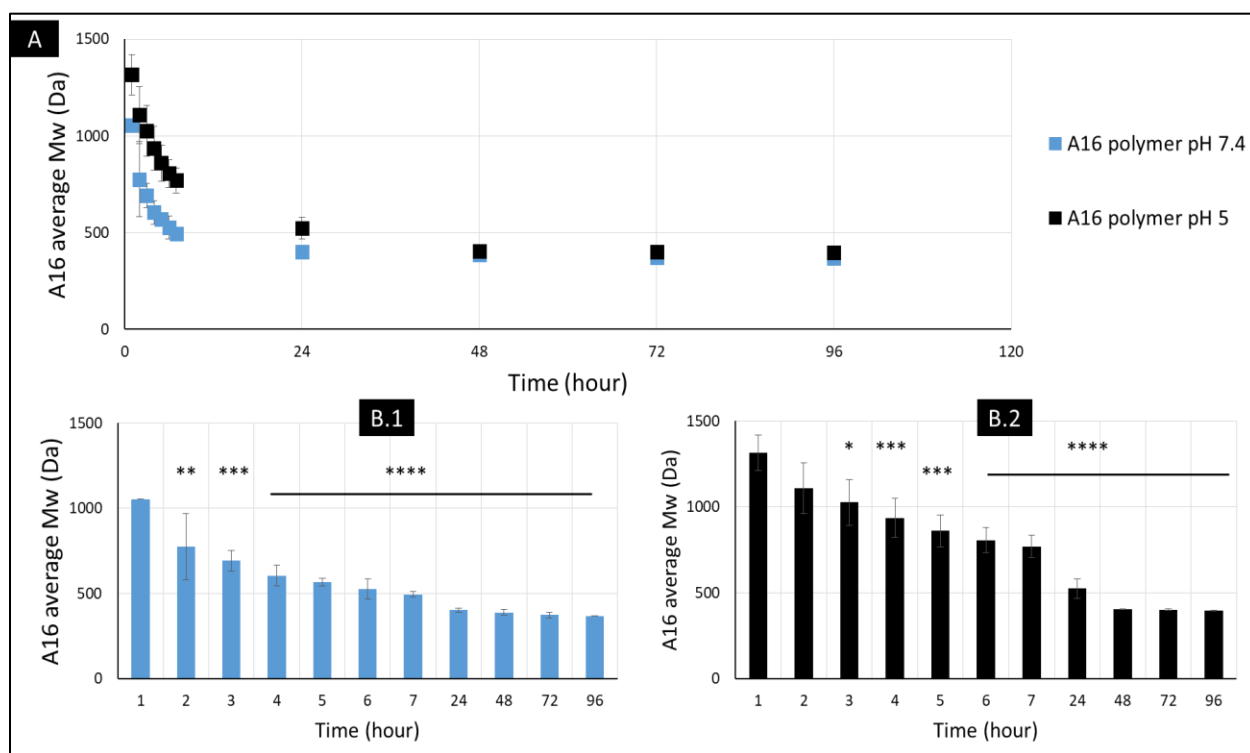
Figure 2.14: The amino-terminated A16 hydrolysis at pH 7.4 and pH 5

The graph (A) is showing a comparison of A16 average Mw reduction at pH 7.4 with pH 5 with the respect to the incubation times. Squires represent the mean ± SD of n=3. The pH 7.4 graph (B.1) is comparing the A16 average Mw at 1 hour to other time points. The pH 5 graph (B.2) is comparing the A16 average Mw at 1 hour to other time points. Bars represent the mean ± SD of n=3. Significant * ($P<0.05$), ** ($P<0.01$), *** (<0.001), **** ($P<0.0001$) compared to A16 at the first hour.

2.3.4.2.3 **A87 hydrolysis study**

Figure 2.15 shows the hydrolysis rate study of amino-terminated A87 at pH 7.4 and pH 5. At both pH conditions, a significant reduction in average Mw begins after 2 hours of incubation at 37℃. Comparing the average Mw of A87 at pH 7.4 against pH 5 with respect to the incubation time points shows a lower average Mw at 6 and 7 hours at pH 7.4 compared to pH 5 (Figure 2.15 A). Additionally, a numerically higher reduction of average Mw at pH 7.4 when compared to pH 5 was observed throughout the time points. Therefore, the hydrolysis rate of A87 at pH 7.4 could be faster than pH 5, even though the hydrolysis of the polymer has shown no statistical difference between pH 7.4 and pH 5 except at incubation times of 6 and 7 hours.
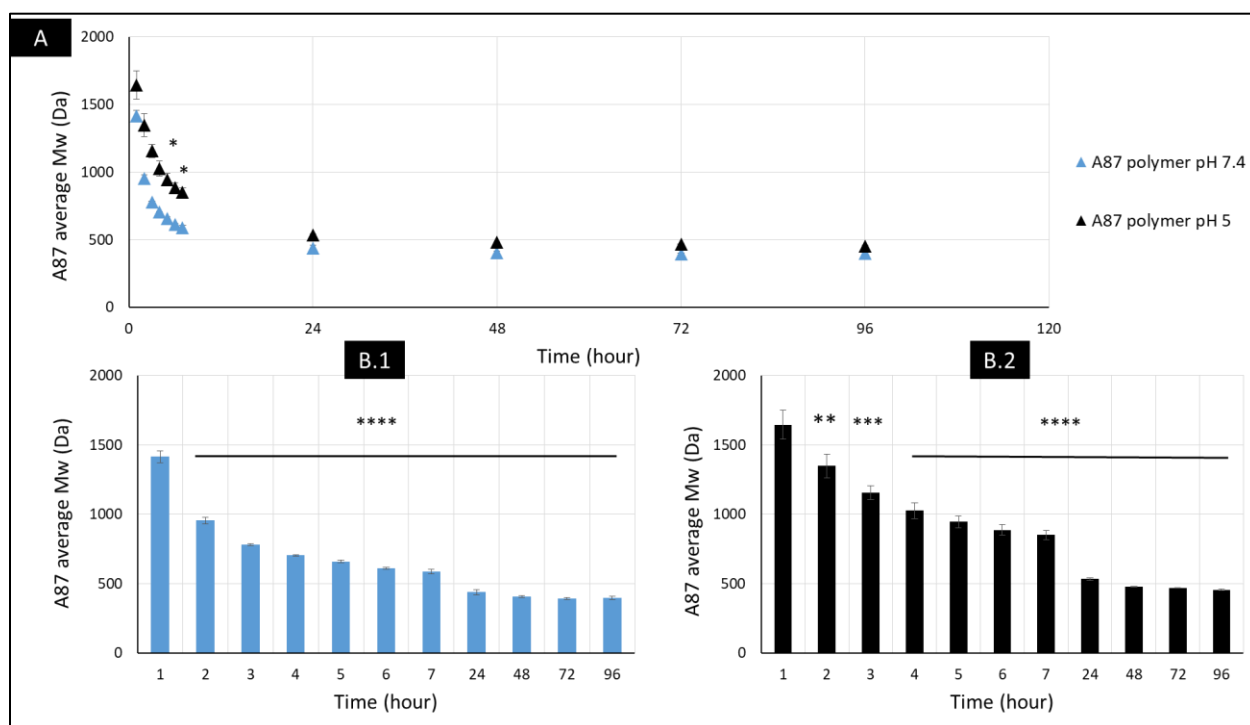
Figure 2.15: The amino-terminated A87 hydrolysis at pH 7.4 and pH 5

Graph A compares the A87 average Mw reduction at pH 7.4 with pH 5 with the respect to the incubation times. Triangles represent the mean ± SD of n=4. Significant * (P<0.05) comparing A5 Mw at pH 7.4 with pH 5. Graph B.1 compares the A87 average Mw at 1 hour to other time points at pH 7.4. Graph B.2 compares the A87 average Mw at 1 hour to each time points at pH 5. Bars represent the mean ± SD of n=3. Significant ** (P<0.01), *** (<0.001), **** (P<0.0001) compared to A87 at the first hour.

73

2.3.5 The polymers net surface charge

The net surface charge of amino-terminated **A5**, **A16**, and **A87** was measured at pH 7.4 and pH 5. In both pH conditions, all three polymers showed a net positive charge (Table 2.7). The net surface charge of **A5**, **A16**, and **A87** at pH 7.4 is 12 ± 3, 7, and 7 (mV), respectively, while 14 ± 2, 7, and 13 ± 1 (mV), respectively at pH 5. The amino-terminated **A5**, and **A87** have shown a higher positive surface charge at pH 5 compared to pH 7.4, whereas **A16** has shown a similar net positive surface charge at both pH conditions. Amino-terminated **A5** has the highest net surface positive charge under both pH conditions compared with amino-terminated **A16** and **A87**. At pH 7.4, **A87** and **A5** have reported the lowest positive charge (7 mV), while the lowest positive charge at pH 5 was observed with **A16** (7 mV).

Table 2.7: Net surface charge of A5, A16, and A87 at pH 7.4 and pH 5 (Mean ± SD, n=6)

Amino-terminated	Surface charge at pH 7.4	Surface charge at pH 5
A5	12 ± 3 (mV)	14 ± 2 (mV)
A16	7 (mV)	7 (mV)
A87	7 (mV)	13 ± 1 (mV)

2.4 **Discussion**

The disease modifying osteoarthritis drugs (DMOADs) performed poorly in clinical trials due to low resident time within the joint space and side effects.(3, 11-19) The hydrophilicity and negatively charged nature of the cartilage play a significant role in lowering the uptake and retention time of these drugs.(173, 193) The current study aims to enhance the uptake and retention time of OA therapeutics in the cartilage by covalently attaching DMOADs to positively charged PBAE polymers. The overall positive charge of these conjugates will allow their strong electrostatic interaction with the negatively charged cartilage components. The attraction would allow DMOADs to be transferred into a deeper cartilage zone and remain in the cartilage for a longer period of time. This will enhance the therapeutic effect, reduce the therapeutic dose, and reduce the risk of side effects. According to previous studies, cationic delivery systems diffuses through the cartilage network deeper and faster than neutral systems.(140, 172, 173) Additionally, conjugating OA therapeutics with positively charged delivery systems has enhanced their therapeutic effect.(140, 170, 172-174)

The strategy for achieving this aim begins with the synthesis of PBAE polymers, which is the primary aspect of this chapter. Three PBAE polymers with diverse structures and properties were selected to investigate the impact of various factors on the uptake and retention time. These factors are the degree of the positive charge and the number of the conjugation site, which were discussed earlier in this chapter (2.1, Figure 2.1). In this chapter, the positively charged A5, A16, and A87 polymers formation, chemical structure identification, and characterization have been studied.

2.4.1 **Synthesis and NMR identification of A5, A16, and A87 polymers**

The polymerization condition and procedure of amino and acrylate-terminated A5, A16, and A87 were identical and adapted from literature (Table 2.2).(143, 180, 184-186) The yield of PBAE polymers is conventionally high since there is no side product formation and the mechanism of the reaction is simple (143, 180, 181). The obtained product of A5, A16, and A87 polymers in diethyl ether or hexane was approximately 1 to 2 g (Table 2.4). However, the investigational study of quantifying the precipitated polymer after adding the anti-solvents was

conducted primarily to determine the anti-solvent that should be added after the conjugation reaction. A5 polymers yielded roughly a similar quantity in both anti-solvents. In contrast, A16 and A87 polymers yielded approximately 290 mg and 750 mg more in hexane than in diethyl ether, respectively, which could be related to the polarity of these polymers (Figure 2.1). A16 and A87 polymers contain strong polar groups and hydrogen donor groups (-OH) in their repeating units, which could cause a lower yield in diethyl ether. However, A5 polymer does not contain a hydrogen bond donor in its repeating units so the solubility in diethyl ether remain low. Therefore, the collection of A16 and A87 conjugates should be in hexane, while A5 conjugate should be in diethyl ether. The structure of synthesised polymers was constant and reproducible, which is confirmed by the ^{1}H-NMR spectra, where multiple ^{1}H-NMR spectra of individually synthesised amino and acrylate A5, A16, and A87 polymers have shown identical proton signals.

The structure identification of amino and acrylate A5, A16, and A87 was determined using ^{1}H-NMR (Figures 2.7 – 2.12). The starting materials ^{1}H-NMR spectra assist significantly in determining the key peaks of PBAE polymers. Additionally, the proton signals interpretation were confirmed according to previous studies that reported the ^{1}H-NMR spectra of PBAE structure.(177, 182, 186, 191, 192) The A5, A16, and A87 polymers share some proton signals because of the presence of the exact diacrylate monomer. The typical acrylate proton peaks at 5.9 - 6.3 ppm are the distinction peaks between acrylate and amino polymers. Additionally, the new signals at 2.4 and 2.7 ppm confirm the polymers formations.(177, 182, 186, 191, 192)

2.4.2 A5, A16, and A87 polymers characteristic studies

Table 2.8 summarises the average Mw and the net surface charge results of A5, A16, and A87 polymers. The average Mw weight of PBAE is often determined according to the Mw of PEG standards or polystyrene standards using the GPC.(180, 186) Numerous PBAE studies have reported that the molecular weight of PBAE is greater than 2000 Da, which can be controlled based on the starting material quantity and the reaction condition.(179, 180, 194) Similar average Mw of A5, A16, and A87 with literature were observed. Both methods of determining the average Mw of the three polymers showed relatively comparable results (Table 2.8). Measuring and optimising the average Mw is essential for the efficiency of A5, A16, and A87 polymers as a delivery system for DMOADs because the size of the carrier affects its cartilage penetration.

According to previous studies on other OA delivery systems that have penetrated the cartilage, A5, A16, and A87 polymers should be able to penetrate the cartilage mesh.(140, 170-173, 176).

The variation in the positive charge of A5, A16, and A87 will further assist in investigating the impact of the positive charge degree on the uptake and retention time of OA therapeutics.(170, 171, 173) The net surface charge of A5, A16, and A87 was simultaneously influenced by the number of the amine group and the polymer size, which was observed in the experiments. The positive charge of PBAE polymers is derived from the tertiary amino groups on the backbone of the polymer, which are protonated at both physiological and inflammatory pH.(180, 181) Accordingly, the number of amino groups should be proportional to the degree of positive charge. The A5 polymer positive charges were 12 ± 3 and 14 ± 2 (mV) at pH 7.4 and pH 5, respectively, which are the highest compared to A16 and A87 because A5 has the largest Mw and also two tertiary amines in each of its repeating units. Even though A87 has two tertiary amines per repeating units, the positive charges are 7 and 13 ± 1 at pH 7.4 and pH 5, respectively. A87 has almost the same chemical structure of A5. The only difference is the presence of the additional two methyleneoxy groups (Figure 2.1). However, A87 has demonstrated a lower positive surface charge compared to A5, which could be related to the two hydroxyl groups in each of its repeating units. Additionally, the NMR analysis has shown that in polymer A5 the number of repeating unit is 6.4 ± 1.1, whereas in A87, n is 5.9 ± 0.43, which also could be the reason of A87 low positive charge. The A16 positive charge was 7 mV at both pH, which is lower compared to A5 because A16 contains one tertiary amine and one hydroxyl group in each of its repeating units, while A5 contains two tertiary amines. At pH 7.4, A16 and A87 showed similar positive charge, while at pH 5, A87 positive charge was significantly higher than that of A16. A87 has two tertiary amines, one hydroxyl group, and 5.9 ± 0.43 repeating units, while A16 has one tertiary amine, one hydroxyl group, and 6.6 ± 0.27 repeating units. Comparing the polymers charges individually at both pH conditions shows that the positive net surface charge of A5 and A87 at pH 7.4 was lower than pH 5, because the tertiary amines are basic functional groups so as the pH decreases the protonation should increase.

Table 2.8: A summary of A5-E1, A5, A16, and A87 characterization studies (Mean ± SD)

PBAE polymer	Surface charge (mV)		GPC average Mw (Da)		NMR Repeating units (n)	NMR average Mw (Da)
	pH 7.4	pH 5	pH 7.4	pH 5		
A5	12 ± 3	14 ± 2	2,580 ± 378	2,546 ± 137	6.4 ± 1.1	2,119 ± 330
A16	7	7	1,138 ± 55	1,315 ± 103	6.6 ± 0.27	2,010 ± 76
A87	7	13	1,756 ± 260	1,739 ± 95	5.9 ± 0.43	2,324 ± 154

2.4.3 **A5, A16, and A87 polymers hydrolysis studies**

PBAE polymers are a hydrolysable polymer because of the ester function group in the backbone of the polymer, which is another significant factor in selecting the PBAE polymers to be evaluated for OA therapeutic delivery. Studies have mentioned that PBAE degradation begins within hours, and the polymers are more stable at pH 5 than pH 7.4.(179-181, 194) Similar results were observed in the hydrolysis studies of A5, A16, and A87, which show a fast average molecular weight reduction of A5, A16, and A87 within the first 8 hours (Figure 2.13, Figure 2.14, and Figure 2.15). Additionally, the hydrolysis of A5, A16, and A87 was faster at pH 7.4 compared to pH 5. Eventually, A5, A16, and A87 are hydrolysable delivery systems at physiological and inflammatory pH. The advantage of developing a degradable delivery system is to ensure that the DMOADs would be fully released and not trapped within the delivery system. Additionally, a fast released DMOADs would potentially has an immediate therapeutic activity.(161)

2.5 **Conclusion**

The aim of the study was to enhance DMOADs uptake and retention time so these drugs can be more effective therapeutically. This could be achieved by conjugating DMOAD to the cationic hydrolysable PBAE polymers. The conjugation to PBAE polymers would enhance the DMOADs penetration through the cartilage mesh network, increase DMOADs cartilage uptake value and drug retention time, and reduce DMOAD drains to the systemic circulation. Potentially, each of these factors can improve DMOADs therapeutic effect and reduce the risk of side effects. A5, A16, and A87 were the PBAE polymer candidates to investigate their influence on the DMOAD uptake and retention time within the cartilage after conjugation. A5, A16, and A87 have demonstrated a positive surface charge at pH 7.4 and pH 5. Additionally, the polymers were hydrolysed within 24 hours at both pH conditions. Accordingly, the chemical properties of these polymers met our previously discussed criteria: the positive charge of these polymers will enhance the penetration through the cartilage mesh, increase the retention time via the attraction to the cartilage electrostatically, and reduce the cartilage-repellence behaviour against lipophilic drugs. Another significant aim for the current study was the synthesis of PBAE polymers with different net positive charges to investigate the charge effect on the delivery system efficiency, which was achievable because of the PBAE structure diversity. Additionally, the uptake and the retention time of DOMADs can be influenced by the drug-loaded capacity on the carrier; therefore, A5, A16, and A87 can contain different drug quantities based on the number of the conjugation sites, which is an additional investigation aim of this study (Figure 2.1). The first objective was achieved, and the preliminary results were expanded further by conjugating these polymers to OA therapeutics. Therefore, in the next chapter, A5, A16, and A87 will be covalently conjugated to the two model drugs of DMOADs (licofelone or NBQX).

Chapter 3: **NBQX and Licofelone Conjugation to PBAE Polymers**

3.1 **Introduction**

The covalent conjugation of two model drugs of DMOAD to our PBAE polymers prepared in the second chapter is the primary objective of this chapter. The reason for preferring a covalent hydrolysable link between the delivery systems and the DMOADs instead of a physical link (such as physical encapsulation and electrostatic interaction) is that in OA, the covalent conjugation has shown a longer residence time of the drug in the joint and a lower drug quantity has reached the systemic circulation.(18, 144) NBQX and licofelone (Figure 3.1) were chosen as models of DMOADs for multiple reasons. Therapeutically, NBQX has been proven to reduce OA symptoms and the disease progression by reducing the glutamate concentration and blocking the glutamic receptor's (AMPA) catalytic site, which has been discussed previously (1.1.4.4.1).(104) Additionally, NBQX targets three essential elements in the progression of OA, which are cytokine release, protease production, and osteoclast/osteoblast activity.(103, 104) Furthermore, licofelone was selected to be a second model for DMOADs because of its excellent therapeutic profile during *in vitro* and *in vivo* studies against OA progression (1.1.4.4.3), and the drug is in phase III clinical trial.(111, 112, 115-117). Furthermore, from a study design perspective, these drugs are commercially available and less expensive compared to the other DMOADs. Moreover, licofelone has a carboxylic acid group, which is a good conjugation point (Figure 3.1).
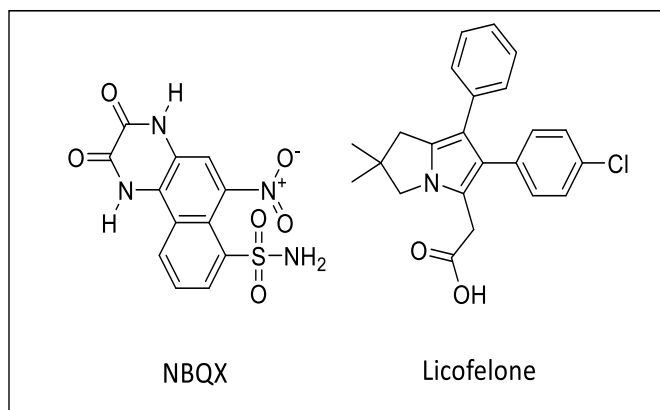
Figure 3.1: NBQX and licofelone structure

Unfortunately, NBQX conjugation attempts were unsuccessful because the sulphonamide group was not a strong nucleophile group, which prevented NBQX from being chemically bonded to the polymers. Therefore, the negatively charged NBQX was physically mixed with the positively charged A5 polymer, which will attach NBQX to the A5 polymer via electrostatic interaction. However, the objective of the study is to attach DMOAD to PBAE polymers via a covalent hydrolysable bond, which will be accomplished by conjugating licofelone to A5, A16, and A87 polymers. The diversity of these polymers aids in analysing the impact of the positive charge and the quantity of licofelone linked to the polymers on the uptake and retention time studies. According to the previous chapter, A5, A16, and A87 showed different degrees of positive charge, which allows studying the effect of positive charge on the uptake and retention time of licofelone. Moreover, A16 and A87 allow more licofelone to be loaded onto the polymer because of the hydroxyl groups in the repeating units of the polymers. Additionally, the hydroxyl group would form a hydrolysable ester bond with licofelone. This chapter focuses on covalently conjugating licofelone to three characteristically different PBAE polymers (A5, A16, and A87).

3.2 **Materials and methods**

Thionyl chloride (SOCl$_2$), DCC (N,N'-Dicyclohexylcarbodiimide), and NHS (N-Hydroxysuccinimide) were purchased from Sigma-Aldrich. Licofelone was purchased from Santa Cruz Biotechnology. NBQX was ordered from Sigma-Aldrich. Potassium permanganate (KMnO$_4$) was purchased from Fisher Scientific.

3.2.1 **Licofelone conjugation reactions**

The conjugation reaction that was applied to conjugate licofelone to A5 is the acylation reaction using thionyl chloride. However, licofelone was conjugated to A16 and A87 using the coupling reaction DCC with NHS. The primary reason for switching from acylation reaction to coupling reaction was the low yields of A5-licofelone and A16-licofelone conjugates that were obtained after acylation reactions.

3.2.1.1 **Acylation reaction using thionyl chloride**

To activate the licofelone carboxylic acid, we attempted its transformation into its chloride derivative via reaction with thionyl chloride (Figure 3.2).(195) Then, the nucleophilic groups on the A5 polymer attack the carbonyl group of the acyl-licofelone and form a covalent bond. The reaction procedure consisted of dissolving 25 mg of licofelone in 3 ml of DCM, then adding 14.3 µl of SOCl$_2$ (3 equivalents). The reaction was running at 0℃ for an hour, then at room temperature for 5 hours, under argon and magnetic stirring. After 6 hours, the DCM and the excess thionyl chloride were evaporated using a rotary evaporator for 45 minutes. The acyl-licofelone product was dissolved in 5 ml DCM, then added to 5 ml DCM, which contains 75 mg of amino-terminated A5. The reaction mixture was placed at room temperature with magnetic stirring for overnight. Then, the reaction solution was transferred into a 50 ml tube. For purification, 50 ml of diethyl ether was added to precipitate the A5-licofelone conjugate. The free licofelone and other starting materials are soluble in diethyl ether, which has been removed with the supernatant. Therefore, the precipitate of the A5-licofelone conjugate tube was washed three times with diethyl ether. After each wash, the tube was centrifuged for 5 minutes at 1500 rpm, and then the supernatant was removed. The precipitate dried using a rotary evaporator for

45 minutes. The product was analysed by ^{1}H-NMR. Figure 3.2 shows the reaction mechanism of A5-licofelone formation through acylation reactions.

In acyl-licofelone, the aromatic rings protons 6.95 – 7.36 ppm (9H, m), -N-**CH₂**-C 3.71 ppm (2H, s), -C-**CH₂**-C=C 3.45 ppm (2H, s), -**CH₂**-COCl 2.78 (2H, s), and **CH₃**-C-**CH₃** 1.23 ppm (6H, s). In A5-licofelone conjugate, the aromatic rings protons 6.95 – 7.36 ppm (9H, m), 4.0 ppm (8H, br, -COO-**CH₂**-), 3.71 ppm (2H, s, -N-**CH₂**-C), 3.45 ppm (2H, s, -C-**CH₂**-C=C), 3.1 ppm (18H, br, -N-**CH₃**), 2.78 ppm (2H, br, -**CH₂**-CON-), 2.6-2.7 ppm (8H, br, -N-**CH₂**-CH₂-COO-), 2.39-2.48 ppm (8H, m, -OOC-**CH₂**-and -N-**CH₂**-), 2.1 ppm (4H, br, CO-N-**CH₂**-), 1.7-1.8 ppm (6H, br, -N-CH₂**CH₂**-CH₂-N-), 1.6 ppm (8H, br, -OCH₂-**CH₂CH₂**-CH₂O-), and 1.23 ppm (6H, s, **CH₃**-C-**CH₃**).
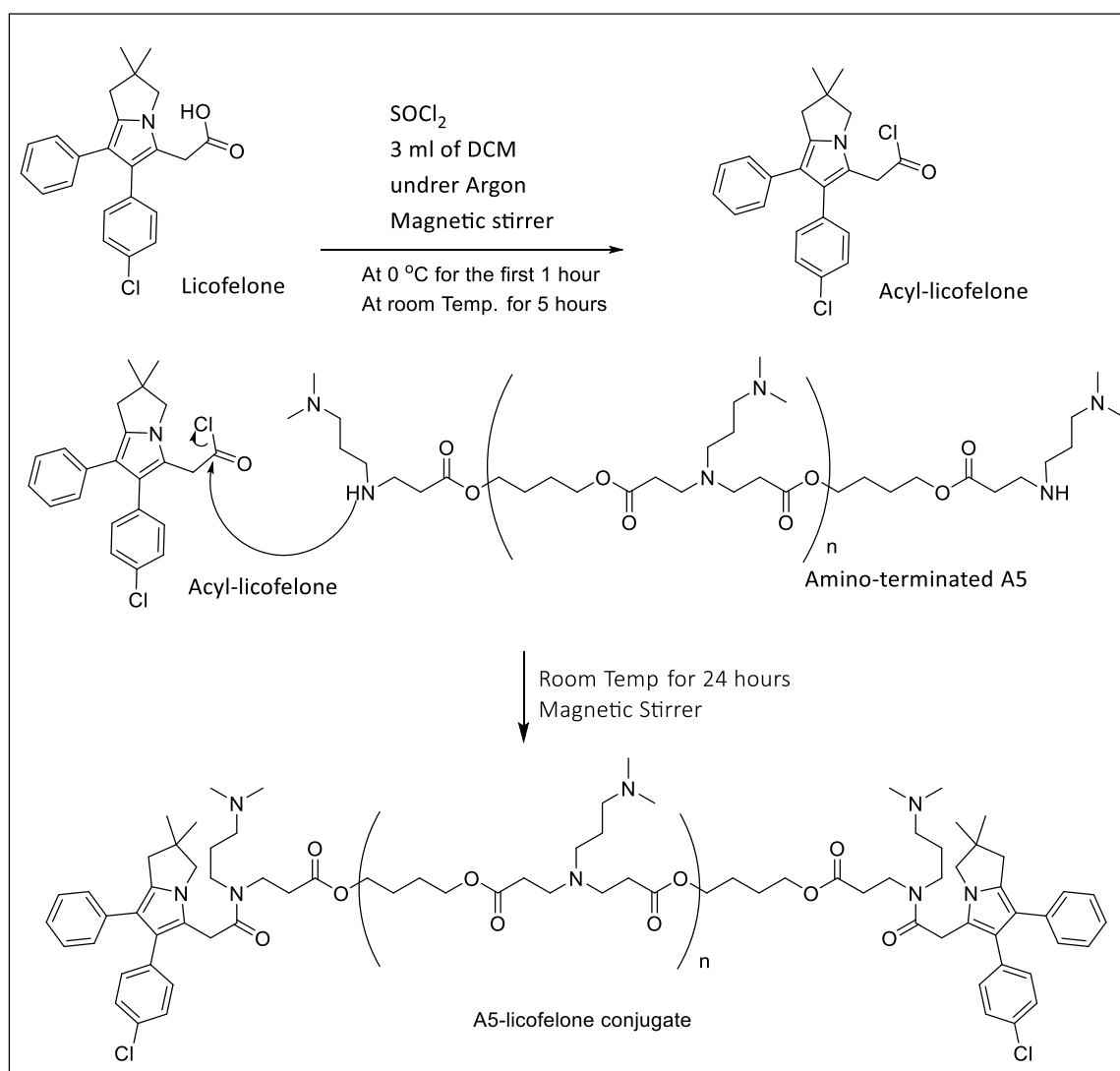
Figure 3.2: The conjugation reaction of licofelone and amino-terminated A5

3.2.1.2 **Coupling reaction using DCC with NHS**

In a 50 ml round bottom flask, 110 mg of amino-terminated A87 or A16, 53 mg of licofelone (3 equivalents), 64 mg of DCC (6.6 equivalents), and 64 mg of NHS (6.6 equivalents) were dissolved in 25 ml of anhydrous DCM. The reaction was at 0 °C for the first 30 minutes, then at room temperature for the next 48 hours under argon and a magnetic stirrer. After 24 hours, there was white precipitate formation of DCU, and the precipitate formation has increased over 48 hours (Figure 3.3). After 48 hours, the solution was filtered using filter papers (185 mm) to remove the DCU precipitate. After filtration, 200 ml of hexane or diethyl ether were added to the reaction mixture to precipitate A16-licofelone and A87-licofelone conjugates, respectively. The supernatant, which contains the unreacted licofelone and other reaction materials, was removed. The precipitates of A16-licofelone and A87-licofelone conjugates were washed with hexane and diethyl ether three times, respectively. After each wash, the supernatant was discarded, then both conjugates were dried using a rotary evaporator for 45 minutes, and the products were analysed by ^{1}H-NMR Figure 3.4 and Figure 3.5 show the reaction mechanism for the formation of A16-licofelone and A87-licofelone conjugates using coupling reagents, respectively.

In A16-licofelone conjugate, the aromatic rings protons 6.95 – 7.36 ppm (10H, m), 4.0 ppm (14H, s, -COO-C**H₂**-), 3.7 ppm (1H, s, -N-C**H₂**-C), 3.47 ppm (1H, s, -C-C**H₂**-C=C), 3.3 ppm (6H, m, -N-CH₂CH₂-C**H₂**-OH), 2.9 ppm (2H, br, -C**H₂**-COO-CH₂), 2.7-2.8 ppm (8H, br, -N-C**H₂**-CH₂-COO-), 2.35-2.48 ppm (14H, br, -OOC-C**H₂**- and N-C**H₂**-), 1.6 ppm (8H, br, -OCH₂-C**H₂**C**H₂**-CH₂O-), 1.4 ppm(6H, br, -N-CH₂C**H₂**-CH₂-OH), and 1.23 ppm (6H, s, C**H₃**-C-C**H₃**). In A87-licofelone conjugate, the aromatic rings protons 6.95 – 7.36 ppm (10H, m), 4.0 ppm (20H, br, -COO-C**H₂**-), 3.7 ppm (1H, s, -N-C**H₂**-C), 3.47 ppm (1H, s, -C-C**H₂**-C=C), 2.7 ppm (2H, br, -C**H₂**-COO-CH₂), 2.6-2.7 ppm (8H, br, -N-C**H₂**-CH₂-COO-), 2.3-2.4 ppm (14H, br, -OOC-C**H₂**- and -N-C**H₂**-), 1.6 ppm (8H, br, -OCH₂-C**H₂**C**H₂**-CH₂O-), 1.4-1.5 ppm(2H, m, -N-CH₂C**H₂**-CH₂-N-), and 1.23 ppm (6H, s, C**H₃**-C-C**H₃**).
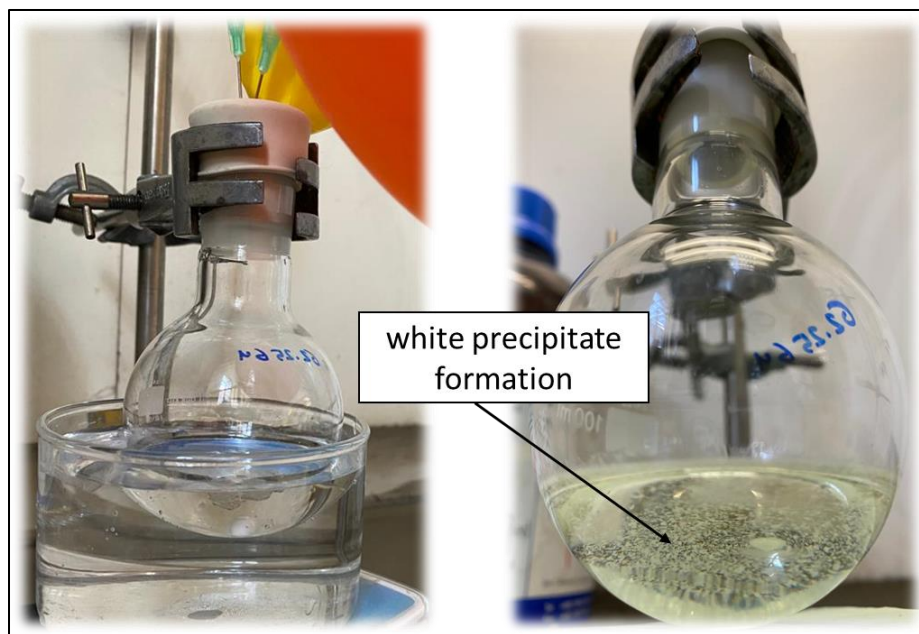
Figure 3.3: The DCC conversion to DCU, which appears as a white precipitate
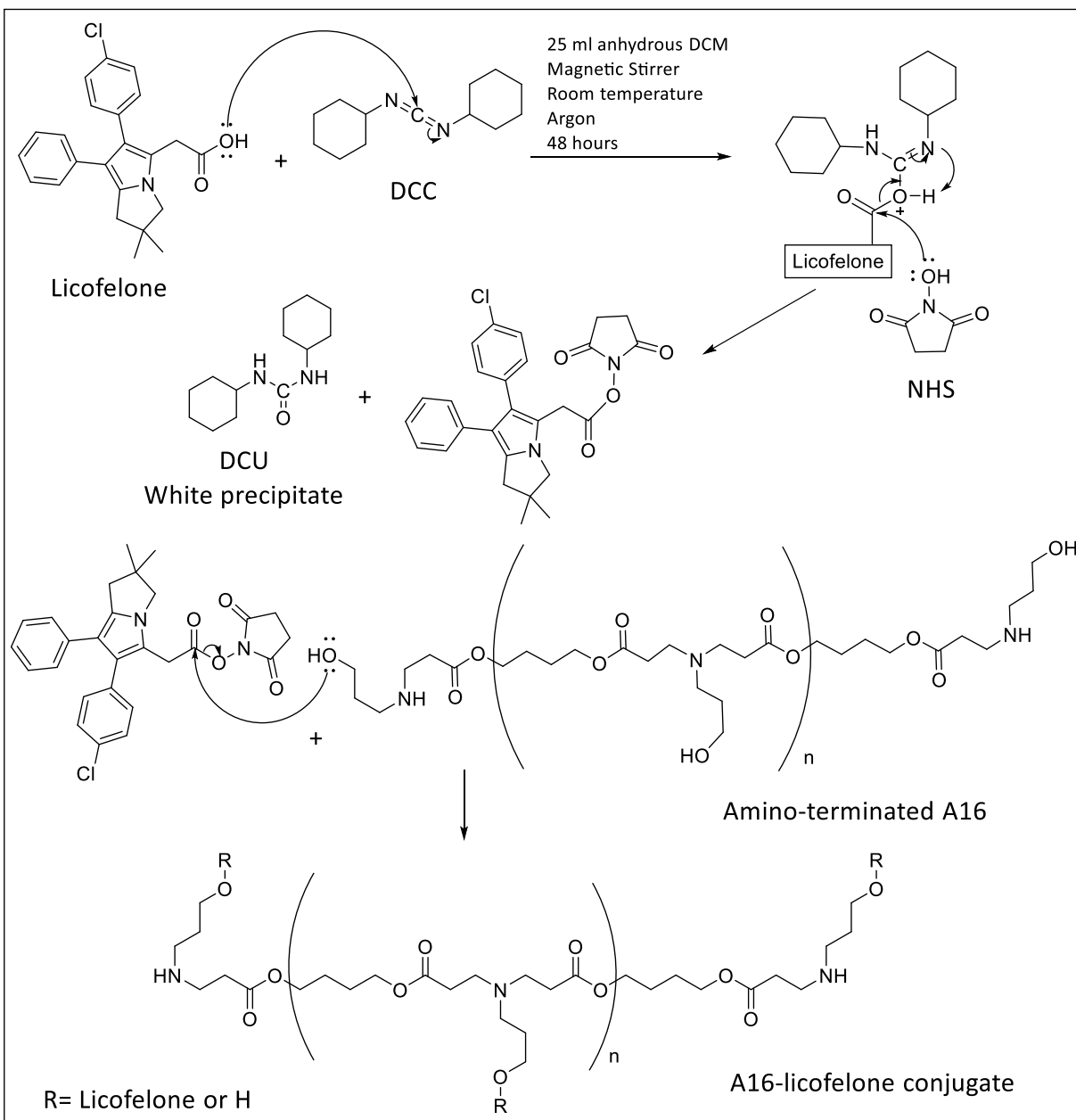
Figure 3.4: The conjugation reaction mechanism of licofelone with amino-terminated A16 using DCC/NHS
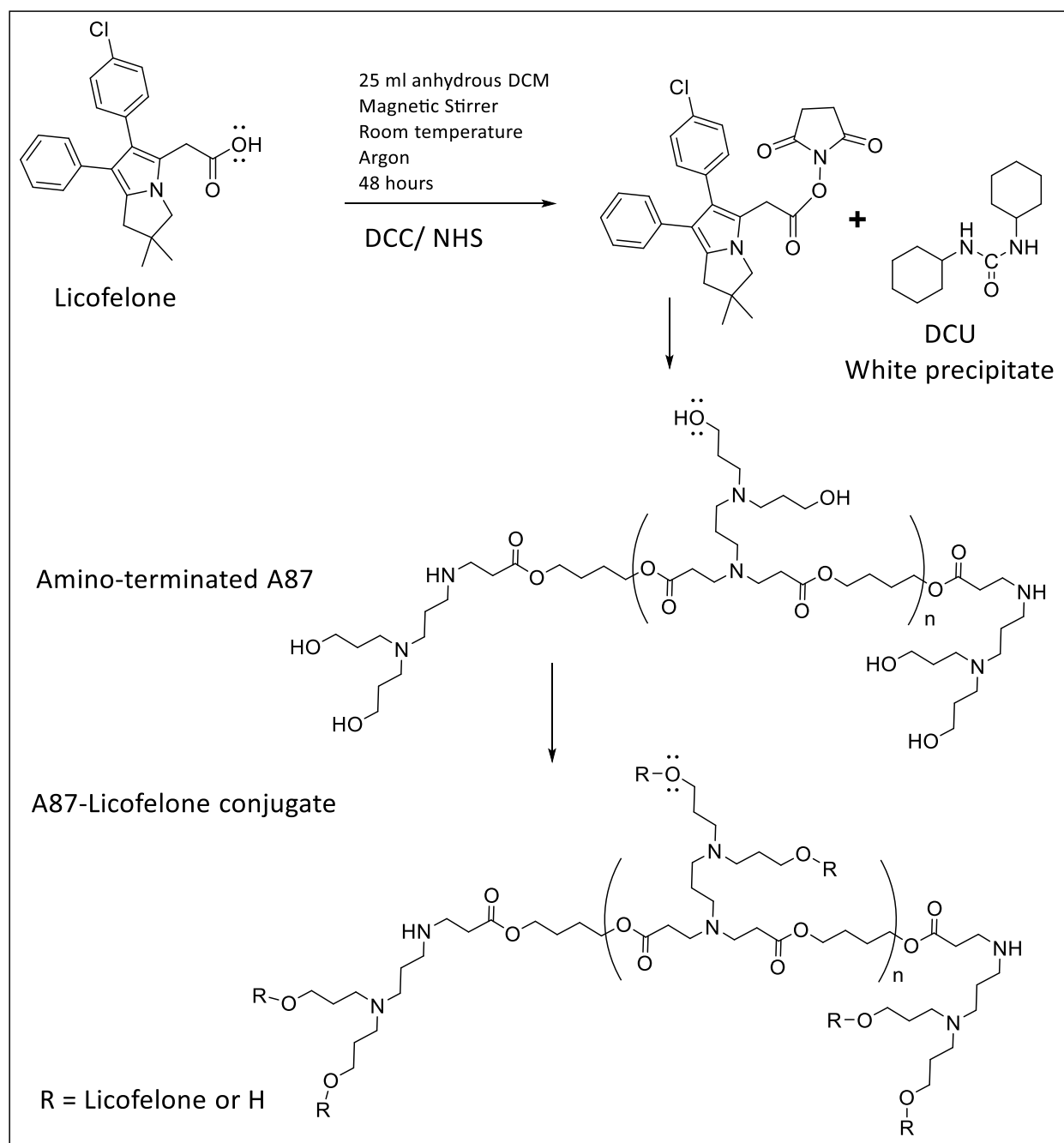
Figure 3.5: The reaction of licofelone with amino-terminated A87

3.2.2 **The net surface charge**

Malvern Zetasizer nano ZS (Malvern Instruments Limited) was used to measure the net surface charge of A5-, A16-, and A87-licofelone conjugates at physiological pH (7.4). The three conjugates were prepared at a concentration of 2 mg/ml of PBS buffer. Moreover, the surface charge of NBQX was determined at a concentration of 0.95 mg/ml (2.5 mM) in PBS buffer, whereas the surface charge of licofelone was measured at 1 mg/ml in 50% PBS buffer and 50% DMSO. 1 ml of the prepared solution was placed in a zeta potential cuvette. The PBS buffer was prepared following the previous procedure, which was mentioned in 2.2.2. The outcome of the surface charge is an indication of the polymer surface charge as explained previously (2.2.3.3).

3.3 Results

The interpretation of ^{1}H-NMR of acyl-licofelone and A5, A16, and A87-licofelone conjugates was based on the ^{1}H-NMR of reactants.

3.3.1 Licofelone conjugation reaction using thionyl chloride

The reaction product of A5-licofelone conjugate was analysed using proton NMR. The overlay of both licofelone and acyl-licofelone ^{1}H-NMR spectra show the disappearance of the carboxylic acid proton at 12.5 ppm (red spectra) after the acylation reaction (Figure 3.6). Other proton signals of licofelone and acyl-licofelone were identical. At 6.95 – 7.4 ppm appear the proton signals of the aromatic rings protons in licofelone and acyl-licofelone. The protons signal of (-N-CH_2-C) appears at 3.71 ppm, and the proton signal of (-C-CH_2-C=C) appears at 3.45 ppm. The signal at 2.78 is linked to the protons on the α-carbon next to the carboxylic acid or next to the acyl chloride. Additionally, the protons signal of (CH_3-C-CH_3) appears at 1.23 ppm for both molecules. There was no signal for the carboxylic acid proton on the ^{1}H-NMR spectra of acyl-licofelone, which confirms the formation of acyl-licofelone.
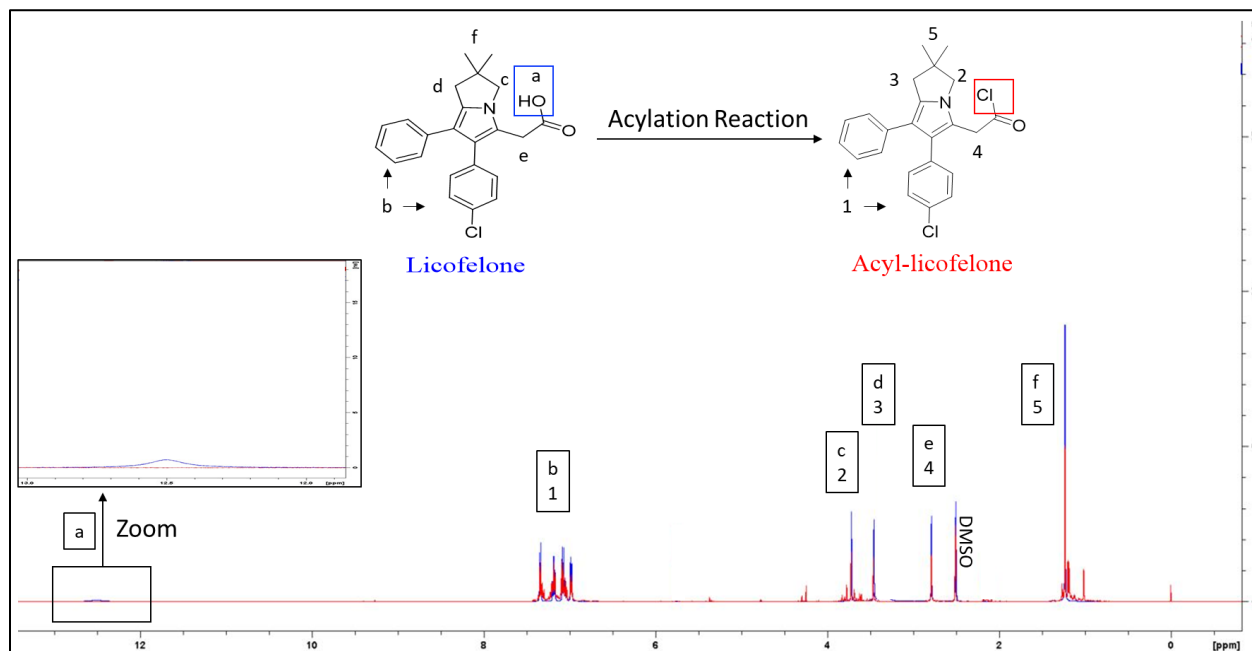
Figure 3.6: Overlay of the ^{1}H-NMR spectrum (500 MHz, DMSO-d6) of licofelone (blue) and acyl-licofelone (red)

Figure 3.7 shows the ^{1}H-NMR spectrum of the A5-licofelone conjugate. The appearance of licofelone proton signals in the ^{1}H-NMR spectrum of the conjugation reaction product after multiple washes confirms the conjugation of licofelone to A5. The aromatic ring protons signals were at 6.95 – 7.4 ppm, the protons signal of (-N-C**H₂**-C) was at 3.71 ppm, the protons signal of (-C-C**H₂**-C=C) was at 3.45 ppm, the protons signal of (-C**H₂**-C=O-) was at 2.78 ppm, and the protons signal of (C**H₃**-C-C**H₃**) was at 1.23 ppm. Additionally, the A5 polymer proton signals appeared in the A5-licofelone conjugates. The protons signal at 4.0 ppm is corresponding to (-C**H₂**-O-CO-), the proton signal at 2.45 - 2.48 ppm is corresponding to (-C**H₂**-N-), the protons signal at 2.39-2.47 ppm is corresponding to (-C**H₂**-COO-), the proton signal at 1.6 ppm is corresponding to (-C**H₂**-C**H₂**-), and the protons signal at 1.8 ppm is corresponding to (-N-CH₂CH₂CH₂-N-). The proton signal at 2.1 ppm is for the proton next to the newly formed amide bond (CO-N-C**H₂**-). The key peaks are the proton of the aromatic ring and the proton of *alpha*-carbon next to the amide group, which further confirm the conjugation of licofelone and the A5 polymer. The yield of the reaction was 10 – 15 mg.
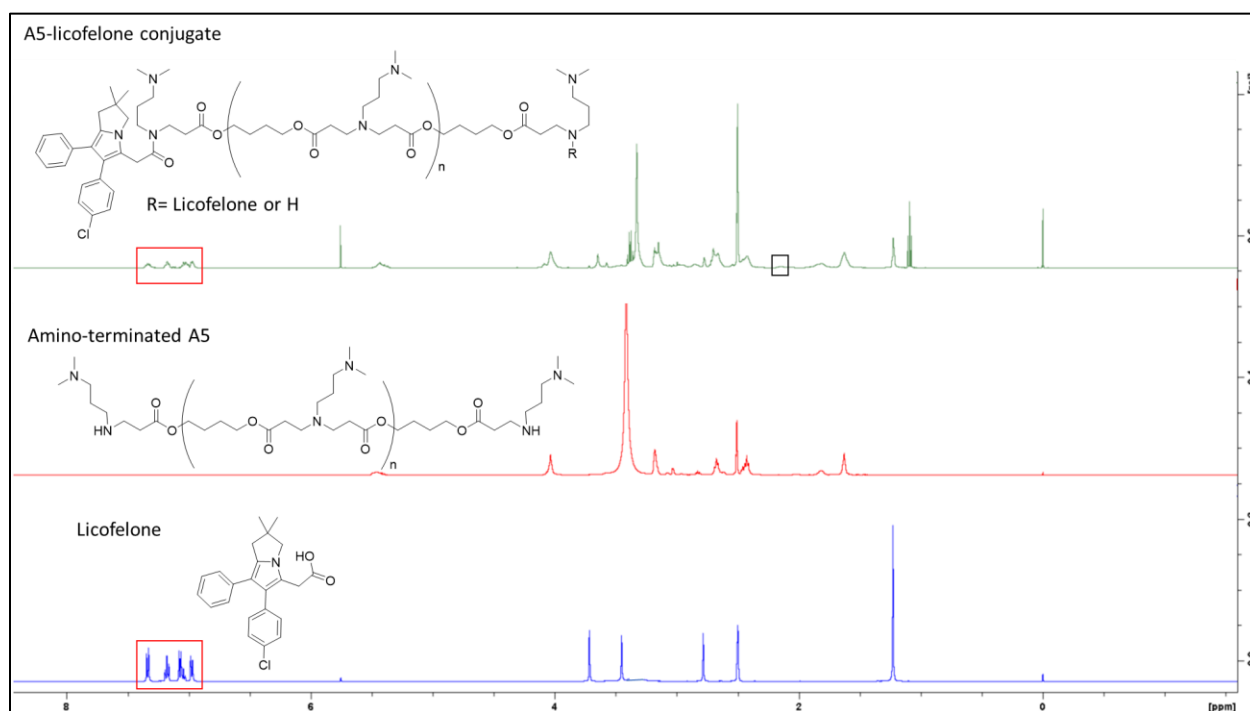
Figure 3.7: Overlay of the ^{1}H-NMR spectrum (500 MHz, DMSO-d6) of A5-licofelone, A5 polymer, and licofelone

3.3.2 Licofelone conjugation reaction using DCC with NHS

Figure 3.8 and Figure 3.9 show the ^{1}H-NMR spectra of the A16-licofelone and the A87-licofelone, respectively, which confirm the formation of the conjugates. The disappearance of the carboxylic acid proton signal of licofelone at 12.5 ppm and the appearance of licofelone aromatic rings protons peaks at 6.95 – 7.4 ppm on the ^{1}H-NMR spectra confirm the formation of A16-licofelone and A87-licofelone conjugates. Additionally, the other licofelone proton signals appear at 3.71 ppm, 3.45 ppm, 2.78 ppm, and 1.23 ppm on ^{1}H-NMR spectra of the A16-licofelone conjugate, which further confirm the conjugate formation. Similar signals were observed on the ^{1}H-NMR spectra of the A87-licofelone conjugate. Furthermore, the proton signals of A16 and A87 polymers appear in the ^{1}H-NMR spectra of their respective licofelone conjugates. Significantly, the conjugation reaction of A16 or A87 to licofelone using DDC/NHS has produced a high yield. The yield of A16-licofelone conjugate was 102.4 mg, and the yield of A87-licofelone conjugate was 111.8 mg.
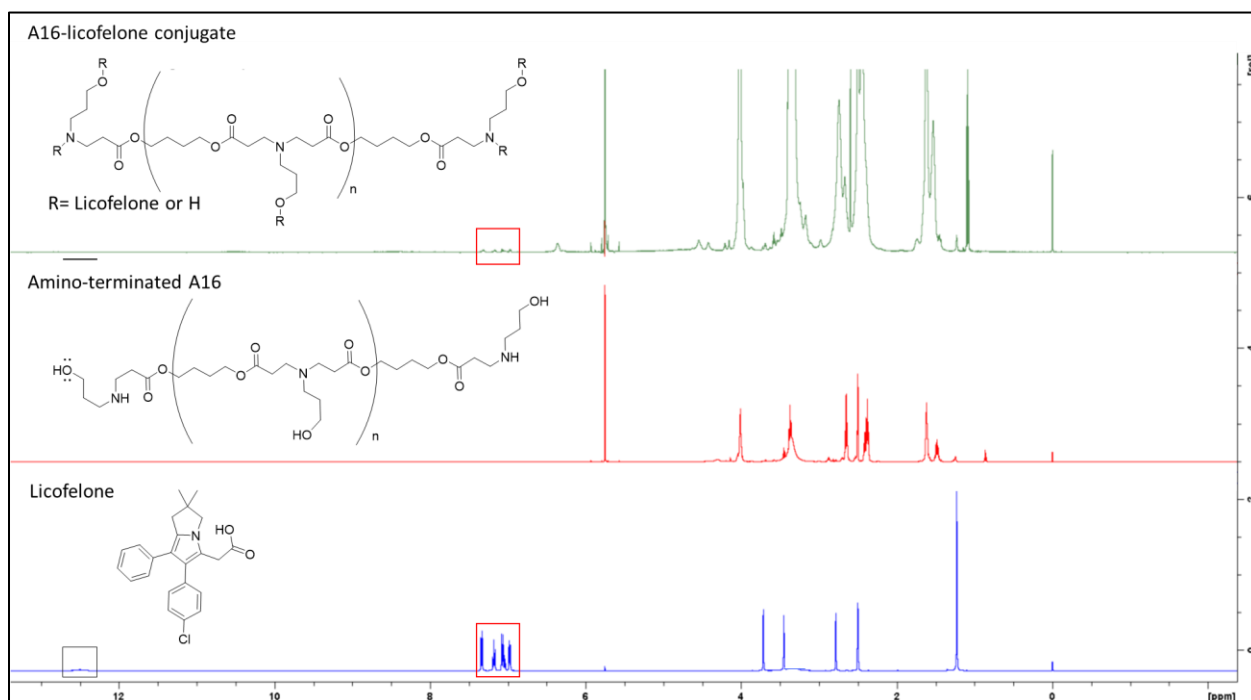
Figure 3.8: Overlay of the ^{1}H-NMR spectrum (500 MHz, DMSO-d6) of A16-licofelone, A16 polymer, and licofelone
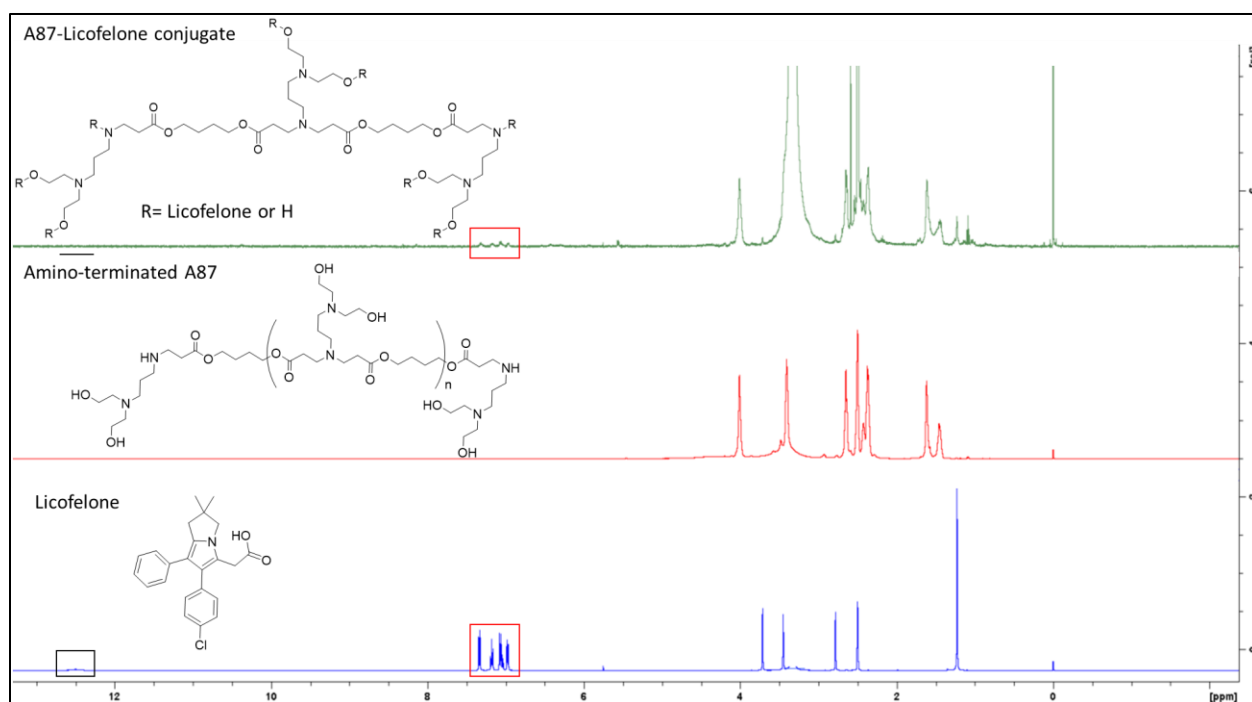
Figure 3.9: Overlay of the ^{1}H-NMR spectrum (500 MHz, DMSO-d6) of A87-licofelone, A87 polymer, and licofelone

3.3.3 **The net surface charge**

Table 3.1 shows the net surface charge of A5, A16, and A87-licofelone conjugates, NBQX, and licofelone at physiological pH. The net surface charge was measured to confirm that the PBAE-licofelone conjugates are positively charged at pH 7.4 and to investigate the influence of the conjugation on the polymer charge. A5 polymer surface charge is 12 ± 3 mV, which has been reduced after licofelone conjugation to be 9 ± 3 mV. The reason for the positive charge reduction could be related to the licofelone net surface, which is negative (9 ± 2 mV), or to the transformation of the terminal secondary amines to amide after the conjugation reaction. However, A16 and A87 polymers surface charges, which was 7 mV have been increased after licofelone conjugation to be 15 ± 2 mV and 12 mV, respectively. The primary reason for the higher surface charges could be associated with converting multiple hydroxyl groups to ester after the conjugation reaction. Significantly, the variation of the licofelone conjugates positive charge was expected and it was essential to investigate the impact of the positive charge on the licofelone uptake and retention time within the cartilage. Additionally, the change of the polymer surface charges is further evidence of successful conjugate formation.

Table 3.1: The net surface charge of A5, A16, and A87-licofelone conjugates, NBQX, and licofelone at pH 7.4 (Mean ± SD)

Compound	Surface charge in pH 7.4
A5-licofelone	9 ± 3 (mV)
A16-licofelone	15 ± 2 (mV)
A87-licofelone	12 (mV)
NBQX	- 17 ± 1 (mV)
Licofelone	- 9 ± 2 (mV)

3.4 **Discussion**

This chapter concentrates on conjugating A5, A16, and A87 polymers to NBQX and licofelone through a hydrolysable covalent bond. These conjugates aid in determining the effect of A5, A16, and A87 polymers on the uptake and retention time of drug within cartilage.

3.4.1 **Attempts to NBQX conjugation reaction**

Conjugating NBQX to A5 polymer was challenging because the reaction condition must be maintained to avoid polymer degradation, oxidation, or structure alteration. Therefore, we have adapted various strategies to covalently conjugate NBQX to A5. Briefly, several conjugation attempts have failed. At the beginning, we wanted to conjugate NBQX directly to the amino groups on the A5 polymer using reagents such as dimethyl malonate and acrylate ester, which have been used previously to crosslink polymers (Figure 3.10).(196-199) The principle behind this selection is that the amine of the sulphonamide group attacks the carbonyl carbon of the dimethyl malonate, then the methanol evaporates, which will be the driving force of the reaction. In the case of the acrylate ester, the amine on the A5 polymer attacks the acrylate moiety, and the NBQX attacks the ester side of the reagent.(196, 200) However, the NMR spectra showed no signals in the aromatic peak ranging from 6.8 to 7.5 ppm after the conjugation reactions, which correspond to the aromatic protons in the NBQX. Therefore, 1,8-Diazabicyclo[5.4.0]undec-7-ene (DBU) or 4-Dimethylaminopyridine (DMAP) was added to the reaction medium as a catalyst.(201, 202) Unfortunately, the reaction was unsuccessful, according to the NMR spectra. We concluded that the reason could be related to steric hindrance since the sulphonamide group in the NBQX could be in close proximity to the A5 polymer chain. Therefore, we decided to react NBQX with succinic anhydride first, and then the NBQX-succinate will be conjugated to the A5 polymer. The succinate will provide a five carbons chain between NBQX and A5 to reduce the hindrance, which has been applied previously.(143) However, the reaction of NBQX with the succinic anhydride was not successful. Therefore, we decided to use licofelone instead of NBQX since we cannot proceed with the NBQX conjugation plan. Additionally, it is not possible to perform any further experiments using more NBQX since it is an expensive molecule.
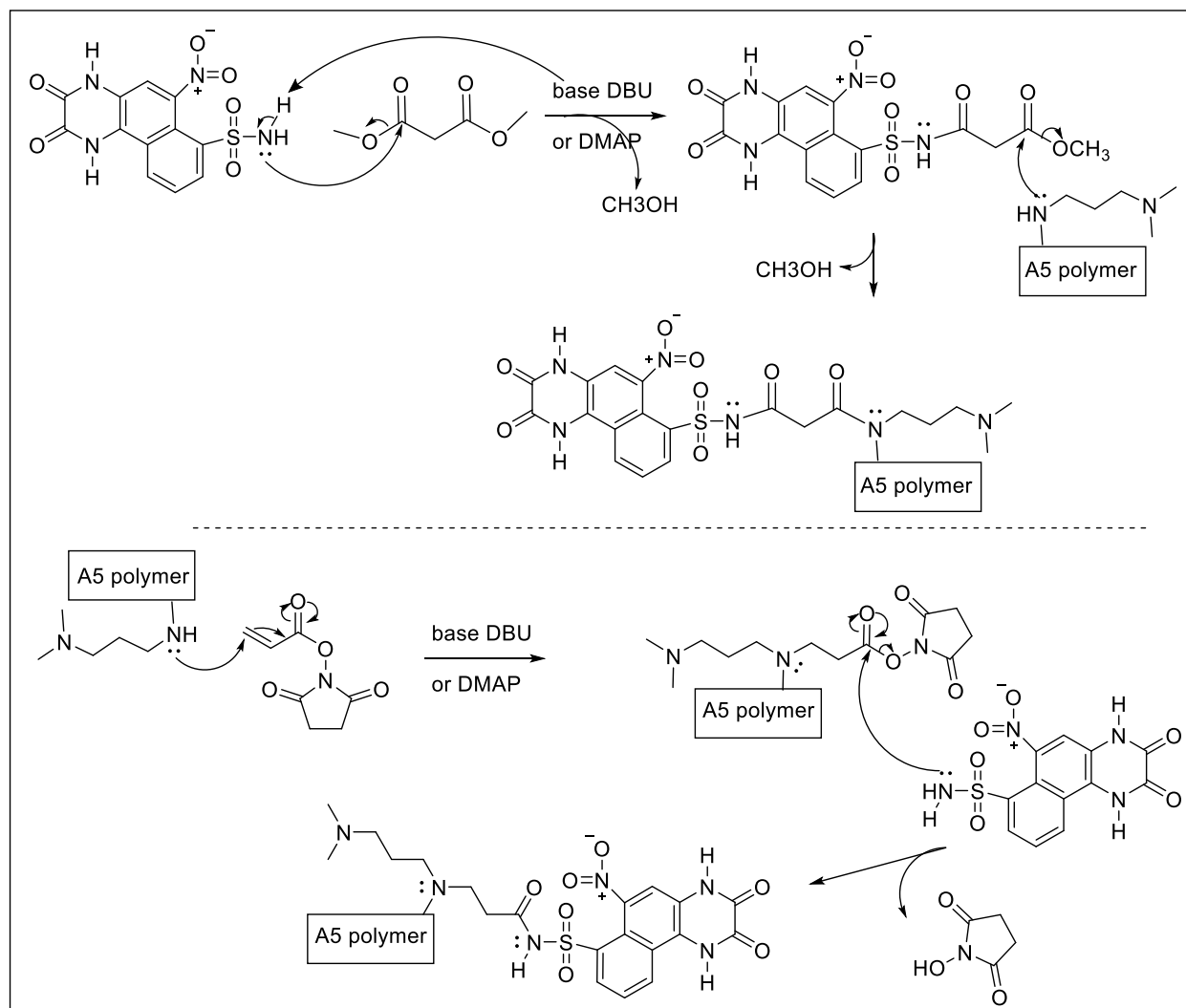
Figure 3.10: The reaction attempts to conjugate NBQX to the amino-terminated A5

3.4.2 Licofelone conjugation reaction

Licofelone was conjugated to A5 via an acylation reaction using thionyl chloride, and the ¹H-NMR spectra of the product have confirmed the formation of A5-licofelone. The conjugation of licofelone by the acylation reaction has produced 10 – 15 mg of A5-licofelone. The low yield could be associated with a possible formation of di-licofelone anhydride, which is the result of two licofelones reacting together.(203) The formation of di-licofelone anhydride occurs when a second licofelone molecule attacks the acyl-chloride group in the acyl-licofelone (Figure 3.11).(203) Although there is a possibility of di-licofelone anhydride formation, the anhydride product can be conjugated to A5. However, the di-licofelone anhydride formation results in licofelone waste, since the licofelone containing the carboxylic acid group will be the living group and will be washed with diethyl ether during the purification processes. Licofelone is a precious drug, so we decided to seek another conjugation reaction to obtain a higher yield, which was the DCC coupling reaction.
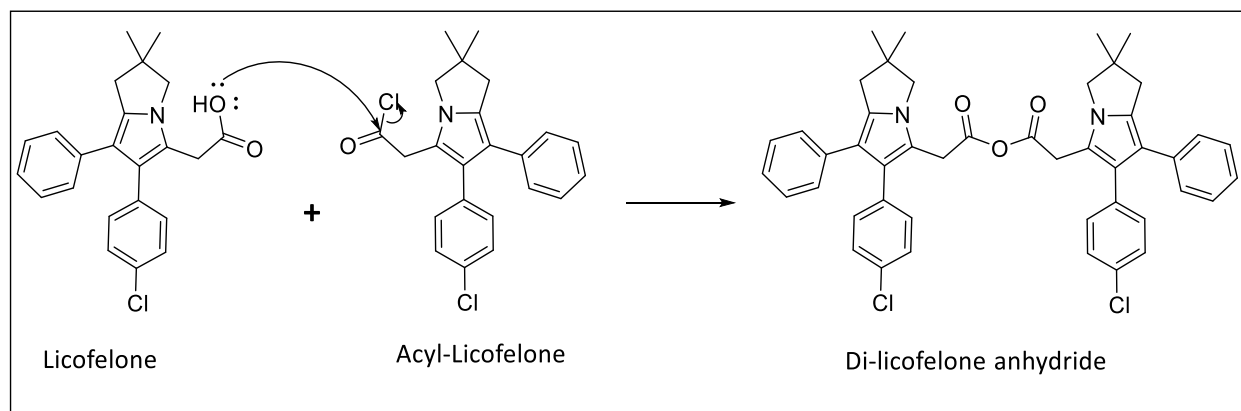
Figure 3.11: The anhydride-licofelone formation form the reaction of licofelone and acyl-licofelone

The purpose of using DCC and NHS is to convert the carboxylic acid group of licofelone to an ester with a good leaving group, which was reported in the reaction mechanism (Figure 3.4). The nucleophilic functional groups on the A16 and A87 polymers will attack the carbonyl carbon of the ester and form their respective conjugates. DCC was chosen as a coupling agent for the conjugation reaction because DCC is a common coupling reagent for esterification reactions, and DCC converts to DCU (Dicyclohexylurea) as a by-product of the esterification reactions.(204-206) Significantly, the DCU is insoluble in dichloromethane (DCM) and forms a white precipitate, which

is easily removed using filter paper.(205, 206) Additionally, the precipitation of DCU drives the reaction in one direction and could be an indication of a successful reaction. The NHS was added to the reaction because the DCC-carboxylic acid intermediate is not very stable.(204) DCC-carboxylic acid intermediate could be hydrolysed back to carboxylic acid and DCU by water molecules.(204) The NHS reacts with the DCC-carboxylic acid intermediate and forms a more stable NHS-ester molecule.(204) Therefore, DCC and NHS were adapted as coupling agents for the future conjugation of A16 and A87 to licofelone to avoid wasting licofelone and obtain a higher yield, which was 102.4 mg and 111.8 mg, respectively. The yield of both conjugates is 10 times higher than the conjugates produced from the acylation reaction. The ^{1}H-NMR spectra of the products after purification have confirmed A16-licofelone and A87-licofelone formation using the DCC/NHS coupling reaction.

3.4.3 The net surface charge

Significantly, the net surface charge of A5-licofelone, A16-licofelone, and A87-licofelone conjugates was positive with different degrees (Table 3.1). Although licofelone was highly negatively charged, the conjugation to highly positively charged A5, A16, and A87 polymers has masked the negative charge and the lipophilicity of licofelone. Accordingly, the results have supported the current study hypothesis that the positively charged PBAE polymers can mask the negative charge and the lipophilicity of DMOADs, which will reduce the cartilage-repellence activity against the drug. The negative charge of licofelone was derived by the carboxylic acid, which is also the conjugation point of licofelone to the polymers. Therefore, after conjugation, the carboxylic acid is converted to a neutral functional group (ester or amide). Furthermore, after conjugation, licofelone blocked multiple hydroxyl groups on the polymer backbone, increasing the net surface positive charge of A16 and A87 polymers. However, the A5 polymer's overall positive charge was reduced after conjugation because the secondary amines were the conjugation point. The variation of the conjugates' net surface charge will allow observing the effect of the positive charge on the uptake and retention time of licofelone.

3.5 Conclusion

The primary aim of the study was to increase the uptake and retention time of DMOADs within the cartilage after covalent conjugation to A5, A16, and A87 polymers. Since licofelone is considered a DMOADs model, the increase in licofelone uptake and retention time after conjugation will be considered an increase in DMOADs. This chapter showed the development of an optimised reaction method for conjugation and confirmed the formation of A5-licofelone, A16-licofelone, and A87-licofelone conjugates. These conjugates will be involved in the uptake and retention time studies to analyse the effect of A5, A16, and A87 polymers on the conjugated licofelone uptake and retention time within the cartilage. Additionally, the variation of the net positive charge of the conjugates will allow analysis of the effect of the positive charge on the drug uptake and retention time. In order to perform these studies, we must develop cartilage models and a quantification method for licofelone, which will be the focus of the next chapter's experimental work.

Chapter 4: **Quantification Methods and *Ex-vivo* OA Cartilage Model Development**

4.1 **Introduction**

This chapter includes the essential works for the project, such as the development of a reverse phase high-performance liquid chromatography (RP-HPLC) quantification method for NBQX and licofelone. The quantification method will determine the quantity of the drug after the uptake and retention time studies as well as the release study of the drug from the conjugates. The RP-HPLC methods for NBQX and licofelone quantifications were developed based on the calibration curves of their standards. The RP-HPLC was preferred because the samples after the experiment will require a separation of the drug from other compounds involved in the experiment prior to the quantification to avoid compound reading interference. Furthermore, this chapter will include the development of an *ex-vivo* bovine cartilage model for the uptake and retention time studies. Regarding the cartilage models, bovine cartilage is a suitable model for the studies because of its structural similarity to human cartilage as well as the fact that it is the most used model in the literature that has investigated cartilage uptake and retention time studies.(140, 143, 172, 185, 207) The bovine cartilage was treated with trypsin-protease to mimic the cartilage content loss that was observed in the early stages of OA.(143, 208, 209) Furthermore, the cartilage content loss was determined based on quantifying the glycosaminoglycan (GAG) content and collagen content. Developing a healthy cartilage model and an early simulated OA cartilage model assists in observing the behaviour of the polymer-licofelone conjugates in both conditions. In addition, the cartilage content depletion effect on the conjugates' uptake and retention would support our hypothesis that the positively charged conjugates will electrostatically interact with negatively charged cartilage content.

4.2 Materials and methods

The materials that were purchased from Fisher Scientific are phosphate buffered saline (PBS) tablets, acetic acid, citric acid, anhydrous sodium acetate, sodium hydroxide, and HPLC grade acetonitrile (ACN). Sodium acetate trihydrate was purchased from Honeywell. Trypsin powder was purchased from Gibco. Papain, Chloramine T reagent, ethylenediaminetetraacetic acid (EDTA), perchloric acid, p-dimethylaminobenzaldehyde (DMAB), and hydroxyproline were purchased from Sigma-Aldrich. Dithiothreitol (DTT) was purchased from IBI Scientific. The order of n-propanol was from Alfa Aesar. Glycine was ordered from Lancaster. The cartilage media materials that were purchased from Thermo Fisher Scientific are Dulbecco's Modified Eagle Medium (DMEM 11885-084), insulin-transferrin-selenium, and minimum non-essential amino acids (MEMNEAA) by Gibco. Penicillin/streptomycin, amphotericin B, and proline were purchased from Sigma Aldrich.

4.2.1 NBQX quantification method

RP-HPLC was used for NBQX quantification (Shimadzu, LC-2030C Plus). A serial dilution of NBQX standard in PBS was prepared to develop the calibration curve (Figure 4.1). Table 4.1 shows the RP-HPLC parameters of NBQX quantification method.

Table 4.1: The RP-HPLC parameters of NBQX quantification method

Stationary Phase	Kinetex 5µm C18 100 Å, LC Column 250 x 4.6 mm
Mobile Phase	85% of AcOH/NaOAc pH 5 & 15% ACN
Flow Rate	1 ml/min
Column Temperature	25°C
Wavelength of the UV-detector	254 nm
Injection Volume	10µl
Experiment time	15 min
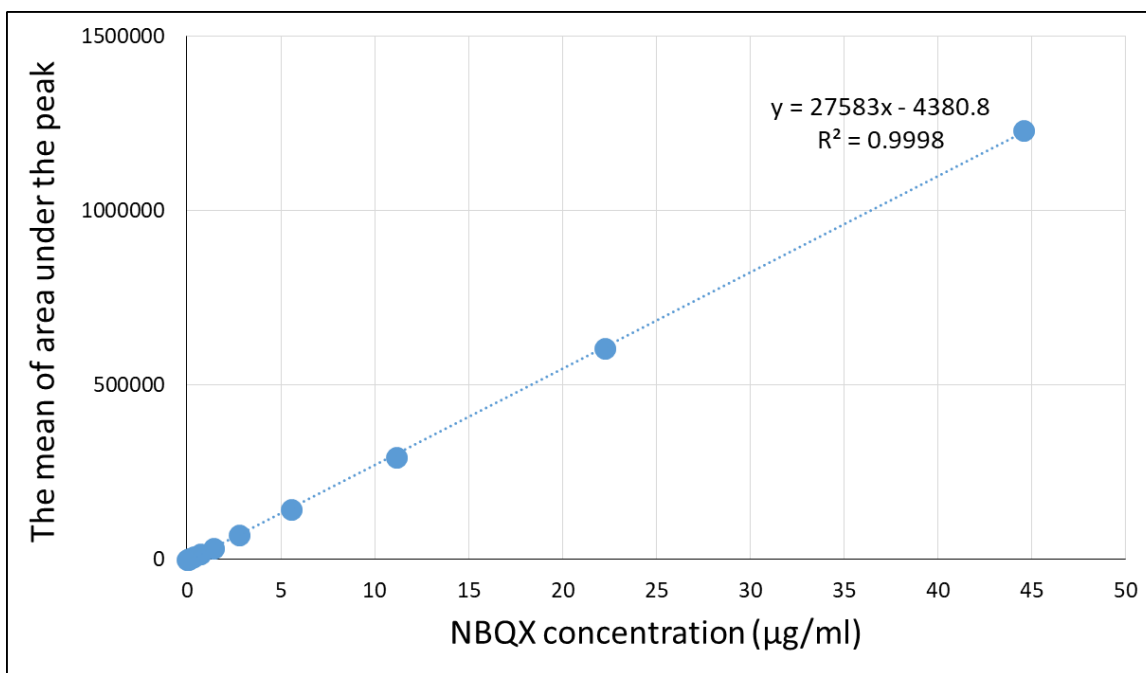
Figure 4.1: The calibration curve of NBQX

Bars represent (Mean ± SD of n=2)

4.2.2 Licofelone quantification method

A calibration curve of standard licofelone was developed using the RP-HPLC technique (Shimadzu, LC-2030C Plus). A serial dilution of the licofelone standard was dissolved in DMSO and PBS pH 7.4 (50%:50%, **v:v**) for the calibration curve development (Figure 4.2). Table 4.2 shows the RP-HPLC parameters of the licofelone quantification method.

Table 4.2: The RP-HPLC parameters for licofelone quantification method

Stationary Phase	Kinetex 5µm C18 100 Å, LC Column 250 x 4.6 mm
Mobile Phase	PBS pH 7.4 and ACN (50%:50%, v:v)
Flow Rate	1 ml/minute
Column Temperature	25℃
Wavelength of the UV-detector	248 nm (based on the manufacturer recommendation)
Injection Volume	10µl
Experiment time	18 min
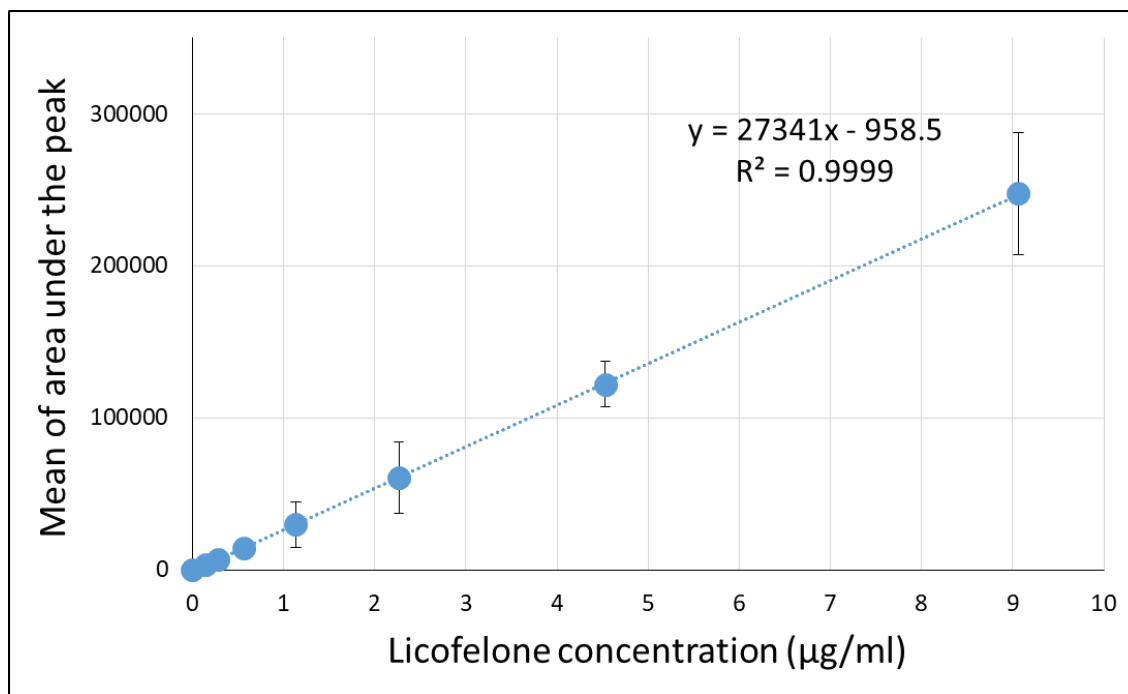
Figure 4.2: The calibration curve of licofelone

Bars represent (Mean ± SD of n=2)

4.2.3 The conjugated licofelone release studies

The licofelone conjugates solution was prepared at a concentration of 3 mg/ml in a mixture of 75% PBS and 25% DMSO (**v:v**). During the first day, the licofelone quantity was measured hourly. Following that, the quantity of the released licofelone was determined at 24, 48, 72, 96, and 120 hours. The unknown licofelone quantity was determined based on the licofelone calibration curve using the exact RP-HPLC method (Figure 4.2 and Table 4.2).

4.2.4 The preparation of buffers and reagents

Buffer pH was measured by a pH meter (Hanna HI-2002 Edge®). Buffers and reagents were prepared according to the following procedures:

- PBS buffer (pH 7.4) and sodium acetate buffer (pH 5) were prepared following the previously reported procedure in 2.2.2.
- Trypsin solution contains 1 mg of trypsin powder per 1 ml of PBS buffer, pH 7.4.
- Digestion buffer was prepared by mixing 2 mM of DTT and 0.3 mg/ml of papain at pH 6.8 buffer, which contains 20 mM sodium phosphate buffer and 1 mM of EDTA.(210)
- The dimethyl-methylene blue (DMMB) reagent was prepared according to the last modification by the Farndale group.(210) The reagent solution contained 3.04 g of glycine, 2.37 g of NaCl, and 95 ml of 0.1 M HCl, which were added to 1000 ml of dH_2O, followed by 16 mg of DMMB.
- The preparation of solutions that were used in measuring collagen content experiments according to the Athanasiou group.(211)

  o Buffer (pH 6 buffer) was prepared by adding 46.1 g of citric acid anhydrous, 119.75 g of sodium acetate trihydrate, 72.19 g of sodium acetate anhydrous, 34 g of sodium hydroxide, and 12 ml of acetic acid in 1000 ml of dH_2O.

  o The assay buffer was obtained by combining n-propanol, dH_2O, and pH 6 buffer in a 2:3:10 ratio.

  o The chloramine T reagent was prepared by adding 0.14 g of chloramine T to a solution containing 500 μl dH_2O, 4 ml pH 6 buffer, and 500 μl n-propanol.

4.2.5 The preparation of cartilage complete medium

The complete medium contains 500 ml of DMEM, 5 ml of insulin-transferrin-selenium, 5 ml of penicillin/streptomycin, 5 ml of MEMNEAA, 0.5 ml of amphotericin B, 0.5 ml of ascorbic acid, and 0.5 ml of proline. The 250 µg of amphotericin B, 20 mg of ascorbic acid, and 4 moles of proline were individually prepared in 1 ml of sterile PBS buffer pH 7.4.(185)

4.2.6 The harvest of bovine cartilage

The cartilages were harvested from the metacarpophalangeal joint (MCP joint) of an immature bovine, which was collected from a local abattoir (Figure 4.3). A 5 mm dermal punch was used to obtain cylindrical cartilage discs with a 5 mm diameter and approximately 0.5 mm thickness. The cartilage was pre-equilibrated in deionized water.(140, 143, 185)

Figure 4.3: The cartilage collection steps

4.2.7 The *ex*-vivo bovine cartilage model of healthy and early simulated OA

The harvested cartilage was considered a healthy cartilage model, whereas for an early simulated OA cartilage model, the healthy cartilage was treated with 1 mg/ml trypsin (a protease enzyme) for 24 hours.(143, 209) The cartilage was placed in an Eppendorf vial containing 500 µl of trypsin solution for 24 hours at 37°C. In order to confirm the depletion of cartilage contents, the glycosaminoglycan content and the collagen content were measured.

4.2.7.1 The measurement of glycosaminoglycan (GAGs) content

Glycosaminoglycan content was measured using the dimethyl-methylene blue (DMMB) assay.(210) The DMMB assay is a colorimetric assay that forms a complex with the sulfated-GAGs, which change its colour density, and the colour density is proportional to the sulfated-GAGs

content in the cartilage. A calibration curve was conducted using a chondroitin sulphate standard to assist in measuring the chondroitin sulphate within non-treated and trypsin-treated cartilage (Figure 4.4). The concentration range of the chondroitin sulphate standard was from 10 to 60 µg/ml in dH_2O. The procedure of the DMMB assay is adding 40 µl of chondroitin sulphate standards, non-treated digested cartilage (control), trypsin-treated digested cartilage, or dH_2O with digestion buffer (blank) in a 96-well plate, followed by 200 µl of DMMB. Then, the colour density was measured using a plate reader at 525 nm.
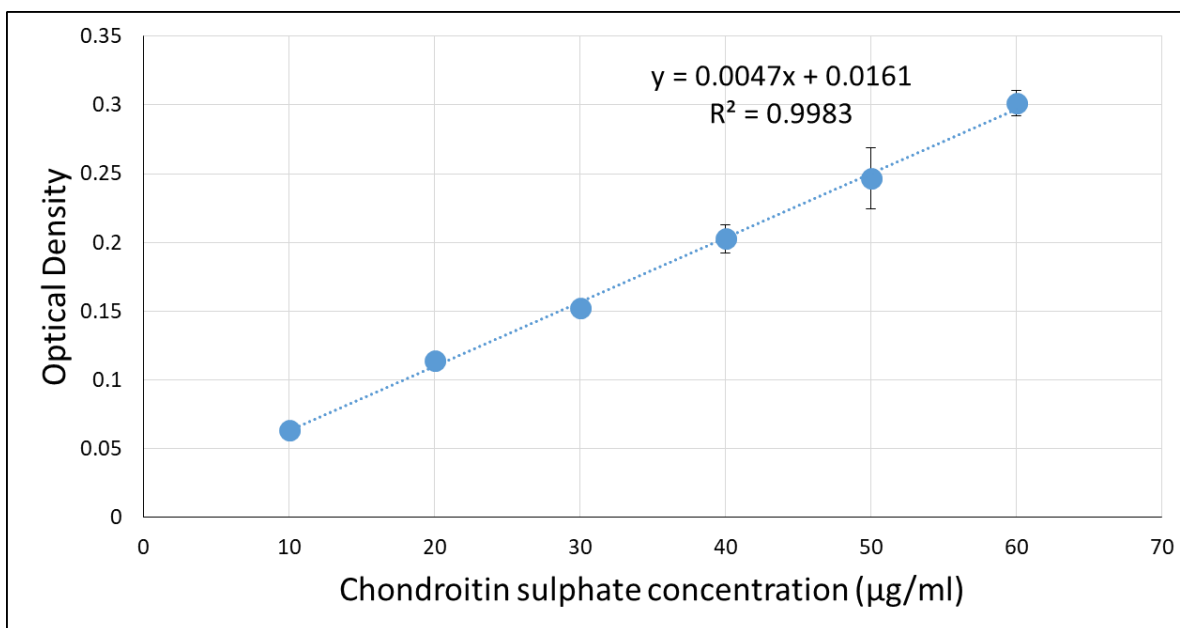
Figure 4.4: The calibration carve of chondroitin sulfate standard

Bars represent (Mean ± SD of n=3).

4.2.7.2 **The measurement of collagen content**

In the process of collagen synthesis, proline is hydroxylated in position 3' or 4', which is essential for collagen structure stability.(212) Collagen content was measured using the hydroxyproline assay, which is based on converting the hydroxyproline within the cartilage to a chromophore product (Figure 4.5).(211) Then, the chromophore product density will be measured at 570 nm using a plate reader, and the chromophore product density is proportional to the quantity of hydroxyproline, which represents the cartilage collagen content. Figure 4.6 shows the calibration curve of the hydroxyproline standard at a concentration range of 1 - 6 mg/ml of dH_2O. The assay protocol involves breaking down 100 µl of the digested cartilage into

individual amino acids using 500 μl of 12N hydrochloric acid. Then, the solution was placed in an Eppendorf vial that was capped and left for 18 hours in an oven set at 100℃. After 18 hours of peptide hydrolysis, the Eppendorf vials were opened and placed in a 55℃ oven for 48 - 72 hours, which allows the solution to evaporate. The residue of the individual amino acids was fully dissolved in 150 μl of dH$_2$O, then transferred into a 96-well plate and left in the fume hood to dry again. The wells of the 96-well plate contain dH$_2$O only (blank), residue of non-treated cartilage (control), residue of trypsin-treated cartilage, or hydroxyproline standards. In this order, 60 μl of dH$_2$O, 20 μl of the assay buffer, and 40 μl of the chloramine T reagent were added to each well. The plate was left at room temperature for 15 minutes, allowing the reagents to react. Finally, 20 μl of n-propanol and 30 μl of perchloric acid were added, followed by 30 μl of p-dimethylaminobenzaldehyde (DMAB) to each well, and left in a 70℃ oven for 20 minutes. After 20 minutes, the chromophore product of hydroxyproline is produced. The final step is measuring the colour density using a plate reader at 570 nm.
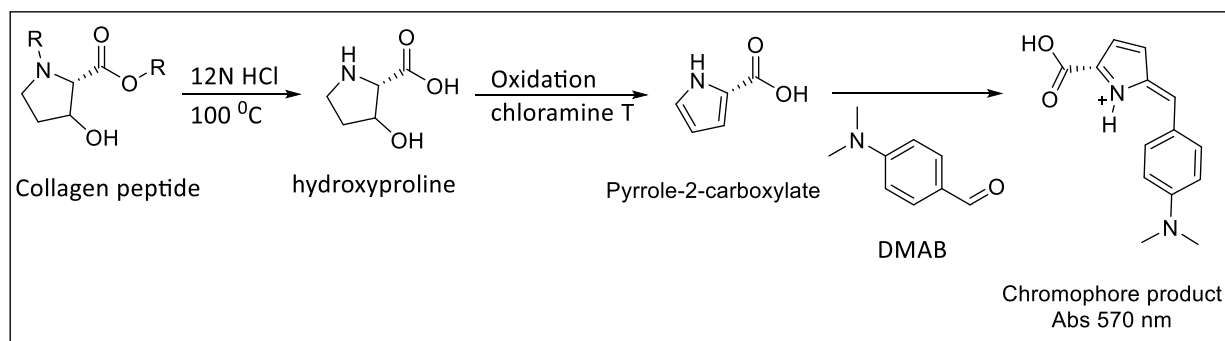
Figure 4.5: The overview of hydroxyproline assay
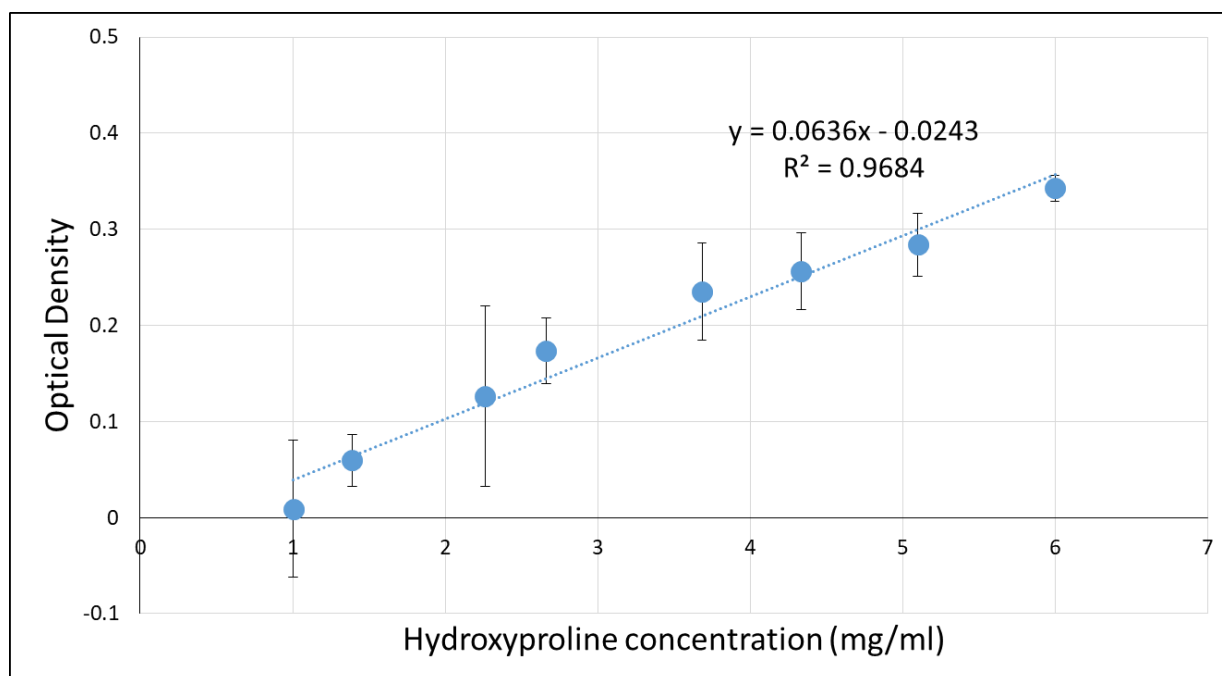
Figure 4.6: The calibration curve of hydroxyproline standard

Bars represent (Mean ± SD of n=3)

4.2.7.3 The preparation of IL-1 solution and IL-1 treated cartilage

Interleukin-1 at 1 µg/ml of sterile PBS pH 7.4 was used as a positive control for GAGs and collagen content studies.(172, 185) Fresh cartilage discs were collected and placed in a 24-well plate containing 1 ml of complete cartilage media for 24 hours in a 37℃ incubator. On the second day, the media was replaced with fresh cartilage complete media. On the third day, the media was discarded, and 1 ml of fresh complete media containing 1 µg of IL-1 was added to the well and incubated for 48 hours. The media was then replaced with fresh media containing 1 µg/ml of IL-1 for an additional 48 hours. After 4 days of treatment, the IL-1 treated cartilage was placed in the digestion buffer for 24 hours prior to GAG and collagen content measurement studies.

4.2.8 Statistical analysis

The statistical analysis was performed as previously reported (2.2.4).

4.3 Results

4.3.1 Quantification methods of NBQX and licofelone

The calibration curves of NBQX and licofelone standards were developed using RP-HPLC. The unknown concentration of NBQX and licofelone in future experiments will be determined based on the standard calibration curve. NBQX can be detected at multiple wavelengths.(213, 214) However, the two main wavelengths are 254 and 400 nm, which were investigated to determine the most sensitive wavelength to NBQX (Figure 4.7 A). At similar conditions, the area under the peak of NBQX was 453,449 in 254 nm, while the area under the peak of NBQX was 137,737 in 400 nm. Accordingly, the 254 nm wavelength is a more sensitive wavelength to detect NBQX, and it was used during the quantification of NBQX. Another significant factor in the NBQX and licofelone quantification methods is separating the drug peak from molecules that were used during the uptake and retention time studies. Therefore, the NBQX and licofelone quantification method must separate the NBQX and licofelone from other components that were used in the uptake and retention experiments. Figure 4.7 and Figure 4.8 show the elution times of all components involved in the uptake and retention studies experiment (blank), the elution times of NBQX and licofelone alone, and a sample contains both blank and NBQX or licofelone. In both quantification methods, the drug peak was distinguishable from other component peaks.
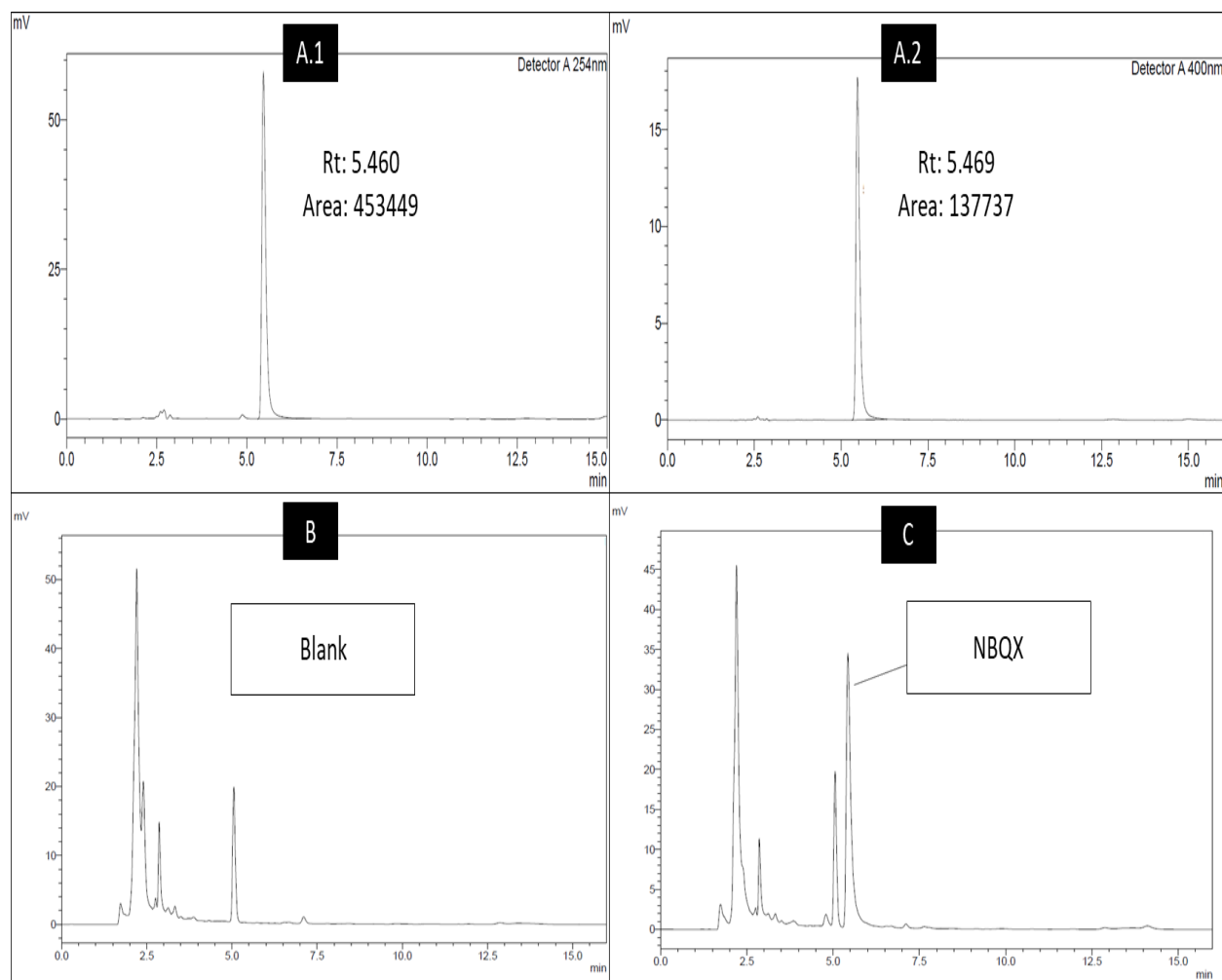
Figure 4.7: The RP-HPLC chromatograms of NBQX

A) The peak area of same NBQX concentration and same RP-HPLC parameters at different wavelengths; A.1) UV detector at 254 nm and A.2) UV detector at 400 nm, B) The RP-HPLC chromatograms of digestion solution without NBQX, and C) The RP-HPLC chromatograms of digestion solution with NBQX
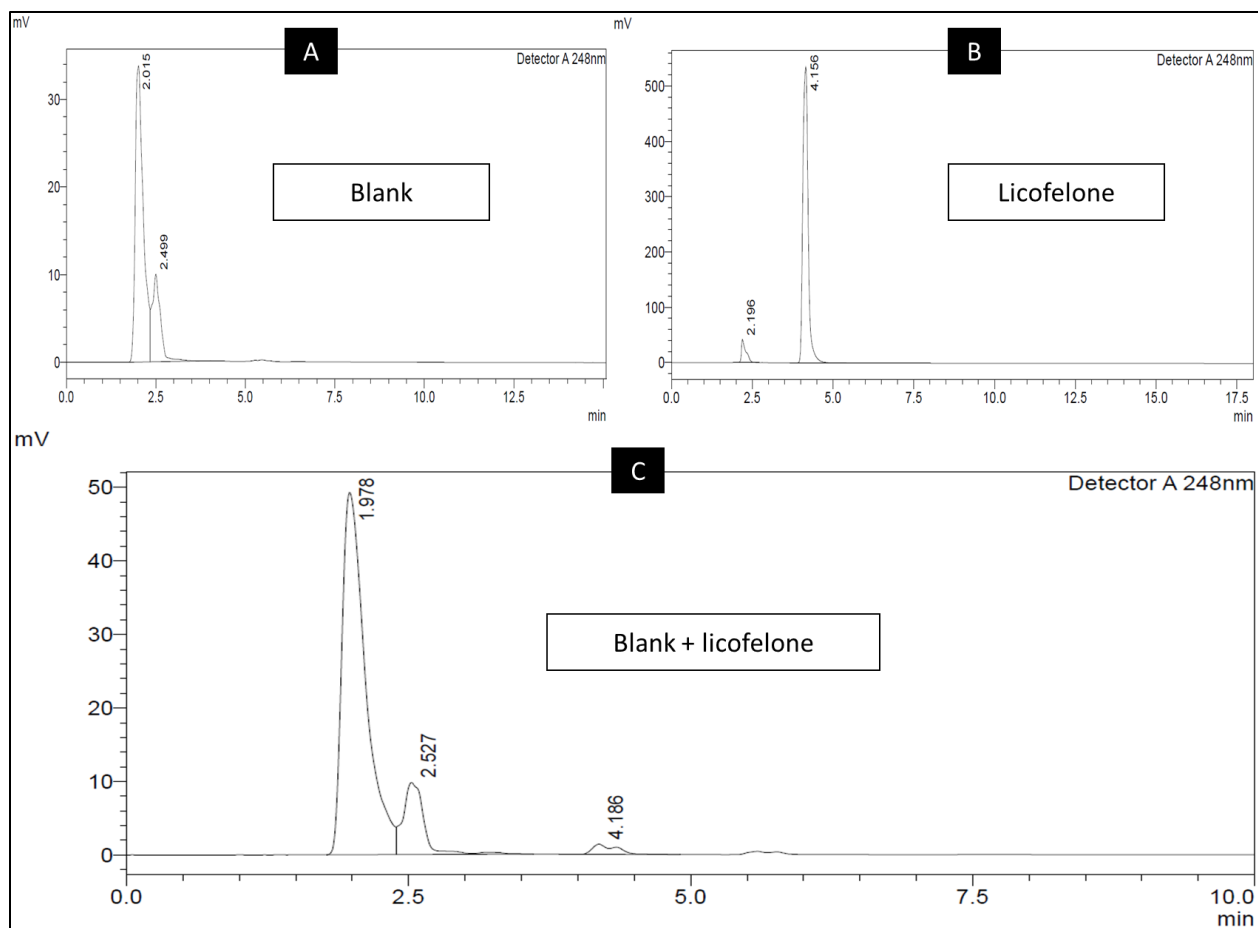
Figure 4.8: The RP-HPLC chromatograms of licofelone

A) RP-HPLC chromatogram shows components involve in the uptake and retention time study, B) RP-HPLC chromatogram of licofelone alone, and C) RP-HPLC chromatogram shows the separation of licofelone retention time from other components.

4.3.2 **Licofelone release study**

The A16-licofelone and A87-licofelone conjugates were completely soluble in PBS buffer. However, DMSO was added to solubilize the released licofelone from the conjugate. Figure 4.9 and Figure 4.10 show the % release of licofelone from A16-licofelone and A87-licofelone conjugates over time, respectively. A relevantly fast release of licofelone was observed from both conjugates. At 4 hours, 25.46 % of licofelone was released from A16-licofelone, while 30.52 % of licofelone was released from A87-licofelone. Then, the release of licofelone from the A16-licofelone conjugate increased slowly until it reached 97.85 % at 96 hours. However, the released licofelone has reached 95.22 % within 48 hours in the case of A87-licofelone conjugate. 50 % of the conjugated licofelone was released from A87 during the first day, while 50 % of the released licofelone from A16 was observed at 48 hours.
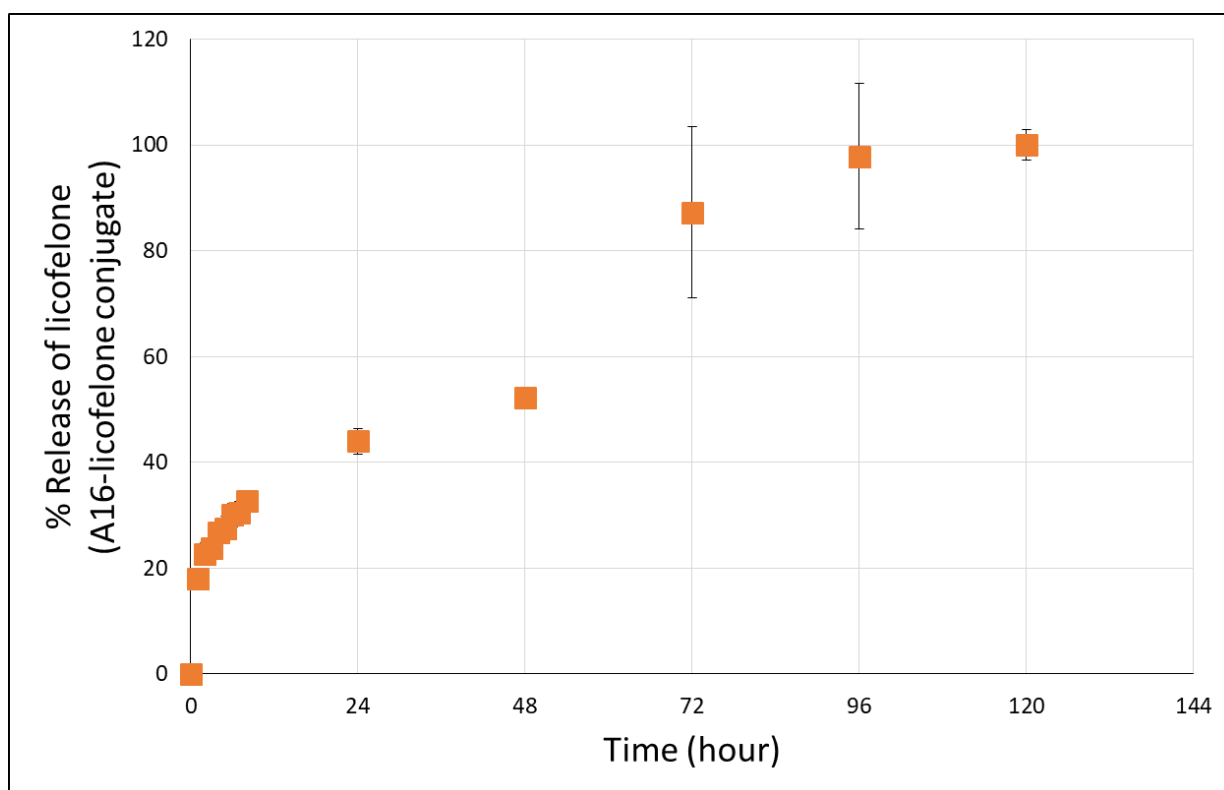
Figure 4.9: The licofelone % release over time from A16-licofelone conjugate

Bars represent (Mean ± SD of n=3)
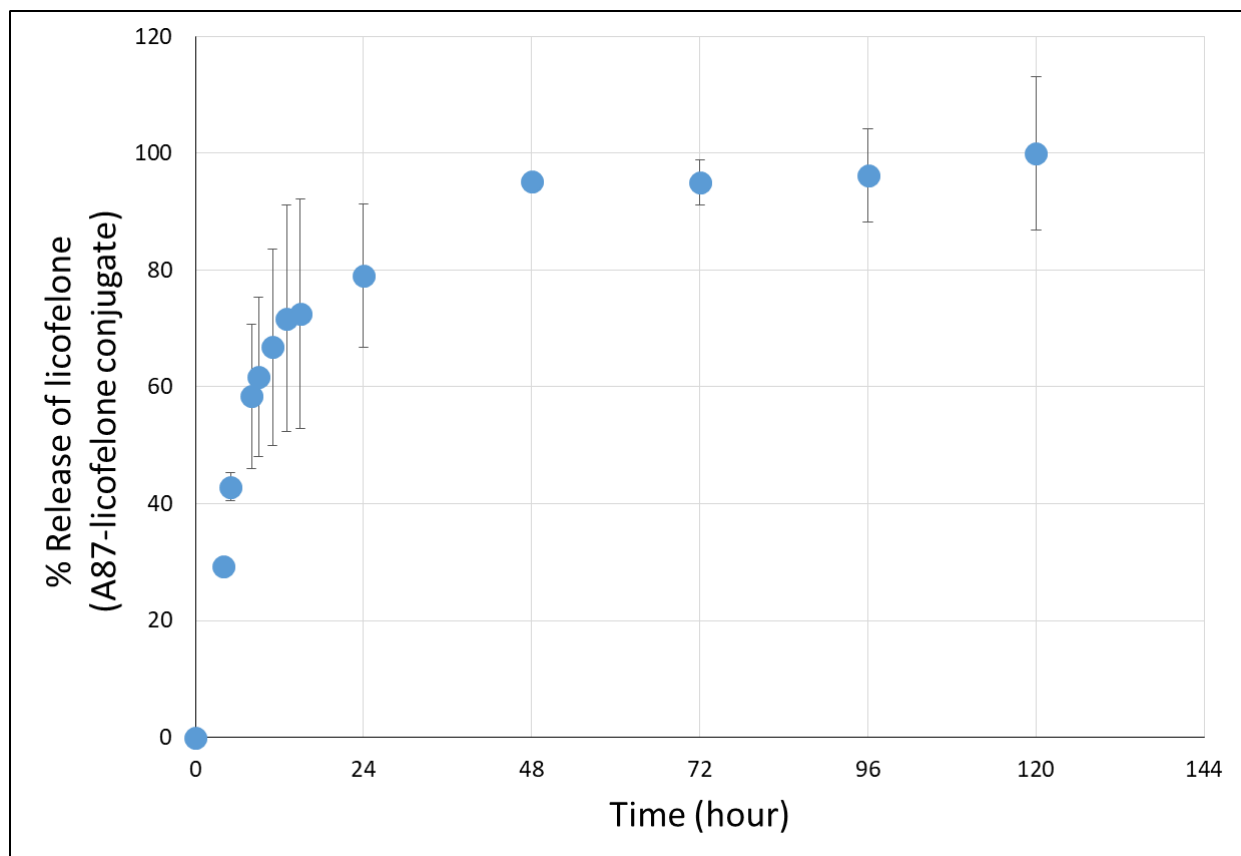
Figure 4.10: The licofelone % release over time from A87-licofelone conjugate

Bars represent (Mean ± SD of n=4)

Furthermore, the quantity of the released licofelone from the A16-licofelone and the A87-licofelone conjugates was determined based on the calibration curve of licofelone (Figure 4.11). The quantity of the released licofelone plateaued after 3 days and 2 days in the release medium pH 7.4 of the A16-licofeon and A87-licofelone conjugates, respectively. The 3 mg/ml of A16-licofelone conjugate contained 6.66 ± 0.19 μg licofelone, while the 3 mg/ml of A87-licofelone contained 26.22 ± 3.4 μg. Significantly, the HPLC chromatogram has proven that the released licofelone has a similar chemical structure to the standard licofelone since both molecules have a similar elution time.
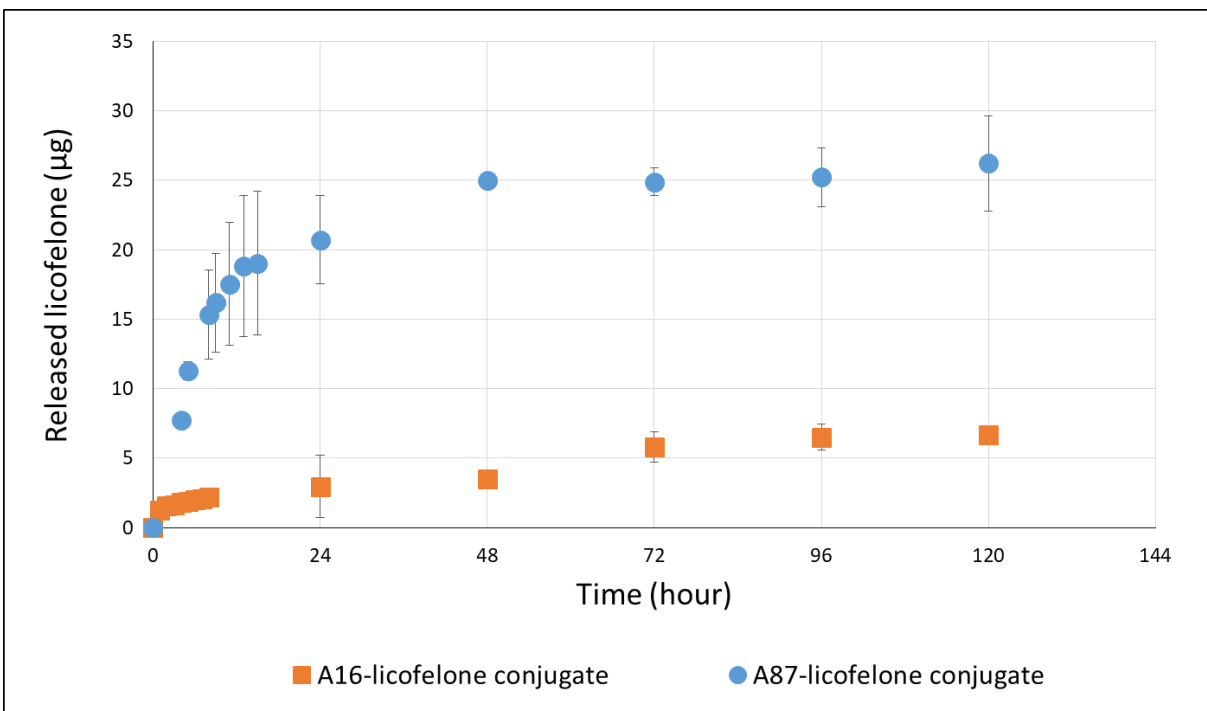
Figure 4.11: The licofelone released quantity over time from A16-licofelone conjugate and A87-licofelone conjugate

Bars represent (Mean ± SD of n=3 for A16-licofelone, n=4 for A87-licofelone)

4.3.3 Early OA *ex*-vivo bovine cartilage model development

The cartilage was treated with trypsin at a concentration of 1 mg/ml to simulate an early-OA cartilage model. The 50 % GAG and collagen depleted cartilage will mimic an early stage of osteoarthritic cartilage. The GAG content and collagen content were measured to confirm the 50 % depletion. The model is beneficial because it will determine the efficiency of the polymers delivering licofelone in GAG depleted cartilage because the drug delivery system is charge-based between the polymer and the negatively charged GAGs.

4.3.3.1 GAG contents

Figure 4.12 shows the percentage of GAG content in non-treated cartilage, trypsin-treated cartilage, and IL-1 treated cartilage. Trypsin or IL-1 treated cartilage showed a significant loss of GAG contents compared to non-treated cartilage (control). Treating cartilages with trypsin at 1 mg/ml for 24 hours showed a statistically significant reduction of 45.74 ± 3.8 % in GAG contents compared to non-treated cartilages. The positive control (IL-1) has statistically depleted the GAG content by 51.69 ± 4.8 % compared to the non-treated cartilage.
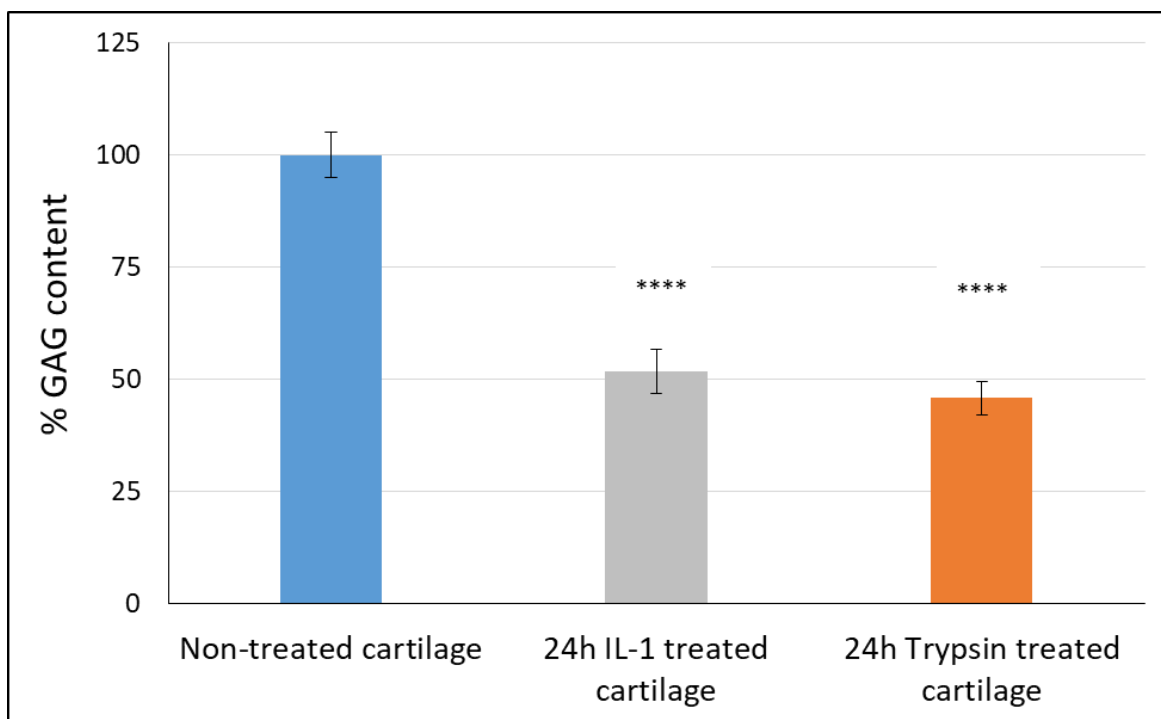
Figure 4.12: The percent of GAG contents.

Bars represent (Mean ± SD of n=3). Significant **** (P<0.0001) compared to the control (non-treated cartilage).

114

4.3.3.2 **Collagen contents**

Cartilages that were treated with trypsin at 1 mg/ml for 24 hours and IL-1 at 1 μg/ml for 96 hours showed a significant inhibition in collagen content compared to the non-treated cartilage (Figure 4.13). There was a 51.89 ± 12 % and a 68.62 ± 15.1 % reduction of collagen content after treating the cartilage with trypsin and IL-1, respectively.
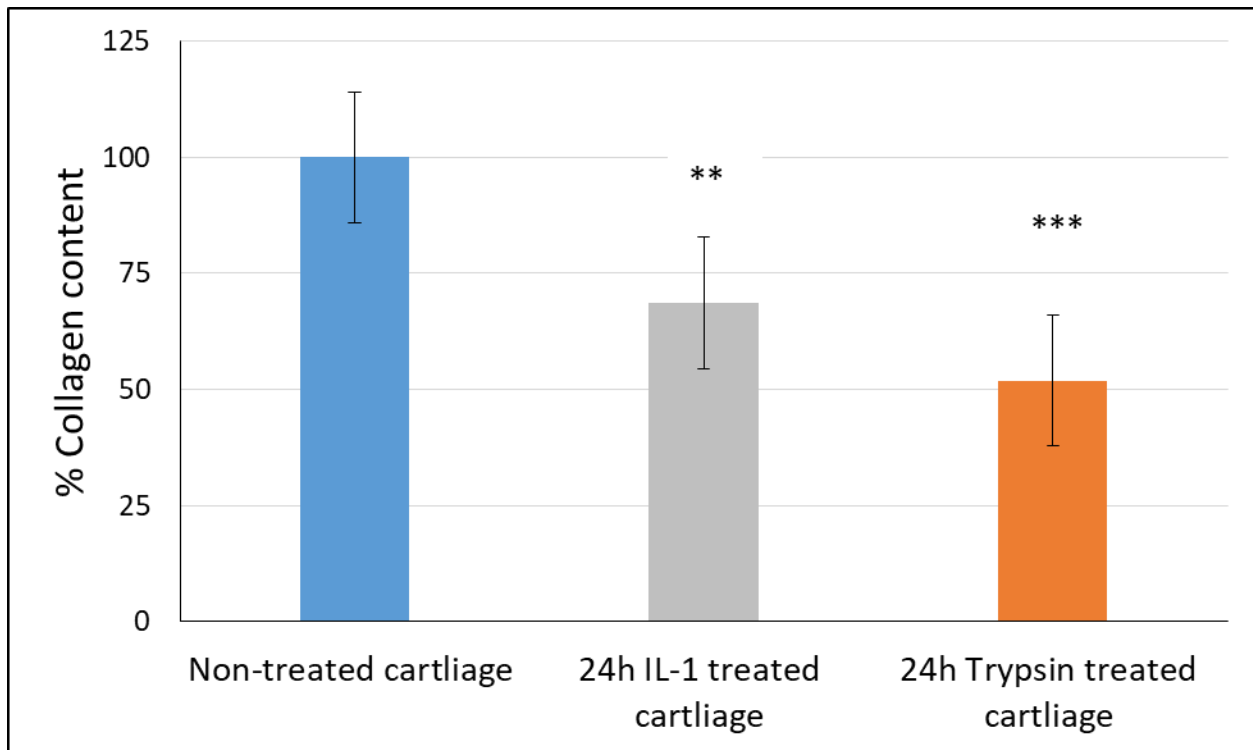
Figure 4.13: The percent of collagen contents

Bars represent (Mean ± SD of n=5). Significant ** (P<0.01), and *** (P<0.001) compared to the control

4.4 Discussion

4.4.1 NBQX and licofelone quantification methods

The RP-HPLC methods showed a separation between the peaks of compounds that will be applied in the experimental mixture solution and the peak of NBQX or licofelone. Figure 4.7 and Figure 4.8 show no interference between the peak of NBQX or licofelone and the other peaks from the digestion solution. Both methods have detected NBQX and licofelone at minimum concentrations of 0.04 μg and 0.1 μg, respectively. NBQX peak area was investigated in two conditions of UV-detector 254 nm and 400 nm, but the 254 nm was more sensitive towards NBQX. These RP-HPLC methods will be used to determine the quantity of NBQX and licofelone after the uptake study, retention time study, and drug release study, based on their respective calibration curves.

4.4.2 Release study of licofelone

Both conjugates have shown a full release of licofelone within 2 to 3 days. A study that conjugated dexamethasone to avidin through an ester bond, reported that 50 % of the drug was released within 14.4 ± 1 hours at pH 7.4, which supports the current study findings.(172) The A16-licofelone had a slower release profile of licofelone than the A87-licofelone, which was expected because the A87 polymer (26.2 μg) was loaded with a higher quantity of licofelone compared to the A16 polymer (6.6 μg). In fact, the release study of the conjugates was performed primarily to confirm that the A87 polymer can carry more licofelone than the A16, and then to investigate the release profiles of both conjugates. One of the current study's investigational aims is to study the influence of the drug loading quantity on the drug uptake and retention time. Therefore, the quantity of licofelone loaded was determined based on the licofelone calibration curve, which showed that A87-licofelone conjugate has four times the amount of released licofelone than A16-licofelone conjugate. Furthermore, the A87 polymer was selected because of the multiple conjugation sites on the polymer backbone, and the release study of A87-licofelone has proven that more licofelone is conjugated to A87 than to A16. According to the release study results, the conjugation strategy of linking licofelone with a hydrolysable covalent bond to ensure that the drug is released from the carrier without altering its chemical structure

was successful. In addition, the release study revealed that the drug is released from the conjugate within 48 to 72 hours, which would provide an immediate therapeutic effect.(161)

4.4.3 *Ex vivo* bovine cartilage models for healthy and early simulated OA cartilage

The *ex vivo* models of healthy bovine cartilage and early simulated OA cartilage were developed to study the uptake and the retention time of the drugs and conjugates inside both models. The untreated bovine cartilage was considered a model of healthy cartilage. In the case of the OA cartilage model, healthy cartilage was treated for 24 hours with 1 mg/ml of trypsin. Trypsin is a serine protease that degrades cartilage components such as GAG and collagen, which also leads to cartilage thinning.(208) At 1 mg/ml, trypsin showed an approximate 50 % depletion in GAG and collagen content compared to non-treated healthy cartilage (Figure 4.12 and Figure 4.13). The 50 % inhibition of cartilage content mimics the loss of GAG and collagen content in the early stages of OA.(143) Numerous studies have used trypsin to simulate an early OA cartilage model.(143, 209) IL-1 was used as a positive control in the GAG and collagen content measurements, which also inhibited the cartilage content by 50 %. This inhibition of cartilage content will play a significant role in the uptake and retention time studies since the cartilage content has the ability to resist and prevent molecules from penetrating. We hypothesised, and it is being supported by other studies, that the DMOADs low therapeutic effect is mainly caused by cartilage-repellence activity, which prevents drugs from reaching their therapeutic target within the cartilage.(17, 18) In order to overcome the biological barrier and penetrate the cartilage deeply, we took advantage of the overall negative charge of the cartilage, which comes from GAG, collagen, and proteoglycan, by conjugating DMOAD to a positively charged carrier.(21, 25) Accordingly, the cartilage content depletion in the early simulated OA cartilage models can influence the drug and conjugate uptake and retention studies. Significantly, the three licofelone conjugates depend on the electrostatic interaction between the negatively charged cartilage content and the positively charged conjugates to infiltrate through the cartilage. Furthermore, the healthy and early simulated OA cartilage models will assist in studying the efficiency of the conjugates by determining their impact on the licofelone uptake and retention time in both models.

4.5 **Conclusion**

The release study of licofelone shows that the polymers were linked to licofelone via a hydrolysable bond, the A87 polymer was loaded with a higher quantity of licofelone than A16, and the structure of the released licofelone was unaltered. In addition, licofelone was completely released between 48 and 72 hours. This chapter also showed that the early simulated OA cartilage model was 50 % GAG and collagen depleted compared to the healthy cartilage model. The depletion of cartilage content can play a significant role in drug uptake and retention time, which will be further discussed in the next chapter, as well as the influence of these carriers on licofelone uptake and retention time within both ex vivo bovine cartilage models.

Chapter 5: **The Uptake and Retention Time Studies of the Conjugates in both Cartilage Models and Cell Viability Assay**

5.1 **Introduction**

Osteoarthritis treatments have failed to produce a significant therapeutic effect during clinical trials because of the limited drug quantity reaching its therapeutic target.(11, 13-16) Therefore, the current study aims to enhance OA therapeutic uptake and retention time within the cartilage, which can improve their therapeutic effect. According to this study's hypothesis, the positively charged drug-delivery system can electrostatically interact with the negatively charged proteoglycans to penetrate through the cartilage, assisting DMOADs to reach a deeper therapeutic target with a high quantity. In addition to the penetration aspect, the electrostatic interaction can attach the delivery system to the cartilage, increasing the retention time and the DMOADs quantity inside the cartilage. Both factors will improve the DMOADs therapeutic effect, uptake, and retention time within the cartilage. Particularly in this study, the goal will be enhancing licofelone quantity within both cartilage models, where licofelone represents a model drug of DMOADs. Licofelone was covalently conjugated to A5, A16, and A87 polymers via a hydrolysable bond. In the case of NBQX, the negatively charged NBQX was physically loaded on the positively charged acrylate-terminated A5 (self-assembled). The PBAE polymers were previously self-assembled with DNA and other negatively charged compounds, so a similar strategy was adapted for NBQX since the conjugation attempts were unsuccessful.(179-181) In this chapter, the uptake and the retention time of NBQX, self-assembled NBQX, licofelone, and licofelone conjugates in the healthy cartilage model and the developed early simulated OA cartilage model will be investigated. In the early stage of OA, a reduction in aggrecan (the abundant type of proteoglycans) was observed, which can influence the conjugates performance since the delivery system is charge-based.(24, 143) Therefore, the 50 % cartilage content depletion in the OA cartilage model will assist in predicting the behaviour of the drug alone and with delivery systems inside osteoarthritic cartilage. Therefore, the efficiency of the self-assembled NBQX and licofelone conjugates systems will be evaluated in both cartilage models based on the percentage uptake and retention time of both drugs within the cartilage models.

Furthermore, A5, A16, and A87-licofelone conjugates have different physiochemical characteristics, which will determine the factors that influence the uptake and retention time of the drug within the cartilage. These factors are the degree of the conjugate positive charge and the conjugated quantity of licofelone to the polymer.

5.2 Materials and Methods

The materials of cartilage complete media orders were reported in 4.2. The cell proliferation assay kit II (XTT) by Roche was purchased from Sigma Aldrich.

5.2.1 Samples and buffer preparations

The PBS buffer, trypsin solution, and digestion buffer preparation methods were described in the second chapter materials and methods section (2.2.2). The sample preparation method of NBQX, self-assembled NBQX, licofelone, and licofelone conjugates for the uptake and retention study is described below.

5.2.1.1 NBQX solution preparation

The chosen NBQX concentration is 2.5 mM (0.95 mg/ml) because it showed a therapeutic effect against OA progression factors (1.1.4.4.1). 0.95 mg/ml was solubilized in PBS buffer pH 7.4.

5.2.1.2 Self-assembly method of acrylate-terminated A5 with NBQX

Two different methodologies for the preparation of acrylate-terminated A5 and 2.5 mM NBQX self-assembly were adapted (Figure 5.1).(180) The first method was **(v/w)** and started by mixing 2 ml of a 2 mg/ml solution of acrylate-terminated A5 in PBS buffer with 1.9 mg of NBQX. The final concentration of the **(v/w)** formula was 2.5 mM NBQX and 2 mg/ml A5 polymer. The second method was **(v/v)**, and it started by preparing two separate solutions of 5 mM NBQX and 4 mg/ml acrylate-terminated A5 in PBS buffer. Then, combine both solutions in a 1:1 ratio for a final concentration of 2.5 mM NBQX and 2 mg/ml A5 polymer.
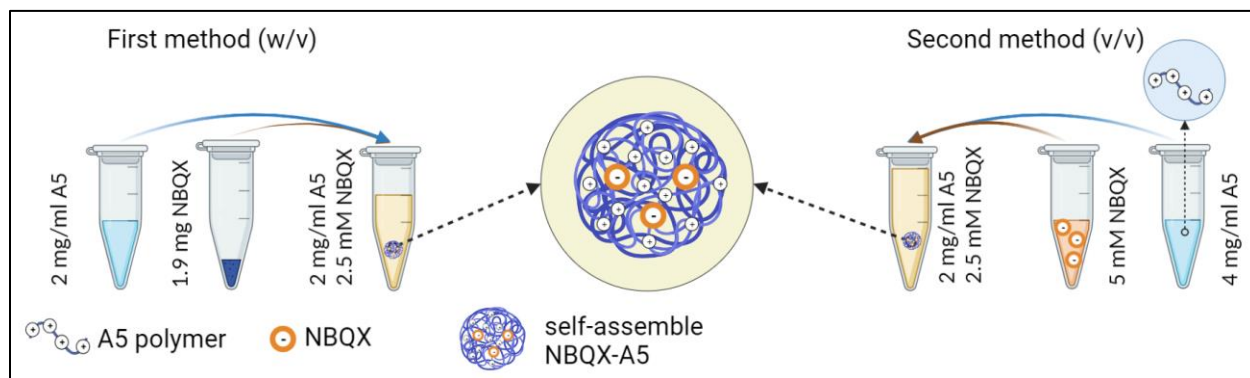
Figure 5.1: NBQX self-assembled with A5 acrylate-terminated polymer

The figure created with BioRender.com.

5.2.1.3 Licofelone solution preparation

Licofelone control solution was prepared by dissolving 1 mg of licofelone in 1 ml of PBS buffer/DMSO. DMSO was mixed with PBS in a 50:50 **(v/v)** ratio because licofelone is insoluble in PBS alone.

5.2.1.4 Licofelone conjugates solutions preparation

4 mg of licofelone conjugates were dissolved in 1 ml of 50% PBS and 50% DMSO **(v/v)**. The conjugate solutions were divided into two tubes.

5.2.2 The uptake and retention time study

In both studies, the quantity of the drug inside the cartilage was determined using the RP-HPLC method after full cartilage digestion. The steps of the uptake and retention study are described in Figure 5.2 and will be reported in detail next.(140, 143, 185) Briefly, the plan is to incubate the drug with cartilage, then digest the cartilage and measure how much of the drug uptake and retention quantity was in the cartilage. Additionally, the quantity of conjugated licofelone to the polymer that was applied to the cartilage was measured to determine the 100 percent of licofelone that was used during the experiments of the uptake and retention time. The reason for this is that the results of the uptake and retention time studies will be represented as a percentage of the drug quantity, which was calculated based on Equation 5.1 because the experiments started with different quantities of NBQX, licofelone, and licofelone conjugates. Adjusting the results of the uptake and retention time studies to be percentages will allow an accurate comparison between the studies. Additionally, the area under the curve of both studies was calculated to determine the total percent of the uptake and the retained drug inside the cartilage over time.

Equation 5.1:

$$\% \text{ Uptake of the drug} = \frac{\text{The uptake of the drug within the cartilage } (\mu g)}{\text{The total given drug quantity to the cartilage } (\mu g)} \times 100$$

$$\% \text{ Retention of the drug} = \frac{\text{The retained drug within the cartilage } (\mu g)}{\text{The total given drug quantity to the cartilage } (\mu g)} \times 100$$
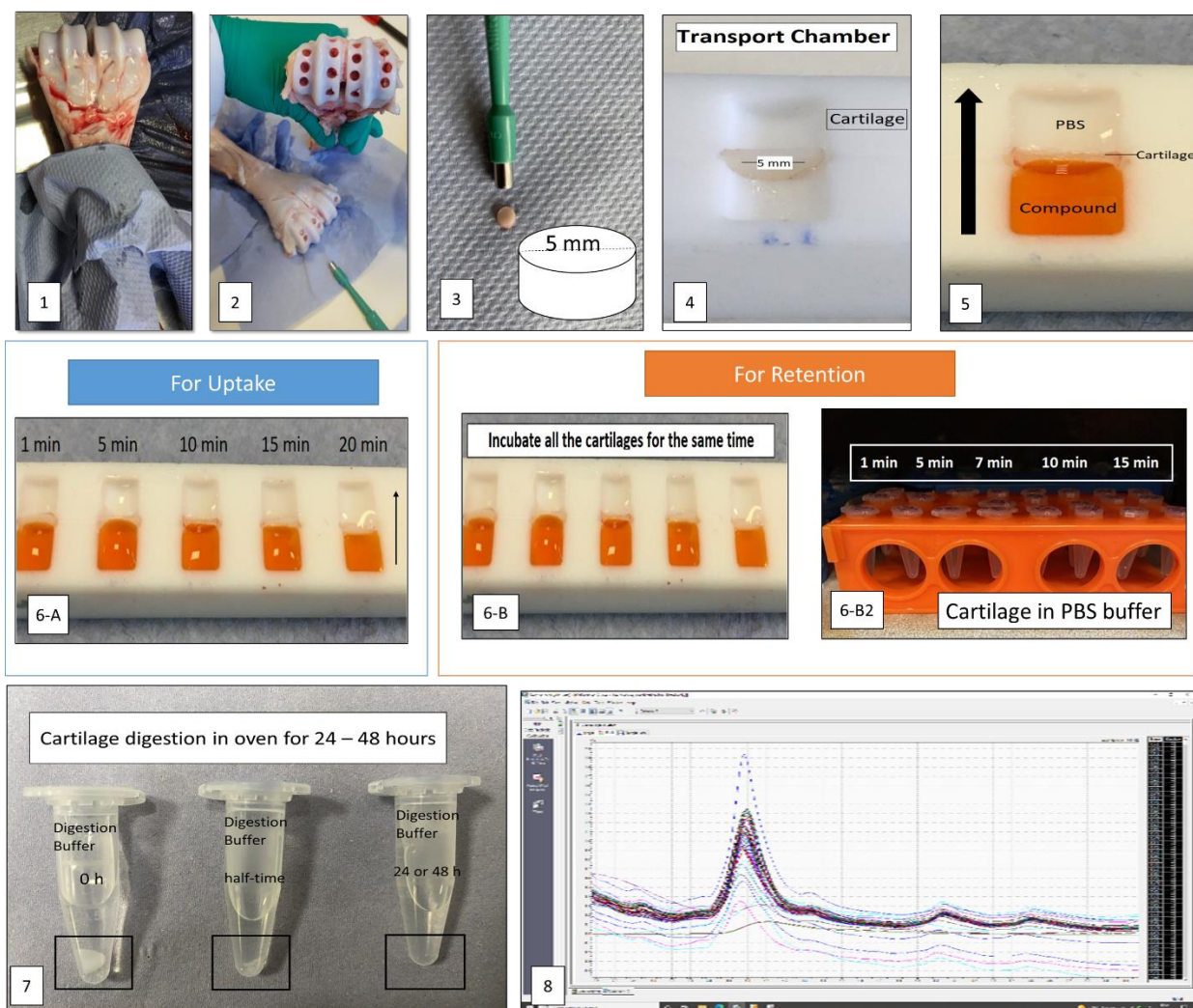
Figure 5.2: The process of cartilage collection, uptake, and retention time study:

1-3) The cartilages were collected from MCP joint using 5 mm dermal punch. 4-5) Semi-circle cartilage placed in transport chamber. 6) Either going for uptake study (A) or retention time study (B). 6-A) At the uptake study the samples left for different time points 6-B) while at the retention study the samples left for a similar time 6-B2) Then Eppendorf containing the samples left at the incubator for different release time. 7) The picture shows the digestion of the cartilage during the incubation time 8) the solution transferred into the HPLC vials, and then analysed using the HPLC method.

5.2.2.1 **The uptake study**

The healthy and early simulated OA cartilages were harvested and prepared as described previously in 4.2.6 and 4.2.7. The cartilage discs were sliced to a semi-circular shape (5 mm in diameter with a thickness of about 0.5 mm). After weighing the cartilage, the samples for the healthy model were placed on the transport chamber, whereas the samples for the OA cartilage

model were placed in an Eppendorf tube containing 500 ml of trypsin solution for 24 hours in a 37℃ incubator. After 24 hours, the early simulated OA cartilage was washed with deionized water and then placed in the transport chamber. The transport chamber, which was manufactured and designed to perform a one-way diffusion study, was composed of six chambers, each with a 5 mm diameter, and has a capacity of 50 μl on each side.. On the transport chamber, the superficial side of the cartilage faced the prepared sample solution, while the deeper side (close to the bone) faced the PBS solution. This cartilage position was set up to mimic the situation when the intra-articular formula is injected, in which the formula will be facing the superficial cartilage side. On the transport chamber, 50 μl of the prepared sample solution was added on one side, and 50 μl of PBS buffer pH 7.4 was added on the opposite side. Then, the transport chamber was placed in a closed Petri dish containing water to minimise evaporation and incubated at 37℃, allowing for passive diffusion through the cartilage. The transport chamber was incubated for different time points, which allowed variant drug concentrations to penetrate and remain within the cartilage (Figure 5.2, step 6-A). At the end of each time point, the cartilage was washed in PBS buffer pH 7.4 and then placed in an Eppendorf tube containing 1 ml of the digestion buffer for 24 - 96 hours at 55℃ (Figure 5.2, step 7). After 24 – 96 hours in the oven, the cartilage was digested, and the drug within the cartilage was quantified using the previously developed RP-HPLC method (4.2.1 and 4.2.2). In the uptake study, the digestion solution contains the quantity of drug inside the cartilage.

5.2.2.2 **The retention study**

The cartilage collection and preparation were done following a similar procedure that was reported in the uptake study. After placing the cartilage on the transport chamber, 50 μl of the prepared sample solution was added on the superficial side, and 50 μl of PBS buffer pH 7.4 was added on the opposite side. Then, the transport chamber was incubated for a specific fixed time point at which the drug uptake concentration within the cartilage started to plateau (Figure 5.2, step 6-B). During this fixed incubation time, the cartilage will uptake the maximum concentration of the drug. Then the cartilages were placed in Eppendorf tubes containing 1 ml PBS buffer pH 7.4 for different time points in a 37 ℃ incubator, allowing the drug to be released from the cartilage into the PBS solution (Figure 5.2, step 6-B2). At the end of each time point, the cartilage

was dipped in PBS buffer and then placed in an Eppendorf tube containing 1 ml of digestion buffer for 24 - 96 hours at 55℃ (Figure 5.2, step 7). After a full digestion of the cartilage, the quantity of the drug retained within the cartilage will be determined using the RP-HPLC method and based on the drug's respective calibration curve.

5.2.2.3 The uptake study of NBQX

The prepared solutions in the transport chamber contained either 50 µl of 2.5 mM NBQX or NBQX self-assembled with acrylate-terminated A5. The transport chamber was incubated at 37℃ for 1 – 120 minutes, allowing the NBQX to cross through the cartilage via passive diffusion. Then, the cartilage was placed in an Eppendorf tube containing 1 ml of digestion solution. The solution was transferred into HPLC vials after digestion. The quantity of NBQX was determined based on the calibration curve equation for NBQX (Figure 4.1).

5.2.2.4 The retention time study of NBQX

After placing the cartilage in the transport chamber, 2.5 mM NBQX or NBQX self-assembled with acrylate-terminated A5 was added on the superficial side of the cartilage and PBS on the other side. Then, the cartilage was incubated for a fixed period of time, at which point the 2.5 mM of NBQX cartilage uptake started to plateau. After incubation, the cartilage should contain the maximum quantity of NBQX. The cartilage was then placed in Eppendorf tubes containing 1 ml of PBS buffer for different time points (1 – 360 minutes), allowing the NBQX to be released into the PBS medium. At the end of each time point, the cartilage was transferred into the digestion solution to measure the quantity of NBQX remaining inside the cartilage. After complete digestion, the solution was prepared for quantification using the RP-HPLC method.

5.2.2.5 The uptake study of licofelone

Following the same procedure, licofelone, A5-licofelone, A16-licofelone, or A87- was incubated for 1 – 30 minutes at 37℃. After each time point, the cartilage was placed in an Eppendorf tube containing 1 ml of digestion solution. After 24 – 96 hours in the oven, the digestion solution containing the digested cartilage and drug were transferred into HPLC vials and prepared for licofelone quantification. Since the licofelone is not soluble in buffers, 100 µl of the digestion solution was replaced by 100 µl of DMSO. Additionally, the licofelone conjugates

uptake studies included an additional HPLC vails of the conjugates solution as a control to determine the 100 % licofelone that was applied to the cartilage.

5.2.2.6 **The retention time study of licofelone**

The transport chamber, which contained the cartilage and 50 µl of licofelone or licofelone conjugates solutions, was incubated for a similar amount of time, at which point the licofelone uptake started to show consistency in uptake quantity. After incubation, the cartilages should contain the maximum quantity of licofelone. The cartilages were then placed in Eppendorf tubes containing 1 ml of PBS buffer pH 7.4 for different time points in a 37℃ incubator. During this time point, some of the drug will remain in the cartilage and other will be released in the PBS buffer pH 7.4. The incubation times for licofelone, A5-licofelone, and A16-licofelone were 1 – 60 minutes, while that for the A87-licofelone was 1 - 120 minutes. Then, the cartilage was transferred into Eppendorf containing 1 ml of the digestion buffer. After complete cartilage digestion, the quantity of licofelone retained within the cartilage was determined using the RP-HPLC method. Similar to the licofelone uptake study, 100 µl of the digestion solution was substituted with 100 µl of DMSO, and a control vial for the licofelone conjugates retention study was prepared. This control vail was obtained from the solution of A5-licofelone, A16-licofelone, or A87-licofelone conjugates, and will represent the 100 % licofelone quantity that was applied to the cartilage.

5.2.2.7 **The effect of DMSO on uptake and retention study**

A healthy cartilage uptake of 0.95 mg/ml of NBQX in PBS pH 7.4 or DMSO was observed to determine the effect of DMSO. The reason for this is that DMSO must be used in licofelone studies. There was no effect observed between the uptake of NBQX dissolved in PBS and DMSO (Figure 5.3).
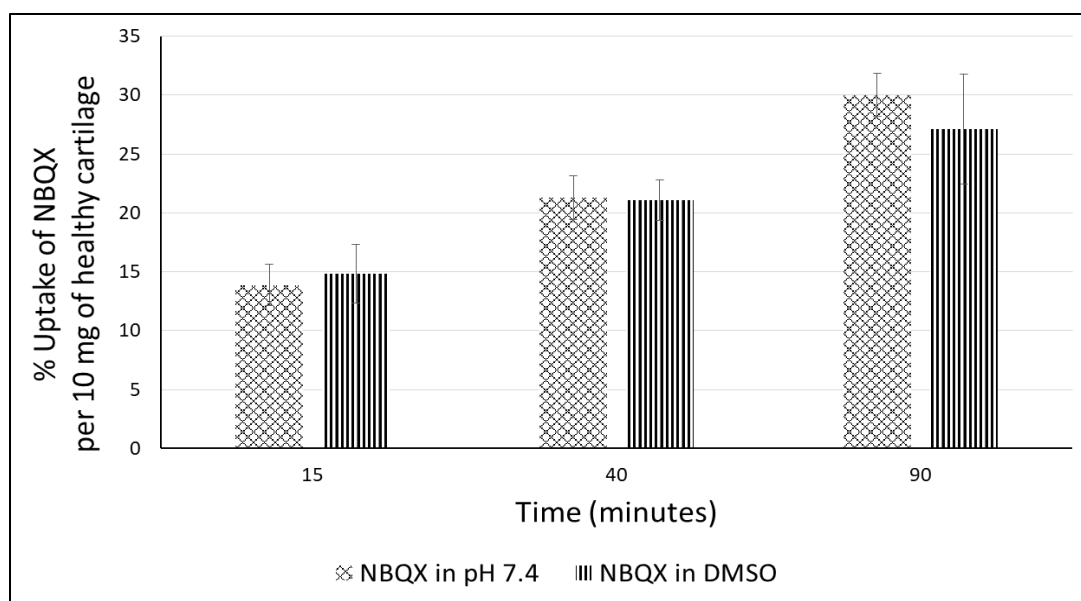
Figure 5.3: The percent uptake of NBQX per 10 mg of healthy cartilage that was dissolved in either PBS pH 7.4 or DMSO. Bars represent (Mean ± SD of n=3)

5.2.3 **XTT cell proliferation assay**

The XTT assay is a colorimetric assay that determines viable cells based on the reduction of the tetrazolium salt by mitochondrial dehydrogenase in metabolically active cells to generate a coloured formazan product (Figure 5.4). The formazan product was detected by measuring the absorbance at 450 nm with a microplate reader (Tecan, Infinite 200 PRO). The colour density is proportional to the cell viability. The XTT cell proliferation kit contains XTT labelling (sodium 3´-[1- (phenylaminocarbonyl)- 3,4- tetrazolium]-bis (4-methoxy-6-nitro) benzene sulfonic acid hydrate) reagent (1) and an electron coupling (PMS (N-methyl dibenzopyrazine methyl sulphate)) reagent (2). The assay reagent was prepared by mixing 98 % of reagent 1 with 2 % of reagent 2, as instructed by the manufacturer.
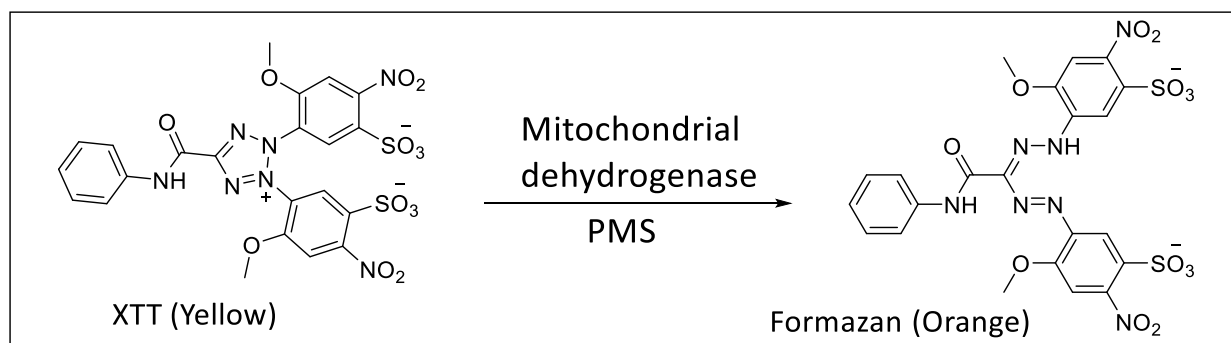
Figure 5.4: The cleavage of tetrazolium salt XTT to produce the orange formazan product

127

5.2.3.1 **XTT assay sample concentration**

The cartilage cell viability assay was performed for the A87-licofelone conjugate because it has shown a preferable licofelone uptake and retention time profile compared to the A16-licofelone and A5-licofelone conjugates. The A87-licofelone concentrations chosen for the XXT assay were 119 and 325 µg/ml of A87-licofelone conjugate, which contained 1 and 2.7 µg of licofelone, respectively. These concentrations were based on the results of the uptake and retention time studies of the A87-licofelone conjugate, which will be discussed in detail in 5.3.3. Additionally, the cytotoxicity of 119 and 325 µg/ml of the A87 polymer alone was observed.

5.2.3.2 **Cartilage cell viability**

The XTT cell viability experiments were performed in accordance with the manufacturer's instructions with minor modifications. Fresh cartilage discs were harvested as mentioned previously in 4.2.6, and then placed in a 48-well plate containing 500 µl of cartilage complete medium for 72 hours in a 37 °C and 5 % CO_2 incubator. The preparation of the cartilage complete medium was previously reported in 4.2.5. On the third day, the medium was discarded, and 500 µl of 119 µg/ml A87-licofelone, 119 µg/ml A87 polymer, 1 µg/ml licofelone, 325 µg/ml A87-licofelone, 325 µg/ml A87 polymer, 2.7 µg/ml licofelone, or complete medium (control) were added to the wells. The cartilage discs were incubated for 24 or 48 hours at 37 °C and 5% CO_2. After the incubation times, the supernatant was discarded, and 500 µl of fresh medium was used to remove the remaining residues of the treatment (licofelone, A87 polymer, or the conjugate). Then, the cartilage discs were sliced into 3 pieces, and 500 µl of XTT solution was added to each well for 4 hours in a 37 °C and 5 % CO_2 incubator. After 4 hours, the XTT solution was transferred to a new 48-well plate. Then, 250 µl of DMSO was added to the cartilage pieces and incubated for 1 hour in a 37 °C and 5% CO_2 incubator in order to dissolve the formazan crystal. Then,250 µl of DMSO was added and mixed with the 500 µl of XTT in the 48-well plate. Then, the colour density was measured at 450 nm and 690 nm using the plate reader. The reference absorption was measured at 690 nm to be subtracted from the formazan absorption at 450 nm, which was instructed by the manufacturer. Furthermore, 0.135 % DMSO was used to solubilize 1 and 2.7 µg/ml licofelone, whereas the A87-licofelone and A87 polymer were soluble in complete medium. Therefore, the cytotoxicity of 0.135 % DMSO was investigated. At 24 and 48 hours,

0.135 % DMSO-treated cartilage showed no statistical difference compared to the untreated cartilage (control) (Figure 5.5), so no toxicity associated with the use of 0.135 % DMSO was observed.
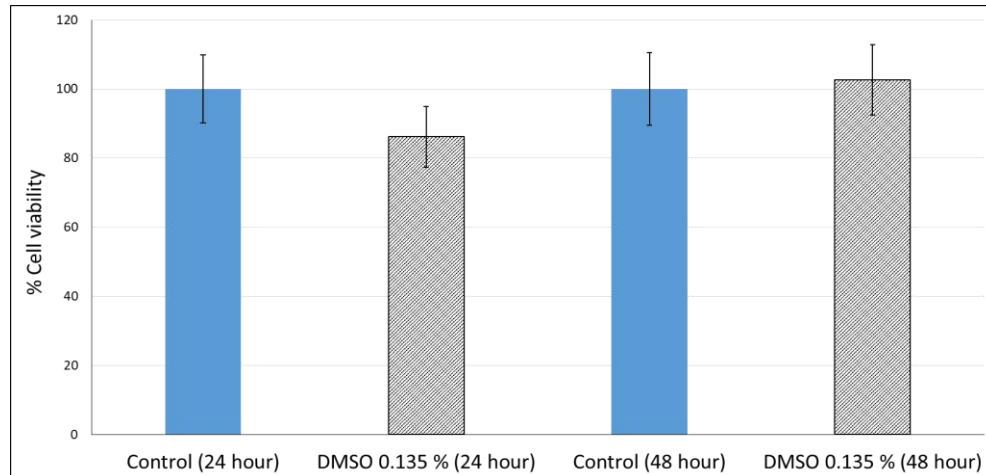
Figure 5.5: The effect of 0.135% DMSO on cell viability. Bars represent (Mean ± SD of n=3).

5.2.4 **Statistical analysis**

The statistic was conducted as described in the second chapter (2.2.4). The area under the curve (AUC) was calculated by the trapezoid rule.(215)

5.3 Results

5.3.1 The uptake study

The uptake of NBQX, licofelone, A5, A16, and A87-licofelone was studied in healthy and early simulated OA cartilage. Overall, the % uptake of NBQX and licofelone has increased in a time-dependent manner.

5.3.1.1 The uptake study of NBQX in healthy or early simulated OA cartilage

At 120 minutes, the uptake of NBQX reached its maximum percent (27.5 ± 2.1 %) in healthy cartilage, while in early simulated OA cartilage, the maximum percent (25 ± 1.9 %) was reached at 90 minutes (Figure 5.6). At both cartilage models, the % uptake of NBQX started to plateau at 60 minutes. Comparing each time point showed no significant difference in the % NBQX uptake between healthy and OA cartilage. Furthermore, the total NBQX uptake in healthy and OA cartilage, which was 2,542 ± 85.2 and 2,391 ± 131.3 %, respectively, was another indicator of a similar uptake percentage in both cartilage models. Over the first 40 minutes, a fast increase of NBQX uptake was observed; the % NBQX started from 3.47 ± 0.8 % to 21.3 ± 1.8 % in healthy cartilage, while the % NBQX started from 3.46 ± 0.5 % to 18.7 ± 4.7 % in OA cartilage. However, over the next 80 minutes, the % uptake of NBQX increased 6.24 % in the healthy model and 6.32% in the OA model.
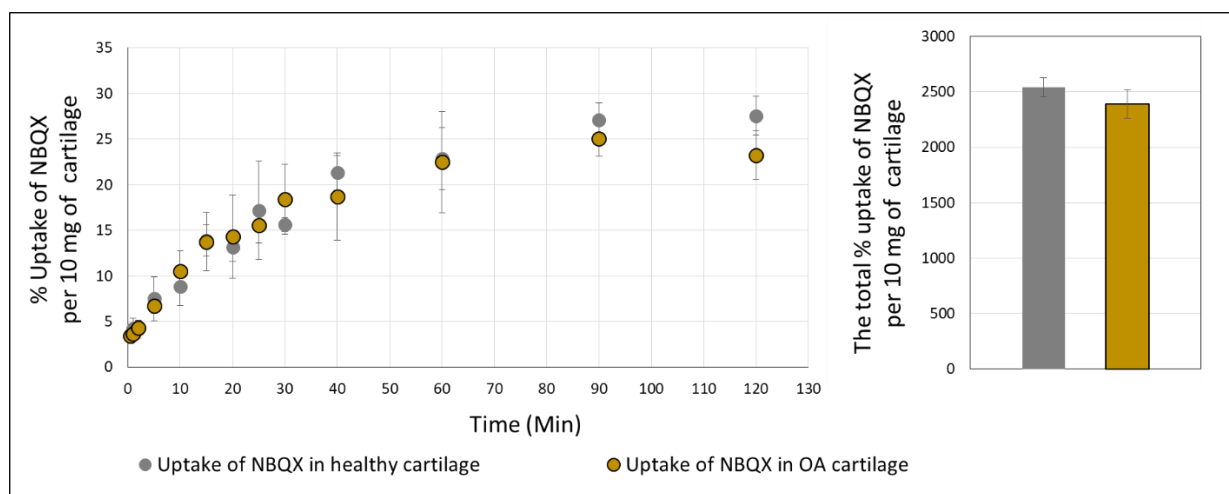
Figure 5.6: The percent uptake of NBQX alone per 10 mg of healthy or early simulated OA cartilage model

Bars represent (Mean ± SD of n=3).

The NBQX was self-assembled with acrylate-terminated A5 in order to mask the negative charge of NBQX and increase its uptake. However, the self-assembly of NBQX and acrylate-terminated A5 has shown lower NBQX uptake compared to NBQX alone (Figure 5.7). The 1st and 2nd self-assembled NBQX have shown maximum NBQX % uptake of 10.1 ± 2.3 % and 15 ± 1.5 %, respectively, which is significantly lower than NBQX alone. Moreover, each time point after 7 minutes in the NBQX alone uptake study was statistically higher compared to the self-assembled NBQX studies. Furthermore, the total % of NBQX uptake showed that the NBQX alone (2,542 ± 85.2) was significantly higher than the 1st self-assembled (835 ± 68.2) and the 2nd self-assembled (1,242 ± 66.9) (Figure 5.7). The reason for the unexpectedly low uptake of self-assembled NBQX was the precipitation of NBQX during the self-assembly and the uptake experiment (Figure 5.8). Comparing both self-assembled NBQX methods showed that at 30, 90, and 120 minutes, the % uptake of NBQX self-assembled (v/v) was significantly higher compared to (v/w) (Figure 5.7). The total NBQX uptake percentage of the 1st self-assembled (v/w) (835 ± 68.2) was statistically lower than the 2nd self-assembled (w/v) (1,242 ± 66.9). As a result of the precipitation, the uptake study of both self-assembly methods was conducted only on the healthy cartilage model to avoid losing the valuable NBQX.
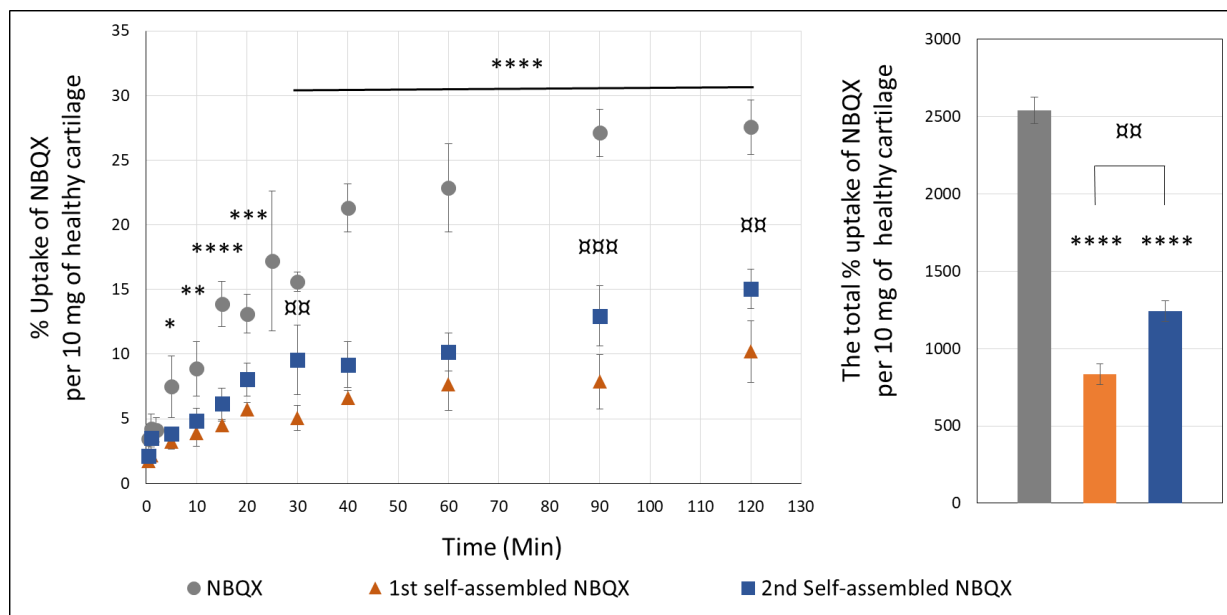
Figure 5.7: The percent uptake of the NBQX alone, 1st self-assembled NBQX (w/v), and the 2nd self-assembled NBQX (v/v) per 10 mg of healthy cartilage

Bars represent (Mean ± SD of n=3). Significant * ($P<0.05$), ** ($P<0.01$), *** ($P<0.001$), **** ($P<0.0001$) the NBQX alone compared to the 2nd self-assembled and significant ¤¤ ($P<0.01$), ¤¤¤ ($P<0.001$) the 1st self-assembled compared to the 2nd self-assembled.
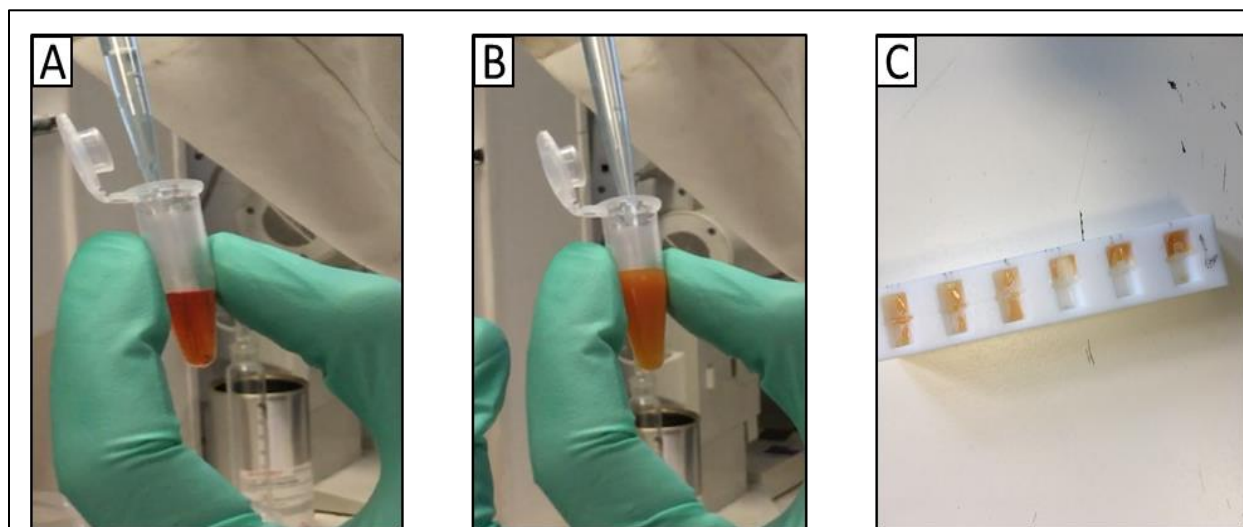
Figure 5.8: The preparation of self-assembled NBQX with acrylate-terminated A5

A) A clear solution of NBQX before adding the acrylate-terminated A5 solution, B) The NBQX solution mixed with the acrylate-terminated A5 and formation of a turbid solution, and C) The precipitation of NBQX in the transport chamber during the uptake study

5.3.1.2 **The uptake study of licofelone (control)**

Figure 5.9 shows the % uptake of licofelone alone per 10 mg of healthy and early simulated OA cartilage. At the first minute, the % uptake of licofelone was 0.3 ± 0.06 % and reached a maximum uptake of 1.3 ± 0.8 % at 30 minutes. Additionally, a similar result of licofelone % uptake per 10 mg of early simulated OA cartilage over time was observed. In early simulated OA cartilage, licofelone reached a maximum uptake of 1.7 ± 0.6 % at 30 minutes, and the lowest uptake of 0.4 ± 0.03 % was at 2 minutes. The percentage uptake of licofelone in both cartilage models started to plateau between 15 and 20 minutes. Although the % uptake of licofelone in OA cartilage was numerically higher than the uptake in healthy cartilage, the comparison shows no statistically significant difference. Moreover, the total % uptake of licofelone in healthy cartilage (27.5 ± 5.2 %) was not statistically different compared to the total % uptake in OA cartilage (32.1 ± 2.9 %) (Figure 5.9).
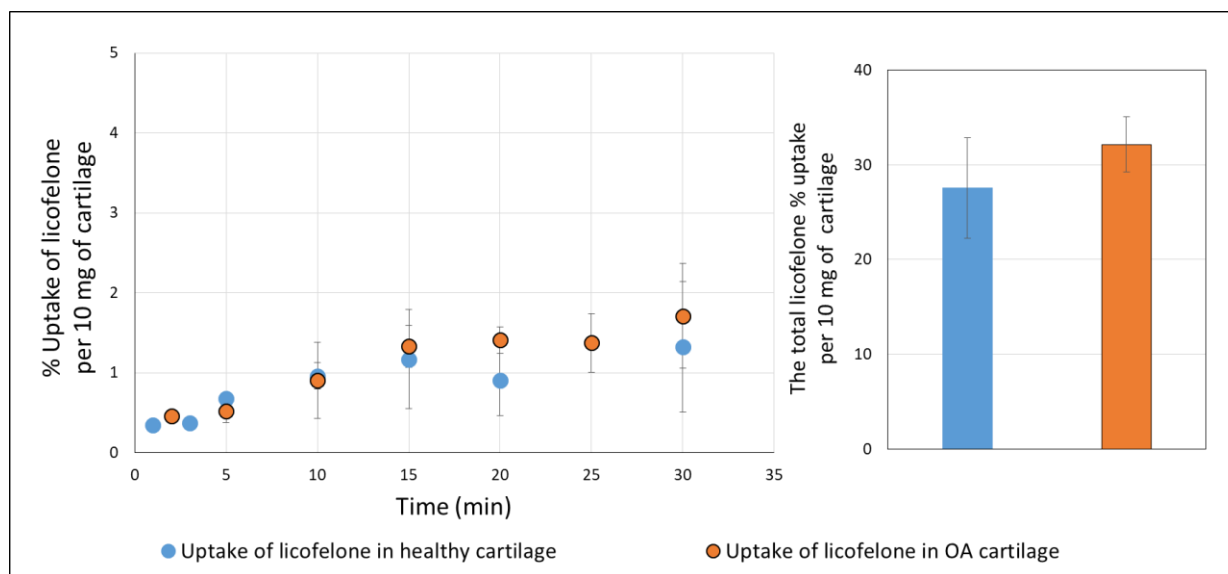
Figure 5.9: The percent uptake of licofelone per 10 mg of the healthy cartilage and early simulated OA cartilage models

Bars represent (Mean ± SD of n=3).

5.3.1.3 **The uptake study of A5-licofelone conjugate**

Figure 5.10 shows the % uptake of licofelone conjugated to A5 per 10 mg of healthy and OA cartilage over time. The uptake of conjugated licofelone showed a statistically significant difference between the two cartilage models. At 2 minutes, the % uptake of licofelone in healthy cartilage was 0.46 ± 0.03 %, and the maximum uptake was 1.7 ± 0.65 %, which was reached at 30 minutes. However, in an early simulated OA cartilage model, the % conjugated licofelone uptake was 8.21 ± 0.66 % at 2 minutes and 10.07 ± 1.08 % at 30 minutes. Comparing the % of conjugated licofelone uptake in healthy cartilage versus OA cartilage has demonstrated that the % uptake of licofelone was significantly higher in the OA cartilage models at each time point. The licofelone conjugated to A5 uptake was 7.12 - 9.08 % higher in OA cartilage compared to healthy cartilage. The total % of conjugated licofelone in the early simulated OA cartilage was 271.4 ± 5.65 %, while in healthy cartilage was significantly lower (28.56 ± 4.29 %). Overall, the % uptake of conjugated licofelone to A5 shows different % uptake of licofelone between the healthy cartilage and the early simulated OA cartilage model, and the % uptake of conjugated licofelone was higher in the OA cartilage models.
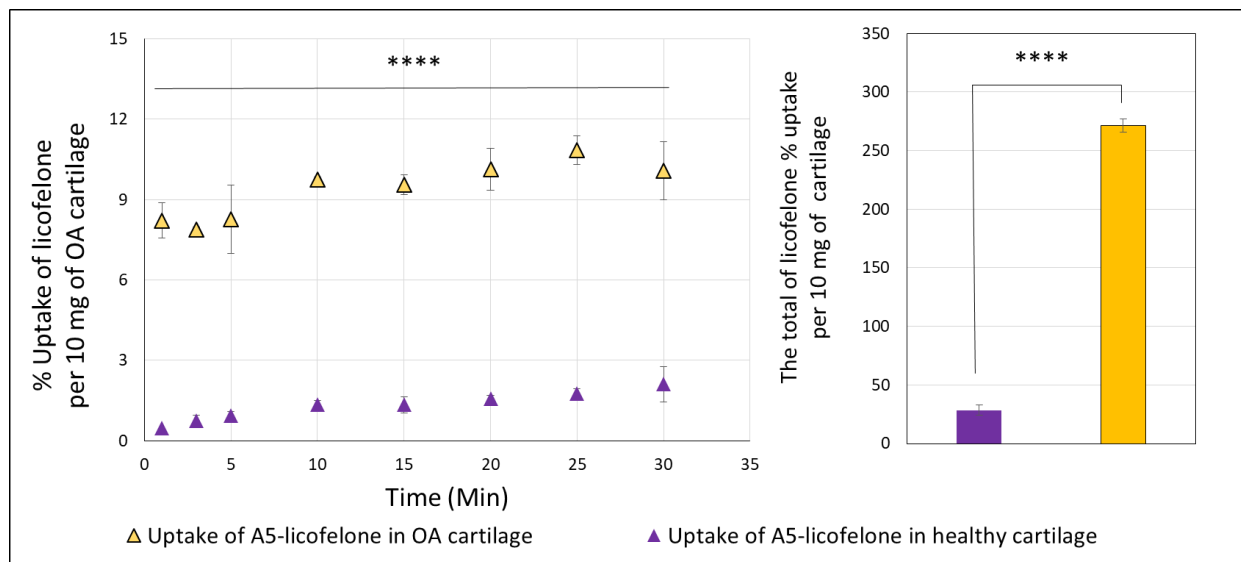
Figure 5.10: The percent uptake of licofelone conjugated to A5 per 10 mg of the healthy cartilage and early simulated OA cartilage

Bars represent (Mean ± SD of n=3). Significant **** (P<0.0001)

5.3.1.4 **The uptake study of A16-licofelone conjugate**

The % uptake of conjugated licofelone to A16 was conducted in healthy and early simulated OA cartilage (Figure 5.11). Both showed a comparable uptake profile. At 0.5 minutes, the % uptake of conjugated licofelone was 16.55 ± 1.02 % in healthy cartilage and 17 ± 3.23 % in the OA model. Moreover, the maximum uptake percentage of licofelone was 23.4 ± 0.85 in healthy cartilage and 23.4 ± 0.26 % in OA cartilage. The uptake percentage of licofelone in the comparison between the health and early simulated OA cartilage models with respect to the time point showed no significant difference except at 7 minutes. In OA cartilage models, the % uptake of conjugated licofelone was 18.7 ± 0.63 %, which is statistically higher than the uptake of licofelone in healthy cartilage by 3.6 %. Statistically, the total % of licofelone uptake shows no difference between both cartilage models, whereas numerically, the uptake of licofelone in healthy cartilage (566.2 ± 16.75 %) was lower than the uptake of licofelone in OA cartilage (595 ± 8.36 %). The uptake study of A16-licofelone conjugate in healthy and OA cartilage showed a gradually increasing percentage of licofelone uptake over time.
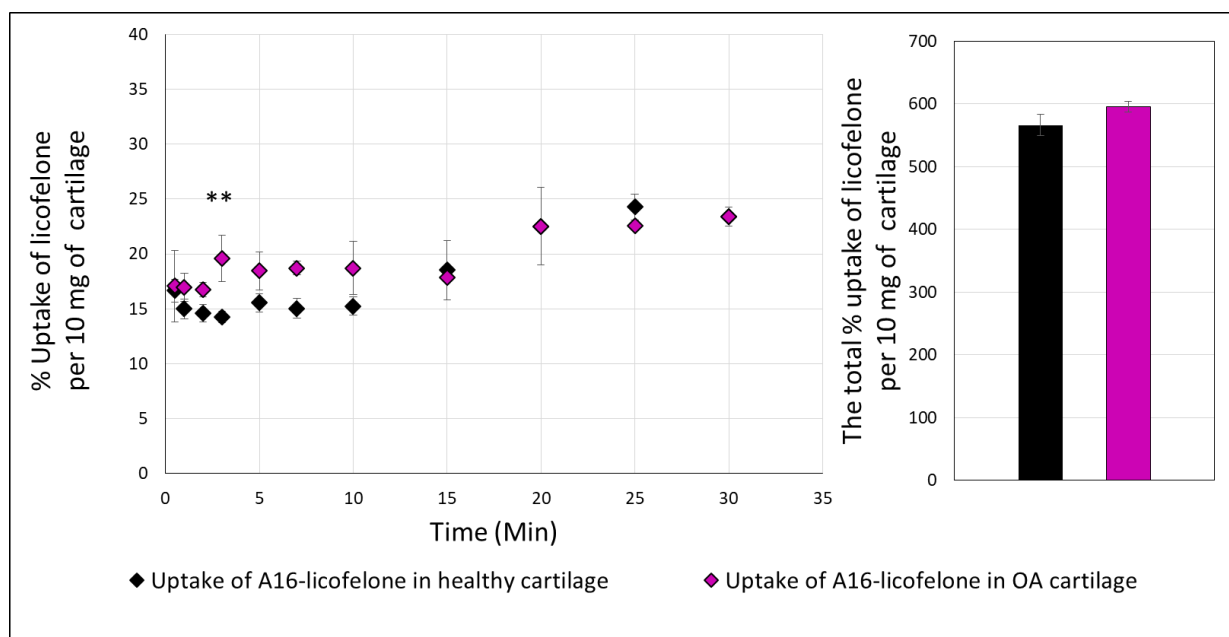
Figure 5.11: The percent uptake of licofelone conjugated to A16 per 10 mg of healthy cartilage and early simulated OA cartilage

Bars represent (Mean ± SD of n=3). Significant ** (P<0.01)

5.3.1.5 **The uptake study of A87-licofelone conjugate**

Figure 5.12 shows the % uptake of licofelone conjugated to A87 per 10 mg of healthy and early simulated OA cartilage over time. The percentage uptake of conjugated licofelone was significantly higher in the healthy cartilage compared to the OA cartilage models. During the first 5 minutes of the uptake studies, the % uptake of licofelone showed no statistical difference between the two cartilage models, but from 7 to 30 minutes, the uptake of licofelone in the healthy cartilage was significantly higher compared to the OA cartilage model. The % uptake of licofelone has started at 15.4 ± 0.79 % in healthy cartilage and 11.2 ± 0.58 % in OA cartilage, which showed no statistical difference. After the first 7 minutes, the % uptake of licofelone in healthy cartilage was 7.9 to 19.3 % higher than the % uptake of licofelone in OA cartilage. At 30 minutes, the % uptake of licofelone conjugated to A87 in healthy cartilage has reached a maximum uptake of 44 ± 4.3 %, while in OA cartilage, the maximum uptake of licofelone was 26.6 ± 3.1 % at 25 minutes. Additionally, the total % uptake of the conjugated licofelone in healthy cartilage (1,012 ± 22.42 %) was statistically higher compared to the licofelone uptake in OA cartilage (679.6 ± 28.72).
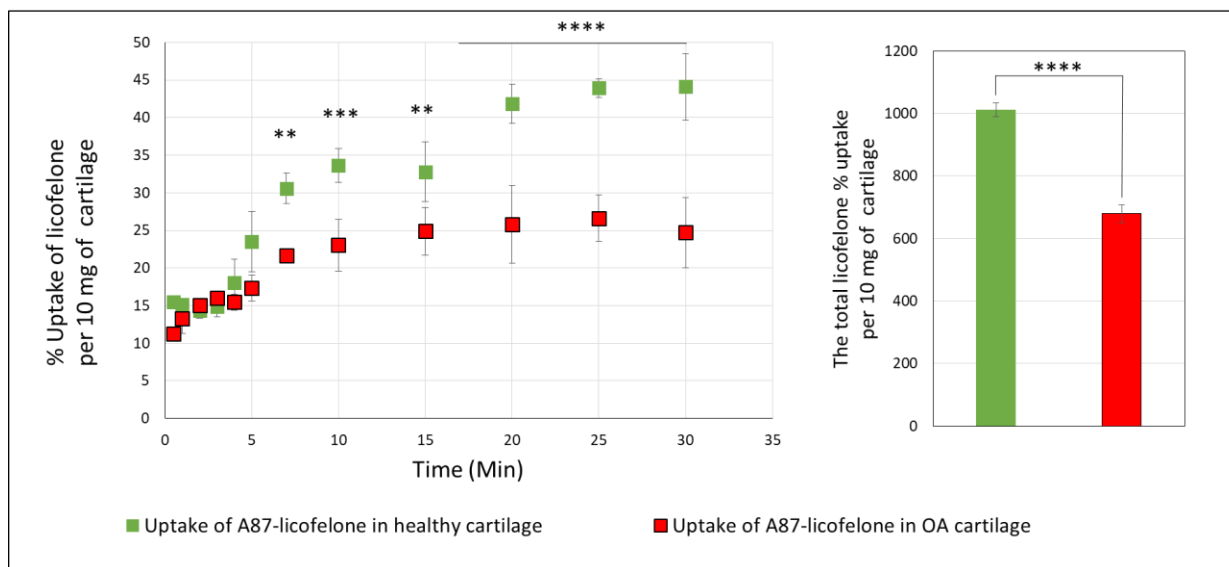
Figure 5.12: The percent uptake of licofelone conjugated to A87 per 10 mg of healthy and early simulated OA cartilage

Bars represent (Mean ± SD of n=3). Significant ** (P<0.01), *** (P<0.001), **** (P<0.0001)

5.3.1.6 The uptake study of NBQX compared to licofelone

A comparison between the uptake of NBQX and licofelone was observed to investigate the physiochemical properties of small molecules that could influence the uptake. The uptake of NBQX in healthy and OA cartilage has demonstrated a significantly higher percentage uptake compared to licofelone (Figure 5.13 and Figure 5.14). At the first minute, the % uptake of NBQX was 4.2 ± 1.1 % in healthy cartilage and 4.3 ± 0.8 % in OA cartilage, while the % uptake of licofelone was 0.3 ± 0.06 % and 0.4 ± 0.03 %, respectively. At 60 minutes, the maximum % uptake of NBQX was 22.8 ± 3.4 % in healthy cartilage and 18.4 ± 3.8 % in OA cartilage, while the % uptake of licofelone was 1.4 ± 0.6 % and 1.7 ± 0.6 %, respectively. Additionally, the % uptake of NBQX was statistically superior compared to the % uptake of licofelone at every time point in both cartilage models. Furthermore, the total % uptake of NBQX was significantly higher in healthy cartilage (332.4 ± 15.5 %) and in OA cartilage (359 ± 34 %) compared to the total % uptake of licofelone (27.5 ± 5.2 % and 32.1 ± 2.9 %, respectively).
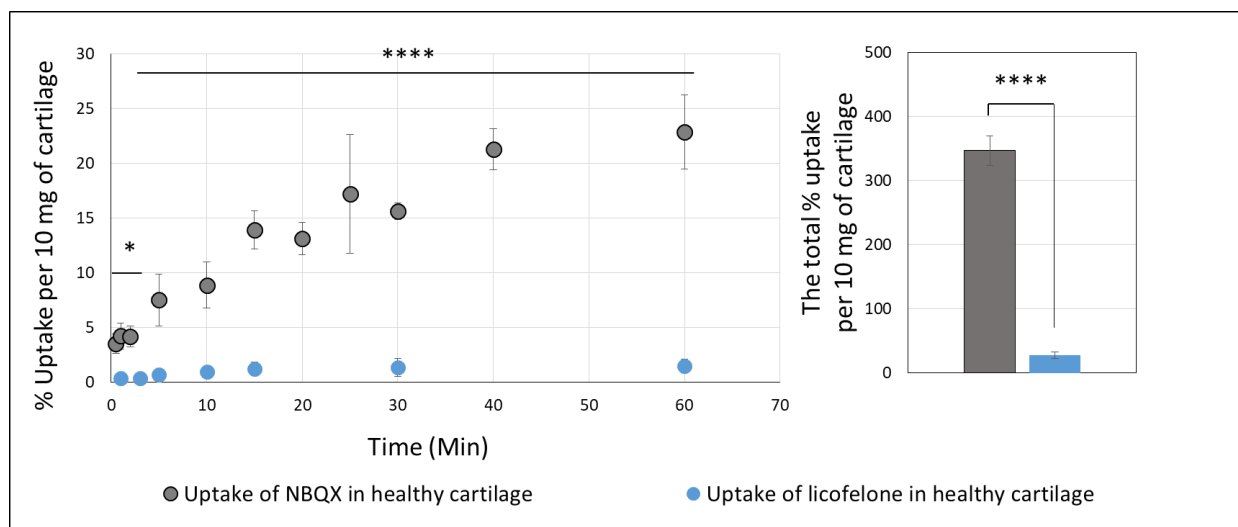
Figure 5.13: The percent uptake of NBQX and licofelone per 10 mg of healthy cartilage over time Bars represent (Mean ± SD of n=3). Significant * (P<0.05), **** (P<0.0001)
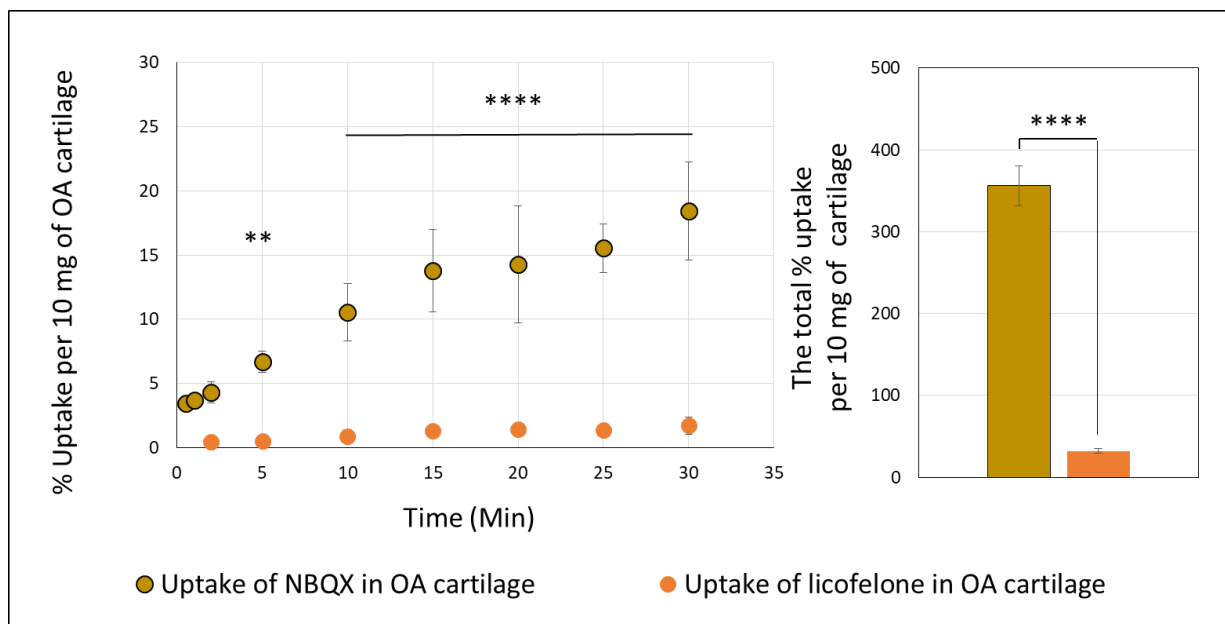
Figure 5.14: The percent uptake of NBQX and licofelone per 10 mg of OA cartilage over time

Bars represent (Mean ± SD of n=3). Significant ** (P<0.01), **** (P<0.0001)

5.3.1.7 **The uptake study of licofelone and licofelone conjugates**

Figure 5.15 shows the comparison of licofelone % uptake between licofelone alone, A5-licofelone, A16-licofelone, and A87-licofelone conjugates in healthy cartilage. Licofelone conjugates except A5-licofelone have statistically enhanced the conjugated licofelone uptake compared to licofelone alone. A5-licofelone conjugate has shown a numerical increase in the % uptake of licofelone compared to licofelone alone (Figure 5.15). The maximum % uptake of unconjugated licofelone was 1.4 ± 0.6 %, whereas the maximum % uptake of conjugated licofelone to A5, A16, and A87 were 1.7 ± 0.65 %, 23.4 ± 0.85 %, and 44 ± 4.3 %, respectively. Additionally, the total uptake % of licofelone alone was 27.5 ± 5.2 %, while the conjugated licofelone to A5, A16, and A87 were 28.56 ± 4.29 %, 566.2 ± 16.75 %, and 1,012 ± 22.42 %, respectively. Similar results were observed in the early simulated OA cartilage model, where A5-licofelone, A16-licofelone, and A87-licofelone conjugates produced a significantly higher uptake percentage of conjugated licofelone compared to unconjugated licofelone (Figure 5.16). In the OA cartilage model, the maximum % uptake of licofelone alone was 1.7 ± 0.6 % at 30 minutes, and the total % uptake of licofelone was 32.1 ± 2.9 %. However, the uptake % of the conjugated drug increased to reach the maximum uptake of 10.07 ± 1.08 % and the total % uptake of 271.4 ± 5.65 % when licofelone conjugated to A5. In OA cartilage, A5-licofelone conjugate has increased

138

the % uptake of conjugated licofelone significantly compared to the control (licofelone alone), whereas in healthy cartilage, the increase in conjugated licofelone to A5 % uptake was not statistically significant compared to the control. Additionally, A16-licofelone and A87-licofelone have increased the uptake % of licofelone even more than the A5-licofelone conjugate to reach maximum % uptake of 23.4 ± 0.26 % and 26.6 ± 3.1 % when conjugated to A16 and A87, respectively. The total % uptake of conjugated licofelone to A16 and A87 was 595 ± 8.36 % and 679.6 ± 28.72 %, respectively, which is approximately 20 times higher than the uptake of licofelone alone.

Comparing the licofelone conjugates against each other has shown that the A87-licofelone conjugate was significantly the highest to enhance the conjugated licofelone uptake compared to the A5-licofelone and A16-licofelone conjugates in both cartilage models. In healthy cartilage, A16-licofelone and A87-licofelone conjugates showed a significantly superior level of conjugated licofelone uptake compared to A5-licofelone at all time points. From 0.5 to 4 minutes, the % uptake of conjugated licofelone to A16 and A87 were approximately similar, whereas from 5 to 30 minutes, the % uptake of conjugated licofelone to A87 has increased significantly compared to A16 (Figure 5.15). In the OA cartilage model, the % uptake of conjugated licofelone to A16 and A87 were significantly greater than the uptake % of conjugated licofelone to A5 at all time points, even though the total uptake % of conjugated licofelone to A5 in OA cartilage has enhanced about 10 times more than in healthy cartilage. In the early simulated OA cartilage, the licofelone conjugated to A16 and A87 was comparable with no significant different except at 0.5 minutes, when the A16-licofelone conjugated showed a higher uptake percent of licofelone. The uptake percentage of the conjugated licofelone to A87 was gradually increased over 10 minutes, at which point it became significantly higher compared to the % uptake of licofelone conjugated to A16. In both cartilage models, A87-licofelone has produced the highest uptake percentage of licofelone, followed by A16-licofelone conjugates, and then the A5-licofelone conjugate and licofelone alone (Figure 5.15 and Figure 5.16).
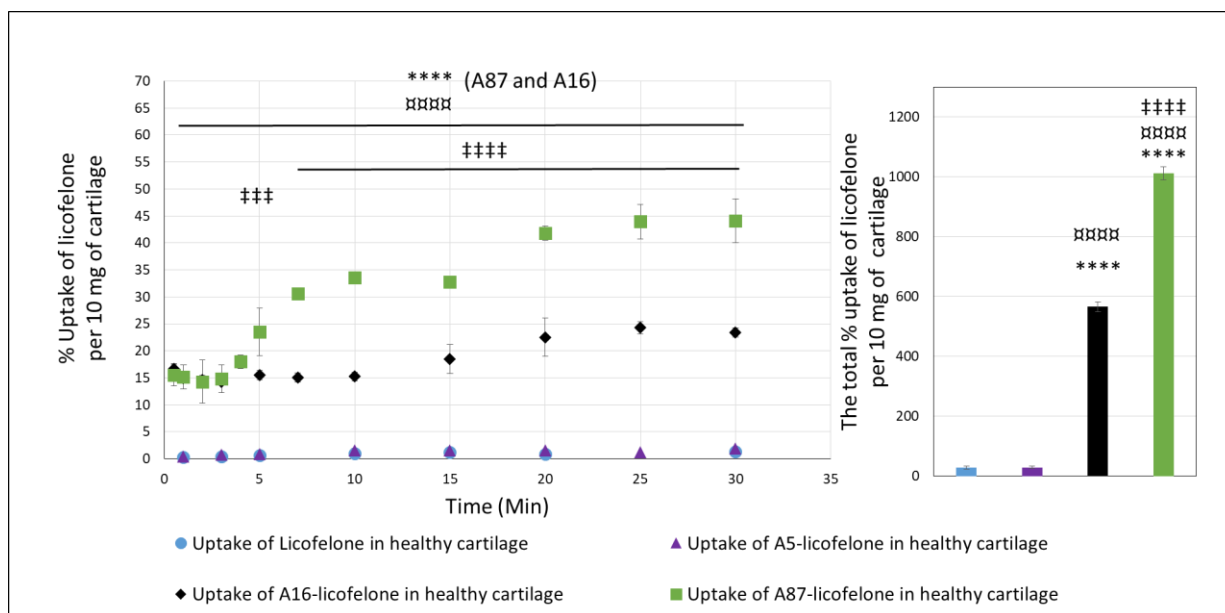
Figure 5.15: The percent uptake of licofelone alone and conjugated licofelone to A5, A16 and A87 per 10 mg of healthy cartilage

Bars represent (Mean ± SD of n=3). Significant **** (P<0.0001), the three licofelone conjugates compared to the control (licofelone alone), significant ¤¤¤¤ (P<0.0001), A16-licofelone and A87-licofelone conjugates compared to the A5-licofelone conjugate, and significant ‡‡‡ (P<0.001), ‡‡‡‡ (P<0.0001), A87-licofelone conjugate compared to the A16-licofelone conjugate.
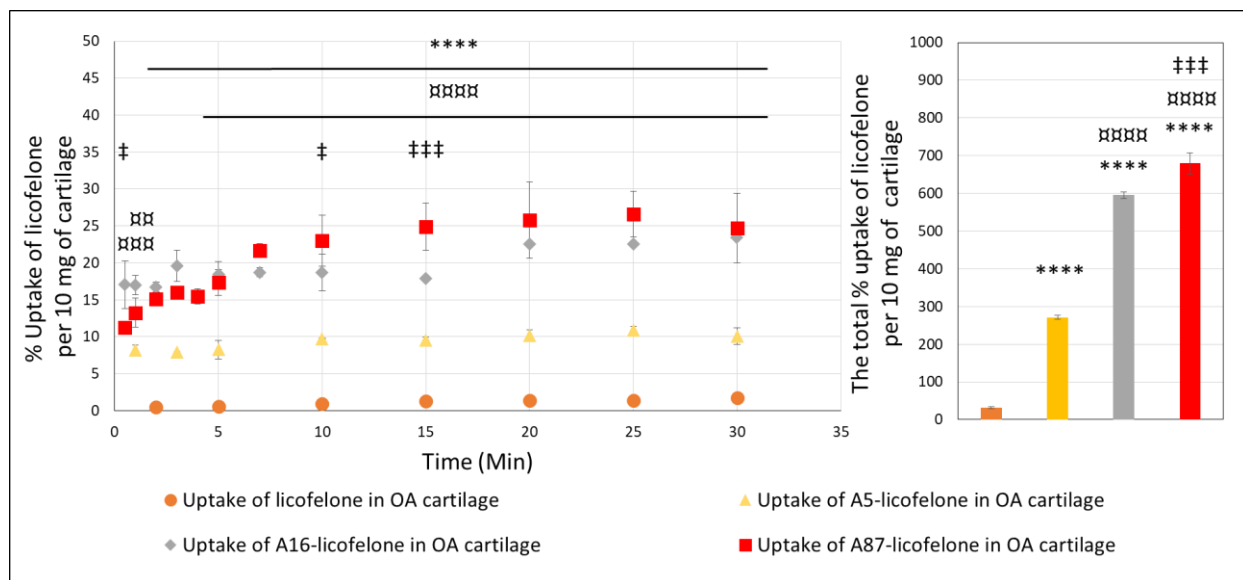
Figure 5.16: The percent uptake of licofelone alone and conjugated licofelone to A5, A16 and A87 per 10 mg of early simulated OA cartilage

Bars represent (Mean ± SD of n=3). Significant **** ($P<0.0001$), the three licofelone conjugates compared to the control (licofelone alone), significant ¤¤ ($P<0.01$), ¤¤¤ ($P<0.001$), ¤¤¤¤ ($P<0.0001$), A16-licofelone and A87-licofelone conjugates compared to the A5-licofelone conjugate, and significant ‡ ($P<0.05$), ‡‡‡ ($P<0.001$), ‡‡‡‡ ($P<0.0001$), A87-licofelone conjugate compared to the A16-licofelone conjugate

5.3.2 The retention study

The retention of NBQX, licofelone, A5, A16, and A87-licofelone was studied in healthy and early simulated OA cartilage. As discussed in 5.2.2.2, the cartilage was incubated with the drug alone or the formulated drug with the polymers until the uptake of the drug within the cartilage plateaued, which was 60 minutes for NBQX and 20 minutes for licofelone (Figure 5.6 and Figure 5.9, respectively). After that, the cartilage containing the maximum percentage of the drug or the formulated drug was incubated in PBS pH 7.4 medium for different time points, allowing the drug to be either released or retained in the cartilage. Then, the quantity of NBQX and licofelone retained within the cartilage was determined after complete cartilage digestion, as reported in 5.2.2.2. However, only in the self-assembled NBQX study was the released quantity of the drug in the PBS pH 7.4 medium calculated based on Equation 5.2. Overall, the retention time profiles have shown a reduction of NBQX and licofelone percentages within the cartilage in a time-dependent manner.

Equation 5.2:

% NBQX released from the cartilage =

(the uptake % of NBQX at 60 minutes - the retained % of NBQX)

5.3.2.1 The retention study of NBQX and self-assembled NBQX

The percentage of NBQX uptake started to plateau at 60 minutes, which was discussed previously (Figure 5.6). Therefore, the transport chamber was incubated for 60 minutes during the retention time studies of NBQX. Figure 5.17 shows the retention time study of NBQX in the healthy and early simulated OA cartilage models. At the first minute, the % NBQX retained was 21.04 ± 4.7 % in healthy cartilage and 21.1 ± 2.6 % in OA cartilage, and then the % NBQX was gradually reduced, reaching 1 ± 0.01 % in healthy cartilage and 4.1 ± 0.97 % in OA cartilage. Comparing each time point shows no significant difference between the % of NBQX retained in both cartilage models except at 60 minutes, which showed the retained % of NBQX in OA cartilage (12.14 ± 0.73 %) was statistically higher compared to the % NBQX retained in healthy cartilage (5.98 ± 0.75 %). Overall, the % NBQX retained in OA cartilage was numerically higher than healthy cartilage. Moreover, the total percentage of NBQX retained in OA cartilage (2,396 ± 90.29 %) was significantly higher than that of healthy cartilage (1,314 ± 135.3). These comparisons indicated that the retention % of NBQX is higher in OA cartilage.
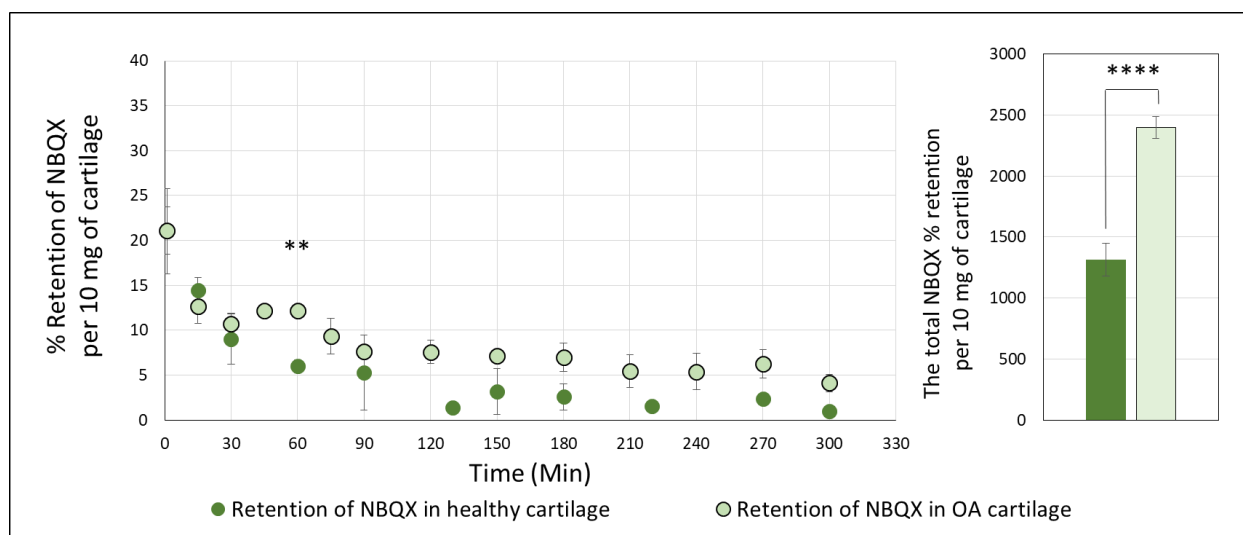
Figure 5.17: The percent retained of NBQX per 10 mg of healthy and early simulated OA cartilage Bars represent (Mean ± SD of n=3). Significant ** (P<0.01), **** (P<0.0001)

The retention study was only conducted for the second methodology of self-assembled NBQX **(v/v)**, because the first methodology **(w/v)** has shown more precipitation of NBQX during preparation and lower uptake of NBQX compared to the second methodology **(v/v)**. Figure 5.18 shows the retention time study of self-assembled NBQX with acrylate-terminated A5 and NBQX

alone in healthy cartilage. NBQX-A5 self-assembled has shown a gradual inhibition of % NBQX from healthy cartilage. The self-assembled NBQX % retained within the cartilage was comparable to NBQX alone, despite the low uptake percentage of self-assembled NBQX because of the precipitation. The exceptions were at 15 and 30 minutes, when the percentage of NBQX retained was significantly higher in NBQX alone (14.4 ± 1.4 % and 10.7 ± 1.2 %) when compared to self-assembled NBQX (9.5 ± 0.1 % and 4.9 ± 1.6 %). Accordingly, the total % of NBQX retained was 1,314 ± 135.3 % in the study of NBQX alone and 880 ± 76.5 % in the study of self-assembled NBQX, which showed a statistically significant difference. The low percentage of NBQX retained that was observed in the self-assembled NBQX when compared to NBQX alone was expected because of the precipitation during the retention study. However, the self-assembled NBQX will have a higher percentage of NBQX retained within the cartilage if the uptake value of NBQX versus the retained value of NBQX were to be considered. For instance, if we subtracted the % of NBQX that is absorbed by the cartilage from the % of NBQX retained within the cartilage in order to obtain the % of NBQX that was released from the cartilage, the % of NBQX released from the cartilage would be lower in the self-assembled NBQX compared to the NBQX alone (Equation 5.2). The current study aims to increase the NBQX retained within the cartilage or lower the NBQX release from the cartilage. Figure 5.19 shows the calculated percentage of NBQX released from the cartilage after subtracting the retained % of NBQX from the uptake % at 60 minutes, which was the uptake time before conducting the retention time study. At 60 minutes, the average NBQX alone % uptake was 22.8 %, and the average self-assembled NBQX % uptake was 10.1 %. Comparing each time point has shown that the % release of NBQX alone from the cartilage was significantly higher compared to self-assembled NBQX. In addition, the total % of NBQX released from the cartilage was statistically lower in the self-assembled NBQX (33.6 ± 1.2 %) compared to NBQX alone (90.7 ± 2.1 %). Overall, the self-assembled NBQX with A5 has significantly decreased the % NBQX released from the cartilage compared to the NBQX alone.
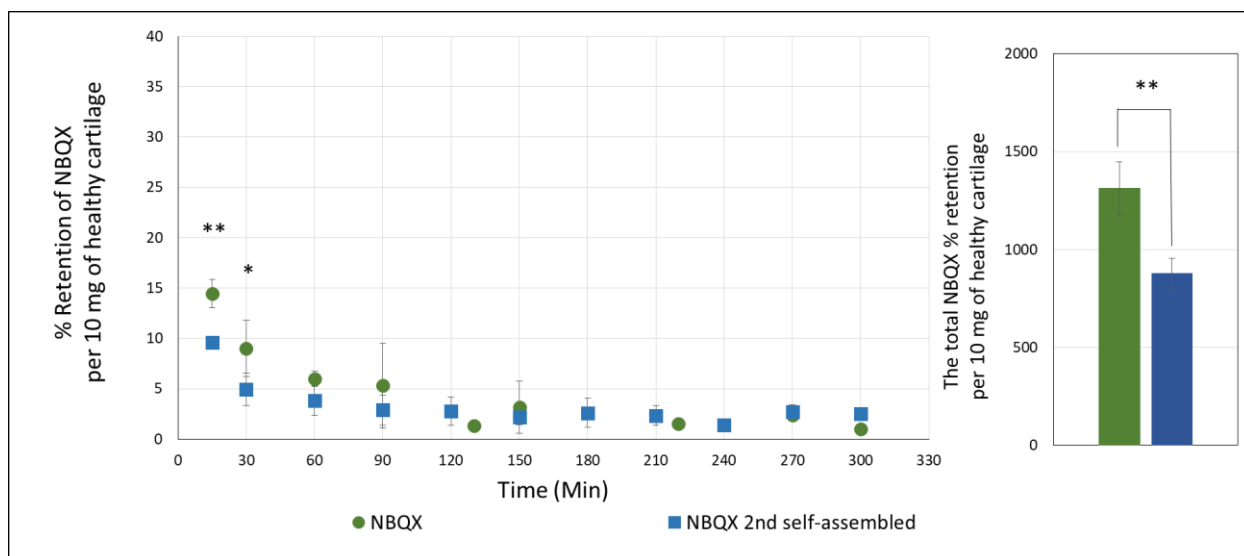
Figure 5.18: The percent retained of NBQX and self-assembled NBQX (v/v) per 10 mg of healthy cartilage

Bars represent (Mean ± SD of n=3). Significant * (P<0.05), ** (P<0.01)
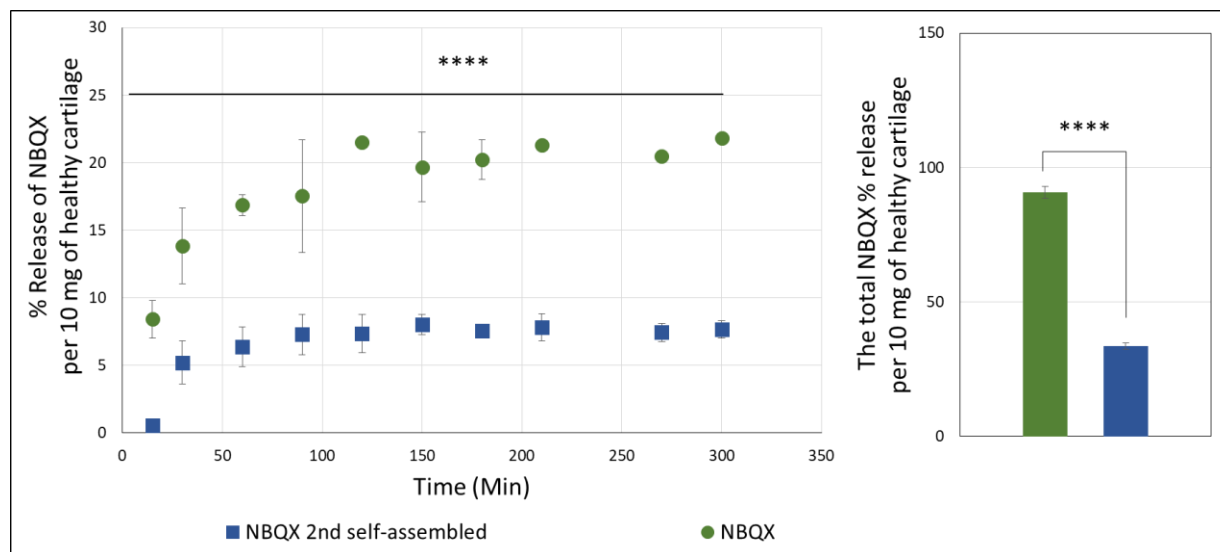
Figure 5.19: The calculated percent of the released NBQX and self-assembled NBQX (v/v) per 10 mg of healthy cartilage over time

Bar represents (Mean ± SD). Significant **** (P<0.0001)

5.3.2.2 **The retention study of licofelone (control)**

At 20 minutes, the % uptake of licofelone started to plateau, which was discussed previously (Figure 5.9). Therefore, the uptake incubation time of 20 minutes was chosen for the licofelone retention time studies. Figure 5.20 shows the % retention of licofelone alone over time in the healthy cartilage and the OA cartilage. In both models, licofelone was not detected after 60 minutes. Additionally, the percentage of licofelone retained within both cartilage models was similar, with no significant difference. In the healthy cartilage, the reduction of licofelone % was rapid during the first 7 minutes and then was steady from 15 to 60 minutes. At the first minute, the retained % of licofelone was 1.8 ± 0.5 % in healthy cartilage and 1.6 ± 0.2 % in OA cartilage, while at the 15th minute, the % of licofelone retained within the cartilage was 0.9 ± 0.3 % and 0.75 ± 0.2 %, respectively, which indicate that 50 % of licofelone has been released from the cartilage during 15 minutes. After 15 minutes, the % retention of licofelone was steady until the 60th minute in both models, where the % retention of licofelone was 0.9 ± 0.1 % in healthy cartilage and 0.64 ± 0.1 % in OA cartilage. Comparing the time points of the retention time study of licofelone in healthy versus in OA cartilages has shown no significant difference. Additionally, the total % of licofelone retained in healthy cartilage (58.29 ± 6.2 %) was not statistically higher than in OA cartilage (56.03 ± 3.2 %).
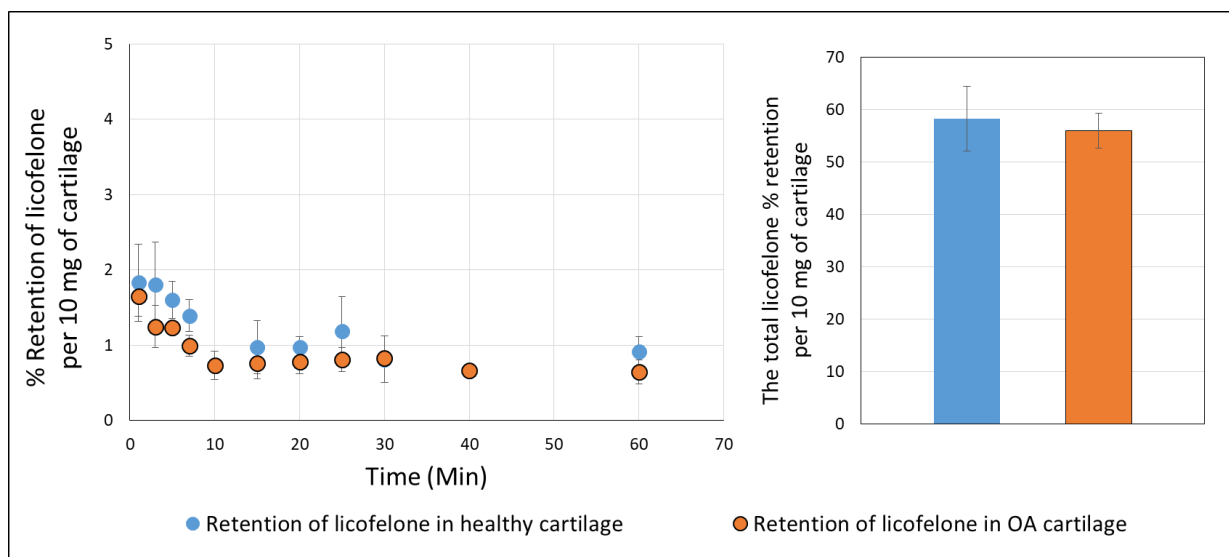
Figure 5.20: The percent retention of licofelone per 10 mg of healthy and early simulated OA cartilage

Bars represent (Mean ± SD of n=3)

146

5.3.2.3 The retention study of A5-licofelone conjugate

Figure 5.21 shows the retention time study of licofelone conjugated to A5 per 10 mg of healthy cartilage and early simulated OA cartilage over time. The percentage of conjugated licofelone retained in the OA cartilage was significantly higher compared to the healthy cartilage. In healthy cartilage, during the first 15 minutes, the release of licofelone was steady and slow. At the first minute, the % of licofelone was 4.1 ± 0.2 %, and 3.7 ± 1.2 % at the 15th minute, which means only 0.3 % of licofelone has been released from the healthy cartilage. After 15 minutes, the % of licofelone retained dropped significantly, reaching 1.4 ± 0.6 % at 20 minutes. Similarly, in OA cartilage, the first 15 minutes showed a constant % of conjugated licofelone retained, which was 11.5 ± 0.6 % at 1 minute and 10.6 ± 1.3 % at 15 minutes. During the first 15 minutes, only 0.8 % of licofelone was released from the cartilage to the PBS medium, while after 15 minutes to the 40th minute, 9.1 % of licofelone was released. At each time point, the % of licofelone retained within OA cartilage was statistically higher than the % of licofelone within healthy cartilage. Additionally, the total % of licofelone retained within healthy cartilage (103 ± 24 %) is significantly lower than OA cartilage (266.1 ± 26.2 %). Although the percentage of licofelone retained within the cartilage was significantly higher in OA cartilage compared to healthy cartilage, the retention time profile in healthy and OA cartilage seems similar. In which both models showed a constant retention % of licofelone for the first 15 minutes, but beyond that time, a large % of licofelone was released from the cartilage into the PBS medium.

Figure 5.21: The percent retention of the licofelone conjugated to A5 per 10 mg of healthy and early simulated OA cartilage

Bars represent (Mean ± SD of n=3). Significant * (P<0.05), ** (P<0.01), *** (P<0.001), **** (P<0.0001)

5.3.2.4 The retention study of A16-licofelone conjugate

Figure 5.22 shows the percentage of licofelone conjugated to A16 retained inside the healthy and early simulated OA cartilage. In both cartilage models, the % of licofelone retained was gradually reduced over time. However, the percentage of conjugated licofelone retained in healthy cartilage was significantly higher compared to the OA cartilage. Comparing each time point of the retention study of A16-licofelone in healthy cartilage against OA cartilage has shown a significantly higher % of licofelone retained in healthy cartilage. During the first 10 minutes, the % of licofelone retained has dropped significantly from 28.4 ± 1.2 % in healthy cartilage and 16.5 ± 2.2 % in OA cartilage to 17.1 ± 0.3 % and 11.7 ± 0.3 %, respectively. After 10 minutes, the % retained of licofelone was steady, and the % retained of licofelone was 14.1 ± 0.1 % in healthy cartilage and 9.1 ± 0.2 % in OA cartilage at 60 minutes. Accordingly, during the first 10 minutes, the released licofelone % was 11.3 % in healthy cartilage and 4.7 % in OA cartilage, while during the next 10 to 60 minutes, only 3 % and 2.6 % of licofelone were released into the PBS medium, respectively. Furthermore, the total % of the licofelone retained has demonstrated that the healthy cartilage (1,179 ± 11.8 %) has retained more licofelone conjugated to A16 than OA cartilage (787.2 ± 8.9 %). Even though a higher percentage of licofelone was retained in healthy cartilage than in OA cartilage, both models have shown a similar retention time profile.
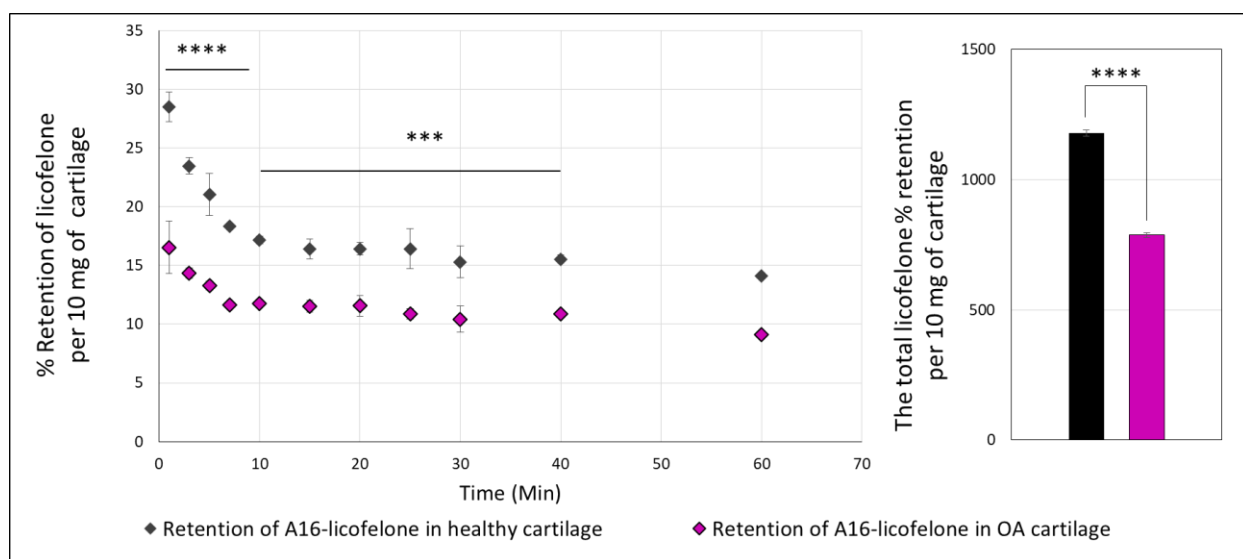
Figure 5.22: The percent retention of the licofelone conjugated to A16 per 10 mg of healthy and early simulated OA cartilage

Bars represent (Mean ± SD of n=3). Significant *** (P<0.001), **** (P<0.0001)

5.3.2.5 The retention study of A87-licofelone conjugate

The % retention of licofelone conjugated to A87 was conducted over time (0 – 120 minutes) in healthy cartilage and OA cartilage (Figure 5.23). The conjugated licofelone to A87 showed an increase on licofelone retention time in the healthy cartilage and OA cartilage. The licofelone was still detectable at 120 minutes in both cartilage models. When the percentage of conjugated licofelone to A87 was compared in healthy cartilage versus OA cartilage, three distinct phases were observed during the retention time study. At the first phase, which was between the first and 10th minute, the % of licofelone retained was significantly higher in healthy cartilage compared to OA cartilage. During the second phase, which was between 15 and 40 minutes, the retention showed no significant difference between both cartilage models. At the third phase (60 – 120 minutes), in the OA cartilage, the retained percentage of licofelone was significantly higher than in the healthy cartilage. At the beginning, the retained licofelone was 31.3 ± 2.8 % within the healthy cartilage and 25.8 ± 2.8 % within the OA cartilage, but over time the retention % of licofelone was reduced to 10.8 ± 0.6 % and 13.4 ± 1.5 % at 120 minutes, respectively. In healthy cartilage, a fast reduction of the % retained licofelone from 31.3 ± 2.8 % to 22.2 ± 3 % was observed during the first 10 minutes, while the % retained licofelone underwent a gradual reduction within OA cartilage during the first 25 minutes, going from 25.8 ± 2.8 % to 21.1 ± 0.8 %. At 120 minutes, the % of conjugated licofelone was 10.8 ± 0.6 % in healthy cartilage and 13.4 ± 1.5 % in OA cartilage, which showed no statistical difference between the models. Although the % of licofelone at four time points (1, 3, 5, and 7 minutes) in healthy cartilage was significantly higher compared to OA cartilage, the total % retained of conjugated licofelone within OA cartilage (2,040 ± 57 %) was higher compared to healthy cartilage (1,829 ± 54.7 %).
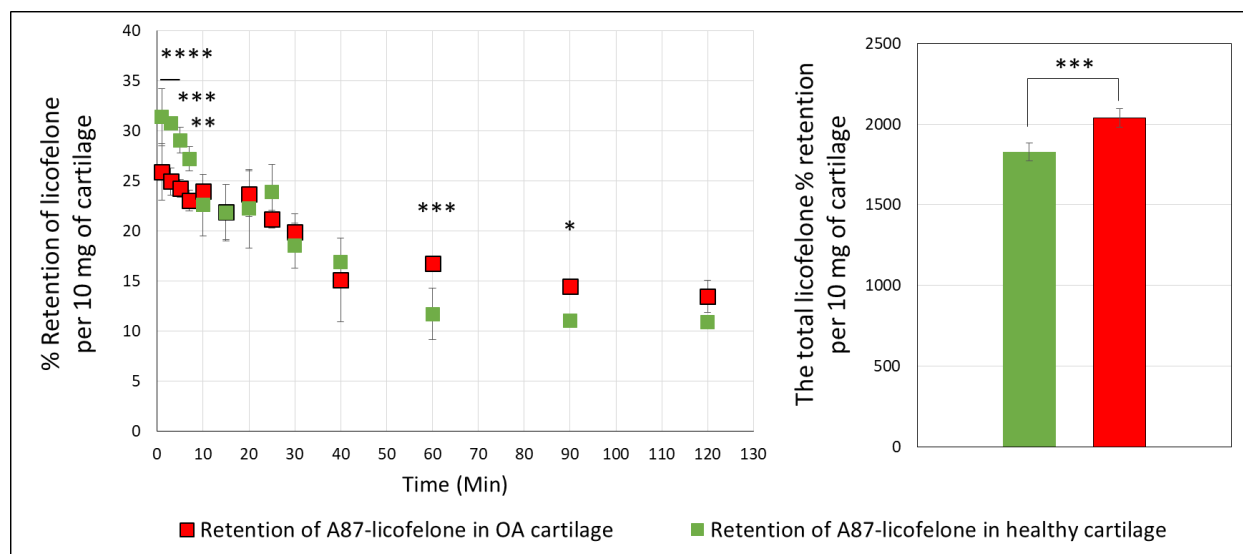
Figure 5.23: The percent retention of the licofelone conjugated to A87 per 10 mg of healthy and early simulated OA cartilage

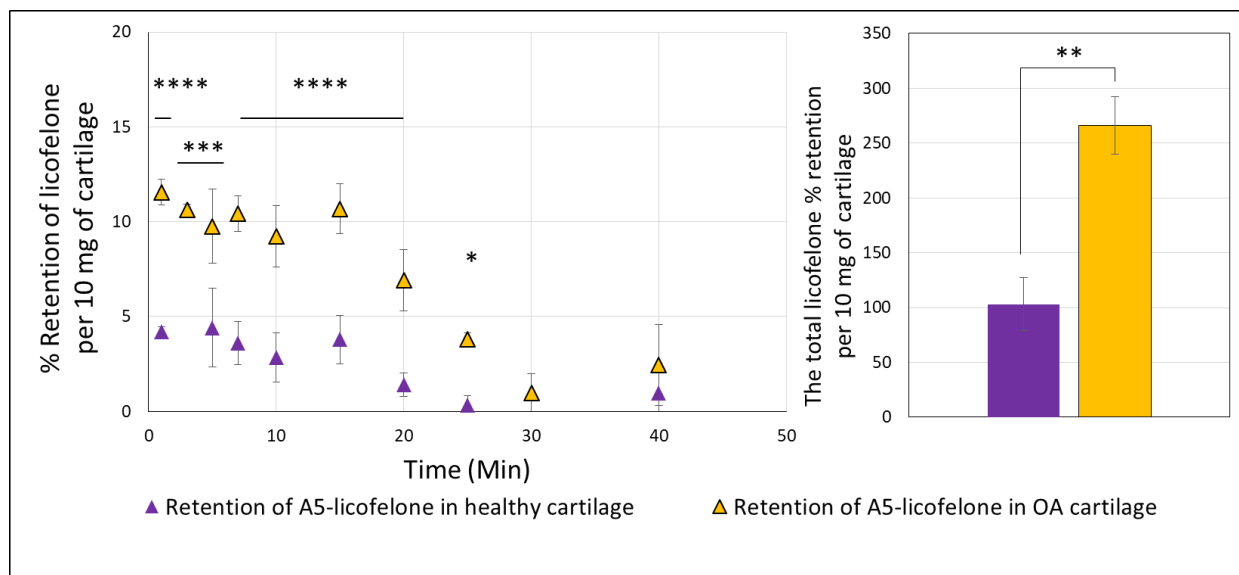Bars represent (Mean ± SD of n=3). Significant * ($P<0.05$), ** ($P<0.01$), *** ($P<0.001$), **** ($P<0.0001$)

5.3.2.6 The retention study of licofelone and licofelone conjugates

The retention time and the retained percentage of licofelone have enhanced after conjugation in healthy and early simulated OA cartilage models (Figure 5.24 and Figure 5.25). The comparison of the % retention of licofelone alone against the % retention of conjugated licofelone showed that A5-licofelone, A16-licofelone, and A87-licofelone significantly increased the retention % of conjugated licofelone in both cartilage models (Figure 5.24 and Figure 5.25).

In healthy cartilage, the % retention of licofelone conjugated to A5 was slightly enhanced compared to the licofelone alone (Figure 5.24). The licofelone retained decreased significantly after 15 minutes when unconjugated, while it decreased significantly after 25 minutes when conjugated to A5. In addition, A16-licofelone and A87-licofelone conjugates showed a significant improvement in the % retention of conjugated licofelone when compared to the unconjugated licofelone. At each time point, the % retention of conjugated licofelone to A16 and A87 was statistically higher by 26 to 14 % and 29 to 17 %, respectively, when compared to licofelone alone.

In the early simulated OA cartilage model, the retention % of licofelone conjugated to A5, A16, and A87 was significantly enhanced compared to the % retention of free licofelone (Figure 5.25). A5-licofelone conjugate has shown a significant increase in conjugated licofelone retention % in the first 25 minutes compared to licofelone alone, but between 30 and 60 minutes the difference was not statistically significant. However, A16-licofelone and A87-licofelone conjugates have increased the % retention of conjugated licofelone compared to licofelone alone at each time point by 15 to 9 % and 24 to 18 %, respectively.

Accordingly, the conjugation of licofelone to A5, A16, and A87 has enhanced the drug retention within both cartilage models. The total retained % of conjugated licofelone to A16 and A87 within the healthy cartilage (1,179 ± 11.8 % and 1,829 ± 54.7 %) were significantly higher compared to the licofelone alone (58.2 ± 6.2 %) (Figure 5.24). Similar results were observed in the OA cartilage model, in which A5, A16, and A87-licofelone conjugates showed a statistically higher retention percentage of the total licofelone (266.1 ± 26.2%, 787.2 ± 8.9 %, and 2,040 ± 57 %) compared to the licofelone alone (56 ± 3.2 %) (Figure 5.25).

Figure 5.24 also shows which licofelone conjugate has increased the % retention of conjugated licofelone the most inside the healthy cartilage model by comparing the results of A5-licofelone, A16-licofelone, and A87-licofelone conjugates. The A5-licofelone conjugate has retained a significantly lower percentage of licofelone compared to the other conjugates at each time point. Additionally, the total % of conjugated licofelone to A16 and A87 were approximately 12 and 18 times higher than the total % of conjugated licofelone to A5. The comparison of the conjugated licofelone % retention between A16-licofelone and A87-licofelone has shown that A87-licofelone has significantly retained more licofelone during the time period of 1 to 30 minutes. However, at 1, 40, and 60 minutes, the retention percentage of conjugated licofelone was not statistically different. Furthermore, the A87-licofelone conjugate has retained a significantly higher total % of licofelone compared to the A16-licofelone conjugate. Accordingly, A87-licofelone has improved the retention % of licofelone in healthy cartilage the most, followed by A16-licofelone and A5-licofelone conjugates.

Figure 5.25 shows the comparison of the % retention of conjugated licofelone between A5, A16, and A87-licofelone conjugates in the early simulated OA cartilage model. Although the % of retained conjugated licofelone to A5 enhanced significantly in OA models compared to the healthy cartilage model, it remains significantly low compared to A16 and A87-licofelone conjugates. Additionally, the % retention of conjugated licofelone to A5 and A16 at each time point and the total % of retained licofelone were statistically low when compared to the A87-licofelone conjugate. . The A87-licofelone conjugate has a higher percentage of licofelone retention and a higher total percentage of retained licofelone compared to the A5-licofelone and A16-licofelone conjugates in the OA cartilage models. According to these comparisons in both cartilage models, A87-licofelone has enhanced the % retention of licofelone the most. Additionally, the retained licofelone was detectable up to 120 minutes when conjugated to A87, whereas in the other retention time study, the licofelone was not detectable after 60 minutes.
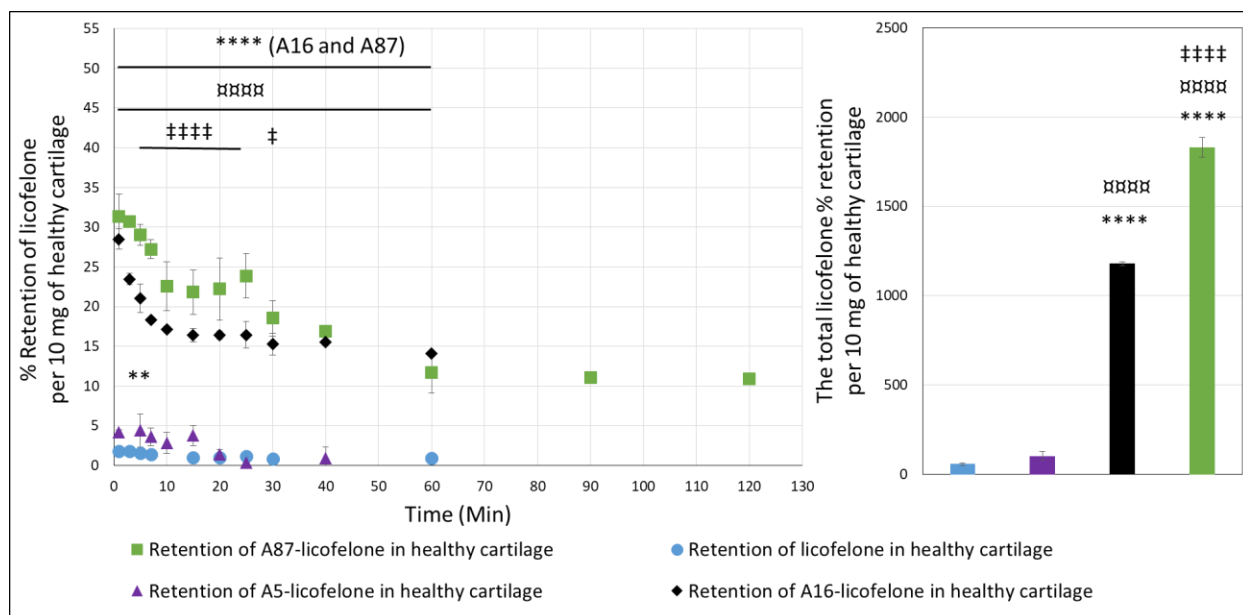
Figure 5.24: The percent retention of licofelone alone and conjugated licofelone to A5, A16, and A87 per 10 mg of healthy cartilage

Bars represent (Mean ± SD of n=3). Significant ** (P<0.01), **** (P<0.0001), the three licofelone conjugates compared to the control (licofelone alone), significant ¤¤¤¤ (P<0.0001), A16-licofelone and A87-licofelone conjugates compared to the A5-licofelone conjugate, and significant ‡ (P<0.05), ‡‡‡‡ (P<0.0001), A87-licofelone conjugate compared to the A16-licofelone conjugate.
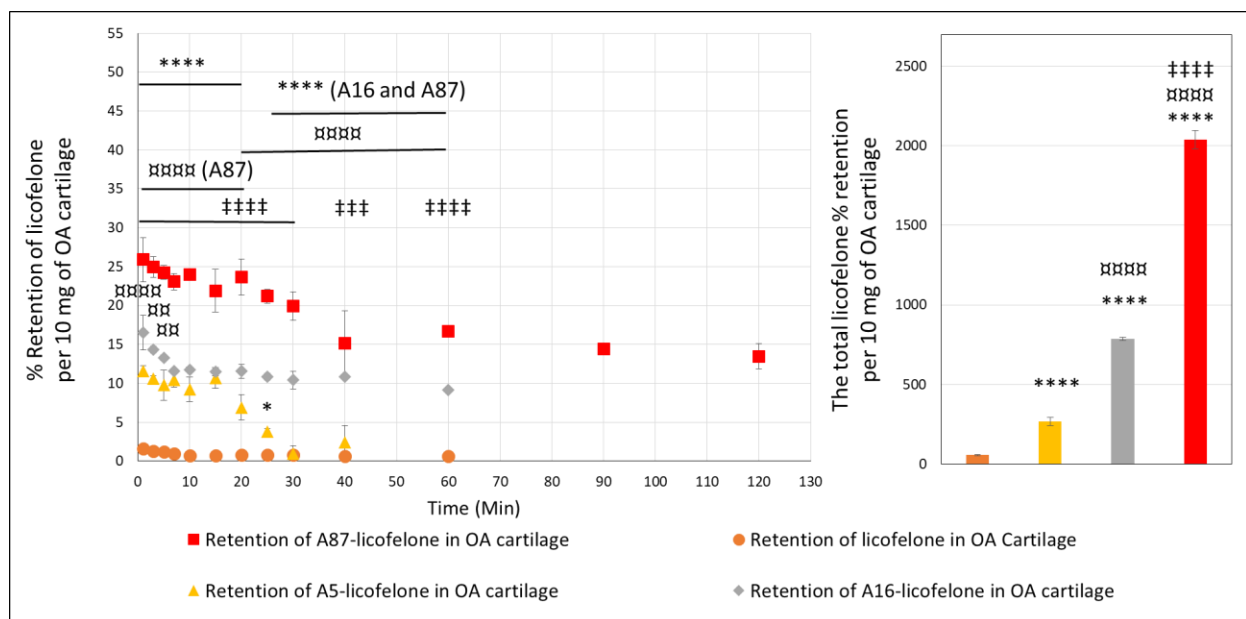
Figure 5.25: The percent retention of licofelone alone and conjugated licofelone to A5, A16 and A87 per 10 mg of OA cartilage

Bars represent (Mean ± SD of n=3). Significant * ($P<0.05$), **** ($P<0.0001$), the three licofelone conjugates compared to the control (licofelone alone), significant ¤¤ ($P<0.01$), ¤¤¤¤ ($P<0.0001$), A16-licofelone and A87-licofelone conjugates compared to the A5-licofelone conjugate, and significant ‡‡‡ ($P<0.001$), ‡‡‡‡ ($P<0.0001$), A87-licofelone conjugate compared to the A16-licofelone conjugate

5.3.3 **The cartilage cell viability**

At 30 minutes, the uptake of conjugated licofelone to A87 in healthy cartilage was 44 ± 4.3 %, which is the highest conjugated licofelone uptake improvement achieved when compared to A5-licofelone and A16-licofelone conjugates. The quantity of the conjugated licofelone in the 44 % is 0.8 ± 0.08 µg, and the total quantity of A87-licofelone conjugate applied to the cartilage was 1.8 ± 0.1 µg. However, in the OA cartilage model, the total applied A87-licofelone conjugate was 2.7 ± 0.2 µg. Therefore, the cell viability of licofelone was performed at 1 µg, which was the maximum uptake of licofelone quantity within the cartilage, and 2.7 µg, which was the highest quantity of licofelone applied to the cartilage. Moreover, the release study of licofelone from the A87-licofelone conjugate showed that 3 mg/ml of A87-licofelone contains approximately 26 µg of licofelone (4.3.1, Figure 4.11). Accordingly, 119 and 325 µg/ml of A87-licofelone conjugate should contain 1 and 2.7 µg of licofelone respectively. Therefore, 1 and 2.7 µg of licofelone, 119 and 325 µg/ml of A87-licofelone conjugate, as well as 119 and 325 µg/ml of A87 polymer alone, were chosen as the concentrations for the cytotoxicity assay.

Figure 5.26 and Figure 5.27 show the cartilage cell viability of licofelone, A87 polymer, or A87-licofelone after 24 and 48 hours of treatment, respectively. At 24 and 48 hours, 1 and 2.7 µg/ml of licofelone alone have shown no statistically significant difference in cell viability compared to the control (an untreated cartilage cell). A similar result was observed during the A87 polymer cytotoxicity study. Additionally, at 24 or 48 hours, A87-licofelone conjugate-treated cartilage cells at 119 or 325 µg/ml showed no significant effect on cell viability compared to the control.
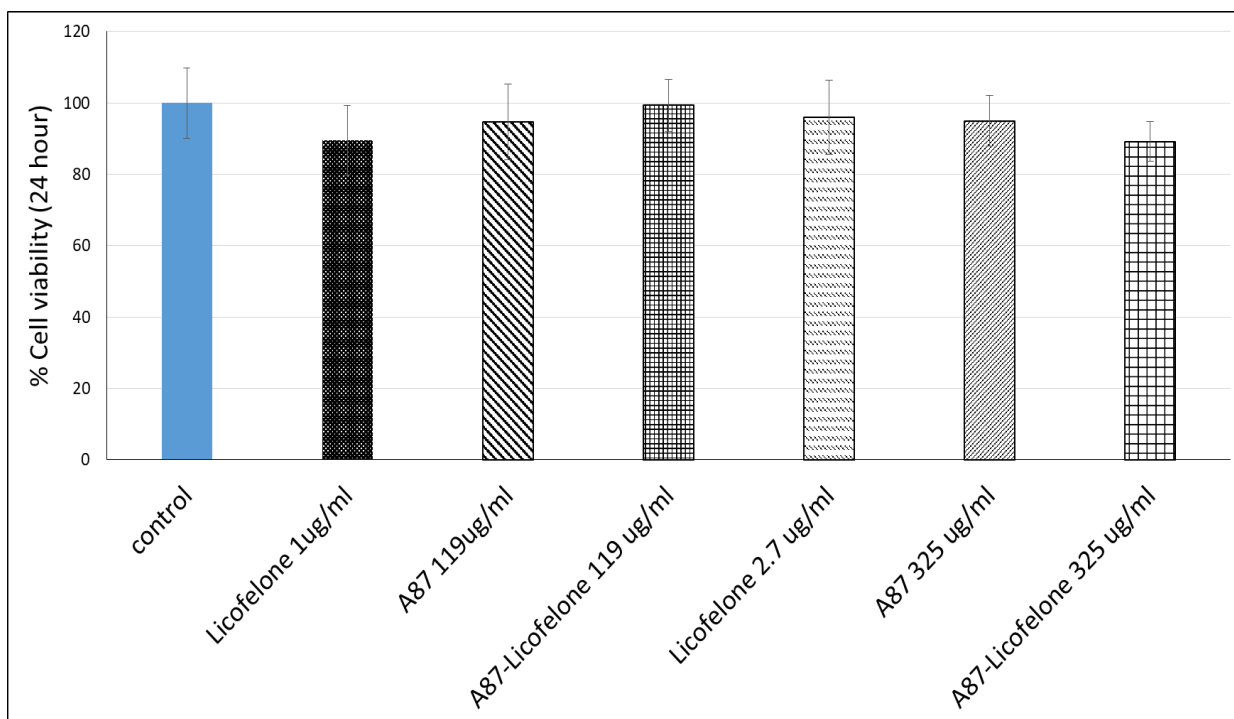
Figure 5.26: The effect of licofelone, A87 polymer, and A87-licofelone on cartilage cell viability after 24 hours of treatment

Bars represent (Mean ± SD of n=3). The control is the cartilage complete medium.
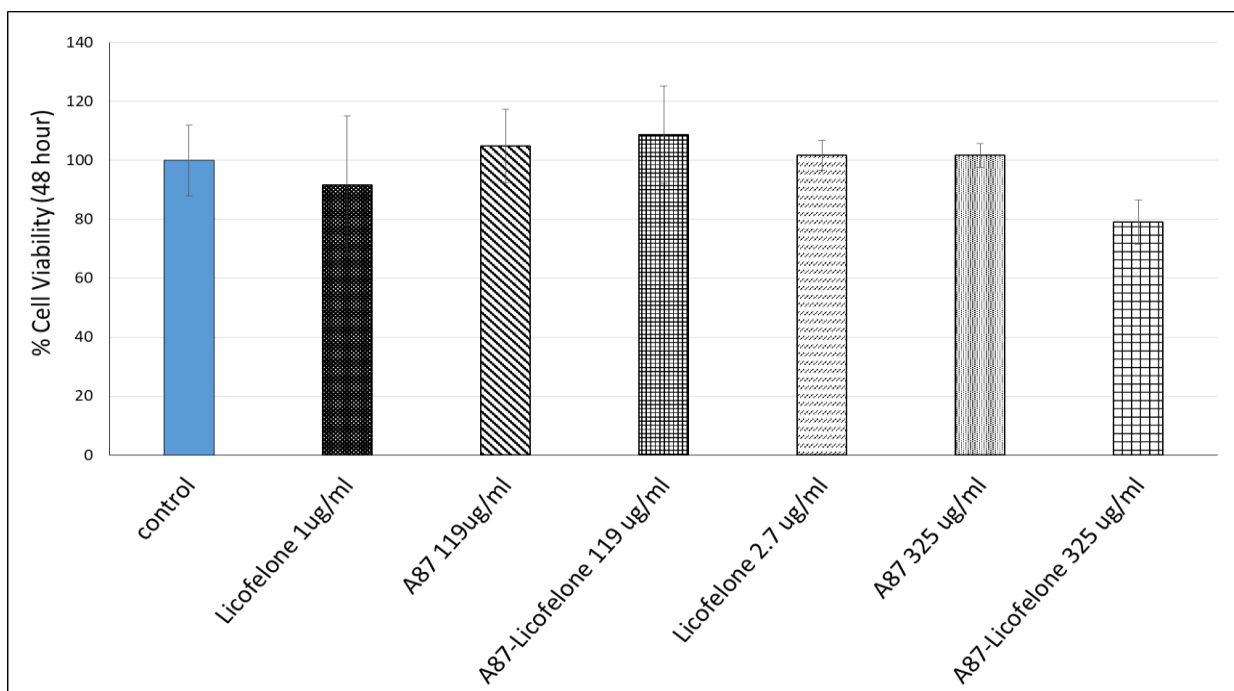
Figure 5.27: The effect of licofelone, A87 polymer, and A87-licofelone on cartilage cell viability after 48 hours of treatment

Bars represent (Mean ± SD of n=3). The control is the cartilage complete medium.

5.4 **Discussion**

The percentage uptake and retention of NBQX, self-assembled NBQX, licofelone, and licofelone conjugates were influenced by the physiochemical properties, the net surface charges, the conjugates size, the quantity of the drug loaded to the polymers, and the cartilage content condition. These factors have simultaneously affected the uptake and the retention percentages of both drugs, which will be discussed in detail during the following sections.

5.4.1 **NBQX uptake and retention time studies**

The uptake of NBQX alone was similar in healthy and early simulated OA cartilage (Figure 5.6). However, the total percent of NBQX retention was approximately two times higher in the OA models compared to the healthy cartilage, which could be related to the negative net surface charge of NBQX and to the cartilage content condition (Figure 5.17). The cartilage acts as a biological barrier, preventing drugs from penetrating and being retained within the cartilage because of the cartilage condensed structure and negatively charged hydrophilic components.(17, 18) The cartilage content is reduced by 50 % in the OA cartilage model compared to the healthy cartilage model, and the net surface charge of NBQX is negative 17.97 ± 1.7 mV, which were reported previously in (4.3.3) and (Table 3.1), respectively. Accordingly, the OA cartilage has lower negatively charged cartilage content (GAGs), which can reduce the resistance against the negatively charged NBQX and increase its retention percentage, which was the case in enhancing the % retention of NBQX in the OA cartilage model.(24) The comparison of the NBQX percentage in both cartilage models has supported the hypothesis that the cartilage acts as a biological barrier and repels negative charge molecules. Therefore, NBQX was self-assembled with the positively charged acrylate-terminated A5, which could mask the NBQX negative charge and reduce the repulsion effect caused by negatively charged cartilage GAGs. Unfortunately, mixing NBQX with the acrylate-terminated A5 results in NBQX precipitation during preparation and during the uptake experimental procedures. In the case of **(v/v)**, the precipitation of NBQX-A5 self-assembly was reduced compared to the **(w/v)** method. Therefore, **(v/v)** self-assembly has increased the total NBQX uptake percentage by about 400 % when compared with **(w/v)** (Figure 5.7). Overall, both self-assembled NBQX methods showed a lower uptake percentage compared to NBQX alone, which was caused by the high quantity of NBQX

precipitation during the preparation and uptake procedures (Figure 5.8). However, the % retention of NBQX self-assembled showed no significant difference compared to the % retention of NBQX alone between 60 and 300 minutes, despite the significantly lower uptake of self-assembled NBQX compared to NBQX alone (Figure 5.18). This indicates that the positive charge of the acrylate-terminated A5 has reduced the repulsion against the self-assembled NBQX and maintained its retention % to be comparable with NBQX alone. The calculated release % of NBQX was determined based on Equation 5.2, which showed that the % release of NBQX from the cartilage was significantly lower when the NBQX was self-assembled (Figure 5.19). The retention study showed encouraging results, supporting the hypothesis that the positively charged acrylate-terminated A5 can mask the negative charge of NBQX and the positively charged NBQX-A5 self-assembled can be attracted to the negatively charged GAGs via electrostatic interaction, thereby enhancing the retention % of NBQX.

The acrylate-terminated A5 could be the reason for NBQX precipitation during the self-assembly process.(179, 180) Studies have stated that the acrylate-terminated PBAE polymers have shown lower cartilage uptake and formulation stability issues in self-assembly studies compared to amino-terminated PBAE.(179, 180) According to the study by the Green group, the use of an end-capping group with acrylate-terminated PBAE would enhance the formulation stability and the uptake of acrylate-terminated PBAE.(179) Therefore, the possible solutions to improve the self-assembly formulation stability are adjusting the concentration of acrylate-terminated A5, using amino-terminated A5, or end-capping the acrylate-terminated A5.(179, 180) However, the aim of the current study is to conjugate PBAE to DMOAD covalently via a hydrolysable bond. The covalent conjugation is preferred due to the limitation of self-assembly. The major disadvantages of self-assembly technology are limited to ionised DMOADs, short lifetime, and lack of formulation stability.(194) In contrast, the covalently linked drugs to the delivery systems had a longer residence time in the synovial fluid than the physically mixed drug with the delivery system, according to a study that compared both techniques.(144)

5.4.2 Licofelone uptake and retention studies

In the uptake and retention studies of licofelone, the percentage of licofelone showed no statistical difference between the two models. However, the % uptake and % retention of licofelone in both cartilage models were relatively low, reaching less than 2 % of licofelone in the cartilage, which could be related to the physiochemical properties of licofelone. Licofelone is a small lipophilic molecule that is negatively charged (-9± 2mV), so the expectation that licofelone would cross the negatively charged cartilage barrier and reach the therapeutic target would be significantly low.(11-16) Additionally, the limited uptake and retention percentages of licofelone could be affected more by the lipophilicity than the negative charge of the drug. Licofelone has reported a lower negatively charged surface than NBQX, and thus the NBQX uptake and retention time study profiles are significantly greater than those of licofelone (Figure 5.13 and Figure 5.14). This higher NBQX uptake could be due to the fact that NBQX is a water-soluble molecule with a lower degree of lipophilicity than licofelone, whereas licofelone is a very lipophilic molecule that is insoluble in water. The comparison of NBQX and licofelone has revealed that the degree of lipophilicity of DMOADs plays a role in the uptake of DMOAD by the cartilage. A study by our group has reported the dexamethasone phosphate (water-soluble) uptake in healthy cartilage, which was approximately 25 %.(143) The high uptake percentages of NBQX and dexamethasone phosphate when compared with licofelone show how significantly the lipophilicity can affect the therapeutic quantity within the cartilage. Unfortunately, the majority of therapeutics are lipophilic molecules; therefore, developing a delivery system to enhance DMOADs uptake and retention time could be essential for these drugs to be effective therapeutics against OA progression. Consequently, licofelone was conjugated to three positively charged PBAE polymers in order to study the effect of A5, A16, and A87 on the % uptake and retention time of licofelone. Furthermore, the licofelone studies have also supported the hypothesis that the cartilage limits the drug quantity within the cartilage.

5.4.3 Licofelone conjugates uptake and retention studies

The comparison of conjugated licofelone percentage between the healthy cartilage and the 50 % depleted cartilage content showed the effect of the cartilage as a biological barrier and provided an evidence that the delivery was charge-based. The % uptake and % retention of

conjugated licofelone to A5 showed a significant difference between the two cartilage models, which was caused simultaneously by the size of the A5 polymer, the charge of the conjugate, and the cartilage content condition (Figure 5.10 and Figure 5.21). In healthy cartilage, the size of the A5-licofelone conjugate could limit its penetration through the cartilage pores, while the electrostatic interaction between the conjugate's positive charge and the cartilage components assisted the conjugate to remain on the cartilage surface. According to the study on the WYRGRL peptide conjugated to a fluorescent nanoparticle, a 90 nm particle size has restricted access to the cartilage surface.(216) The cartilage mesh network is composed of a collagen network pore size of 60 - 200 nm and an aggrecan network pore size of 20 nm (18), which may limit the ability of the A5-licofelone conjugate to cross through the healthy cartilage.(140) When the cartilage content was depleted by 50 %, the positively charged A5-licofelone conjugate deeply penetrated the OA cartilage and significantly increased the % uptake and % retention of licofelone compared to the healthy cartilage (Figure 5.10). Although the increase of the cartilage pore assisted the conjugates to infiltrate through and increase the licofelone uptake percent, the A5-licofelone may have remained in the superficial zone of the cartilage, which explains the fast release of the drug in the retention study. The difference between the healthy and OA cartilage models results of the A5-licofelone conjugate is additional evidence of the condensed cartilage network action as a biological barrier.

A16-licofelone conjugate showed similar % uptake of licofelone conjugate in both cartilage models, while the % retention of licofelone has enhanced significantly in the healthy cartilage, which was expected (Figure 5.11 and Figure 5.22). The positive charge of A16-licofelone conjugate was the reason for increasing the retention % of licofelone in healthy cartilage. As discussed previously, the cartilage components quantity (specifically GAGs) is higher in the healthy cartilage model, which means a stronger electrostatic interaction between the positively charged A16-licofelone conjugate and the negatively charged GAGs. The interaction between the conjugate and the cartilage component has increased the % of conjugated licofelone retention inside the healthy cartilage, while in the 50 % GAGs depleted cartilage the % retention was reduced. Accordingly, the conjugation of licofelone to the positively charged A16 polymer has increased the quantity of licofelone inside the cartilage, which supports the current study

hypothesis that the negatively charged cartilage components could be used as an advantage to enhance the conjugated DMOADs penetration and retention inside the cartilage.

Furthermore, the intensity of the electrostatic interaction and the cartilage content condition played a similar role in the A87-licofelone conjugate uptake study, where the % uptake of conjugated licofelone was statistically higher in healthy cartilage compared to the OA cartilage (Figure 5.12). The 50 % reduction of GAG content in early simulated OA cartilage caused less electrostatic attraction between the negatively charged cartilage component and the positively charged A87-licofelone conjugate, which reduced the uptake % of licofelone. The retention study of A87-licofelone has shown similar observations. The percentage increase of conjugated licofelone to A16 and A87 in the healthy cartilage compared to the GAG-depleted cartilage is evidence that the delivery system is charge-based. (Figure 5.23).

5.4.4 **Licofelone verses licofelone conjugates uptake and retention studies**

The aim of the current study was to increase licofelone uptake and retention time within the cartilage. Hypothetically, the positively charged conjugates will be attracted to the negatively charged GAG via electrostatic interaction, which will assist licofelone to penetrate the cartilage network faster and deeper and to extend the conjugate retention time within the cartilage. A study has reported that the positively charged delivery system allows faster and deeper penetration through the cartilage, which was observed in the A5-licofelone, A16-licofelone, and A87-licofelone conjugates studies when compared to the drug alone.(173) In both cartilage models, comparing the licofelone alone with the licofelone conjugates has shown that the positively charged A5, A16, and A87 polymers have significantly increased the % uptake and retention of conjugated licofelone (Figure 5.15, Figure 5.16,Figure 5.24, and Figure 5.25). These conjugates assisted licofelone to penetrate through the cartilage, or the positive charge of A5, A16, and A87 has masked the lipophilicity and the negative charge of licofelone, which reduced the repelling activity of the hydrophilic and negatively charged cartilage components against negative molecules.(24) A study that compared the retention of anionic and cationic nanoparticles in the cartilage reported a significant increase in the retention time of cationic nanoparticles compared to the anionic nanoparticles.(217) Additionally, conjugating dexamethasone to a cationic biological polymer (Avidin) has increased dexamethasone uptake

by the cartilage compared to dexamethasone alone.(172) These studies findings have suggested that using a cationic delivery system could assist drugs in overcoming the biological nature of the cartilage and have supported the results of the current study.(172, 217)

Significantly, all three conjugates have increased the uptake and the retention time of conjugated licofelone compared to the drug alone. The uptake of conjugated licofelone to A87, A16, and A5 has reached 44 ± 4.3 %, 23.4 ± 0.85 %, and 1.7 ± 0.65 %, respectively, compared to licofelone alone (1.4 ± 0.6 %) in healthy cartilage, whereas the uptake in the OA cartilage model was 26.6 ± 3.1 %, 23.4 ± 0.26 %, and 10.07 ± 1.08 %, respectively, compared to the unconjugated licofelone (1.7 ± 0.6 %). The majority of literature on drug delivery systems for OA therapeutics has reported the effect of the delivery system based on the therapeutic improvement of the drug, drug quantity within the systemic circulation, or the duration of the drug retained within the joint space.(144, 153, 157, 169, 174) Nevertheless, some studies have determined the effect of the delivery system on the cartilage uptake of OA therapeutics, which can be compared to our developed system.(143, 218) For example, the uptake of conjugated insulin-like growth factor 1 (IGF-1) to polyamidoamine (PAMAM) dendrimers showed 51 % and 71 % uptake in the bovine cartilage discs after 24 hours of incubation, whereas the conjugated licofelone to A87 polymer showed 44 % uptake of licofelone in a half-disc of a healthy bovine cartilage model after 30 minutes of incubation.(218) Although the PAMAM dendrimers showed a higher percentage of the drug, the IGF-1 study was performed on a full cartilage disc for 24 hours, and the diffusion of the formulated IGF-1 was not one-way passive diffusion.(218) Furthermore, the percentage uptake of conjugated dexamethasone to A1 and A2 were 60 % and 50 % in the healthy bovine cartilage model after 10 minutes of incubation, respectively, while the uptake of unconjugated dexamethasone was 25 % at the same time point.(143) A1 and A2 polymers are the products of piperazine and 4,4'-trimethylenedipipreridine polymerization with 1,4-butanediol diacrylate, respectively.(143) Accordingly, the A1 and A2 polymers have enhanced the uptake of dexamethasone by approximately 2.4 and 2 times, respectively, while the A87 and A16 polymers showed approximately 17 and 32 times improvement in licofelone uptake in healthy cartilage following similar experimental procedures.

A87-licofelone conjugate has increased the uptake percentage of conjugated licofelone approximately 40 times more than unconjugated licofelone. Therefore, the conjugation to A87 polymer could increase the quantity of DMOADs in the synovial joint, which will enhance the therapeutic effect of these drugs. Additionally, the licofelone conjugates to A16 and A87 have enhanced the uptake and the retention time of licofelone in the healthy cartilage significantly compared to the GAG depleted cartilage model, which confirms that the mechanism of this improvement is the electrostatic interaction.

5.4.5 Licofelone conjugates uptake studies

In the current study, A5, A16, and A87 polymers were selected as drug delivery systems because of the structural diversity, which allowed controlling the degree of the positive charge and the quantity of licofelone loaded on the polymers. The comparison of between licofelone conjugates has shown the effect of the polymer MW, the positive charge degree, and the quantity of conjugated licofelone on the drug uptake. The A5-licofelone conjugate has shown the lowest uptake percent of licofelone, primarily because the A5 polymer has the lowest positive charge degree and a relatively large size that could limit the conjugate penetration, as well as only two conjugation sites on the terminal side of the polymer (Figure 5.15)

Another significant observation was the effect of the conjugates' surface charge and the quantity of licofelone loaded within the conjugates on cartilage uptake and retention time studies. The hypothesis of the current study is that the positively charged PBAE will increase the uptake and retention time of DMOAD due to the electrostatic interaction between the positively charged conjugate and the negatively charged GAG. Accordingly, the positive charge of the licofelone conjugates should be proportional to the licofelone uptake. However, the results of comparing A87-licofelone against A16-licofelone have revealed that was not the case (Figure 5.15 and Figure 5.16). Although the positive surface charge of A16-licofelone was higher, the uptake of conjugated licofelone to A87 within both cartilage models was higher, which was caused by the strong electrostatic interaction between A16 and the GAGs on the cartilage superficial zone, preventing a deeper penetration.(170) This finding could explain how both conjugates have similar licofelone uptake during the first 5 minutes before the % of the conjugated licofelone to A87 significantly increased in the healthy model (Figure 5.15). Additionally, the uptake of

conjugated licofelone to A87 was comparable to A16-licofelone conjugate in the depleted cartilage model because the strong electrostatic interaction between A16-licofelone and GAGs was reduced (Figure 5.16). The higher % uptake of conjugated licofelone to A16 at the first 4 minutes (healthy cartilage) and the first 7 minutes (OA cartilage) when compared to A87-licofelone conjugate is another evidence that A16-licofelone conjugate penetration is hindered. Therefore, the positive charge of a delivery system should be maintained to avoid a strong interaction with the negatively charged cartilage components on the surface, which will potentially reduce the infiltration through the cartilage network. Furthermore, 3 mg/ml A16-licofelone and A87-licofelone conjugates contain 6.66 ± 0.19 μg and 26.22 ± 3.4 μg licofelone, respectively. The high loaded quantity of licofelone could have played a significant role in enhancing the uptake % of licofelone when conjugated to A87.

5.4.6 Licofelone conjugates retention time studies

Figure 5.24 and Figure 5.25 show the retention time studies of licofelone conjugates in the healthy and OA cartilage models, respectively. Similar factors that have influenced the uptake of A5-licofelone, A16-licofelone, and A87-licofelone have affected the retention time of the licofelone conjugates, which are the degree of the conjugate surface charge, the intensity of the electrostatic interaction, the polymer average Mw, and the quantity of licofelone conjugated into the polymer. Furthermore, in both cartilage models, A16 and A87-licofelone conjugates have significantly enhanced the % retention of the drug compared to the A5-licofelone conjugate, which is primarily related to the A5-licofelone low positively charged surface and limited conjugation sites. The surface positive charge has assisted the conjugates to remain attracted to the cartilage components, which has increased the retention of conjugated licofelone within the cartilage. Comparing A16-licofelone and A87-licofelone has revealed that the factors that have been investigated can influence the retention of conjugated licofelone simultaneously. For instance, the positive surface charge of A16-licofelone is higher than that of A87-licofelone, but the % retention of licofelone conjugated to A87 is significantly higher, which is related to the strong electrostatic interaction between the A16-licofelone conjugate and GAG, as well as the high quantity of loaded licofelone in the A87 polymer. Therefore, the % retention of conjugated

licofelone in both cartilage models was highest when conjugated to A87, followed by A16 and A5.

5.4.7 Cartilage cell viability

At the concentrations tested, A87-licofelone conjugate has no effect on the chondrocyte viability after 24 and 48 hours of treatment. According to previous studies that investigated the cytotoxicity of PBAE polymers on various cell lines, the polymers showed no toxicity.(143, 177-180) A study by the Prokopovich group has shown that there was no toxicity on chondrocyte viability during 72 hours of exposure to A1 and A2 polymers, which are the products of piperazine or 4,4'-trimethylenedipipreridine polymerization with 1,4-butanediol diacrylate, respectively.(143)

5.5 **Conclusion**

Overall, A5, A16, and A87-licofelone conjugates have improved licofelone retention time in healthy and OA cartilage compared to licofelone alone. The results have provided evidence supporting the hypothesis of the current study, which is the electrostatic interaction between the negatively charged PGs and the positively charged conjugate can enhance the DMOADs uptake and retention time within the cartilage. Additionally, the outcome of licofelone conjugates has achieved the aim of the current study, which was enhancing the uptake and the retention time of DMOAD within the cartilage. The positively charged A5, A16, and A87 polymers have managed to enhance the uptake and retention of licofelone (the model drug of DMOADs) in both cartilage models by hiding the physiochemical properties of licofelone and interacting electrostatically with the negatively charged cartilage components.

This chapter also focused on investigating the factors that influence the NBQX and licofelone uptake and retention time studies in both cartilage models, which revealed several factors that play a significant role in altering the percentage of both drugs within the cartilage. For instance, the comparison between the uptake of licofelone and NBQX showed that the degree of lipophilicity and water solubility of DMOADs could affect the uptake of the drug. Additionally, the uptake and retention time of DMOADs or drug delivery systems could be impacted by the cartilage health state, confirming that the cartilage acts as a biological barrier preventing therapeutics from penetration and the hydrophilic negatively charged GAGs repel therapeutics.

The cartilage content depletion can affect the pore size and the repellence activity of the cartilage, which has played a significant role in a variety of uptake and retention studies. For example, in the A5-licofelone conjugate, the reduction of the cartilage contents has extremely enhanced the percentage of conjugated licofelone in the cartilage due to the increase in pore size.(140) According to the Jeffrey group, large nanoparticles adhere to the cartilage surface rather than diffusing deep into the cartilage as small nanoparticles do.(216) In contrast, in the A16-licofelone and A87-licofelone conjugates, the reduction of cartilage contents has reduced

the % uptake and retention of conjugated licofelone because of the inhibition of the electrostatic interaction intensity.(140)

Furthermore, the degree of positivity could be involved in affecting the uptake and the retention time study of licofelone conjugates, which was discussed when comparing the licofelone conjugates against each other (5.4.5 and 5.4.6). Additionally, the degree of the positive charge should be maintained to avoid a strong electrostatic interaction with the superficial cartilage GAGs, which has limited A16-licoflone penetration through the cartilage (170), and to avoid low uptake of licofelone in cases of low charge, which was observed with A5-licofelone conjugate.

Chapter 6: **General Discussion and Future Work**

6.1 **General discussion**

Osteoarthritis is a chronic inflammatory disease affecting the structure integrity of synovial joints. The current disease managements target the symptoms but not the progression, but DMOADs have managed to slow and prevent the progression of OA.(7, 8, 11-16) Unfortunately, none of the DMOADs are available for prescription because of their low therapeutic effect in clinical trials and adverse effects, which are related to the low drug quantity penetrated, absorbed, and retained inside the cartilage.(17, 18, 25, 33, 34) Therefore, we optimised a conjugation method between the positively charged A5, A16, and A87 polymers and a model drug of DMOADs (licofelone) to increase the drug quantity and time inside two models of cartilage without affecting the chemical structure of licofelone. A16 and A87 polymers have enhanced licofelone percentage about 17 to 32 times within the cartilage, both polymers can be also conjugated to other DMOAD that showed low resident time within the joint. Furthermore, the conjugates have increased the licofelone time within the cartilage, and each conjugate has distinctively affected the licofelone resident time based on the polymer physiochemical properties. Consequently, investigating the effect of other PBAE polymers with different physiochemical properties on licofelone uptake and retention time within the cartilage can further improve the drug's quantity and time.

The cartilage is acting as a biological barrier, preventing and repelling therapeutics, which results in low drug uptake by the cartilage and drug elimination with synovial fluid exchange into the blood circulation, increasing the risk of systemic side effects.(3, 18-20, 24, 141, 142, 173, 193, 217) Therefore, a drug delivery system for OA therapeutics is essential to penetrate and retain inside the cartilage in order to reach their therapeutic targets and effects. A87 and A16 could be a solution for DMOADs that have failed clinical trials due to an insignificant therapeutic effect caused by a low drug quantity in the cartilage or an adverse reaction caused by increasing the drug concentration to obtain the therapeutic effect, such as cartilage catabolism inhibitors, inflammatory cytokine inhibitors, and bone resorptions. After conjugating these drugs to A87 or A16, the drug quantity within the cartilage would be increased, and we could use a lower drug

concentration to reach the therapeutic effect and minimise the risk of side effects. Furthermore, A87 and A16 could be a solution for DMOADs that are insoluble in water, such as kartogenin and rhein, as the polymers would have a dual effect of enhancing drug uptake and retention time as well as water solubility for IA injection formulation.

The conjugation of licofelone to the polymers will have a positive impact on the therapeutic effect and the pharmacokinetic of licofelone. Therapeutically, licofelone is a DMOAD in phase III clinical trial and showed activity against OA by inhibiting leukotriene-B4 (LTB$_4$), prostaglandin E2, IL-1β synthesis, and iNOS level, as well as reducing oedema, erythema, and cartilage/bone degradation.(111-115) Furthermore, doses of 2.5 and 5 mg/kg/day inhibited the apoptosis of chondrocytes in dogs with osteoarthritic cartilage.(116) Licofelone protecting the chondrocytes from apoptosis during OA will significantly enhance the cartilage condition in OA and reduce its degradation.(116) In dogs, at 2.5 mg/kg for 8 weeks, licofelone produces a significant therapeutic effect against the progression of OA by decreasing collagen degradation and the activity of MMP, inhibiting the expression of MMP-1, MMP-13, ADAMTS-5, and cathepsin K, and reducing the width of osteophytes.(115) A study on dogs reported that at 2.5 and 5 mg/kg/day, licofelone protected a deep zone of the cartilage (classified cartilage) and reduced the osteoclast count, but only at the high dose of licofelone were the MMP-13 and cathepsin K levels in subchondral bone significantly inhibited.(219) A study that investigated the mechanism of licofelone to inhibit the level of prostaglandin E2 and leukotriene-B4 (LTB$_4$) suggested that it was related to COX-2 and 5-LO inhibition, respectively, but the inhibition of OA progression may not be related to the activity of licofelone on these enzymes.(113) Additionally, the inhibition of IL-1β synthesis by licofelone is associated with the drug reducing the level of LTB$_4$, which plays a role in IL-1β synthesis.(113) The inhibition of MMP-1, MMP-3, and IL-1β by licofelone could be the reason for the cartilage protective effect that was observed in licofelone-treated dogs.(113) In OA patients, licofelone reduces cartilage loss and suppresses the symptoms of OA.(117) According to these studies' conclusions, licofelone mechanism of action as DMOAD involves its activity on chondrocytes and subchondral bone cells, which are located within the cartilage and deep cartilage area, respectively. Therefore, delivering the drug into a deeper cartilage zone will assist licofelone in providing a higher therapeutic effect. The conjugation of licofelone to A16 and

A87 aids the drug to infiltrate the cartilage and retain within the cartilage in higher quantity compared to the drug alone. Regarding the pharmacokinetics of licofelone in humans, a maximum blood concentration of 1.66 µg/ml after an oral administration of 200 mg/day of licofelone was reported.(112) Additionally, licofelone oral administration of 2.5 and 5 mg/kg/day has reached a maximum serum concentration of 371 and 629 µg/ml after 2 hours, respectively, which is about 14 and 12.5 % of the dose.(116) An additional pharmacokinetic study on rats reported that the highest licofelone concentrations were found in the heart, lung, intestine, kidney, and liver.(112) Therefore, intraarticular injection of the conjugated licofelone will localise licofelone within the joint space, increase licofelone residence time in the therapeutic region, reduce the licofelone dose, and limit licofelone from reaching other organs. Additionally, the risk of systemic side effects will be inhibited. A study has stated that the drugs that can reduce cell death could also enhance the risk of malignant disease when the drug is systemically administered.(116) Therefore, giving licofelone locally in the synovial joint will reduce the risk of systemic side effects, except that licofelone alone is not soluble in aqueous solution. However, A87-licofelone and A16-licofelone conjugates are soluble in PBS buffer pH 7.4, which provides a carrier for licofelone to be injected in the joint. In addition to providing a carrier, these polymers will increase the time that licofelone remains within the joint and assist the drug in penetrating the cartilage to reach the therapeutic target.

In conclusion, the covalent conjugation of A87, A16, and A5 to licofelone increased the drug uptake and retention in both cartilage models, which will significantly enhance licofelone therapeutically and pharmacokinetically. In the future, we desire to investigate the effect of these polymers on other DMOADs, which were discussed previously in 1.1.4.

References

1.   Lyn March MC. Epidemiology and risk factors for osteoarthritis. 2022 [accessed 30 Augest]. Available from: https://www.uptodate.com/contents/epidemiology-and-risk-factors-for-osteoarthritis
2.   Arthritis V. The State of musculoskeletal health 2021. 2021 [accessed. Available from: https://www.versusarthritis.org/media/24238/state-of-msk-health-2021.pdf
3.   Mancipe Castro LM, García AJ, Guldberg RE. Biomaterial strategies for improved intra-articular drug delivery. Journal of biomedical materials research Part A. 2021;109(4):426-36. doi: 10.1002/jbm.a.37074
4.   Arthritis Research UK. State of musculoskeletal health 2018. 2018 [accessed 16 May 2019]. Available from: https://www.arthritisresearchuk.org/~/media/Files/Data%20and%20stats/State%20of%20MSK/PHS-08_StateOfMSKReport.ashx?la=en
5.   Lyn March MC. Epidemiology and risk factors for osteoarthritis. 2019 [accessed 7 May]. Available from: https://www.uptodate.com/contents/epidemiology-and-risk-factors-for-osteoarthritis
6.   The National Joint Registry for England W, Northern Ireland and the Isle of Man. National joint registry the national joint rgistry; 2018 [accessed 19/ May/ 2019]. Available from: http://www.njrreports.org.uk/Portals/0/PDFdownloads/NJR%2015th%20Annual%20Report%202018.pdf
7.   Nelson AE, Allen KD, Golightly YM, Goode AP, Jordan JM. A systematic review of recommendations and guidelines for the management of osteoarthritis: the chronic osteoarthritis management initiative of the U.S. bone and joint initiative. Seminars in arthritis and rheumatism. 2014;43(6):701-12. doi: 10.1016/j.semarthrit.2013.11.012
8.   National Clinical Guideline C. National institute for health and clinical excellence: guidance. Osteoarthritis: care and management in adults. London: National institute for health and care excellence (UK) Copyright (c) National Clinical Guideline Centre, 2014.; 2014.

9.   Concoff A, Sancheti P, Niazi F, Shaw P, Rosen J. The efficacy of multiple versus single hyaluronic acid injections: a systematic review and meta-analysis. BMC musculoskeletal disorders. 2017;18(1):542. doi: 10.1186/s12891-017-1897-2
10.   Hunter DJ, Felson DT. Osteoarthritis. BMJ (Clinical research ed). 2006;332(7542):639-42. doi: 10.1136/bmj.332.7542.639
11.   Huang Z, Ding C, Li T, Yu SP. Current status and future prospects for disease modification in osteoarthritis. Rheumatology (Oxford, England). 2018;57(suppl_4):iv108-iv23. doi: 10.1093/rheumatology/kex496
12.   Karsdal MA, Michaelis M, Ladel C, Siebuhr AS, Bihlet AR, Andersen JR, et al. Disease-modifying treatments for osteoarthritis (DMOADs) of the knee and hip: lessons learned from failures and opportunities for the future. Osteoarthritis and cartilage. 2016;24(12):2013-21. doi: 10.1016/j.joca.2016.07.017
13.   Pelletier JP, Martel-Pelletier J. DMOAD developments: present and future. Bulletin of the NYU hospital for joint diseases. 2007;65(3):242-8.
14.   Cho Y, Jeong S, Kim H, Kang D, Lee J, Kang SB, et al. Disease-modifying therapeutic strategies in osteoarthritis: current status and future directions. Experimental & molecular medicine. 2021;53(11):1689-96. doi: 10.1038/s12276-021-00710-y
15.   Qvist P, Bay-Jensen AC, Christiansen C, Dam EB, Pastoureau P, Karsdal MA. The disease modifying osteoarthritis drug (DMOAD): Is it in the horizon? Pharmacological research. 2008;58(1):1-7. doi: 10.1016/j.phrs.2008.06.001

16.   Ghouri A, Conaghan PG. Update on novel pharmacological therapies for osteoarthritis. Therapeutic advances in musculoskeletal disease. 2019;11:1759720x19864492. doi: 10.1177/1759720x19864492

17.   Geiger BC, Grodzinsky AJ, Hammond P. Designing drug delivery systems for articular joints. Chemical engineering progress. 2018;114(5)

18.   Rahimi M, Charmi G, Matyjaszewski K, Banquy X, Pietrasik J. Recent developments in natural and synthetic polymeric drug delivery systems used for the treatment of osteoarthritis. Acta biomaterialia. 2021;123:31-50. doi: 10.1016/j.actbio.2021.01.003

19.   Cao Y, Ma Y, Tao Y, Lin W, Wang P. Intra-articular drug delivery for osteoarthritis treatment. Pharmaceutics. 2021;13(12) doi: 10.3390/pharmaceutics13122166

20.   Maudens P, Jordan O, Allémann E. Recent advances in intra-articular drug delivery systems for osteoarthritis therapy. Drug discovery today. 2018;23(10):1761-75. doi: 10.1016/j.drudis.2018.05.023

21.   Ng HY, Lee K-XA, Shen Y-F editors. Articular cartilage : structure , composition , injuries and repair. 2017.

22.   Barreto G, Manninen M, K. Eklund K. Osteoarthritis and toll-like receptors: when innate immunity meets chondrocyte apoptosis. Biology. 2020;9(4):65.

23.   Guilak F, Mow VC. The mechanical environment of the chondrocyte: a biphasic finite element model of cell-matrix interactions in articular cartilage. Journal of biomechanics. 2000;33(12):1663-73.

24.   Bhosale AM, Richardson JB. Articular cartilage: structure, injuries and review of management. British medical bulletin. 2008;87:77-95. doi: 10.1093/bmb/ldn025

25.   Sophia Fox AJ, Bedi A, Rodeo SA. The basic science of articular cartilage: structure, composition, and function. Sports health. 2009;1(6):461-8. doi: 10.1177/1941738109350438

26.   Kuettner KE. Biochemistry of articular cartilage in health and disease. Clinical biochemistry. 1992;25(3):155-63. doi: 10.1016/0009-9120(92)90224-g

27.   Davidson RK, Waters JG, Kevorkian L, Darrah C, Cooper A, Donell ST, et al. Expression profiling of metalloproteinases and their inhibitors in synovium and cartilage. Arthritis research & therapy. 2006;8(4):R124. doi: 10.1186/ar2013

28.   Bromme D, Lecaille F. Cathepsin K inhibitors for osteoporosis and potential off-target effects. Expert opinion on investigational drugs. 2009;18(5):585-600. doi: 10.1517/13543780902832661

29.   Ghosh S, Choudhury D, Das NS, Pingguan-Murphy B. Tribological role of synovial fluid compositions on artificial joints - A systematic review of the last 10 years. Lubrication science. 2014;26(6):387-410. doi: 10.1002/ls.1266

30.   Trunfio-Sfarghiu AM, Berthier Y, Meurisse MH, Rieu JP. Multiscale analysis of the tribological role of the molecular assemblies of synovial fluid. Case of a healthy joint and implants. Tribology international. 2007;40(10):1500-15. doi: https://doi.org/10.1016/j.triboint.2007.02.008

31.   Evans CH, Ghivizzani SC, Robbins PD. Arthritis gene therapy and its tortuous path into the clinic. Translational research : the journal of laboratory and clinical medicine. 2013;161(4):205-16. doi: 10.1016/j.trsl.2013.01.002

32.   Goldring SR, Goldring MB. 1 - Biology of the Normal Joint. In: Firestein GS, Budd RC, Gabriel SE, McInnes IB, O'Dell JR, editors. Kelley's textbook of rheumatology (Ninth Edition). Philadelphia: W.B. Saunders; 2013. p. 1-19.e6.

33.   Conaghan PG, Hunter DJ, Cohen SB, Kraus VB, Berenbaum F, Lieberman JR, et al. Effects of a single intra-articular injection of a microsphere formulation of triamcinolone acetonide on knee osteoarthritis pain: a double-blinded, randomized, placebo-controlled, multinational study. The journal of bone and joint surgery American volume. 2018;100(8):666-77. doi: 10.2106/jbjs.17.00154

34.   Bodick N, Lufkin J, Willwerth C, Kumar A, Bolognese J, Schoonmaker C, et al. An intra-articular, extended-release formulation of triamcinolone acetonide prolongs and amplifies analgesic effect in

patients with osteoarthritis of the knee: a randomized clinical trial. The journal of bone and joint surgery American volume. 2015;97(11):877-88. doi: 10.2106/jbjs.n.00918

35.	Manicourt DH, Devogelaer JP, Azria M, Silverman S. Rationale for the potential use of calcitonin in osteoarthritis. Journal of musculoskeletal & neuronal interactions. 2005;5(3):285-93.

36.	Robinson WH, Lepus CM, Wang Q, Raghu H, Mao R, Lindstrom TM, et al. Low-grade inflammation as a key mediator of the pathogenesis of osteoarthritis. Nature reviews rheumatology. 2016;12(10):580-92. doi: 10.1038/nrrheum.2016.136

37.	Schrier L, Ferns SP, Barnes KM, Emons JA, Newman EI, Nilsson O, et al. Depletion of resting zone chondrocytes during growth plate senescence. The journal of endocrinology. 2006;189(1):27-36. doi: 10.1677/joe.1.06489

38.	Bondeson J, Wainwright SD, Lauder S, Amos N, Hughes CE. The role of synovial macrophages and macrophage-produced cytokines in driving aggrecanases, matrix metalloproteinases, and other destructive and inflammatory responses in osteoarthritis. Arthritis research & therapy. 2006;8(6):R187. doi: 10.1186/ar2099

39.	Kevorkian L, Young DA, Darrah C, Donell ST, Shepstone L, Porter S, et al. Expression profiling of metalloproteinases and their inhibitors in cartilage. Arthritis and rheumatism. 2004;50(1):131-41. doi: 10.1002/art.11433

40.	Rose BJ, Kooyman DL. A tale of two joints: the role of matrix metalloproteases in cartilage biology. Disease markers. 2016;2016:4895050. doi: 10.1155/2016/4895050

41.	Murphy G, Knäuper V, Atkinson S, Butler G, English W, Hutton M, et al. Matrix metalloproteinases in arthritic disease. Arthritis research. 2002;4 Suppl 3(Suppl 3):S39-49. doi: 10.1186/ar572

42.	Verma P, Dalal K. ADAMTS-4 and ADAMTS-5: key enzymes in osteoarthritis. Journal of cellular biochemistry. 2011;112(12):3507-14. doi: 10.1002/jcb.23298

43.	Yang CY, Chanalaris A, Troeberg L. ADAMTS and ADAM metalloproteinases in osteoarthritis - looking beyond the 'usual suspects'. Osteoarthritis and cartilage. 2017;25(7):1000-9. doi: 10.1016/j.joca.2017.02.791

44.	Bekhouche M, Colige A. The procollagen N-proteinases ADAMTS2, 3 and 14 in pathophysiology. Matrix biology : journal of the international society for matrix biology. 2015;44-46:46-53. doi: 10.1016/j.matbio.2015.04.001

45.	Luan Y, Kong L, Howell DR, Ilalov K, Fajardo M, Bai XH, et al. Inhibition of ADAMTS-7 and ADAMTS-12 degradation of cartilage oligomeric matrix protein by alpha-2-macroglobulin. Osteoarthritis and cartilage. 2008;16(11):1413-20. doi: 10.1016/j.joca.2008.03.017

46.	Zeng W, Corcoran C, Collins-Racie LA, Lavallie ER, Morris EA, Flannery CR. Glycosaminoglycan-binding properties and aggrecanase activities of truncated ADAMTSs: comparative analyses with ADAMTS-5, -9, -16 and -18. Biochimica et biophysica acta. 2006;1760(3):517-24. doi: 10.1016/j.bbagen.2006.01.013

47.	Pratta MA, Scherle PA, Yang G, Liu RQ, Newton RC. Induction of aggrecanase 1 (ADAM-TS4) by interleukin-1 occurs through activation of constitutively produced protein. Arthritis and rheumatism. 2003;48(1):119-33. doi: 10.1002/art.10726

48.	Fosang AJ, Rogerson FM, East CJ, Stanton H. ADAMTS-5: the story so far. European cells & materials. 2008;15:11-26.

49.	Glasson SS, Askew R, Sheppard B, Carito B, Blanchet T, Ma HL, et al. Deletion of active ADAMTS5 prevents cartilage degradation in a murine model of osteoarthritis. Nature. 2005;434(7033):644-8. doi: 10.1038/nature03369

50.	Maruotti N, Corrado A, Cantatore FP. Osteoblast role in osteoarthritis pathogenesis. Journal of cellular physiology. 2017;232(11):2957-63. doi: 10.1002/jcp.25969

51.	Mabey T, Honsawek S. Cytokines as biochemical markers for knee osteoarthritis. World journal of orthopedics. 2015;6(1):95-105. doi: 10.5312/wjo.v6.i1.95

52.   Walsh DA, Stocks J. New therapeutic targets for osteoarthritis pain. SLAS discovery : advancing life sciences R & D. 2017;22(8):931-49. doi: 10.1177/2472555217716912

53.   Creamer P. Intra-articular corticosteroid injections in osteoarthritis: do they work and if so, how? Annals of the rheumatic diseases. 1997;56(11):634-6. doi: 10.1136/ard.56.11.634

54.   Wenham CY, Hensor EM, Grainger AJ, Hodgson R, Balamoody S, Dore CJ, et al. A randomized, double-blind, placebo-controlled trial of low-dose oral prednisolone for treating painful hand osteoarthritis. Rheumatology (Oxford, England). 2012;51(12):2286-94. doi: 10.1093/rheumatology/kes219

55.   Ivers N, Dhalla IA, Allan GM. Opioids for osteoarthritis pain: benefits and risks. Canadian family physician medecin de famille canadien. 2012;58(12):e708.

56.   Karlsson J, Pivodic A, Aguirre D, Schnitzer TJ. Efficacy, safety, and tolerability of the cyclooxygenase-inhibiting nitric oxide donor naproxcinod in treating osteoarthritis of the hip or knee. The journal of rheumatology. 2009;36(6):1290-7. doi: 10.3899/jrheum.081011

57.   Geusens P. Naproxcinod, a new cyclooxygenase-inhibiting nitric oxide donor (CINOD). Expert opinion on biological therapy. 2009;9(5):649-57. doi: 10.1517/14712590902926071

58.   Naproxcinod: AZD 3582, HCT 3012, naproxen nitroxybutylester, nitronaproxen, NO-naproxen. Drugs in R&D. 2007;8(4):255-8. doi: 10.2165/00126839-200708040-00006

59.   Wallace JL, Viappiani S, Bolla M. Cyclooxygenase-inhibiting nitric oxide donors for osteoarthritis. Trends in pharmacological sciences. 2009;30(3):112-7. doi: 10.1016/j.tips.2009.01.001

60.   Lohmander LS, McKeith D, Svensson O, Malmenäs M, Bolin L, Kalla A, et al. A randomised, placebo controlled, comparative trial of the gastrointestinal safety and efficacy of AZD3582 versus naproxen in osteoarthritis. Annals of the rheumatic diseases. 2005;64(3):449-56. doi: 10.1136/ard.2004.023572

61.   Bay-Jensen AC, Thudium CS, Mobasheri A. Development and use of biochemical markers in osteoarthritis: current update. Current opinion in rheumatology. 2018;30(1):121-8. doi: 10.1097/bor.0000000000000467

62.   Bellamy N, Buchanan WW, Goldsmith CH, Campbell J, Stitt LW. Validation study of WOMAC: a health status instrument for measuring clinically important patient relevant outcomes to antirheumatic drug therapy in patients with osteoarthritis of the hip or knee. The journal of rheumatology. 1988;15(12):1833-40.

63.   Collins NJ, Misra D, Felson DT, Crossley KM, Roos EM. Measures of knee function: International Knee Documentation Committee (IKDC) Subjective Knee Evaluation Form, Knee Injury and Osteoarthritis Outcome Score (KOOS), Knee Injury and Osteoarthritis Outcome Score Physical Function Short Form (KOOS-PS), Knee Outcome Survey Activities of Daily Living Scale (KOS-ADL), Lysholm Knee Scoring Scale, Oxford Knee Score (OKS), Western Ontario and McMaster Universities Osteoarthritis Index (WOMAC), Activity Rating Scale (ARS), and Tegner Activity Score (TAS). Arthritis care & research. 2011;63 Suppl 11(0 11):S208-28. doi: 10.1002/acr.20632

64.   Murphy G, Knäuper V, Atkinson S, Butler G, English W, Hutton M, et al. Matrix metalloproteinases in arthritic disease. Arthritis Research & Therapy. 2002;4(3):S39. doi: 10.1186/ar572

65.   da Costa BR, Nuesch E, Reichenbach S, Juni P, Rutjes AW. Doxycycline for osteoarthritis of the knee or hip. The Cochrane database of systematic reviews. 2012;11:Cd007323. doi: 10.1002/14651858.CD007323.pub3

66.   Krzeski P, Buckland-Wright C, Balint G, Cline GA, Stoner K, Lyon R, et al. Development of musculoskeletal toxicity without clear benefit after administration of PG-116800, a matrix metalloproteinase inhibitor, to patients with knee osteoarthritis: a randomized, 12-month, double-blind, placebo-controlled study. Arthritis Res Ther. 2007;9(5):R109. doi: 10.1186/ar2315

67.   Leff RL, Elias I, Ionescu M, Reiner A, Poole AR. Molecular changes in human osteoarthritic cartilage after 3 weeks of oral administration of BAY 12-9566, a matrix metalloproteinase inhibitor. The Journal of rheumatology. 2003;30(3):544-9.

68.   Engel CK, Pirard B, Schimanski S, Kirsch R, Habermann J, Klingler O, et al. Structural basis for the highly selective inhibition of MMP-13. Chemistry & biology. 2005;12(2):181-9. doi: 10.1016/j.chembiol.2004.11.014

69.   Xie XW, Wan RZ, Liu ZP. Recent Research Advances in Selective Matrix Metalloproteinase-13 Inhibitors as Anti-Osteoarthritis Agents. ChemMedChem. 2017;12(15):1157-68. doi: 10.1002/cmdc.201700349

70.   Chockalingam PS, Sun W, Rivera-Bermudez MA, Zeng W, Dufield DR, Larsson S, et al. Elevated aggrecanase activity in a rat model of joint injury is attenuated by an aggrecanase specific inhibitor. Osteoarthritis and cartilage. 2011;19(3):315-23. doi: 10.1016/j.joca.2010.12.004

71.   Lindström E, Rizoska B, Tunblad K, Edenius C, Bendele AM, Maul D, et al. The selective cathepsin K inhibitor MIV-711 attenuates joint pathology in experimental animal models of osteoarthritis. Journal of translational medicine. 2018;16(1):56. doi: 10.1186/s12967-018-1425-7

72.   Runger TM, Adami S, Benhamou CL, Czerwinski E, Farrerons J, Kendler DL, et al. Morphea-like skin reactions in patients treated with the cathepsin K inhibitor balicatib. Journal of the American Academy of Dermatology. 2012;66(3):e89-96. doi: 10.1016/j.jaad.2010.11.033

73.   Khosla S, Hofbauer LC. Osteoporosis treatment: recent developments and ongoing challenges. The lancet Diabetes & endocrinology. 2017;5(11):898-907. doi: 10.1016/s2213-8587(17)30188-2

74.   Lindstrom E, Rizoska B, Henderson I, Terelius Y, Jerling M, Edenius C, et al. Nonclinical and clinical pharmacological characterization of the potent and selective cathepsin K inhibitor MIV-711. Journal of translational medicine. 2018;16(1):125. doi: 10.1186/s12967-018-1497-4

75.   Conaghan PG, Bowes MA, Kingsbury SR, Brett A, Guillard G, Rizoska B, et al. Disease-Modifying Effects of a Novel Cathepsin K Inhibitor in Osteoarthritis: A Randomized Controlled Trial. Annals of internal medicine. 2020;172(2):86-95. doi: 10.7326/m19-0675

76.   Lindstrom E, Grabowska U, Jerling M, Edenius C. Miv-711, a Highly Selective Cathepsin K Inhibitor, Reduces Biomarkers of Bone Resorption and Cartilage Degradation in Healthy Subjects. Osteoarthritis and cartilage. 2014;22:S197-S. doi: DOI 10.1016/j.joca.2014.02.376

77.   Conaghan PG, Bowes MA, Kingsbury SR, Brett A, Guillard G, Thunblad K, et al. Safety and Efficacy of Six Months' Open Label Extension Post-Rct Using the Novel Cathepsin K Inhibitor Miv-711 in Patients with Knee Osteoarthritis. Osteoarthritis and cartilage. 2019;27:S501-S2. doi: DOI 10.1016/j.joca.2019.02.564

78.   Cheleschi S, Cantarini L, Pascarelli NA, Collodel G, Lucherini OM, Galeazzi M, et al. Possible chondroprotective effect of canakinumab: an in vitro study on human osteoarthritic chondrocytes. Cytokine. 2015;71(2):165-72. doi: 10.1016/j.cyto.2014.10.023

79.   Tamura T, Ohmori K. Rhein, an active metabolite of diacerein, suppresses the interleukin-1alpha-induced proteoglycan degradation in cultured rabbit articular chondrocytes. Japanese journal of pharmacology. 2001;85(1):101-4. doi: 10.1254/jjp.85.101

80.   Boileau C, Tat SK, Pelletier JP, Cheng S, Martel-Pelletier J. Diacerein inhibits the synthesis of resorptive enzymes and reduces osteoclastic differentiation/survival in osteoarthritic subchondral bone: a possible mechanism for a protective effect against subchondral bone remodelling. Arthritis research & therapy. 2008;10(3):R71. doi: 10.1186/ar2444

81.   Dougados M, Nguyen M, Berdah L, Maziéres B, Vignon E, Lequesne M. Evaluation of the structure-modifying effects of diacerein in hip osteoarthritis: ECHODIAH, a three-year, placebo-controlled trial. Evaluation of the Chondromodulating Effect of Diacerein in OA of the Hip. Arthritis and rheumatism. 2001;44(11):2539-47. doi: 10.1002/1529-0131(200111)44:11<2539::aid-art434>3.0.co;2-t

82.   Pelletier JP, Yaron M, Haraoui B, Cohen P, Nahir MA, Choquette D, et al. Efficacy and safety of diacerein in osteoarthritis of the knee: a double-blind, placebo-controlled trial. The Diacerein Study Group. Arthritis and rheumatism. 2000;43(10):2339-48. doi: 10.1002/1529-0131(200010)43:10<2339::aid-anr23>3.0.co;2-p

83.   Panova E, Jones G. Benefit-risk assessment of diacerein in the treatment of osteoarthritis. Drug safety. 2015;38(3):245-52. doi: 10.1007/s40264-015-0266-z

84.   Langdahl BL. Overview of treatment approaches to osteoporosis. British journal of pharmacology. 2021;178(9):1891-906. doi: 10.1111/bph.15024

85.   Laslett LL, Doré DA, Quinn SJ, Boon P, Ryan E, Winzenberg TM, et al. Zoledronic acid reduces knee pain and bone marrow lesions over 1 year: a randomised controlled trial. Annals of the rheumatic diseases. 2012;71(8):1322-8. doi: 10.1136/annrheumdis-2011-200970

86.   Bingham CO, 3rd, Buckland-Wright JC, Garnero P, Cohen SB, Dougados M, Adami S, et al. Risedronate decreases biochemical markers of cartilage degradation but does not decrease symptoms or slow radiographic progression in patients with medial compartment osteoarthritis of the knee: results of the two-year multinational knee osteoarthritis structural arthritis study. Arthritis and rheumatism. 2006;54(11):3494-507. doi: 10.1002/art.22160

87.   Buckland-Wright JC, Messent EA, Bingham CO, 3rd, Ward RJ, Tonkin C. A 2 yr longitudinal radiographic study examining the effect of a bisphosphonate (risedronate) upon subchondral bone loss in osteoarthritic knee patients. Rheumatology (Oxford, England). 2007;46(2):257-64. doi: 10.1093/rheumatology/kel213

88.   Han W, Fan S, Bai X, Ding C. Strontium ranelate, a promising disease modifying osteoarthritis drug. Expert opinion on investigational drugs. 2017;26(3):375-80. doi: 10.1080/13543784.2017.1283403

89.   Loca D, Smirnova A, Locs J, Dubnika A, Vecstaudza J, Stipniece L, et al. Development of local strontium ranelate delivery systems and long term in vitro drug release studies in osteogenic medium. Scientific reports. 2018;8(1):16754. doi: 10.1038/s41598-018-35197-7

90.   Alexandersen P, Karsdal MA, Qvist P, Reginster JY, Christiansen C. Strontium ranelate reduces the urinary level of cartilage degradation biomarker CTX-II in postmenopausal women. Bone. 2007;40(1):218-22. doi: 10.1016/j.bone.2006.07.028

91.   Tat SK, Pelletier JP, Mineau F, Caron J, Martel-Pelletier J. Strontium ranelate inhibits key factors affecting bone remodeling in human osteoarthritic subchondral bone osteoblasts. Bone. 2011;49(3):559-67. doi: 10.1016/j.bone.2011.06.005

92.   Pelletier JP, Roubille C, Raynauld JP, Abram F, Dorais M, Delorme P, et al. Disease-modifying effect of strontium ranelate in a subset of patients from the Phase III knee osteoarthritis study SEKOIA using quantitative MRI: reduction in bone marrow lesions protects against cartilage loss. Annals of the rheumatic diseases. 2015;74(2):422-9. doi: 10.1136/annrheumdis-2013-203989

93.   Lafeber FPJG, van Laar JM. Strontium ranelate: ready for clinical use as disease-modifying osteoarthritis drug? Annals of the Rheumatic Diseases. 2013;72(2):157-61. doi: 10.1136/annrheumdis-2012-202453

94.   Hamdy RC, Daley DN. Oral calcitonin. International journal of women's health. 2012;4:471-9. doi: 10.2147/ijwh.s24776

95.   Karsdal MA, Byrjalsen I, Henriksen K, Riis BJ, Lau EM, Arnold M, et al. The effect of oral salmon calcitonin delivered with 5-CNAC on bone and cartilage degradation in osteoarthritic patients: a 14-day randomized study. Osteoarthritis and cartilage. 2010;18(2):150-9. doi: 10.1016/j.joca.2009.08.004

96.   Manicourt DH, Azria M, Mindeholm L, Thonar EJ, Devogelaer JP. Oral salmon calcitonin reduces Lequesne's algofunctional index scores and decreases urinary and serum levels of biomarkers of joint metabolism in knee osteoarthritis. Arthritis and rheumatism. 2006;54(10):3205-11. doi: 10.1002/art.22075

97.   Karsdal MA, Byrjalsen I, Alexandersen P, Bihlet A, Andersen JR, Riis BJ, et al. Treatment of symptomatic knee osteoarthritis with oral salmon calcitonin: results from two phase 3 trials. Osteoarthritis and cartilage. 2015;23(4):532-43. doi: 10.1016/j.joca.2014.12.019

98.   Yoneda Y, Kuramoto N, Kitayama T, Hinoi E. Consolidation of transient ionotropic glutamate signals through nuclear transcription factors in the brain. Progress in neurobiology. 2001;63(6):697-719.

99.   Wen ZH, Chang YC, Jean YH. Excitatory amino acid glutamate: role in peripheral nociceptive transduction and inflammation in experimental and clinical osteoarthritis. Osteoarthritis and cartilage. 2015;23(11):2009-16. doi: 10.1016/j.joca.2015.03.017

100.   Szymanska E, Nielsen B, Johansen TN, Cunado Moral AM, Pickering DS, Szczepanska K, et al. Pharmacological characterization and binding modes of novel racemic and optically active phenylalanine-based antagonists of AMPA receptors. European journal of medicinal chemistry. 2017;138:874-83. doi: 10.1016/j.ejmech.2017.07.007

101.   McNearney T, Baethge BA, Cao S, Alam R, Lisse JR, Westlund KN. Excitatory amino acids, TNF-alpha, and chemokine levels in synovial fluids of patients with active arthropathies. Clinical and experimental immunology. 2004;137(3):621-7. doi: 10.1111/j.1365-2249.2004.02563.x

102.   Jean YH, Wen ZH, Chang YC, Huang GS, Lee HS, Hsieh SP, et al. Increased concentrations of neuro-excitatory amino acids in rat anterior cruciate ligament-transected knee joint dialysates: a microdialysis study. Journal of orthopaedic research : official publication of the Orthopaedic Research Society. 2005;23(3):569-75. doi: 10.1016/j.orthres.2004.12.015

103.   Flood S, Parri R, Williams A, Duance V, Mason D. Modulation of interleukin-6 and matrix metalloproteinase 2 expression in human fibroblast-like synoviocytes by functional ionotropic glutamate receptors. Arthritis and rheumatism. 2007;56(8):2523-34. doi: 10.1002/art.22829

104.   Bonnet CS, Williams AS, Gilbert SJ, Harvey AK, Evans BA, Mason DJ. AMPA/kainate glutamate receptors contribute to inflammation, degeneration and pain related behaviour in inflammatory stages of arthritis. Ann Rheum Dis. 2015;74(1):242-51. doi: 10.1136/annrheumdis-2013-203670

105.   Zhang GH, Yoon YW, Lee KS, Min SS, Hong SK, Park JY, et al. The glutamatergic N-methyl-D-aspartate and non-N-methyl-D-aspartate receptors in the joint contribute to the induction, but not maintenance, of arthritic pain in rats. Neuroscience letters. 2003;351(3):177-80.

106.   Piepoli T, Mennuni L, Zerbi S, Lanza M, Rovati LC, Caselli G. Glutamate signaling in chondrocytes and the potential involvement of NMDA receptors in cell proliferation and inflammatory gene expression. Osteoarthritis and cartilage. 2009;17(8):1076-83. doi: 10.1016/j.joca.2009.02.002

107.   Vuolteenaho K, Moilanen T, Knowles RG, Moilanen E. The role of nitric oxide in osteoarthritis. Scandinavian journal of rheumatology. 2007;36(4):247-58. doi: 10.1080/03009740701483014

108.   Sciences NCfAT. CINDUNISTAT HYDROCHLORIDE MALEATE. 2001 [accessed 25/03]. Available from: https://drugs.ncats.io/drug/S39P2D3CM9

109.   Hellio le Graverand MP, Clemmer RS, Redifer P, Brunell RM, Hayes CW, Brandt KD, et al. A 2-year randomised, double-blind, placebo-controlled, multicentre study of oral selective iNOS inhibitor, cindunistat (SD-6010), in patients with symptomatic osteoarthritis of the knee. Annals of the rheumatic diseases. 2013;72(2):187-95. doi: 10.1136/annrheumdis-2012-202239

110.   Laufer SA, Augustin J, Dannhardt G, Kiefer W. (6,7-Diaryldihydropyrrolizin-5-yl)acetic Acids, a Novel Class of Potent Dual Inhibitors of Both Cyclooxygenase and 5-Lipoxygenase. Journal of Medicinal Chemistry. 1994;37(12):1894-7. doi: 10.1021/jm00038a021

111.   Cicero AF, Laghi L. Activity and potential role of licofelone in the management of osteoarthritis. Clinical interventions in aging. 2007;2(1):73-9. doi: 10.2147/ciia.2007.2.1.73

112.   Kulkarni SK, Singh VP. Licofelone--a novel analgesic and anti-inflammatory agent. Current topics in medicinal chemistry. 2007;7(3):251-63. doi: 10.2174/156802607779941305

113.   Jovanovic DV, Fernandes JC, Martel-Pelletier J, Jolicoeur FC, Reboul P, Laufer S, et al. In vivo dual inhibition of cyclooxygenase and lipoxygenase by ML-3000 reduces the progression of experimental osteoarthritis: suppression of collagenase 1 and interleukin-1beta synthesis. Arthritis and rheumatism. 2001;44(10):2320-30. doi: 10.1002/1529-0131(200110)44:10<2320::aid-art394>3.0.co;2-p

114.   Gay RE, Neidhart M, Pataky F, Tries S, Laufer S, Gay S. Dual inhibition of 5-lipoxygenase and cyclooxygenases 1 and 2 by ML3000 reduces joint destruction in adjuvant arthritis. The Journal of rheumatology. 2001;28(9):2060-5.

115.   Moreau M, Boileau C, Martel-Pelletier J, Brunet J, Laufer S, Pelletier JP. Licofelone reduces progression of structural changes in a canine model of osteoarthritis under curative conditions: effect on protease expression and activity. The Journal of rheumatology. 2006;33(6):1176-83.

116.   Boileau C, Martel-Pelletier J, Jouzeau JY, Netter P, Moldovan F, Laufer S, et al. Licofelone (ML-3000), a dual inhibitor of 5-lipoxygenase and cyclooxygenase, reduces the level of cartilage chondrocyte death in vivo in experimental dog osteoarthritis: inhibition of pro-apoptotic factors. The Journal of rheumatology. 2002;29(7):1446-53.

117.   Raynauld JP, Martel-Pelletier J, Bias P, Laufer S, Haraoui B, Choquette D, et al. Protective effects of licofelone, a 5-lipoxygenase and cyclo-oxygenase inhibitor, versus naproxen on cartilage loss in knee osteoarthritis: a first multicentre clinical trial using quantitative MRI. Ann Rheum Dis. 2009;68(6):938-47. doi: 10.1136/ard.2008.088732

118.   Blaney Davidson EN, van der Kraan PM, van den Berg WB. TGF-beta and osteoarthritis. Osteoarthritis and cartilage. 2007;15(6):597-604. doi: 10.1016/j.joca.2007.02.005

119.   Blaney Davidson EN, Vitters EL, van der Kraan PM, van den Berg WB. Expression of transforming growth factor-beta (TGFbeta) and the TGFbeta signalling molecule SMAD-2P in spontaneous and instability-induced osteoarthritis: role in cartilage degradation, chondrogenesis and osteophyte formation. Annals of the rheumatic diseases. 2006;65(11):1414-21. doi: 10.1136/ard.2005.045971

120.   Blaney Davidson EN, Scharstuhl A, Vitters EL, van der Kraan PM, van den Berg WB. Reduced transforming growth factor-beta signaling in cartilage of old mice: role in impaired repair capacity. Arthritis research & therapy. 2005;7(6):R1338-47. doi: 10.1186/ar1833

121.   Hunter DJ, Pike MC, Jonas BL, Kissin E, Krop J, McAlindon T. Phase 1 safety and tolerability study of BMP-7 in symptomatic knee osteoarthritis. BMC musculoskeletal disorders. 2010;11:232. doi: 10.1186/1471-2474-11-232

122.   Yao X, Zhang J, Jing X, Ye Y, Guo J, Sun K, et al. Fibroblast growth factor 18 exerts anti-osteoarthritic effects through PI3K-AKT signaling and mitochondrial fusion and fission. Pharmacological research. 2019;139:314-24. doi: 10.1016/j.phrs.2018.09.026

123.   Moore EE, Bendele AM, Thompson DL, Littau A, Waggie KS, Reardon B, et al. Fibroblast growth factor-18 stimulates chondrogenesis and cartilage repair in a rat model of injury-induced osteoarthritis. Osteoarthritis and cartilage. 2005;13(7):623-31. doi: 10.1016/j.joca.2005.03.003

124.   Mori Y, Saito T, Chang SH, Kobayashi H, Ladel CH, Guehring H, et al. Identification of fibroblast growth factor-18 as a molecule to protect adult articular cartilage by gene expression profiling. The Journal of biological chemistry. 2014;289(14):10192-200. doi: 10.1074/jbc.M113.524090

125.   Power J, Hernandez P, Guehring H, Getgood A, Henson F. Intra-articular injection of rhFGF-18 improves the healing in microfracture treated chondral defects in an ovine model. Journal of orthopaedic research : official publication of the Orthopaedic Research Society. 2014;32(5):669-76. doi: 10.1002/jor.22580

126.   Ellsworth JL, Berry J, Bukowski T, Claus J, Feldhaus A, Holderman S, et al. Fibroblast growth factor-18 is a trophic factor for mature chondrocytes and their progenitors. Osteoarthritis and cartilage. 2002;10(4):308-20. doi: 10.1053/joca.2002.0514

127.   Lohmander LS, Hellot S, Dreher D, Krantz EF, Kruger DS, Guermazi A, et al. Intraarticular sprifermin (recombinant human fibroblast growth factor 18) in knee osteoarthritis: a randomized, double-blind, placebo-controlled trial. Arthritis & rheumatology (Hoboken, NJ). 2014;66(7):1820-31. doi: 10.1002/art.38614

128.   Roemer FW, Aydemir A, Lohmander S, Crema MD, Marra MD, Muurahainen N, et al. Structural effects of sprifermin in knee osteoarthritis: a post-hoc analysis on cartilage and non-cartilaginous tissue alterations in a randomized controlled trial. BMC musculoskeletal disorders. 2016;17:267. doi: 10.1186/s12891-016-1128-2

129.   Hochberg MC, Guermazi A, Guehring H, Aydemir A, Wax S, Fleuranceau-Morel P, et al. Effect of Intra-Articular Sprifermin vs Placebo on Femorotibial Joint Cartilage Thickness in Patients With Osteoarthritis: The FORWARD Randomized Clinical Trial. Jama. 2019;322(14):1360-70. doi: 10.1001/jama.2019.14735

130.   Guehring H, Moreau F, Daelken B, Ladel C, Guenther O, Bihlet AR, et al. The effects of sprifermin on symptoms and structure in a subgroup at risk of progression in the FORWARD knee osteoarthritis trial. Seminars in arthritis and rheumatism. 2021;51(2):450-6. doi: 10.1016/j.semarthrit.2021.03.005

131.   Eckstein F, Kraines JL, Aydemir A, Wirth W, Maschek S, Hochberg MC. Intra-articular sprifermin reduces cartilage loss in addition to increasing cartilage gain independent of location in the femorotibial joint: post-hoc analysis of a randomised, placebo-controlled phase II clinical trial. Annals of the rheumatic diseases. 2020;79(4):525-8. doi: 10.1136/annrheumdis-2019-216453

132.   Eckstein F, Hochberg MC, Guehring H, Moreau F, Ona V, Bihlet AR, et al. Long-term structural and symptomatic effects of intra-articular sprifermin in patients with knee osteoarthritis: 5-year results from the FORWARD study. Annals of the rheumatic diseases. 2021;80(8):1062-9. doi: 10.1136/annrheumdis-2020-219181

133.   Zeng WN, Zhang Y, Wang D, Zeng YP, Yang H, Li J, et al. Intra-articular Injection of Kartogenin-Enhanced Bone Marrow-Derived Mesenchymal Stem Cells in the Treatment of Knee Osteoarthritis in a Rat Model. The American journal of sports medicine. 2021;49(10):2795-809. doi: 10.1177/03635465211023183

134.   Kwon JY, Lee SH, Na HS, Jung K, Choi J, Cho KH, et al. Kartogenin inhibits pain behavior, chondrocyte inflammation, and attenuates osteoarthritis progression in mice through induction of IL-10. Scientific reports. 2018;8(1):13832. doi: 10.1038/s41598-018-32206-7

135.   Johnson KA, Woods AK, Joseph SB, Chatterjee AK, Zhu S, Wisler J, et al. Development of KA34 as a cartilage regenerative therapy for Osteoarthritis. Osteoarthritis and cartilage. 2020;28:S518. doi: https://doi.org/10.1016/j.joca.2020.02.814

136.   Deshmukh V, O'Green AL, Bossard C, Seo T, Lamangan L, Ibanez M, et al. Modulation of the Wnt pathway through inhibition of CLK2 and DYRK1A by lorecivivint as a novel, potentially disease-modifying approach for knee osteoarthritis treatment. Osteoarthritis and cartilage. 2019;27(9):1347-60. doi: 10.1016/j.joca.2019.05.006

137.   Yazici Y, McAlindon TE, Fleischmann R, Gibofsky A, Lane NE, Kivitz AJ, et al. A novel Wnt pathway inhibitor, SM04690, for the treatment of moderate to severe osteoarthritis of the knee: results of a 24-week, randomized, controlled, phase 1 study. Osteoarthritis and cartilage. 2017;25(10):1598-606. doi: 10.1016/j.joca.2017.07.006

138.   Yazici Y, McAlindon TE, Gibofsky A, Lane NE, Clauw D, Jones M, et al. Lorecivivint, a Novel Intraarticular CDC-like Kinase 2 and Dual-Specificity Tyrosine Phosphorylation-Regulated Kinase 1A Inhibitor and Wnt Pathway Modulator for the Treatment of Knee Osteoarthritis: A Phase II Randomized Trial. Arthritis & rheumatology (Hoboken, NJ). 2020;72(10):1694-706. doi: 10.1002/art.41315

139.   Tambiah JRS, Kennedy S, Swearingen CJ, Simsek I, Yazici Y, Farr J, et al. Individual Participant Symptom Responses to Intra-Articular Lorecivivint in Knee Osteoarthritis: Post Hoc Analysis of a Phase 2B Trial. Rheumatology and therapy. 2021;8(2):973-85. doi: 10.1007/s40744-021-00316-w

140.   Bajpayee AG, Wong CR, Bawendi MG, Frank EH, Grodzinsky AJ. Avidin as a model for charge driven transport into cartilage and drug delivery for treating early stage post-traumatic osteoarthritis. Biomaterials. 2014;35(1):538-49. doi: 10.1016/j.biomaterials.2013.09.091

141.   Saeedi T, Alotaibi HF, Prokopovich P. Polymer colloids as drug delivery systems for the treatment of arthritis. Advances in colloid and interface science. 2020;285:102273. doi: 10.1016/j.cis.2020.102273

142.   DeJulius CR, Gulati S, Hasty KA, Crofford LJ, Duvall CL. Recent Advances in Clinical Translation of Intra-Articular Osteoarthritis Drug Delivery Systems. Advanced therapeutics. 2021;4(1) doi: 10.1002/adtp.202000088

143. Perni S, Prokopovich P. Poly-beta-amino-esters nano-vehicles based drug delivery system for cartilage. Nanomedicine : nanotechnology, biology, and medicine. 2017;13(2):539-48. doi: 10.1016/j.nano.2016.10.001

144. Yoshioka K, Kisukeda T, Zuinen R, Yasuda Y, Miyamoto K. Pharmacological effects of N-[2-[[2-[2-[(2,6-dichlorophenyl)amino]phenyl]acetyl]oxy]ethyl]hyaluronamide (diclofenac Etalhyaluronate, SI-613), a novel sodium hyaluronate derivative chemically linked with diclofenac. BMC musculoskeletal disorders. 2018;19(1):157. doi: 10.1186/s12891-018-2077-8

145. Kumar A, Bendele AM, Blanks RC, Bodick N. Sustained efficacy of a single intra-articular dose of FX006 in a rat model of repeated localized knee arthritis. Osteoarthritis and cartilage. 2015;23(1):151-60. doi: 10.1016/j.joca.2014.09.019

146. McCormack R, Lamontagne M, Vannabouathong C, Deakon RT, Belzile EL. Comparison of the 3 Different Injection Techniques Used in a Randomized Controlled Study Evaluating a Cross-Linked Sodium Hyaluronate Combined With Triamcinolone Hexacetonide (Cingal) for Osteoarthritis of the Knee: A Subgroup Analysis. Clinical medicine insights Arthritis and musculoskeletal disorders. 2017;10:1179544117725026. doi: 10.1177/1179544117725026

147. Hangody L, Szody R, Lukasik P, Zgadzaj W, Lénárt E, Dokoupilova E, et al. Intraarticular Injection of a Cross-Linked Sodium Hyaluronate Combined with Triamcinolone Hexacetonide (Cingal) to Provide Symptomatic Relief of Osteoarthritis of the Knee: A Randomized, Double-Blind, Placebo-Controlled Multicenter Clinical Trial. Cartilage. 2018;9(3):276-83. doi: 10.1177/1947603517703732

148. Anika Therapeutics I. Cingal. [accessed 20/04]. Available from: https://anika.com/medical/products/cingal/

149. Nishida Y, Kano K, Nobuoka Y, Seo T. Sustained-release diclofenac conjugated to hyaluronate (diclofenac etalhyaluronate) for knee osteoarthritis: a randomized phase 2 study. Rheumatology (Oxford, England). 2021;60(3):1435-44. doi: 10.1093/rheumatology/keaa605

150. Nishida Y, Kano K, Nobuoka Y, Seo T. Efficacy and Safety of Diclofenac-Hyaluronate Conjugate (Diclofenac Etalhyaluronate) for Knee Osteoarthritis: A Randomized Phase III Trial in Japan. Arthritis & rheumatology (Hoboken, NJ). 2021;73(9):1646-55. doi: 10.1002/art.41725

151. Nishida Y, Kano K, Osato T, Seo T. Open-label phase 3 study of diclofenac conjugated to hyaluronate (diclofenac etalhyaluronate: ONO-5704/SI-613) for treatment of osteoarthritis: 1-year follow-up. BMC musculoskeletal disorders. 2021;22(1):233. doi: 10.1186/s12891-021-04108-9

152. Paik J, Duggan ST, Keam SJ. Triamcinolone Acetonide Extended-Release: A Review in Osteoarthritis Pain of the Knee. Drugs. 2019;79(4):455-62. doi: 10.1007/s40265-019-01083-3

153. Kraus VB, Conaghan PG, Aazami HA, Mehra P, Kivitz AJ, Lufkin J, et al. Synovial and systemic pharmacokinetics (PK) of triamcinolone acetonide (TA) following intra-articular (IA) injection of an extended-release microsphere-based formulation (FX006) or standard crystalline suspension in patients with knee osteoarthritis (OA). Osteoarthritis and cartilage. 2018;26(1):34-42. doi: 10.1016/j.joca.2017.10.003

154. Therapeutics F. Flexion Therapeutics Announces New Drug Application for Zilretta™ (FX006) Accepted by U.S. Food and Drug Administration. Flexion Therapeutics; 2017 [accessed 01/07]. Available from: https://ir.flexiontherapeutics.com/news-releases/news-release-details/flexion-therapeutics-announces-new-drug-application-zilrettatm

155. Getgood A, Dhollander A, Malone A, Price J, Helliwell J. Pharmacokinetic Profile of Intra-articular Fluticasone Propionate Microparticles in Beagle Dog Knees. Cartilage. 2019;10(2):139-47. doi: 10.1177/1947603517723687

156. Kandel L, Dolev Y, Rivkind G, Liebergall M, Mattan Y, Barenholz Y, et al. Safety and efficacy of MM-II, an intra-articular injection of liposomes, in moderate knee osteoarthritis. Prospective randomized double-blinded study. Osteoarthritis and cartilage. 2014;22:S193. doi: 10.1016/j.joca.2014.02.367

157.   Yu WN, Wu MJ, Chang PC, Shih SF. Cartilage damage and synovial toxicokinetic study of a sustained release liposomal formulation of dexamethasone sodium phosphate (TLC599) following intra-articular injection in healthy dogs and rabbits. Osteoarthritis and cartilage. 2019;27:S161-S2. doi: https://doi.org/10.1016/j.joca.2019.02.239

158.   Wu T-J, Yu W-N, Wu M-J, Chang P-C, Shih S-F. THU0465 PHARMACOKINETICS AND TOXICOKINETICS STUDIES OF A SUSTAINED RELEASE LIPOSOMAL FORMULATION OF DEXAMETHASONE SODIUM PHOSPHATE (TLC599) FOLLOWING INTRA-ARTICULAR INJECTION IN DOGS. Annals of the rheumatic diseases. 2019;78(Suppl 2):523-. doi: 10.1136/annrheumdis-2019-eular.3880

159.   Hunter DJ, Chang CC, Wei JC, Lin HY, Brown C, Tai TT, et al. TLC599 in patients with osteoarthritis of the knee: a phase IIa, randomized, placebo-controlled, dose-finding study. Arthritis research & therapy. 2022;24(1):52. doi: 10.1186/s13075-022-02739-4

160.   Kang ML, Ko JY, Kim JE, Im GI. Intra-articular delivery of kartogenin-conjugated chitosan nano/microparticles for cartilage regeneration. Biomaterials. 2014;35(37):9984-94. doi: 10.1016/j.biomaterials.2014.08.042

161.   Kang ML, Kim JE, Im GI. Thermoresponsive nanospheres with independent dual drug release profiles for the treatment of osteoarthritis. Acta biomaterialia. 2016;39:65-78. doi: 10.1016/j.actbio.2016.05.005

162.   Kang ML, Jeong SY, Im GI. Hyaluronic Acid Hydrogel Functionalized with Self-Assembled Micelles of Amphiphilic PEGylated Kartogenin for the Treatment of Osteoarthritis. Tissue engineering Part A. 2017;23(13-14):630-9. doi: 10.1089/ten.tea.2016.0524

163.   Fan W, Li J, Yuan L, Chen J, Wang Z, Wang Y, et al. Intra-articular injection of kartogenin-conjugated polyurethane nanoparticles attenuates the progression of osteoarthritis. Drug delivery. 2018;25(1):1004-12. doi: 10.1080/10717544.2018.1461279

164.   Maudens P, Seemayer CA, Thauvin C, Gabay C, Jordan O, Allémann E. Nanocrystal-Polymer Particles: Extended Delivery Carriers for Osteoarthritis Treatment. Small (Weinheim an der Bergstrasse, Germany). 2018;14(8) doi: 10.1002/smll.201703108

165.   Wang SJ, Qin JZ, Zhang TE, Xia C. Intra-articular Injection of Kartogenin-Incorporated Thermogel Enhancing Osteoarthritis Treatment. Frontiers in chemistry. 2019;7:677. doi: 10.3389/fchem.2019.00677

166.   Jain A, Mishra SK, Vuddanda PR, Singh SK, Singh R, Singh S. Targeting of diacerein loaded lipid nanoparticles to intra-articular cartilage using chondroitin sulfate as homing carrier for treatment of osteoarthritis in rats. Nanomedicine : nanotechnology, biology, and medicine. 2014;10(5):1031-40. doi: 10.1016/j.nano.2014.01.008

167.   Gómez-Gaete C, Retamal M, Chávez C, Bustos P, Godoy R, Torres-Vergara P. Development, characterization and in vitro evaluation of biodegradable rhein-loaded microparticles for treatment of osteoarthritis. European journal of pharmaceutical sciences : official journal of the European Federation for Pharmaceutical Sciences. 2017;96:390-7. doi: 10.1016/j.ejps.2016.10.010

168.   Poh S, Lin JB, Panitch A. Release of anti-inflammatory peptides from thermosensitive nanoparticles with degradable cross-links suppresses pro-inflammatory cytokine production. Biomacromolecules. 2015;16(4):1191-200. doi: 10.1021/bm501849p

169.   Lin JB, Poh S, Panitch A. Controlled release of anti-inflammatory peptides from reducible thermosensitive nanoparticles suppresses cartilage inflammation. Nanomedicine : nanotechnology, biology, and medicine. 2016;12(7):2095-100. doi: 10.1016/j.nano.2016.05.010

170.   Vedadghavami A, Zhang C, Bajpayee AG. Overcoming negatively charged tissue barriers: Drug delivery using cationic peptides and proteins. Nano today. 2020;34 doi: 10.1016/j.nantod.2020.100898

171.   Vedadghavami A, Wagner EK, Mehta S, He T, Zhang C, Bajpayee AG. Cartilage penetrating cationic peptide carriers for applications in drug delivery to avascular negatively charged tissues. Acta biomaterialia. 2019;93:258-69. doi: 10.1016/j.actbio.2018.12.004

172.   Bajpayee AG, Quadir MA, Hammond PT, Grodzinsky AJ. Charge based intra-cartilage delivery of single dose dexamethasone using Avidin nano-carriers suppresses cytokine-induced catabolism long term. Osteoarthritis and cartilage. 2016;24(1):71-81. doi: 10.1016/j.joca.2015.07.010

173.   Bajpayee AG, Scheu M, Grodzinsky AJ, Porter RM. Electrostatic interactions enable rapid penetration, enhanced uptake and retention of intra-articular injected avidin in rat knee joints. Journal of orthopaedic research : official publication of the Orthopaedic Research Society. 2014;32(8):1044-51. doi: 10.1002/jor.22630

174.   Bajpayee AG, De la Vega RE, Scheu M, Varady NH, Yannatos IA, Brown LA, et al. Sustained intra-cartilage delivery of low dose dexamethasone using a cationic carrier for treatment of post traumatic osteoarthritis. European cells & materials. 2017;34:341-64. doi: 10.22203/eCM.v034a21

175.   Zhang C, He T, Vedadghavami A, Bajpayee AG. Avidin-biotin technology to synthesize multi-arm nano-construct for drug delivery. MethodsX. 2020;7:100882. doi: 10.1016/j.mex.2020.100882

176.   He T, Zhang C, Vedadghavami A, Mehta S, Clark HA, Porter RM, et al. Multi-arm Avidin nano-construct for intra-cartilage delivery of small molecule drugs. Journal of controlled release : official journal of the Controlled Release Society. 2020;318:109-23. doi: 10.1016/j.jconrel.2019.12.020

177.   Yang C, Xue Z, Liu Y, Xiao J, Chen J, Zhang L, et al. Delivery of anticancer drug using pH-sensitive micelles from triblock copolymer MPEG-b-PBAE-b-PLA. Materials science & engineering C, Materials for biological applications. 2018;84:254-62. doi: 10.1016/j.msec.2017.12.003

178.   Liu Y, Chen J, Tang Y, Li S, Dou Y, Zheng J. Synthesis and Characterization of Quaternized Poly(beta-amino ester) for Highly Efficient Delivery of Small Interfering RNA. Molecular pharmaceutics. 2018;15(10):4558-67. doi: 10.1021/acs.molpharmaceut.8b00549

179.   Green JJ, Langer R, Anderson DG. A combinatorial polymer library approach yields insight into nonviral gene delivery. Accounts of chemical research. 2008;41(6):749-59. doi: 10.1021/ar7002336

180.   Lynn DM, Langer R. Degradable Poly(β-amino esters): Synthesis, Characterization, and Self-Assembly with Plasmid DNA. Journal of the American Chemical Society. 2000;122(44):10761-8. doi: 10.1021/ja0015388

181.   Liu Y, Li Y, Keskin D, Shi L. Poly(β-Amino Esters): Synthesis, Formulations, and Their Biomedical Applications. Advanced healthcare materials. 2019;8(2):e1801359. doi: 10.1002/adhm.201801359

182.   Liu Y, Chen J, Tang Y, Li S, Dou Y, Zheng J. Synthesis and Characterization of Quaternized Poly(β-amino ester) for Highly Efficient Delivery of Small Interfering RNA. Molecular pharmaceutics. 2018;15(10):4558-67. doi: 10.1021/acs.molpharmaceut.8b00549

183.   Devalapally H, Shenoy D, Little S, Langer R, Amiji M. Poly(ethylene oxide)-modified poly(beta-amino ester) nanoparticles as a pH-sensitive system for tumor-targeted delivery of hydrophobic drugs: part 3. Therapeutic efficacy and safety studies in ovarian cancer xenograft model. Cancer chemotherapy and pharmacology. 2007;59(4):477-84. doi: 10.1007/s00280-006-0287-5

184.   Perni S, Prokopovich P. Optimisation and feature selection of poly-beta-amino-ester as a drug delivery system for cartilage. Journal of materials chemistry B. 2020;8(23):5096-108. doi: 10.1039/c9tb02778e

185.   Saeedi T, Prokopovich P. Poly beta amino ester coated emulsions of NSAIDs for cartilage treatment. Journal of materials chemistry B. 2021;9(29):5837-47. doi: 10.1039/d1tb01024g

186.   Kim MS, Lee DS, Choi E-K, Park H-J, Kim J-S. Modulation of poly(β-amino ester) pH-sensitive polymers by molecular weight control. Macromolecular Research. 2005;13(2):147-51. doi: 10.1007/BF03219029

187.   Min KH, Kim JH, Bae SM, Shin H, Kim MS, Park S, et al. Tumoral acidic pH-responsive MPEG-poly(beta-amino ester) polymeric micelles for cancer targeting therapy. Journal of controlled release : official journal of the Controlled Release Society. 2010;144(2):259-66. doi: 10.1016/j.jconrel.2010.02.024

188.	Hwang SJ, Kim MS, Han JK, Lee DS, Kim BS, Choi EK, et al. pH-sensitivity control of PEG-poly(β-amino ester) block copolymer micelle. Macromolecular Research. 2007;15(5):437-42. doi: 10.1007/BF03218811

189.	Paulsen K, Frasco D. Determination of polymer molecular weight and composition using picoSpin NMR spectroscopy. Thermo Fisher Scientific: Thermo Fisher Scientific; 2016 [accessed 04/July]. Available from: https://assets.thermofisher.com/TFS-Assets/CAD/Application-Notes/Case-Western-Polymer-App-Note-r16-11-22.pdf

190.	Software G. Tukey and Dunnett methods. 2017 [accessed 15/ Aug]. Available from: https://www.graphpad.com/guides/prism/7/statistics/index.htm?stat_the_methods_of_tukey_and_dunne.htm

191.	Hammarling K, Sandberg M, Engholm M, Andersson H, Nilsson H-E. Synthesis, Curing Behavior and Swell Tests of pH-Responsive Coatings from Acryl-Terminated Oligo(β-Amino Esters). Chemosensors. 2018;6(1):10.

192.	Li Y, Beitelshees M, Fang L, Hill A, Ahmadi MK, Chen M, et al. In situ pneumococcal vaccine production and delivery through a hybrid biological-biomaterial vector. Science advances. 2016;2(7):e1600264. doi: 10.1126/sciadv.1600264

193.	Kou L, Xiao S, Sun R, Bao S, Yao Q, Chen R. Biomaterial-engineered intra-articular drug delivery systems for osteoarthritis therapy. Drug delivery. 2019;26(1):870-85. doi: 10.1080/10717544.2019.1660434

194.	Liu Y, Li Y, Keskin D, Shi L. Poly(beta-Amino Esters): Synthesis, Formulations, and Their Biomedical Applications. Advanced healthcare materials. 2019;8(2):e1801359. doi: 10.1002/adhm.201801359

195.	Silva LF, Aguilar AM. 4.03 - Functions Incorporating a Halogen and Another Heteroatom Group Other Than a Chalcogen. In: Katritzky AR, Taylor RJK, editors. Comprehensive Organic Functional Group Transformations II. Oxford: Elsevier; 2005. p. 129-91.

196.	Schuh C, Rühe J. Penetration of Polymer Brushes by Chemical Nonidentical Free Polymers. Macromolecules. 2011;44(9):3502-10. doi: 10.1021/ma102410z

197.	Alex He Z, Blank WJ. Crosslinking with malonate blocked isocyanates and with melamine resins. Journal of Coatings Technology. 1999;71(889):85-90. doi: 10.1007/BF02697892

198.	Byrne FP, Assemat JMZ, Stanford AE, Farmer TJ, Comerford JW, Pellis A. Enzyme-catalyzed synthesis of malonate polyesters and their use as metal chelating materials. Green chemistry : an international journal and green chemistry resource : GC. 2021;23(14):5043-8. doi: 10.1039/d1gc01783g

199.	Ghosh Dastidar T, Netravali AN. 'Green' crosslinking of native starches with malonic acid and their properties. Carbohydrate polymers. 2012;90(4):1620-8. doi: 10.1016/j.carbpol.2012.07.041

200.	Aydin D, Arslan M, Sanyal A, Sanyal R. Hooked on Cryogels: A Carbamate Linker Based Depot for Slow Drug Release. Bioconjugate chemistry. 2017;28(5):1443-51. doi: 10.1021/acs.bioconjchem.7b00140

201.	Larrivée-Aboussafy C, Jones BP, Price KE, Hardink MA, McLaughlin RW, Lillie BM, et al. DBU catalysis of N,N'-carbonyldiimidazole-mediated amidations. Organic letters. 2010;12(2):324-7. doi: 10.1021/ol9026599

202.	Boddu SK, Ur Rehman N, Mohanta TK, Majhi A, Avula SK, Al-Harrasi A. A review on DBU-mediated organic transformations. Green Chemistry Letters and Reviews. 2022;15(3):765-95. doi: 10.1080/17518253.2022.2132836

203.	Schaefer BHaW. n-BUTYRYL CHLORIDE. Organic Syntheses. 1929;9:32. doi: 10.15227

204.	Au - Lutjen AB, Au - Quirk MA, Au - Kolonko EM. Synthesis of Esters Via a Greener Steglich Esterification in Acetonitrile. JoVE. 2018(140):e58803. doi: doi:10.3791/58803

205.	Neises Bernhard SW. Simple Method for the Esterification of Carboxylic Acids. Angewandte Chemie : international edition. 1978;17(7):522-424. doi: 10.1002/anie.197805221

206.	Dosta P, Ramos V, Borrós S. Stable and efficient generation of poly(β-amino ester)s for RNAi delivery. Molecular Systems Design & Engineering. 2018;3(4):677-89. doi: 10.1039/C8ME00006A

207.   Temple DK, Cederlund AA, Lawless BM, Aspden RM, Espino DM. Viscoelastic properties of human and bovine articular cartilage: a comparison of frequency-dependent trends. BMC musculoskeletal disorders. 2016;17(1):419. doi: 10.1186/s12891-016-1279-1

208.   Yoo HJ, Hong SH, Choi JY, Lee IJ, Kim SJ, Choi JA, et al. Contrast-enhanced CT of articular cartilage: experimental study for quantification of glycosaminoglycan content in articular cartilage. Radiology. 2011;261(3):805-12. doi: 10.1148/radiol.11102495

209.   McMasters J, Poh S, Lin JB, Panitch A. Delivery of anti-inflammatory peptides from hollow PEGylated poly(NIPAM) nanoparticles reduces inflammation in an ex vivo osteoarthritis model. Journal of controlled release : official journal of the Controlled Release Society. 2017;258:161-70. doi: 10.1016/j.jconrel.2017.05.008

210.   Farndale RW, Buttle DJ, Barrett AJ. Improved quantitation and discrimination of sulphated glycosaminoglycans by use of dimethylmethylene blue. Biochimica et biophysica acta. 1986;883(2):173-7.

211.   Cissell DD, Link JM, Hu JC, Athanasiou KA. A Modified Hydroxyproline Assay Based on Hydrochloric Acid in Ehrlich's Solution Accurately Measures Tissue Collagen Content. Tissue engineering Part C, Methods. 2017;23(4):243-50. doi: 10.1089/ten.tec.2017.0018

212.   Malhotra V, Erlmann P. The pathway of collagen secretion. Annual review of cell and developmental biology. 2015;31:109-24. doi: 10.1146/annurev-cellbio-100913-013002

213.   Dalgaard L, Hjortkjaer RK, Regnier B, Nordholm L. Pharmacokinetics of the neuroprotective glutamate antagonist NBQX (6-nitro-7-sulfamoyl-benzo(f)quinoxaline-2,3-dione) in mice, rats, and dogs. Interactions with probenecid. Drug metabolism and disposition: the biological fate of chemicals. 1994;22(2):289-93.

214.   Elements A. NBQX Disodium Salt. American Elements; [accessed 10/08]. Available from: https://www.americanelements.com/nbqx-disodium-salt-479347-86-9

215.   Jaki T, Wolfsegger MJ. A Theoretical Framework for Estimation of AUCs in Complete and Incomplete Sampling Designs. Stat Biopharm Res. 2009;1(2):176-84. doi: 10.1198/sbr.2009.0025

216.   Rothenfluh DA, Bermudez H, O'Neil CP, Hubbell JA. Biofunctional polymer nanoparticles for intra-articular targeting and retention in cartilage. Nature Materials. 2008;7(3):248-54. doi: 10.1038/nmat2116

217.   Brown S, Pistiner J, Adjei IM, Sharma B. Nanoparticle Properties for Delivery to Cartilage: The Implications of Disease State, Synovial Fluid, and Off-Target Uptake. Molecular pharmaceutics. 2019;16(2):469-79. doi: 10.1021/acs.molpharmaceut.7b00484

218.   Geiger BC, Wang S, Padera RF, Jr., Grodzinsky AJ, Hammond PT. Cartilage-penetrating nanocarriers improve delivery and efficacy of growth factor treatment of osteoarthritis. Science translational medicine. 2018;10(469) doi: 10.1126/scitranslmed.aat8800

219.   Pelletier JP, Boileau C, Brunet J, Boily M, Lajeunesse D, Reboul P, et al. The inhibition of subchondral bone resorption in the early phase of experimental dog osteoarthritis by licofelone is associated with a reduction in the synthesis of MMP-13 and cathepsin K. Bone. 2004;34(3):527-38. doi: 10.1016/j.bone.2003.11.021